RHEUMATOID ARTHRITIS AND CITRULLINATION

TARGETING EPITOPE-SPECIFIC T CELLS AND MODELLING PROTEIN HYPERCITRULLINATION IN RHEUMATOID ARTHRITIS

By DEVON MALHOTRA, BHSc

A Thesis Submitted to the School of Graduate Studies in Partial Fulfilment of the Requirements for the Degree Master of Science

McMaster University MASTER OF SCIENCE (2024) Hamilton, Ontario (Medical Sciences, Infection and Immunity)

TITLE: Targeting Epitope-Specific T cells and Modelling Protein Hypercitrullination in Rheumatoid Arthritis

AUTHOR: Devon Malhotra, BHSc. (McMaster University)

SUPERVISOR: Professor M. Larché

NUMBER OF PAGES: xiii, 180

Lay Abstract

Rheumatoid arthritis (RA) is a long-term condition that reduces quality of life. In RA, the immune system mistakenly attacks and damages the bone and cartilage that make up the joints. The immune response is due to protein modification by an overactive enzyme in the body (PAD). PAD changes one amino acid (arginine) into another (citrulline). The immune system sees this change as a threat and reacts by damaging the joints.

This thesis aims to provide (1) a proof-of-concept for an RA treatment. Immune cells, from patient and control blood, were tested to see how they reacted to unchanged (arginine) and modified (citrulline) proteins, seen in RA. It was found that the immune cells did not have consistent responses, preventing treatment development. The second project (2) tried overproducing PAD in cells to study how it causes RA. Although the protein was produced it was non-functional and could not modify its targets.

Abstract

Introduction: Rheumatoid arthritis (RA) is a debilitating, autoimmune disease of the synovial joints, involving a complex interplay of genetic and environmental risk factors. In RA, an overactive peptidyl-arginine deiminase (PAD) enzyme, citrullinates 'self-proteins', converting positively charged arginine residues to neutral citrulline, generating new immunogenic peptides. These peptides interact favourably with a positively charged pocket within the binding groove of HLA-DR molecules. Peptides are subsequently presented to and activate autoreactive T cells, driving an inflammatory response. The Aims of this research were (1) to demonstrate proof-of-principal for a therapeutic mRNA vaccine substituting glutamine residues for citrulline (non-coded amino acid). T cell responses to native/citrullinated/glutamine-substituted peptides were compared, and (2) to overexpress the PAD4 enzyme and investigate the consequences of protein hypercitrullination in RA pathogenesis.

Methods: In Aim 1, 17 RA patients and healthy controls were recruited from a local Rheumatology clinic. Participants' peripheral blood mononuclear cells were isolated from whole blood to assess T cell responses to native, citrullinated, and glutamine-substituted peptides. In Aim 2, an adeno-associated virus (AAV), encoding a murine PAD4, was transduced into human and mouse cells. Protein hypercitrullination was investigated by western blotting, immunocytochemistry, flow cytometry, and ELISA.

Results: In Aim 1, 4/17 participants demonstrated an equivalent frequency of T cell responses to citrulline and glutamine epitopes. Antigen-specific T cell responses to unmodified peptides were also detected. In Aim 2, the AAV-encoding PAD4 was expressed in human and mouse cells. Cytoplasmic, rather than the expected nuclear and

endoplasmic reticulum distribution was observed. Protein hypercitrullination was not detected suggesting the engineered protein was non-functional.

Discussion/Conclusion: For Aim 1, it was apparent that glutamine was not an appropriate surrogate for citrulline (*in vitro*) in the design of a therapeutic mRNA vaccine. While, for Aim 2, an AAV-expression system to assess PAD4-mediated hypercitrullination led to production of a non-functional enzyme.

Acknowledgements

I am deeply thankful for the unwavering support, guidance, and feedback my supervisor, Dr. Mark Larché has provided me as I embarked on this journey. Being able to engage consistently in meaningful discussions and learning from an expert in the field of immunology and immunotherapy, has left me with an invaluable skillset and sincere appreciation towards autoimmune research.

There are several members of the Larché lab, past and present, that have had a significant impact in my development as a researcher, whom I sincerely thank. Dr. Tom Mu and Cheryl Kipling constantly provided the necessary resources and direction which have been pivotal in learning the laboratory techniques that I hope to utilize in my future endeavours. Amy Wang and Bilal Mohideen, undergraduate students in the lab, were always extremely supportive and I really appreciated their assistance.

The completion of this thesis would not be possible without the guidance and insightful comments from my committee members, Drs. Carl Richards, Maggie Larché, and Elena Tonti.

I am grateful for Barbara Baker's assistance in recruiting patients and controls at the Rheumatology Clinic and in conducting their blood draw for the clinical portion of this thesis. I would like to thank our collaborators at the University of Guelph as well, Dr. Sarah Wootton and Yanlong Pei, with the development of the AAV constructs. I also really appreciate the guidance and expertise provided by Kyle Macdonald, from the Richards Lab, in conducting western blots, and Mouhanad Babi from the Centre for Advanced Light Microscopy (CALM) with the confocal microscope.

I would also like to thank my family for their continued support and courage as I navigated through this project. It has been a wonderful experience developing as a researcher, and I am very thankful to have such a strong support network around me.

Table of Contents

Abstract……iv-v
Acknowledgements……vi-vii
List of Figures and Tables……x-xi
List of Abbreviations……xii
1.0 Introduction……1
1.1 Innate and Adaptive Immunity……1
1.1.1 Antigen Presentation……1-2
1.1.2 Tolerance and Anergy……2-4
1.2 Rheumatoid Arthritis……4
1.2.1 Background……4-5
1.2.2 Epidemiology……5-6
1.2.3 Etiology of disease……6-9
1.2.4 Etiologic Hypotheses……9-10
1.2.5 Clinical Diagnosis……10-12
1.2.6 Active Therapies and Challenges……12-14
1.3 Citrullination and the Peptidyl-arginine deiminase (PAD) enzyme……14-15
1.4 Inflammation and Pathophysiology of RA……16-18
1.5 Adeno-associated viruses……18-19
1.6 Thesis Rationale and Hypotheses……19-21
1.6.1 Research Questions……21-22
1.6.2 Hypotheses……22
1.6.3 Specific Aims……22-23
2.0 Methods……23
2.1 Study Characteristics……23
2.1.1 Study Design and Recruitment……23-24
2.1.2 Inclusion and Exclusion Criteria……24
2.2 ELISPOT Immunoassay……24
2.2.1 PBMC Isolation from Whole Blood……24-25
2.2.2 ELISPOT Preparation, Development, and Reading……25-27
2.2.3 ELISPOT Assay Assessment……27
2.2.4 ELISPOT Assay Troubleshooting……27-28
2.3 Adeno-Associated Virus (AAV) Cell Transduction and Analysis Techniques……28
2.3.1 AAV Vector Designs……28-30
2.3.2 AAV Tissue Tropism……30
2.3.3 Culturing Cells……30-31
2.3.4 Cellular Transduction with AAV……31-32
2.3.5 Cell Supernatant and Lysate……32-33
2.3.6 In-house ELISA (*in vitro*)……33-34
2.3.7 PAD Activity Detection Kit (in vitro)……34-35

2.3.8 EVOS Microscopy……...35-36
2.3.9 Immunocytochemistry and Confocal Microscopy……...36-37
2.3.10 Flow Cytometry…….....37-38
2.3.11 Western Blot…….....38-40
2.4 Statistical Analyses…….....40-41
3.0 Results……..……41
3.1 T Cell Responses (ELISPOT)…….....41-44
3.2 AAV MOI Selection and Confirmation of Transduction (*in vitro*)……..44-45
3.3 Subcellular Location of the PAD4 Enzyme……45-46
3.4 Western Blot…….....46-48
3.5 Optimizing the In-House ELISA…….....48-49
3.6 Peptidyl-Arginine Deiminase (PAD) Activity (*in vitro*) ……49
3.6.1 Citrullinated Protein levels in Untransduced and Transduced Cells……49-53
3.6.2 Citrullinated Protein levels in Untransduced and Transduced Cells – Examining Ionomycin and Calcium Supplementation on PAD Activity…….53-59
3.6.3 Citrullinated Protein levels in Untransduced and Transduced Cells – Addition of CCP as an Assay Control…….....59-61
3.7 PAD Activity using the Commercial Detection Kit……..61-63
4.0 Discussion…….....63-64
4.1 Project 1: Targeting Epitope Specific T Cells……..64
4.1.1 Frequency of T cell Responses is not similar between Citrulline and Glutamine Peptides…….....64-68
4.2 Project 2: Modelling Protein Hypercitrullination…….…..69
4.2.1 PAD4 is not Localized to the Endoplasmic Reticulum……69-71
4.2.2 Detection of PAD4 Expression by Western Blotting……...71-72
4.2.3 Assessment of PAD Activity by ELISA……72-76
4.2.4 Assessment of PAD Activity with a commercial kit……76-77
4.2.5 An Exploration of the following Project Caveats……..……...77-83
4.3 Statistical Significance and Experimental Design Limitations…….…83-87
5.0 Conclusion and Future Directions…….....87-88
6.0 Figures and Tables…….....89-155
7.0 References…….....156-180

List of Figures and Tables

Figure 1. Conversion of Arginine to Citrulline by PAD……...89
Figure 2. Peptide-specific T cell activation……..90
Figure 3. Comparison of Citrulline residues with Glutamine……91
Figure 4. Plasmid and cartoon maps of AAV constructs……92-93
Figure 5. Flow cytometry gating strategy……94
Table 1. Sample characteristics for peptide response clinical study (project 1) ……95
Table 2. Overview of the peptides in the clinical study (project 1) ……..96
Figure 6. Equivalent T cell response examples in the clinical study (project 1) ……...97
Table 3. Magnitude of antigen-specific T cells to native/citrullinated/glutamine-substituted peptides……98-100
Table 4. Summary of all patient and control significant T cell responses……101
Table 5. Interpretation of ELISPOT data……...102
Figure 7. Assessment of cells expressing GFP……103-105
Figure 8. Comparison of GFP-positive cells across several MOIs……106-111
Figure 9. PAD4 subcellular location using the EVOS microscope……..……..112
Figure 10. Assessment of PAD4 distribution within the cell using confocal microscopy……113-116
Figure 11. Expression levels of AAV encoded PAD4 by western blot……..….117-118
Figure 12. Optimizing the in-house ELISA for PAD activity……119
Figure 13. Comparison of citrullinated protein levels in untransduced and transduced cells……120
Tables 6-17. Descriptive statistics and summary results of post hoc multiple comparisons test……..121-125
Figure 14. Comparison of citrullinated protein levels in untransduced and transduced cells using two different sera (high titre ACPA and control) ……126
Tables 18-28. Descriptive statistics and summary results of post hoc multiple comparisons test for infection experiments with and without ionomycin and calcium supplementation……...127-132
Figure 15. Assessment of ionomycin and calcium supplementation on PAD activation (in vitro) ……...133-134
Tables 29-39. Descriptive statistics and summary results of post hoc multiple comparisons test for infection experiments with and without ionomycin and calcium supplementation across three cell types……135-140
Figure 16. Assessment of ionomycin and calcium supplementation on PAD activation in vitro across three cell types……141-142
Figure 17. Assessment of the in-house ELISA assay using a commercial peptide……143

Tables 40-44. Descriptive statistics and summary results of post hoc multiple comparisons test for infection experiments with and without ionomycin and calcium……...144-146
Tables 45-46. Summary of the descriptive statistics using a PAD activity detection kit…….146-147
Figure 18. Assessment of AAV encoded PAD by a commercial kit……148
Figure 19. Assessment of PAD activity with two AAV constructs using the PAD activity detection kit……149
Figure 20. Predicted 3-D model of the GFP-PAD4 fusion protein…….150-151
Supplementary Figure 1. T cell response graphs for RA patients and Healthy controls……..152-155

List of Abbreviations

Adeno-Associated Virus	AAV
AlexaFluor647	AF647
American College of Rheumatology	ACR
Anti-Citrullinated Protein Antibody	ACPA
Anti-Cyclic Citrullinated Peptide Antibody	Anti-CCP
Anti-Modified Citrulline Antibody	AMC
Antigen Presenting Cell	APC
C-reactive Protein	CRP
Clusters of Differentiation	CD
Cyclic Citrullinated Peptide	CCP
Dendritic Cells	DCs
Disease-Modifying Anti-Rheumatic Drugs	DMARDs
Distribution-Free Resampling with Equivalence	DFR(eq)
Enzyme-linked Immunosorbent Assay	ELISA
Enzyme-linked Immunospot	ELISPOT
Fetal Bovine Serum	FBS
Fluorescence-Activated Cell Sorting	FACS
Green Fluorescent Protein	GFP
High titre ACPA Sera	HPS
Human Leukocyte Antigen	HLA
Immunoglobulin	Ig
Interferon-Gamma	IFN-γ
Interleukin	IL
Major Histocompatibility Complex	MHC
Multiplicity of Infection	MOI
Non-steroidal inflammatory drugs	NSAIDs
Nuclear Localization Signal	NLS
Peptidyl-Arginine Deiminase	PAD
Peripheral Blood Mononuclear Cells	PBMCs
Phosphate Buffered Saline	PBS
Phycoerythrin	PE
Healthy Control (ACPA-negative) Pooled Sera	CPS
Relative Centrifugal Force	RCF
Rheumatoid Arthritis	RA
Rheumatoid Factor	RF
Shared Epitope	SE
T Cell Receptor	TCR
T Helper Cells	Th
Tetramethylbenzidine	TMB
Tumour Necrosis Factor-alpha	TNF-α
Woodchuck Hepatitis Virus Posttranscriptional Regulatory Element	WPRE

Declaration of Academic Achievement

I, Devon Malhotra, declare that the work presented in this thesis is my own, including the execution of experiments and analysis of data. The projects discussed in this paper, were designed by Dr. Mark Larché. Barbara Baker assisted with drawing participant blood for the clinical study (project 1). Dr. Tom Mu provided guidance on experimentation and led the collection and analysis of flow cytometry data reported here (project 2). This thesis was reviewed by Dr. Mark Larché.

1.0 Introduction

1.1 Innate and Adaptive Immunity

The innate and adaptive arms of the immune system protect from foreign pathogens. Although both systems work collectively, the innate immune system responds upon exposure to a microorganism once it has breached the body's physical barriers, such as the skin (1). Innate immune cells, including macrophages and neutrophils, try to contain the foreign agents by phagocytosis, secreting proinflammatory cytokines and recruiting more cells to the point of entry (1,2). If the innate immune system cannot eliminate the pathogen, antigen-presenting cells (APCs) interact with adaptive immune cells to initiate the second arm of the response. The adaptive arm is pathogen-specific and maintains immunologic memory to drive a more robust response upon re-exposure to the organism (1).

1.1.1 Antigen Presentation

The innate and adaptive immune responses are bridged by professional APCs, including dendritic cells (DCs), macrophages, and some B cells (1,3,4). These APCs use cell surface molecules, such as the major histocompatibility complex (MHC), also known as the human leukocyte antigen (HLA) in humans, to present epitopes (protein fragments) to adaptive immune cells (e.g., T and B cells) (1,3-5). A highly polymorphic gene complex on chromosome 6 encodes three classes of HLA molecules: I, II and III (5). The class I HLA-(A/B/C) or MHC-I molecules present endogenous pathogens to activate $CD8^+$ T lymphocytes, while class III consists of a range of substances that mediate an immune or inflammatory response such as, complement proteins and tumour necrosis factor-alpha (TNF-α) (5). The class II (HLA-DR/DP/DQ or MHC-II) molecules are vital for exogenous

pathogens and have an important role in autoimmune diseases, a primary focus of the next chapter *1.1.2* (5).

Professional APCs process and present epitopes to 'prime' corresponding T cells, leading to their activation and proliferation, using three signals (1,3-5). The first is the interaction of the MHC-II molecule loaded with the peptide fragment with a T cell receptor (TCR) and a second co-stimulatory signal via the CD28 receptor (T cell surface) binding CD80 ligand of the APC (1,3,4). Inflammatory cytokines, as secreted by mature APCs into the extracellular environment, provide the third signal for the differentiation of a T cell to provide effector function (2,3). In the absence of co-stimulation, however, T lymphocytes enter a state of hypo-responsiveness known as anergy, which is critical for immunoregulation (6,7).

1.1.2 Tolerance and Anergy

In response to a pathogen, the immune system may sometimes become over-reactive. As a result, to prevent the development of autoimmune diseases there are mechanisms that 'turn off' (or tolerize) immune cells (7-10). Immunologic tolerance is the process of decreasing immune cell responsiveness towards specific antigens presented by APCs (7). There are two forms of tolerance: central and peripheral. Early in the development of T lymphocytes within the thymus, a primary lymphatic organ, successful (moderate affinity) binding between the TCR and MHC-antigen complex allows for positive selection of these cells (8,9). These thymocytes are initially positive for both clusters of differentiation (CD) 4 and 8 (8,9). Only after binding with an appropriate MHC or HLA class (I or II) molecules do the cells become singly positive ($CD4^+$ and class II; $CD8^+$ and class I) (8,9). Another component of central tolerance is negative selection

which is the removal of autoreactive T cells to host antigens (8-10). B lymphocytes also undergo negative selection in a different primary lymphoid organ, the bone marrow (11). However, the process of central tolerance is 'incomplete' as some of the autoreactive T cells may survive and persist in the periphery (7). Several potential models for escaping tolerance induction have been hypothesized and elucidated in the literature. These included the lymphocytes receiving minimal exposure to sequestered (hidden) epitopes or encountered less of the subdominant to immunodominant epitopes during development (differential tolerance) (12-14). For instance, Cibotti and colleagues demonstrated that transgenic mice expressing the hen egg-white lysozyme (HEL) were tolerant to the full protein and the immunodominant peptide (13). However, the existing T cell repertoire was still responsive to two subdominant epitopes of HEL, highlighting differential tolerance towards different antigenic determinants of the same protein (13).

There are intrinsic and extrinsic mechanisms of peripheral tolerance, for potential autoreactive T cells not eliminated during central tolerance. Some example mechanisms are clonal deletion (apoptosis), suppression by regulatory T cells, and anergy, as mentioned above (15,16). Clonal deletion has one of two pathways, the first involves strong stimulation of the TCR with an autoantigen in the absence of a secondary signal (16). This prompts the upregulation and release of pro-apoptotic factors from the mitochondria which downstream can disrupt the cell structure and cause death (16). The second pathway, known as 'activation-induced cell death', consists of the surface receptor Fas binding to its ligand FasL to initiate a cascade of signalling events resulting in apoptosis (16-18). Although cell death is one way to maintain self-tolerance, Sakaguchi and colleagues previously demonstrated that $CD4^+CD25^+$ T cells, transferred to BALB/c

mice induced with autoimmune diseases, can suppress lymphocyte activity (19). These regulatory T cells (T_{reg}) had several immunoregulatory properties from secreting inhibitory cytokines, such as interleukin (IL)-10, or the expression of granzyme and perforin that can kill target cells (20-23). Some studies, such as by Dieckmann and colleagues, showed that T_{reg} cocultured with antigen-specific $CD4^+$ and $CD8^+$ T cells, *in vitro*, had a 75% and 60% reduction in proliferation, respectively (24). In addition to T_{reg}, another method of peripheral tolerance is anergy. In this reversible unresponsive state, lymphocytes do not proliferate or differentiate upon stimulation (15,25). To induce anergy involves an absence of the co-stimulatory signal through CD28 when presenting an epitope, along with changes in the intracellular signalling pathways that fail to produce IL-2, a cytokine indicative of activation (15,26,27). Thus, the cells can become tolerant to a particular antigen and are unable to mount an autoimmune response.

1.2 Rheumatoid Arthritis (RA)

1.2.1 Background

The immunoregulatory mechanisms can sometimes be dysfunctional and result in pathogenesis. To date, there are reports of over 100 different autoimmune diseases, from rheumatoid arthritis (RA) to type I diabetes (28). Despite the involvement of different organ systems, autoimmune diseases have overlapping similarities. For instance, the adaptive immune cells cannot differentiate self-antigens from non-self, and the innate immune cells play a critical role in presenting antigenic determinants to autoreactive T and B cells (28). Upon stimulation, the lymphocytes orchestrate a response against the body's tissues, producing autoantibodies and inducing systemic or localized inflammation by secreting proinflammatory cytokines (2-4,28).

Systemic and local inflammation are both associated with RA (27). RA is a chronic autoimmune disease of the synovial joints, symmetrically targeting the hands, knees, and feet (polyarticular) (29). The synovial joint is an anatomical space connecting two bone structures and consists of the articular cartilage, synovial membrane, and synovial fluid (30,31). The articular cartilage is a layer of connective tissue on the surfaces of adjacent bone that protects against damage (30). Continuous with the articular cartilage is the synovial membrane containing synoviocytes that fill the joint cavity with a colourless, viscous fluid (30,31). This fluid helps to reduce the friction caused by the motion of the limbs (30,31). RA presents as a complex, multi-stage disease process with inflammation of the synovial lining, and destruction of bone and cartilage, leading to deformities in the distal upper and lower extremities (32,33). Guo and colleagues recently proposed a four-phase model of RA pathogenesis (33). In phase I, *triggering*, certain genetic and environmental predisposition factors could make an individual susceptible to RA onset (33). The next phase (II), *maturation*, examined the activation of autoreactive immune cells in response to citrullinated self-proteins (33). In phase III, *targeting*, the pathologic mechanisms associated with joint damage were elucidated. While in phase IV, *fulminant*, the clinical and extra-articular manifestations of the disease were characterized (33,34).

1.2.2 Epidemiology

RA affects about 1% (or 350,000) of Canadians and poses a significant concern due to an aging population, as symptoms tend to become prominent in later adulthood (35,36). In multiple population-based investigations on estimates of RA prevalence and incidence, there was an evident rise in disease rates over time (35,37). For instance, Widdifield and colleagues reported a 120% increase in the total number of RA cases from

1996 (42,734) to 2010 (97,499) (35). Interestingly, the crude prevalence rose about two-fold from 490 to 899 total cases per 100,000 people, whereas a stable trend was observed for the incidence rate as it changed from 64 (1996) to 59 (2010) cases per 100,000 persons at risk per year (35). Although studies have reported that crude incidence rates tend to remain moderately stable over time, RA affects the sexes disproportionately (35,37-39). For example, the frequency of RA was two to three times higher in females than in males (39,40). These sex-based differences in RA may be partly explained by underlying genetic and hormonal factors (41,42). In a recent paper by Yu and colleagues, they found a statistically significant difference ($p<0.05$) and lower expression levels of the IL-4 gene in female compared to male RA patients (41). These findings suggested that lower levels of this anti-inflammatory cytokine may have profound implications in disease progression, especially for women (41).

1.2.3 Etiology of Disease

Current understanding of RA has stemmed from the complex interaction of genetic and environmental predisposing factors. Twin and genome-wide association studies (GWAS) have provided insight into the genes and their alleles that increased susceptibility towards RA (43-46). The results from two nationwide investigations demonstrated that the cumulative heritability estimate for RA was about 53% [95% CI (confidence interval): 40-65] (United Kingdom) (43,44) and 65% [95% CI: 50-77] (Finland) (43,45), with much higher concordance rates in monozygotic (12.3%) than dizygotic (3.5%) twins (44). To date, there are over 30 susceptibility genes, such as *PTPN22*, encoding a tyrosine-protein phosphatase non-receptor type 22, responsible for regulating antigen presentation (47,48). More notably, however, are a subset of alleles pertaining to the *HLA-DR beta*

(β)1 gene, such as DRβ1*01:01 (DR1 subtype) or DRβ1*04:01 (DR4 subtype), found in over 80% of RA cases (49). The product of the HLA-DRβ1 gene is an HLA class II molecule that contains a positively charged five amino acid (AA) motif, known as the shared epitope (SE), in the binding groove of the DRβ chain (50). Gregersen and colleagues proposed the SE hypothesis that the HLA-DR molecule presents peptides favourably interacting with the binding groove to activate autoreactive T cells (50,51). In subsequent experimental investigations using DR1 or DR4 transgenic mice engineered to express the human HLA-DR complex, it became clear that this antigen-presenting molecule binds peptides from self-protein, such as type II collagen, with a preference towards citrulline-containing (neutral) sequences over arginine (positively charged; described further in *sections 1.3 and 1.4*) (51-53). The *HLA-DRβ1* SE alleles are also implicated in associating interstitial lung disease (ILD), commonly described as an extra-articular manifestation of RA, with cigarette smoking (described below) (54,55). Recently emerging evidence using Mendelian randomization analysis on pre-existing GWAS data has shown a bi-directional, genetic causal link between ILD and RA (56). The researchers selected single nucleotide polymorphisms as instrumental variables based on pre-defined criteria connected to the risk factor but not directly to the outcome (56). For instance, when the causality of RA (risk factor) on ILD (outcome) was investigated, the risk of the outcome increased by 9.6% (56). Notably, when the occurrence of ILD, as the risk factor, was assessed on RA, it raised the risk of the arthritic disease by 12.8%, with both causal associations being statistically significant ($p<0.05$) (56). Together, these findings illustrated that genetic predisposition has a pivotal role in RA, the risk of which is likely elevated with environmental factors**.**

Numerous studies have highlighted certain environmental factors that increase the risk of RA onset (57-64). For instance, a case-control study on Swedish participants reported the odds of having high birthweight (>4000 g) in adult-onset RA patients was 3.3 times more likely than the controls (strong association) (57). Similarly, the incidence of RA was 40% more likely (relative risk=1.4) in both men and women of a low socioeconomic status (SES) (58). Though the underlying mechanisms for these two factors remain unknown, more extensively elucidated are the independent correlations that cigarette smoke and exposure to *Porphyromonas gingivalis* have with RA status (59). Smoking has a strong link to rheumatoid arthritis as evidence has shown that inhalable exposure increases the expression and activity of a particular peptidyl-arginine deiminase (PAD) enzyme (described in detail in *section 1.3*) implicated in the disease (60). There was also evidence that suggested smoking significantly elevated TNF-α, an inflammatory cytokine, secretion from lymphocytes over non-smokers, providing insight into one plausible mechanism of joint inflammation, as seen in RA (60,61). Glossop and colleagues also found a positive trend between the number of pack-years smoking and TNF-α secretion (61). This relationship was consistent with a population-based study which showed the risk of developing RA was over two-fold with 20 or more pack-years of smoking (62).

In addition to smoking, infection, such as with *P. gingivalis* was associated with RA. This gram-negative bacterium, known to cause periodontitis and contribute to periodontal diseases, has two virulence factors that are targets for the host immune system and relevant to RA (63). These factors include a PPAD enzyme, similar to the human form, and gingipains (63). The overlapping similarities between the bacterial and

human proteins may help explain how autoimmunity against the joints may arise. Current data has shown that *P. gingivalis* DNA was found in the synovial tissue in a significantly greater proportion of RA patients (33.3%) than in controls (5.9%), demonstrating that the oral infection may spread to the joints and play a part in the arthritic disease (64). A study by Kharlamova and colleagues demonstrated the 'additive interaction' effect of combining genetic and environmental risk factors in RA (59). For instance, elevated antibody levels to *P. gingivalis'* gingipain are associated with significantly higher odds of being RA positive (Odds Ratio (OR)=2.96) (59). This relationship strengthened in smokers (additive OR=5.35), and the proportion of the outcome attributable to the combined exposure was 48% (59). The additive effect also increased with anti-gingipain antibodies and the presence of the HLA-DR susceptibility genes (additive OR=16.62), with an attributable proportion of 47% (59). Thus, there is convincing evidence of an interaction among the risk factors with RA status.

1.2.4 Etiologic Hypotheses of Disease

Citrullination can yield new peptides (neoantigens) that although similar to their native counterparts, can be immunogenic. However, it remains unclear how smoking or infection by bacterial agents in the lungs can propel innate and adaptive immune cells to target the structures of the synovial joints. Two potential hypotheses to explain the mechanistic link between environmental exposures and RA were introduced: molecular mimicry and epitope spreading (65-67). The concept of molecular mimicry, first proposed by R. Damian in 1964 (67), suggested that the similarities between foreign antigens of microorganisms and the host they infect may contribute to autoimmune diseases (65, 67). Similarly, epitope spreading refers to the ability of dominant and subdominant (or cryptic)

epitopes to elicit an immune response (66). The subdominant or cryptic epitopes tend to be sequestered, but an event, such as an inflammatory response initiated by the primary epitope or tissue damage, allows APCs to present hidden sequences (secondary epitopes) and prime T cells (66).

Interestingly, however, the extent of disease may vary according to the processed antigen, and epitope spreading can create a hierarchy based on the immunodominance of the epitope (66). A study by Lundberg and colleagues described the cross-reactivity of antibodies to alpha-enolase in humans and enolase from *P. gingivalis* (68). The immunodominant peptide of citrullinated (or modified) alpha-enolase, a protein commonly implicated in RA, shared 82% homology with the bacterial analog (68). The researchers found that the immunoglobulin (Ig) G antibody response against the human and bacterial forms of enolase significantly correlated (r^2=0.8; $p<0.01$) (68). In another investigation, following immunization of HLA-DR1, DR4, and DR15 transgenic mice with immunodominant and cryptic epitopes of lethal factor (an antigen from *Bacillus anthracis*) revealed major differences in the levels of T cell activation and cytokine (e.g., interferon-gamma [IFN-γ]) production (69). When T cells were stimulated with cryptic epitopes, there were fewer cytokine-secreting lymphocytes than seen with the immunodominant peptides (69). Thus, molecular mimicry and epitope spreading can improve understanding of environmental factors and autoimmune diseases while broadening the scope of potential peptide targets that may mediate the disease.

1.2.5 Clinical Diagnosis

The American College of Rheumatology and European League Against Rheumatism (ACR/EULAR) revised a classification system in 2010, to better define RA

(70). Their criteria evaluated patients who may be suspected of RA on a 0 to 10 scale, with a score equal to or above 6, indicating disease (70). When diagnosing RA, it is important to assess the number of joints involved (mono- versus poly-articular) and disease severity, in addition to the circulating serologic markers (70,71). For instance, a characteristic clinical feature of RA is joint swelling caused by the activities of autoreactive immune cells (71). Patients may present with stiff and tender joints, such as those in the hands and feet, which negatively impacts their mobility and overall quality of life (71). RA does not localize only to the small joints and may be associated with extra-articular manifestations, as mentioned above (71,72). For instance, ILD (pulmonary), rheumatoid nodules (dermatologic), and lymphoma (hematologic) are a few of the systemic manifestations of the disease (71). A case-control study by Baecklund and colleagues found that the risk of lymphoma increased almost three-fold in RA cases (73). Thus, it is more likely for patients to experience complications with other organ systems after developing chronic RA.

Though the clinical features of RA primarily include changes to the joint morphology, there are specific serologic markers that aid in diagnosis, including rheumatoid factor (RF) and anti-cyclic citrullinated peptide antibodies (anti-CCP; hereafter referred to by the more inclusive term: anti-citrullinated protein antibodies [ACPA]) (72). Although patients may have seronegative RA, in the absence of RF or ACPA, it is much less common and seen only in about 30% of cases (29). Both RF and ACPA are autoantibodies produced by B cells to self-molecules. More specifically, RF targets the constant domain of IgG, while ACPAs interact with self-protein modified in an enzymatic process that creates neo-peptides, which the body assumes are foreign (74).

Interestingly, studies have demonstrated that these serologic markers form several years before clinical features are completely apparent (75,76). For instance, Nielen and colleagues reported a median time interval of 4.5 years from the first appearance of autoantibodies to symptom onset, with a moderately high positive predictive value (RF: 77% and anti-CCP: 83%) (75,77). To test for antibody status, there are commercially available enzyme-linked immunosorbent assays (ELISAs) and other clinical devices (78). Furthermore, systematic reviews and meta-analyses discovered that the accuracy of detecting autoantibodies was inconsistent with large ranges for sensitivity (12% to 93%) and specificity (63% to 100%) (79). Although specificity is generally higher for ACPA (95%) than RF (79%), their sensitivities are more comparable (67% versus 69%) (77-79). Thus, laboratory testing for these autoantibodies may provide considerable insight into the presence of RA. Another systemic marker indicative of inflammation is the c-reactive protein (CRP) (80). Biologically, CRP regulates immune responses and influences cytokine secretion from immune cells, thereby inducing inflammation (80). Although this protein is not a strong predictor of disease, some evidence has suggested that elevated levels of the marker (>10 mg/L) were present in RA patients and positively associated with disease activity (80). Nonetheless, measuring CRP levels may provide some indication of disease in conjunction with the autoantibody concentrations.

1.2.6 Active Therapies and Challenges

Current treatment options for RA are non-curative, focus on temporary symptom reduction, and pose significant challenges for the patient (81). Early intervention with corticosteroids, non-steroidal inflammatory drugs (NSAIDs), or disease-modifying anti-rheumatic drugs (DMARDs) can help reduce some of the joint inflammation (81,82). Intra-

articular corticosteroid injections of prednisone or NSAIDs, such as aspirin, are first-line therapies for managing RA symptoms as they have rapid effects and can inhibit the transcription of inflammatory genes, improving synovitis and the status of pain (82,83). However, there are also well-documented side effects with their use. For example, patients may experience gastrointestinal complications and even thinning of the bone (81). In a retrospective cohort study, almost 12% of the discontinuation rate for RA treatment was attributable to high risk of adverse events (84), a challenge with many of the current therapies available (33, 84, 85). Also, prescribing a lengthy treatment regimen may prompt nonadherence and worsen the disease, which is especially important with an aging population (29,36,81,86).

DMARDs are second-line therapies that take longer to act but have demonstrated success in reducing joint destruction and achieving clinical remission (81). A common DMARD to treat RA is methotrexate (81). However, as an immunosuppressive agent, this drug increases the patient's susceptibility to subsequent infection (81,87). In a randomized controlled trial (RCT) that compared the efficacy of DMARD combination therapy with monotherapy, there was a significant difference in the proportion of patients that achieved remission (24/97 (combination-DMARD) versus 11/98 (monotherapy-DMARD); $p=0.011$) (86). In a separate prospective follow-up study design, researchers reported that the two-year remission rates were higher and significantly different ($p<0.01$) for the combination therapy group (40%) over the monotherapy (18%), with lower radiographic joint damage also observed in the combination-treatment group (89). Although these studies provide insight into the effectiveness of a combinatory approach to RA treatment over single therapy, it still necessitates finding a cost-effective alternative.

A subclass of DMARDs are biologics that are disease-specific but incur high costs to patients (e.g., over $15000 annually) (90). A biologic approved for RA treatment is abatacept, which blocks the binding of CD80 with CD28 (co-stimulation) (91). An RCT by Kremer and colleagues compared abatacept with a placebo and found a significantly higher likelihood of ACR 20 (or 20% improvement in symptoms and disease status) with the intervention (60%) over the placebo group (35%) (91). Nonetheless, all three therapies may demonstrate some success in treating RA. However, many patients are unresponsive to current therapies, warranting the development of a newer, life-improving drug (33).

1.3 Citrullination and the Peptidyl-Arginine Deiminase (PAD) Enzyme

An important indicator of RA is autoantibodies that target citrullinated (modified) versions of the self-proteins, including vimentin, fibrinogen, and type II collagen (92,93). Citrullination is the post-translational modification of a positively charged L-arginine residue to neutral L-citrulline, intra- and extracellularly (94). A family of peptidyl-arginine deiminase (PAD) enzymes catalyze this calcium-dependent reaction, generating new immunogenic peptides since citrulline is a non-coded AA (**Figure 1**) (95). There is growing evidence that suggests citrullination has a major role in RA (**Figure 1**) (95). For instance, Wang and colleagues identified 182 citrullinated peptides from 83 total autoantigens in the synovial fluids (SF) of RA cases (96). RA patients have elevated levels of circulating autoantibodies and citrullinated autoantigens in their SF (93,97,98). In a recent study, it was evident from serum analysis that the mean ACPA levels were significantly higher in the RA group over osteoarthritis patients (133.93 ± 41.3 ng/L versus 5 ± 13.2 ng/L; $p=0.0001$) (98). Additional support for the association of citrullination and arthritogenicity

comes from pre-clinical investigations (94,99). An experiment with Dark Agouti rats demonstrated that immunization with citrullinated (cit) rat serum albumin (RSA) could break tolerance, as seen by anti-(cit)RSA IgG reacting to the native peptide (94). The researchers also found a positive correlation between the inflammation severity and levels of PAD4 and citrullinated peptides (91).

The PAD enzymes citrullinate peptides, and the two isoforms commonly implicated in RA are PAD2 and PAD4 (100-102). Foulquier and colleagues detected PAD2 and PAD4 mRNA transcripts in the synovial tissue of RA patients and found a positive association between enzyme expression and severity of inflammation (100). Several cells, such as monocytes, lymphocytes, and synoviocytes, express PAD enzymes intracellularly, with some PAD enzymes localizing to extracellular protein deposits (100,103). One source of PADs warranting further examination is neutrophils. Neutrophil-expressed PADs citrullinated peptides extracellularly, and cell death can form neutrophil extracellular traps (NETs) containing the enzyme elastase (104,105). Carmona-Rivera and colleagues recently showed that elastase-mediated release of PAD2 from fibroblast-like synoviocytes similarly modified proteins in the surrounding environment, developing autoantigens and contributing to joint damage (105). Contrarily, inhibiting the PAD enzyme may reduce arthritic symptoms. In a pre-clinical model of collagen-induced arthritis, DBA/1J mice injected with CL-amidine, an irreversible PAD inhibitor, significantly decreased disease activity and inflammation of the synovium (106). Thus, citrullination and PAD enzymes are critical contributors to RA pathogenesis.

1.4 Inflammation and Pathophysiology

Rheumatoid arthritis is an inflammatory disease characterized by erythema, joint pain, synovial hyperplasia, and bone/cartilage loss (33,107). There is accumulating evidence that suggests citrullination, genetic, and environmental factors have the potential to trigger RA (29,81,108). For instance, citrullinated peptides, compared with their native sequence, can form stable complexes with the *HLA-DRB1* gene-encoded product (29,52,81). These HLA-DR molecules contain a net positive, five AA sequence in the binding groove called the SE (described earlier in *section 1.2.3*) (52,108). Since citrulline (neutral AA) replaces a positively charged arginine residue, the antigenic sequence decreases in net charge and has a higher affinity for the SE (**Figure 2**) (109,110). Studies examining gene-environment interactions have highlighted the role of specific oral agents in RA onset. For example, cigarette smoke increased the expression of the PAD2 isoform, resulting in more citrullinated peptides (60). Furthermore, infection with bacterial agents, such as *P. gingivalis*, has helped establish a link between oral infection and joint destruction, emphasizing molecular mimicry and epitope spreading as potential explanations for targeting self-proteins (57,61-64,101,102). In a study by Wegner and colleagues, the group demonstrated how the *P. gingivalis* PAD (PPAD) enzyme and arginine-gingipains (proteases) worked in concert to develop autoantigens (or neo-epitopes) (111). The arginine-gingipains first cleaved the fibrinogen peptide right after an arginine residue, which PPAD then citrullinated (59,63,65,111). Similarly, modified peptides by human PADs are processed and presented by APCs to T lymphocytes in secondary lymphoid tissue that would otherwise have remained inactive upon binding to the native form (52,108). Once primed, these epitope-specific,

autoreactive $CD4^+$ T cells elicit an autoimmune response by secreting signalling molecules (e.g., IFN-γ) to promote inflammation and stimulate B cells to produce ACPAs, signifying the breach of self-tolerance (29,52,81,108).

In RA, ACPAs are found circulating and interacting with endogenous citrullinated proteins in the extracellular matrix or those secreted by cells of the joint tissues (107,112,113). Studies showed that ACPA can also interact with innate immune cells such as macrophages, stimulating them to produce proinflammatory cytokines (i.e., TNF-α and IL-6) and to recruit more leukocytes to infiltrate the joint, eventually resulting in a thickened and swollen synovial membrane (113,114). Other key players in RA are fibroblast-like synoviocytes (FLS) and Type 1 T helper (Th1) cells. FLS are responsive to the cytokines secreted by both innate and adaptive immune cells and produce the receptor activator of nuclear factor-κB-ligand (RANKL) which binds to the receptor RANK initiating the differentiation and activation of osteoclasts (bone-resorbing cells) (107,114-117). Osteoclasts, also stimulated by cytokines secreted from Th1 lymphocytes (e.g., TNF-α, IL-2, IFN-γ), contribute to the destruction of bone and cartilage as seen with RA patients (107, 115,116). In addition to macrophages, FLS have a complex interaction with $CD4^+$ T Cells and B cells. FLS interact with T cells via cell-adhesion molecules (e.g., CD58 on FLS interacts with CD2 on T cells) and secrete transforming growth factor-beta (TGF-β), which differentiates T cells into Th17 cells (in the presence of other cytokines like IL-6 and IL-23) that further orchestrate the immune response using IL-17 (107, 115-117). Several studies have reported an increase in IL-17-secreting $CD4^+$ T cells in the synovial joint of RA patients (118,119). By recruiting neutrophils, promoting osteoclastogenesis, or increasing the level of activated collagen-specific T cells as shown in a collagen-

induced arthritis mouse model (119), IL-17 has significant pathogenic involvement in this autoimmune disease (115-117,119). Moreover, FLS-secreted IL-6 or B-cell activating factor are critical for the survival and maturation of B lymphocytes, permitting continued antibody production (117). All in all, RA is a complicated autoimmune disease that is partly T cell-mediated, and selectively tolerizing these cells may reduce inflammation and joint damage.

1.5 Adeno-Associated Viruses

The use of adeno-associated viruses (AAVs) as a gene therapy vehicle for tackling genetic and autoimmune diseases in clinical medicine has gained extensive support. AAVs are small, non-enveloped *Dependoviruses* incapable of replicating in the absence of a helper virus (e.g., adenovirus) (120-122). These viruses contain a single strand of DNA, limited to approximately 4.7 kilobases, and are not known to cause human disease (121,122). To date, there are 13 AAV serotypes, AAV 1-13, each characterized by tissue tropism (123). When engineering the AAV, the desired transgene replaces the viral genome, developing recombinant AAV (rAAV) (120,121). As a result, these viruses have low immunogenicity and are non-pathogenic, serving as an ideal candidate for delivering therapeutic genes (120-122). In several *in vivo/ex vivo* examinations, it was evident that the virus successfully transduced liver (hepatocytes), kidney (renal), and muscle (myocytes) tissue (120-124). Many therapeutic modalities, such as injection-based treatments, are administered intramuscularly or intravenously, and the liver was frequently reported as the ‘default destination’ for most AAV serotypes (120-122,125-128). Previous investigations have also demonstrated stable and long-term expression of the transgene in muscle and liver cells (121,122,125-129). Manno and colleagues

reported little to no toxicity upon infusion of an rAAV in hemophilic patients when transducing the liver (130). Besides the ongoing clinical trials, a few AAV-based therapies have received approval from the Food and Drug Administration (FDA) for managing neuromuscular and genetic disorders. These included ZOLGENSMA® (Novartis Gene Therapies, Inc.) which used an AAV9-based delivery system for treating spinal muscular atrophy, approved in 2019; and more recently, Roctavian™ (BioMarin Pharmaceutical, Inc.), approved in 2023, an AAV5 vector with the genetic instructions to make Factor VIII, a clotting protein deficient in severe hemophilia A patients (131,132). Furthermore, the AAV vector can persist as an episome and does not integrate into the host genome (122). Thus, the transgene will eventually be released from cells as they replicate multiple times or undergo cell death, thereby having a clearance mechanism (122).

1.6 Thesis Rationale

Existing therapies for managing RA are focused on resolving symptoms but are unable to cure the disease. With the potential for serious adverse events and low clinical remission rates, research should aim to develop a newer disease-specific and life-improving immunotherapy for this autoimmune disease. Previously in the Larché lab, the group identified several potential T cell epitopes *in silico* using prediction software tools (i.e., TEPITOPE and Net-MHC) from a list of the most implicated autoantigens in RA (e.g., fibrinogen, vimentin, etc.) (Personal Communication, Adiga Life Sciences, Inc.). The binding capability to SE+ HLA-DR and solubility (e.g., water-soluble, dimethylsulfoxide (DMSO)-soluble) were assessed for a selection of candidate peptides (Personal Communication, Adiga Life Sciences, Inc.). The challenge with the epitope prediction software tool was the absence of the citrulline residue from the system database, as it is

a non-coded AA formed post-translationally from arginine. To circumvent this issue, citrulline was substituted with glutamine ('Q') for all epitope predictions as it shares a similar amide terminal group and neutral net charge (**Figure 3**). In subsequent investigations (*in vivo*), candidate peptides with binding capabilities to the SE+ HLA-DR (specifically those belonging to DR4 or DR1) alleles were injected into HLA-DR4 transgenic mice for 'induction of $CD4^+$ T cell responses' (133). An IFN-γ ELISPOT (Enzyme-linked Immunospot) was used to detect positive T cell responses by comparing citrullinated with native peptides with harvested mouse splenocytes. Citrullinated antigens capable of inducing T and B cell responses were later used in developing an inflammatory-arthritis mouse model (133).

The T cell response assays performed compared citrullinated and native peptides, which demonstrated that citrulline-containing peptides elicited a positive signal that was absent from their native variants. The group conducted these investigations with the goal of developing a physical peptide vaccine, which would deliver citrullinated peptides to tolerize T cells under the appropriate conditions (e.g., systemically delivered, soluble, low dose, adjuvant-free, etc.). However, the challenge with the physical peptide approach was being unable to get enough peptides into the vaccine. With the advent of nucleotide-based (e.g., RNA) vaccines, it is now possible to encode many peptides at once, circumventing the initial concerns. However, finding an alternative to citrulline was crucial, as this AA cannot be encoded nor directly incorporated during peptide synthesis. Thus, the purpose of the first project (Project 1) was to conduct preliminary feasibility work to assess if glutamine is an appropriate substitute for citrulline by comparing T cell responses (*ex vivo*) from RA patients and healthy controls against native, citrullinated, or

glutamine-substituted variants of the same peptide. If citrulline-specific T cells recognize glutamine, this would have important implications for designing a potentially therapeutic, disease-specific, genetic vaccine.

Protein hypercitrullination is a highly upregulated mechanism in RA pathophysiology and can serve as an important translational element in designing innovative solutions to treat the autoimmune disease. Some groups have tried to force the overexpression of the PAD enzyme but with variable success (134,135). Further, there is currently no direct evidence to suggest that hypercitrullination results in disease. Thus, the second project (Project 2) assessed the role of protein hypercitrullination in RA pathogenesis using an engineered adeno-associated virus serotype 6 (AAV6). The viral construct encodes a PAD4 enzyme and three native/un-citrullinated versions of RA peptides reported in the literature. Two different constructs were designed and tested, with the primary difference being the fusion of a green fluorescent protein (GFP) to the PAD4 in the first construct (AAV6-V1) and a Woodchuck Hepatitis Virus posttranscriptional regulatory element (WPRE) replacing GFP in the second construct (AAV6-V2) in order to amplify transcription of the PAD4 gene. The AAV6 construct was evaluated in cells of human and mouse origin (*in vitro*), including hepatocytes [HEPG2 (human) and HEPA1-6 (mouse)] and human embryonic kidney cells (HEK293 cell line), selected based on the known tissue tropism of AAV6 (described further in *section 2.3.2*).

1.6.1 Research Questions

Project 1:

(1) Can citrulline-specific T cells derived from RA patient blood recognize glutamine-substituted peptides?

Project 2:

(1) Can ‘forced’ PAD4 overexpression, using an AAV6 delivery system, lead to the generation of citrullinated proteins/peptides?

1.6.2 Hypotheses

Project 1:

(1) Citrulline and glutamine variants will elicit equivalent frequencies of T cell responses (*in vitro*).

Project 2:

(1) The delivery of an engineered AAV6 encoding PAD4 and T cell epitopes of disease-associated target proteins will result in the expression and secretion of citrullinated immunogenic peptides (*in vitro*).

1.6.3 Specific Aims

Project 1:

(1) To compare and demonstrate T cell reactivity with native, citrulline, and glutamine substituted RA peptides using an ELISPOT Immunoassay.

Project 2:

(1) To confirm transduction of human and mouse cells by detecting the expression of AAV6-encoded T cell epitopes, PAD4 (and GFP with AAV6-V1), and the cellular location of the PAD4 enzyme, using EVOS and confocal microscopy, flow cytometry, and western blotting.

(2) To validate protein hypercitrullination through the overexpression of the PAD4 enzyme (*in vitro*), by comparing the amount of citrullinated protein between untransduced and virally infected cells (either supplemented with or without ionomycin/calcium).

2.0 Methods

2.1 Study Characteristics

2.1.1 Study Design and Recruitment

To examine the frequency of cytokine-producing epitope-specific T cells against native, citrullinated, and glutamine-substituted peptides, in this cross-sectional clinical investigation, peripheral blood mononuclear cells (PBMCs) were extracted from whole blood and used to assess immunologic responses. At the first clinic visit, participants were assigned an ID (e.g., RA10), provided informed consent, and 80-120 ml of whole blood was collected by a certified phlebotomist. Participants were only requested for an unscheduled visit if a repeat sample was required owing to technical issues with the assay or an insufficient blood draw. Information regarding demographics, medical and smoking history, height and weight, and vital signs were also assessed during the initial visit. The blood draw consisted of a sample for PBMC isolation, tissue typing, serum, complete blood count, inflammatory markers (i.e., c-reactive protein), and autoantibody levels (e.g., ACPA, RF).

Treatment-naïve and RA-diagnosed patients on treatments (n=13), as per the 2010 ACR/EULAR criteria, were recruited from a rheumatology clinic at the St. Joseph's Healthcare Hamilton, Charlton Campus. Age-matched healthy controls (n=4) were recruited from the rheumatology clinic and the McMaster Immunology Research Centre (MIRC). These included family members of RA patients who did not have the disease but may have possessed the genetic susceptibility factors. This thesis only reports data from participants recruited from March 2022 to August 2023. This study was approved by the Hamilton Integrated Research Ethics Board (Project #1031).

2.1.2 Inclusion and Exclusion Criteria

Inclusion Criteria: All aspects of the study were met by enrolled participants. Participants, regardless of biological sex or gender, were between 18 and 65 years of age at the time of inclusion. Participants were capable of providing both verbal and written informed consent, and patients had an active diagnosis of RA according to the 2010 ACR classification system.

Exclusion Criteria: If participants met the following criteria, they were ineligible to partake in the study. A history of drug or alcohol abuse, patients actively using corticosteroids (within the past three months) regardless of the mode of delivery (oral, intravenous, intramuscular), or women of childbearing potential were excluded from the study. In addition, if controls had any history of inflammatory arthritis, they were excluded.

2.2 ELISPOT Immunoassay – Co-Culturing Target Peptides with PBMCs

2.2.1 PBMC Isolation from Whole Blood

This protocol was adopted from the Larché Lab, Human IFN-γ ELISPOT Using Fresh Blood, version 1.0. The whole blood was separated to isolate PBMCs in a sterile environment, a biological safety cabinet (BSC), by way of Ficoll-paque density gradient centrifugation. In sterile 50 ml centrifuge tubes, 15 mL of Ficoll-paque (GE Healthcare, USA) was transferred, with 20-25 mL of whole blood layered gently on top. The 50 mL tubes were placed in an Allegra Centrifuge at 400 RCF (relative centrifugal force) for 30 minutes at 25°C (SLOW acceleration, SLOW deceleration). Using a transfer pipet, the plasma layer at the top was carefully removed and stored at -80°C in sterile 10 mL tubes. The next layer, the buffy coat or PBMC layer, was isolated and transferred into a clean, sterile 50 mL tube, immediately followed by the addition of serum-free wash medium

RPMI 1640 (Life Technologies) to the cells to bring the total solution volume to approximately 40 mL. The 50 mL tubes were spun at 250 RCF for 10 minutes at 25°C (MAX acceleration, MAX deceleration). The supernatant was immediately discarded, and the remining cell pellet was resuspended with 2 mL of serum-free wash media and pipetted up and down gently to obtain a homogenous, single-cell solution (if there were multiple 50 mL tubes of cell pellets, all were combined into one tube). In a clean microcentrifuge tube, cells were diluted 1:10 with serum-free wash media before acquiring the cell count using the Countess Cell Counter. The average live cell concentration was multiplied by 10 to account for dilution and then by the total volume of solution of resuspended cells to get the total number of PBMCs. Next, the volume of serum-free culture medium (Cellular Technology Limited (CTL)-Test Medium, Immunospot) required for a final concentration of $5x10^6$ mL^{-1} was calculated. The 50 mL tube containing the resuspended cells were spun at 220 RCF for 10 minutes at 25°C (MAX acceleration, MAX deceleration), then the supernatant was discarded, and the cell pellet was resuspended in the appropriate volume of serum-free culture media as calculated.

2.2.2 Human IFN-γ T Cell Plate (ELISPOT) Preparation, Development and Reading

Preparing the ELISPOT Plate:

This protocol was adopted from the Larché Lab, Human IFN-γ ELISpot Using Fresh Blood, version 1.0. The Human IFN-γ ELISPOT Pro (Horseradish Peroxidase; HRP) Kit was purchased from Mabtech AB, Inc. The plate was removed from the sealed package and washed 4 times with sterile (0.2-micron (µm) filtered) Phosphate Buffered Saline (PBS), 200 µL/well. The plate was conditioned with serum-free culture medium by adding 200 µL/well and incubating for at least 30 minutes at room temperature. Following

the isolation of PBMCs, as described in *section 2.2.1*, medium was removed from the ELISPOT plate and 100 µL/well of medium (negative control) or peptides (60 nmol/mL) were added. For the positive control wells, anti-CD3 (included in the kit) was diluted 1:1000 with culture medium, and then 100 µL/well was added. Next,100 µL cell suspension was added to each well, i.e. 5 x 10^5 PBMCs per well. The remaining cells were diluted 1:10 in culture medium before adding 100 µL, i.e. 5 x 10^4 PBMC, to each CD3 positive control well. The plate was wrapped in aluminum foil and placed in a 37°C humidified incubator with 5% CO_2 and incubated for 24$\pm$2 hours.

Developing and Reading the ELISPOT Plate:

First, 0.2 µm filtered PBS containing 0.5% FBS was prepared. To make HRP-conjugated detection antibody, 7-B6-HRP (included in the kit) was diluted 1:200 in PBS-0.5% FBS and filtered using a 0.2 µm syringe filter. After 24$\pm$2 hours of incubation the plate was removed from the incubator. The plates contents were removed and then washed 5 times with filtered PBS, 200 µL/well, before 100 µL/well HRP-conjugated detection antibody was added, and the plate was incubated for 2 hours at room temperature. Prior to the completion of the incubation period, TMB (tetramethylbenzidine) substrate was filtered using a 0.45 µm syringe filter. The plates were emptied again and rinsed 5 times with filtered PBS, 200 µL/well, before adding 100 µL/well TMB. The plate was developed for 15 minutes and washed thoroughly with Milli-Q water to stop colour development. The underdrain was carefully removed from the plate to rinse the underside of the membrane. The plate was left to dry in the dark for 2-4 days before reading. The plates were read to detect the number of IFN-γ producing cells using the BioReader 6000-Fβ.

2.2.3 ELISPOT Assay Assessment

To determine the suitability of glutamine as a potential surrogate for citrulline in the design of a vaccine, the following outcomes of the assay needed to be met:

1. An equivalent (or approximately equivalent) immune response between a citrulline peptide and its glutamine-substituted variant. This translates to an equivalent frequency of IFN-γ secreting cells across both peptide conditions.
2. A higher magnitude of antigen-specific T cells for the peptides containing citrulline and glutamine, compared to the same peptide in its native/unmodified conformation.
3. A positive response, as defined by the distribution-free resampling with equivalence [DFR(eq)] statistical tool (explained in *section 2.4*), for the citrulline and glutamine peptides in the pair. The directionality of the relationship is determined by comparing the mean number of spot counts in the stimulation condition to the negative control (cells and media alone).

If analyzed patient samples successfully match the criteria above, these findings would support that glutamine-substituted peptides elicit a similar T cell response to citrulline containing peptides *in vitro*, warranting further examination.

2.2.4 ELISPOT Assay Troubleshooting

Over the course of assessing donor samples and after adding the TMB substrate, the wells immediately changed to a dark blue colour, as opposed to a gradual change observed with the usual development time (15 minutes). This warranted further investigation, as upon reading the plate, there were no detectable spots. In systematically addressing the posed challenge, the following questions needed exploration: (1) Were

too many cells plated? (2) Was the TMB substrate left in for too long? (3) Were there atmospheric issues responsible for the observed phenomenon? (4) What is the pH of the buffers? (5) Are there specific components of the wash or culture media causing the problem?

First, all calculations were reviewed, and it was evident that an appropriate number of cells were plated. In subsequent iterations of the experiment, the development time was decreased from 15 to 10 minutes. However, the TMB reactions continued to occur quickly. To circumvent potential atmospheric issues, post-incubation, the ELISPOT plate was developed in a BSC as opposed to the bench. Lastly, using a pH meter, the pH of the PBS buffer was determined to be within the range of physiological pH near 7.4, aligned with the recommended value. Furthermore, serum-free media was used, and FBS was excluded. With this change to the wash and culture media, the TMB reactions occurred as expected and previously seen. It was concluded that a particular batch of FBS was interfering with assay activity, and its prompt removal from the media and a shift to CTL-Test media permitted continuation and completion of the clinical portion of this thesis.

2.3 Adeno-Associated Virus (AAV) Cell Transduction and Analysis Techniques

2.3.1 AAV Vector Designs

An adeno-associated virus serotype 6 (AAV6) based delivery system was used for transduction experiments. Two separate AAV6 vector constructs were designed in collaboration with Dr. Sarah Wootton's lab at Guelph University and tested *in vitro*. The major differentiating factors between the two constructs was: (a) the presence of a (enhanced) green fluorescent protein (eGFP or GFP) fused to the mouse PAD4 enzyme

with a GGSG linker in the first vector genome (referred to as AAV6-V1) (**Figure 4A**); and (b) a Woodchuck Hepatitis Virus Posttranscriptional Regulatory Element (WPRE) replacing the GFP in the second vector (referred to as AAV6-V2) (**Figure 4B**). The overlapping elements, in sequential order, between the two vectors consisted of: (a) a CASI promoter which allows for ubiquitous transgene expression not limited to select tissues (136,137), a Kozak sequence important for translation initiation (138,139), and a signal peptide, (b) a PAD4 sequence (NM_011061.2) of mouse origin, (c) a KDEL (Lys-Asp-Glu-Leu) sequence at the PAD4 C-terminal, to retain the synthesized product within the endoplasmic reticulum (ER) lumen; (d) a series of 2A peptides beginning with F2A, that originate from different viruses (e.g., F2A: foot-and-mouth disease virus polyprotein; E2A: Equine Rhinitis A virus polyprotein; P2A: Porcine teschovirus-1 polyprotein), used to separate encoded peptides as the eukaryotic ribosome 'skips' forming the peptide bond connecting the glycine and proline residues at the C-terminus, thereby serving as peptide separation elements (140); (e) after F2A was the first of three peptides commonly implicated in RA known as Vimentin (RAVR-42; amino acid (AA) sequence: SSAVRLRSSVPGVRL); (f) Vimentin was separated from the next peptide Aggrecan core (RAAR-54; AA sequence: GVVFHYRPGPTRYSL) by E2A; (g) lastly, Alpha-enolase (RAAER-93; AA sequence: AREIFDSRGNPTVEV) was the final peptide separated from the previous one by P2A and was followed by a stop codon (ATT). All three peptide names end with the letter 'R', which is the native configuration of peptide containing an arginine residue (a detailed description of peptide nomenclature was provided in **Table 2**), and it was hypothesized that all three peptides would be modified (conversion of arginine residue to citrulline) by the encoded PAD4 enzyme.

2.3.2 Tissue Tropism of Virus – Hepatic and Renal Cells

Human embryonic kidney cells (HEK-293 cell line), and hepatoma cell lines, HEPG2 (human) and HEPA1-6 (mouse; provided by Dr. Gregory Steinberg's Lab, McMaster University), were selected based on the tissue tropism documented for the AAV6 serotype (124,141-143), along with their ease of accessibility. In particular, the HEK-293 cell line was crucial for validating the work of the Wootton collaborator lab to ensure the virus performed similarly here. Moreover, HEPG2 and HEPA1-6 are highly secretory liver cells that model their physiologic counterpart (i.e., primary hepatocytes) fittingly (143,144). It was hypothesized that following citrullination with the encoded PAD4 enzyme, modified peptides would readily be released by these cells, serving as the rationale for collecting and analyzing the supernatant alongside lysate. In summary, these cell lines continue to be commonly used for AAV investigations both *in vitro* and in animal models (141,145,146), serving as ideal targets to assess the virus' transduction capabilities and transgene expression.

2.3.3 Culturing Cells

The complete protocols for culturing, thawing, and subculturing the cells were developed in the Larché lab in accordance with the published ATCC (American Type Culture Collection) guidelines and executed in a BSC under aseptic conditions. First, a stock of complete culture media was prepared that contained 500 mL of MEM (Minimum Essential Media) for HEPG2 or DMEM (Dulbecco's Modified Eagle Medium) for HEK-293/HEPA1-6, 10% fetal bovine serum (FBS), 5 mL of 2 mM glutamine and 5 mL of penicillin (100 units/mL)/streptomycin (100 µg/mL) (P/S). After all the reagents were added, the media was considered complete and abbreviated as cMEM or cDMEM. Next,

a vial containing 1 mL of cells, thawed by gentle agitation in a 37°C water bath for 1-2 minutes, was transferred to a 15 mL falcon tube holding 9 mL of complete culture media (cMEM or cDMEM for the respective cell lines), and spun in an ultracentrifuge for 5 minutes at 120 RCF. While the cells were being spun, a T-75 flask with 12-14 mL of complete culture media was placed in a humidified 37°C incubator to allow the media to reach a normal pH range before the vial contents were added. Then, the supernatant was discarded, and the cell pellet was resuspended in 2 mL of complete culture media before using the Countess® II FL Automated Cell Counter (Invitrogen, Thermo Fisher Scientific, USA) to assess viability and concentration. Lastly, the cells were seeded in multi-well plates (and the flask to continually passage cells) at the selected density and placed in an incubator at 37°C with 5% CO_2 conditions. The media in the flask was replaced every 2-3 times per week and subcultured when cells attained 70-80% confluency.

2.3.4 Transduction of Cells using AAV (*in vitro*)

In advance of transducing the above-mentioned cell lines, three solutions were prepared: 1. Complete culture media (as described in *section 2.3.3*); 2. AAV inoculum and 3. AAV top-up media, as described here. The AAV inoculum media consisted of basal MEM or DMEM with 2 mM glutamine. While the AAV top-up media was comprised of cMEM or cDMEM containing 20% FBS (double the amount). The following transduction protocol was provided by the Wootton Lab. The cells, suspended in complete culture media, were first seeded at high densities (e.g., $1.1x10^5$ cells/well for a 24-well plate) in a multi-well plate approximately 16 to 20 hours prior to transduction and kept in an incubator at 37°C with 5% CO_2. Following the overnight incubation, the culture media was aspirated, and the cells were rinsed one time with sterile PBS without calcium (Ca^{2+}) and magnesium

(Mg^{2+}). Next, the AAV inoculum solution was prepared at varying multiplicities of infection (MOI) from 0 to 160,000 vector genomes per cell (e.g., 250 µL of AAV inoculum per well for a 24-well plate) and the transduced cells were placed back into the incubator (37°C and 5% CO_2) for 2 to 4 hours. Finally, the wells received AAV top up media with double the amount of FBS (20%) in an equivalent volume to as the AAV inoculum (e.g., 250 µL of AAV top up media per well for a 24-well plate). The cells were observed under microscopy to confirm transduction prior to lysate collection and incubated for multiple days to provide sufficient time for the virus to uncoat and the transgene to be expressed.

2.3.5 Harvesting Cell Supernatant and Lysate (*in vitro*)

All three adherent cell lines were cultured up to 144-hours. In the preliminary experiments, serial MOIs were tested before one was selected for all future trials, as described further in the Results (*section 3.2*). Moreover, post-transduction, ionomycin (1 µM), and Ca^{2+} (2 to 10 mM) at variable concentrations, were added directly to the virally infected and control cells (*activation phase* – to ensure sufficient calcium concentrations for PAD4 activation and protein citrullination) for 2-4 hours at 37°C. Following the activation phase, the supernatant was collected in microcentrifuge tubes and either immediately plated for the ELISA (enzyme-linked immunosorbent assay) or stored at -80°C until use. Next, the adherent cells were washed once with cold sterile PBS (without Ca^{2+}/Mg^{2+}) and received 0.05% trypsin-EDTA (ethylenediaminetetraacetic acid; 0.5% stock) for 4-5 minutes to detach the cells from the plate's surface before complete culture media was added. The wells belonging to the same condition were appropriately combined into 1.5 mL Eppendorf tubes and spun down at 1200 RPM (revolutions per minute) for 5 minutes. The supernatant was discarded, and the cell pellet was

resuspended in either ELISA coating buffer (in-house) or PAD buffer for the commercial kit. The lysis procedure consisted of freeze-thaw cycles, shifting the tubes between the -80°C freezer for 30 minutes followed by 30 minutes in a 37°C water bath, and repeated three times. The cells were then spun down at 14,000 RCF for 5 minutes in a microcentrifuge and the lysate was collected.

2.3.6 In-house ELISA (*in vitro*)

The ELISA protocol was adapted from the Schellekens and colleagues research paper (147). Through an indirect ELISA system, a high-binding 96-well Costar polystyrene flat bottom assay plate (Corning Incorporated, Durham, NC, USA) was coated overnight for 16-20 hours at 4°C with cell supernatant and lysate (100 µL/well) at variable dilutions using the coating buffer (50 mM carbonate buffer pH9.6). Positive control wells received 15 µg/well of cyclic citrullinated peptide (CCP), as preliminary experiments demonstrated that the CCP could serve as a positive control to confirm that the assay was functional. After the overnight incubation, the coated substances were removed, and the plate was blotted against paper towel. The wells were rinsed once with 250 µL of wash buffer (PBS (without Ca^{2+}/Mg^{2+}) and 0.05% v/v (volume/volume) Tween-20), and then 200 µL per well of 2% bovine serum albumin (BSA; blocking buffer consisted of BSA dissolved in wash buffer) was added for 1 hour at room temperature. Post-incubation with BSA, the wells were washed 6 times with 250 µL of wash buffer, before 100 µL of the primary antibody layer was added for 2 hours at room temperature. The primary antibody layer consisted of either high ACPA patient (HPS) or control (CPS) sera. The HPS was pooled from six patients with a clinical ACPA score >124 units; while the CPS was a composite from three healthy individuals with a clinical ACPA score <18

units or in other words were ACPA negative). The HPS and CPS were diluted 200-fold with RIA buffer (10 mM Tris-HCl buffer pH7.6, 350 mM NaCl, 1% BSA, 1% v/v Triton X-100, 0.5% w/v (weight/volume) sodium deoxycholate, 0.1% sodium dodecyl sulfate) containing 10% normal rabbit serum (RS; Gibco, Grand Island, New York, USA). The primary antibody layer was removed, and the wells were washed another 6 times with 250 µL of wash buffer, before 100 µL of anti-human IgG HRP secondary antibody, diluted 1:2000 in RIA buffer, was added to the appropriate wells and the plate was incubated for 2 hours at room temperature. After removing the secondary antibody and repeating the washing step, 100 µL of TMB substrate was added and left for 15 minutes to allow the plate to develop. Wells used for background reading received 200 µL of PBS (without Ca^{2+}/Mg^{2+}). The reaction was stopped by adding 100 µL of 2 M sulfuric acid to each well, and the plate was immediately read using plate reader at 450 nm.

2.3.7 PAD Activity Detection Kit (*in vitro*)

A commercial PAD enzyme activity detection kit (SignalChem, Richmond, BC, Canada) was used to assess the total activity of the construct-encoded PAD4, and the following procedure was provided by the manufacturer. After transducing cells and collecting the lysate, as outlined in *sections 2.3.4 and 2.3.5,* all assay reagents were prepared. First, a NeutrAvidin-coated 96-well plate was washed 3 times with wash buffer. After each wash, the plate was blotted against paper towel. Next, 100 µL per well of substrate coating solution (a universal PAD substrate (identity undisclosed) dissolved in Milli-Q water and further diluted 1:1000 with wash buffer) was added and incubated for 1 hour at room temperature. Next, the PAD substrate solution was decanted, and the plate was washed 4 times with wash buffer and blotted against paper towel each time. Then,

the wells aptly received one of the following: (a) 50 µL of sample (cell lysate); (b) 50 µL of PAD cocktail (positive control; a mixture of 5 PAD isoforms) diluted in PAD buffer (0.1 M Tris-HCl pH7.4, 10 mM $CaCl_2$, 0.5 mM DTT) to a final concentration of 100 ng/50 µL; or (c) PAD buffer only (negative control). The plate was covered with a plate sealer and placed in a 37°C incubator for 1 hour. Post-incubation, the samples and controls were removed, and the wells were rinsed 4 times with wash buffer. Next, 100 µL of trypsin buffer (50 mM Tris-HCl pH8.0, 2.5 mM EDTA) was briefly added to all the wells and aspirated. Then, 100 µL of trypsin digestion reagent, diluted 1000-fold in trypsin buffer, was loaded into to all the wells, and the covered plate was situated in a 37^{o}C incubator for 1 hour. The trypsin digestion reagent was discarded, and the plate was washed again for 4 times with wash buffer. Next, the detection antibody was diluted 1:500 in wash buffer with 100 µL added to all wells, and the plate was developed for 1 hour at room temperature. After, the detection antibody was decanted, and the wash step was repeated (4 washes with wash buffer). Then 50 µL of TMB substrate was added to all wells and the plate was kept in the dark for 20 minutes before 25 µL of stop solution was added. The plate was then immediately read with the iMark™ Microplate Absorbance Reader (Bio-Rad Laboratories, Inc.) at 450 nm and 595 nm. To account for background noise and optical imperfections all readings taken at 595 nm were subtracted from 450 nm.

2.3.8 EVOS Microscopy

Cells transduced with the AAV6-V1 encoding GFP, were imaged using the Invitrogen EVOS Digital Inverted Fluorescence Microscope. During incubation or before harvesting the cells for further experimentation, images were collected for all cell lines, regardless of infection status, across the different MOIs tested. First, the cells were placed

under transmitted light and the image was captured. Next, the channel was changed to green fluorescence to detect and visualize GFP-positive cells. Across the images captured, the settings for contrast and brightness were maintained.

2.3.9 Immunocytochemistry and Confocal Microscopy

The following immunocytochemistry and immunofluorescence (ICC/IF) steps, to prepare the cells seeded atop of sterile glass cover slips (22 mm x 22 mm; Fisher Scientific, Pittsburgh, PA, USA) in 6-well plates for visualization by confocal microscopy, were adapted from Abcam Limited. To begin, the culture media was first aspirated from the wells, and the cells were rinsed 2 times with PBS (without Ca^{2+}/Mg^{2+}). Next, a freshly prepared 4% paraformaldehyde-PBS pH7.4 solution was added for 15 minutes at room temperature before the cells were washed 3 times with cold PBS (without Ca^{2+}/Mg^{2+}) to remove any leftover fixative. Then each well received 0.1% Triton-X-100 in PBS (without Ca^{2+}/Mg^{2+}) for 20 minutes at room temperature. The cells were washed 3 times with PBS (without Ca^{2+}/Mg^{2+}) for 5 minutes each. Next, the cells were incubated for 60 minutes in 1% BSA with 0.3 M glycine (Bioshop, Canada) in PBST (PBS (without Ca^{2+}/Mg^{2+}) + 0.1% Tween-20). After blocking the cells and decanting the solution, the primary rabbit anti-PAD4 antibody (Abcam, Canada), diluted 1:1000 in 1% BSA in PBST, was added to the plate and incubated overnight at 4°C. The next day, the primary antibody was removed, and the cells were washed 3 times with PBS (without Ca^{2+}/Mg^{2+}) for 5 minutes each time. Then the wells received the biotinylated goat anti-rabbit IgG (secondary; Abcam, Canada) diluted 1:500 in 1% BSA in PBST for 1.5 hours at room temperature. Post-incubation, the secondary antibody was aspirated, and the wash step was repeated (3 times with PBS (without Ca^{2+}/Mg^{2+}) for 5 minutes each). Next, the cells were blocked with 10% RS in

PBST for 60 minutes at room temperature. The blocking solution was decanted, and the AlexaFluor647/AF647 rabbit anti-calreticulin antibody (Abcam, Canada) diluted 1:500 in 1% BSA in PBST was incubated overnight at 4°C in the dark. Following the overnight incubation, the antibody solution was removed, and the cells were rinsed 3 times with PBS (without Ca^{2+}/Mg^{2+}) for 5 minutes each, protected from light. Lastly, streptavidin-phycoerythrin (PE) (Agilent Technologies, Santa Clara, CA, USA) diluted 1:250 in 1% BSA in PBST was added to the cells for 1 hour at room temperature, and the plate was kept in the dark. The cells were then washed 3 times with PBS (without Ca^{2+}/Mg^{2+}) in the dark for 5 minutes each to remove any unbound streptavidin-PE. The cells were kept in PBS (without Ca^{2+}/Mg^{2+}) until the glass cover slips were transferred, one-by-one using pointed forceps, onto glass microscope slides (SATI International Science, Inc., St. Laurent) using 10 µL of Fluoromount-G (SouthernBiotech, Birmingham, AL, USA) mounting media provided by Dr. Joshua Koenig's Lab, MIRC, McMaster University. The glass slides were left to dry, protected from light, prior to imaging.

2.3.10 Flow Cytometry

Sample Preparation and Running the Flow Cytometer:

This protocol was adapted from Ad5-GFP Infectious Units assay by flow cytometry protocol in the Larché Lab, version 5.0. Following cell culturing and AAV transduction, as outlined in *sections 2.3.3 and 2.3.4*, respectively, the cells were observed for 6-days prior to collection. First, the culture media was aspirated, and the cells were rinsed 1 time with PBS (without Ca^{2+}/Mg^{2+}). Next, an appropriate volume of 0.05% trypsin-EDTA was added for 5 minutes, and the plate was kept in an incubator at 37°C. Then, the wells received complete culture media (cMEM or cDMEM) and all cell suspensions of the same condition

were collected in a single 15 mL falcon tube. The cells were ultracentrifuged at 120 RCF for 5 minutes. The supernatant was discarded, and the cells were resuspended in fluorescence-activated cell sorting (FACS) buffer. Then, cells were fixed with BD cytofix fixation buffer (BD Biosciences, San Diego, USA) and kept on ice for 15 minutes. Next, FACS buffer was added to increase the volume of the solution, and the cells were spun at 400 RCF for 5 minutes and resuspended in new FACS buffer. Then the samples were filtered through FACS tubes before loading into the instrument to avoid clumping or aggregation of cells and prevent clogging in the BD LSRFortessa Flow Cytometer. Lastly, analyses were conducted using the Flowjo Software version 10.10.0. The gating strategy applied for cells transduced with AAV6-V1 was explained in detail in **Figure 5**.

2.3.11 Western Blot

Cell lysate Preparation:

Lysates from infected and uninfected cells were collected post-transduction in RIPA (Radioimmunoprecipitation assay) lysis buffer (Thermo Fisher Scientific Inc., Rockford IL, USA). First the media was decanted, and the cells were washed 2 times with ice cold PBS (without Ca^{2+}/Mg^{2+}) and kept on ice. After aspirating the PBS, each well received cold RIPA lysis buffer (25mM Tris-HCl pH7.6, 150 mM NaCl, 1% NP-40, 1% sodium deoxycholate, 0.1% sodium dodecyl sulfate) containing a halt protease phosphatase inhibitor cocktail (diluted 1:100) (Thermo Fisher Scientific Inc., Rockford IL, USA). The adherent cells were gently scraped using a cell scraper and solutions from the same condition were combined into pre-cooled Eppendorf tubes. The Eppendorf tubes containing single-cell suspensions in lysis buffer were kept on ice for 1 hour. After incubation on ice, the cells were spun in a microcentrifuge at 14,000 RCF for 5 minutes

and the supernatant was collected into new Eppendorf tubes and kept on ice until further experimentation.

Bradford Assay, Sample Preparation and Running the Gel:

This protocol was adopted from Dr. Carl Richard's Lab, MIRC, McMaster University. Following lysate collection, protein concentration was assessed using a Bradford Assay. By determining the concentration of protein present, an equal amount of sample was used for each condition measured. Next, a molecular weight ladder (Bio-Rad Laboratories, Inc., USA) and 20 µL of 20 µg of sample and controls, untransduced cell lysate (negative control) and commercial mouse PAD4 (positive control; Cayman Chemicals, Michigan, USA), were loaded into wells on a 15% SDS-PAGE (sodium dodecyl sulfate polyacrylamide gel electrophoresis) gel at a concentration of 20 µg of protein per well. The sample was separated by electrophoresis at 90 V for 90 minutes (Mini-PROTEAN Tetra System and PowerPac™ Basic Power Supply, Bio-Rad Laboratories, Inc., USA). After running the gel for 1.5 hours, the protein was transferred from the gel to nitrocellulose membranes at 400 mA for 1 hour (PowerPac™ Basic Power Supply, Bio-Rad Laboratories, Inc., USA). Following the transfer, the membranes were blocked for 1 hour at room temperature using the Odyssey Blocking Buffer (LI-COR Biosciences, Lincoln, NE, USA) and kept on a rocker. Next, using an appropriate dilution (1:1000) the membrane was probed with the rabbit anti-PAD4 monoclonal antibody (Abcam, Canada) and incubated overnight on a shaking rocker at 4°C. After the overnight incubation, the membranes were washed 3 times with TBS + 0.15% Tween-20 buffer for 7 minutes each. The membranes were then incubated with IRDye® donkey anti-rabbit secondary antibody diluted 1:5000 (LI-COR Biosciences, Lincoln, NE, USA) for 1 hour at

room temperature. The membranes were washed again in 3 washes of TBS + 0.15% Tween-20 buffer for 7 minutes each. Then using the Odyssey LI-COR Imaging System (Lincoln, NE, USA) the blots were imaged.

2.4 Statistical Analyses

All two-sided statistical analyses were conducted using the GraphPad Prism 9 (version 9.5.1) software and The RunDFR Web Tool (https://rundfr.fredhutch.org/). To select the appropriate method of analysis (parametric versus non-parametric), all variables were tested for normality (Shapiro-Wilk: $p>0.05$ is indicative of a normally distributed data set). For datasets that were normally distributed, and samples were in at least triplicates, the following tests were applied as appropriate: 1. a One-way Analysis of Variance (ANOVA) comparing the means of independent groups, and if significant was followed by Dunnett's post hoc test of multiple comparisons to determine which experimental groups were statistically different than the control; 2. an unpaired T-test that directly compared the mean of two independent groups; and 3. Pearson's correlation coefficient (r_p) for assessing the linear relation between two groups. For datasets that were not normally distributed, or normality could not be assessed as the raw data values were in duplicates and not triplicates (or higher), then non-parametric equivalents were used: 1. A Kruskal-Wallis H Test to compare three or more groups, which if significant was followed by Dunn's post hoc test of multiple comparisons; 2. Mann-Whitney U Test comparing only two independent groups directly; and, 3. Spearman's rank correlation coefficient (r_s). The level of significance selected a priori was 0.05, thus all reported adjusted p-values below this threshold were considered statistically significant. Moreover, all ELISPOT data were analyzed using the distribution-free resampling with equivalence

[DFR(eq)] technique. The tool, based on a non-parametric statistical test rather than an empirical rule, calculated the mean difference in spot counts between the experimental and negative control wells, and generated a test statistic for all permutations (148). The null hypothesis was that there was no difference in the means between the groups (in other words they were equal). The null hypothesis was rejected if the antigen condition was statistically different than the control and was reported as a positive response. The DFR(eq) output was binary, with 1 indicating a positive response and 0 being the absence of a positive immune response.

3.0 Results

Project 1 Aim: To compare and demonstrate T cell reactivity with citrulline and glutamine substituted RA peptides using an ELISPOT Immunoassay.

3.1 T Cell Responses (ELISPOT)

The study enrolled 17 participants, consisting of RA patients [n=13; mean (SD) age of 55.85 (14.87)] and healthy controls [n=4; 49.50 (21.83)], with approximately 71% of the sample comprised of females. A fraction of the patients were treatment-naïve (23%). However, the study sample also consisted of patients who previously received treatment for their RA before entering remission, followed by relapse. These patients started a new treatment cycle at the same clinic visit as their blood donation. Furthermore, more than 50% of patients were seropositive (ACPA and RF positive) with high mean autoantibody titres. **Table 1** summarizes the descriptive and serologic characteristics of the enrolled sample.

To assess T cell responses to specific autoantigen sequences, the number of peptide-specific IFN-γ secreting T cells were enumerated, in response to each of three

versions of the sequence: the unmodified native (Nat or R; arginine-containing), modified citrulline (Cit) and glutamine (Glut or Q). The selected RA candidate proteins, as established in the literature (93,149-152), for which the three 15mer variants were developed, included β-fibrinogen (peptides 23 and 28), aggrecan core (peptide 54), and anti-thrombin III (peptides 69 and 76) with their sequences highlighted in **Table 2**. To establish whether glutamine was an appropriate surrogate for citrulline in the design of a potential vaccine, criteria were developed, as outlined in *section 2.2.3*, that would need to be met. A possible outcome of the experiment that would have supported glutamine substitution, would be an equivalent mean spot count for the citrulline-glutamine peptide pair (e.g., 54 and 76), and that the peptide response was positive according to the statistical test [DFR(eq)] applied. These findings coupled with a lower average value of ag-specific T cells obtained with the native counterpart, would have satisfied all three criteria aspects. It therefore follows that the next step would have been to assess if the response was consistent across RA patients and absent from controls.

From the enrolled cohort, data from the following participants, such as RA1 and RA8, showed an equivalent immune response, albeit a low frequency of cytokine-secreting cells (**Figure 6**). For instance, the mean (standard deviation; SD) number of antigen(ag)-specific cells were 4.67 (1.53) for RA1 across the citrulline and glutamine versions of peptide 23 (Cit23 and Glut23), and 5.67 (2.89) for Nat23. The mean spot count for the negative control well was 3.67 (2.34). Here, it was evident that the modified peptides had a higher magnitude of response relative to the negative control wells but less than the original peptide. Similarly, Cit28 and Glut28 variants of peptide 28, for patient RA8, had an equivalent mean spot count at 0.33 (0.58). The magnitude of cytokine-

secreting cells to the antigen-stimulated Nat28 condition was the same as the citrulline and glutamine peptides, but all three had a lower frequency of T cell responses as compared to the unstimulated wells [0.67 (1.21)]. The average IFN-γ secreting cells across each peptide, analyzed in triplicates, for both patients and controls, were displayed in **Table 3**. While, all participant response graphs were provided in **Supplementary Figure 1**. The last parameter to be assessed was whether the immune response was 'positive', as measured using the web-based DFR(eq) tool (**Table 4)**. It was determined that neither peptide, 23 and 28, was statistically different than the background condition for patients RA1 and RA8, respectively (**Table 4**).

Only four (of 17) participants (i.e., patients – RA1, RA8, and RA13; and control RA15) demonstrated an equivalent T cell response between a citrulline-glutamine pair, as seen for peptides 23 and 28. Although three participants had an equivalent response for peptide 28, neither was significant relative to the unstimulated condition (**Table 5**). Upon assessing participants independently, data from some fulfilled a few but not all the parameters established for interpreting the immunoassay. In the present study, no participant's ELISPOT assay data completely satisfied all three criteria. Relative to the healthy controls, RA patients had a greater breadth of positive responses. Notably, there was a higher magnitude of significant responses against the epitopes substituted with Q54 and Q69, as seen in five out of 13 patients and two out of four controls. For RA patients, at least one positive response was found to peptides 23 and 54 containing citrulline (e.g., Cit23, Cit54) and all five glutamine forms. Contrastingly, in the control group, a positive response was only observed against peptides Cit54, Cit76, Q28, and Q69 conditions. Holistically, these findings suggested that not only were there more

positive T cell responses for patients, as expected, but these responses were also widespread over several antigens.

These results indicate that the frequency of ag-specific T cell responses, *ex vivo*, were not equivalent between glutamine and citrulline modified sequences. Furthermore, a peptide substituted with citrulline or glutamine may have demonstrated an equal immune response (e.g., Cit23 and Glut23), but this did not translate to a significant immune response. Thus, there were detectable T cell responses across an array of peptides tested and it was apparent that the cells from RA patients recognized both the unmodified and modified epitopes. However, these findings were inconsistent and did not support the rationale of glutamine serving as a reliable substitute for citrulline in the design of an RNA immunotherapy.

Project 2 Aim 1: To confirm transduction of human and mouse cells by detecting the expression of AAV-encoded T cell epitopes, PAD4 and GFP, and the cellular location of the PAD4 enzyme, using microscopy, flow cytometry, and western blotting.

3.2 AAV MOI Selection and Confirmation of Transduction (*in vitro*)

To determine the optimal multiplicity of infection (MOI) for experiments, human hepatocytes (HEPG2) and human embryonic kidney cells (HEK-293) were transduced with AAV6-V1 at varying MOIs (e.g., starting at 1250 and doubling to 160,000) to generate a dose-dependent curve and monitored and imaged over the course of 144 hours using an EVOS microscope. Preliminary images of the infected and uninfected cells confirmed viral transduction by way of detecting the fluorescing GFP. In an early experiment, in which cells were infected at a single MOI of 5000, there detectable fluorescing cells both 4- and 5-days post-transduction (**Figure 7A**). Flow cytometry data confirmed the

presence of GFP in infected relative to non-infected cells (**Figure 7B-C**). When serial MOIs were tested across multiple time points, as early as 48 hours post-transduction, microscopy confirmed cellular GFP expression, with more detectable signals at 144 hours (**Figure 8A**). Visually, the number of fluorescing HEPG2 cells increased with higher MOI, as expected. Further, flow cytometry quantified the proportion of GFP-positive (GFP+) cells at varying MOIs (**Figure 8B**). It was evident that with an increasing MOI, more cells were expressing GFP and there was a statistically significant positive correlation between MOI and percentage of GFP+ cells, using Spearman's coefficient (r_s=0.996, $p<0.0001$), supporting the microscopy findings. As seen in the dose-dependent curve (**Figure 8C**), at an MOI of 160,000, there were greater than 50% of GFP+ cells and what also appears to be the beginning of the curve plateauing. A similar increasing trend was also observed with HEK-293 cells (*data not shown*, *experiment conducted by Jing Bo Amy Wang*). Thus, an MOI of 160,000 was selected as an appropriate experimental condition for all future assays and sufficient to address research aims with the resources available.

3.3 Subcellular location of the PAD4 enzyme

At 48 hours post-transduction, the cells were fixed for imaging at the Centre for Advanced Light Microscopy (CALM). Even at high magnifications (40x and 50x), with the EVOS microscope, the location of the fusion protein was inconclusive, as the entire cell fluoresced (**Figure 9**). In an attempt to better detect the subcellular location of the PAD4 enzyme, cells underwent multi-colour staining with a primary non-conjugated anti-PAD4 antibody, followed by a biotinylated secondary antibody, streptavidin-PE, and with a fluorophore (AlexaFluor647; AF647) conjugated anti-calreticulin antibody to outline the ER. Both HEPG2 and HEPA1-6 cells were infected (MOI=160,000) for 96 hours before

the samples were prepared for microscopy. Since the HEPA1-6 cells did not adhere well to the glass cover slips, only the findings for HEPG2 are presented, with the experimental condition consisting of infection with the AAV6-V1 construct (GFP-PAD4 fusion), and controls [non-infected cells (0 MOI) interrogated with all staining antibodies (**Figure 10A**) or only anti-calreticulin (**Figure 10B**)]. As seen in **Figure 10B**, the anti-calreticulin antibody, shown in cyan (AF647), outlined the ER of the cell. When each of the fluorophore channels were viewed independently, it was evident that the GFP (green), and streptavidin-PE (red) bound to the secondary detection antibody binding to the primary anti-PAD4, overlap as both recognized the same chimeric protein (**Figure 10C**). However, when all three channels were overlayed into a single image (**Figure 10C**), the GFP and PE regions did not overlap with the cyan ER section. Thus, it was concluded that the fusion protein did not localize to the ER, despite the presence of the KDEL sequence, but rather it was spread throughout the cell/cytoplasm. Interestingly, despite the presence of a naturally occurring nuclear localization sequence (NLS), the protein was not found in the nucleus.

3.4 Western Blot

HEPG2, HEK-293, and HEPA1-6 cells were infected with either AAV6-V1 (GFP-PAD4 fusion) or AAV6-V2 (PAD4 + WPRE) constructs for 96 hours before collecting lysate to detect the PAD4 protein levels. There were four wells for each cell type: with untransduced cell lysate in lanes 1/5/9, lysate from cells transduced with the older AAV6-V1 batch in lanes 2/6/10, lysate from cells transduced with the transduced with new AAV6-V1 batch in lanes 4/8/12, and lysate from cells transduced with the transduced with AAV6-V2 in lanes 3/7/11, with 20 μg of protein sample was loaded into each well and probed

with an anti-PAD4 antibody. The positive control consisted of 0.5 μg of a commercial recombinant mouse PAD4 protein with a band near 75 kDa, as expected. For **Figure 11**, the positive control of a separate blot was used, as supra-optimal concentrations of protein led to spill-over into adjacent wells and a smear that spanned the length of the well making the blot difficult to interpret (*not shown*). Western blot analysis demonstrated that even in the absence of viral infection (lanes 1, 5, and 9), there was a basal level of endogenous PAD4 expression near 75 kDa, as evident across all three cell types (**Figure 11A-C**). No clear increase in 75 kDa PAD4 protein expression was observed between the wells containing lysate from uninfected or infected cells. For HEPA1-6 cells, a second band was present at an approximate molecular weight of 100 kDa. This species was more prominent for HEPA1-6 cells than for HEPG2 or HEK-293 (**Figure 11A-B**). The 100 kDa band was consistent with a GFP-PAD4 fusion protein (PAD4 ~76 kDa + GFP ~27 kDa), as encoded by AAV6-V1. As shown in **Figure 11**, only wells containing lysates from AAV6-V1 infected cells (lanes 2/4/6/8/10/12) demonstrated the 100 kDa species.

In contrast to production of the 100 kDa fusion protein following transduction with the AAV6-V1 construct, western blotting failed to demonstrate increased expression of the 75 kDa PAD4 species following infection of cells with the AAV6-V2 construct, suggesting that the WPRE enhancer was non-functional. Three independent blotting experiments produced consistent results. In all experiments, no increase was observed in the intensity of the 75 kDa species following infection with either AAV6-V1 or AAV6-V2 construct. Since AAV6-V1 encoded the larger fusion protein, this result is expected. In contrast, a functional AAV6-V2 construct would be expected to result in increased band density at 75 kDa, but this was not observed.

Project 2 Aim 2: To validate protein hypercitrullination through the overexpression of the PAD4 enzyme in vitro, by comparing the amount of citrullinated protein between untransduced and virally infected cells.

3.5 Optimizing the In-House ELISA

To validate the in-house ELISA based on the Schellekens and colleagues' paper (147), the detection of a commercial cyclic citrullinated peptide (CCP) (Genscript, New Jersey, USA), plated at different concentrations, by donor sera of varying ACPA titres was conducted. Initially, three peptide concentrations ranging from 2.5 μg/well doubling to 10 μg/well, demonstrated a linear increase in absorbance (A). Thus, as the amount of coated peptide increased, it correlated positively and significantly with absorbance levels (r_p= 0.999, p=0.014) (**Figure 12A**). This warranted further investigation with different ACPA titres and higher concentrations of peptide to determine an optimal CCP amount for experiments. Relative to ACPA negative (<18 units; pooled healthy control sera) or low (weak positive) ACPA (20-39 units) sera, a dose-dependent relationship was observed between CCP concentration and absorbance (A) for high (strong positive) ACPA sera (>124 units) (**Figure 12B**). As evident in **Figure 12B**, at 15 μg/well (or 150 ng/μL) of CCP, the absorbance was A=2.015, which was only slightly less than that observed with double the amount of CCP present (A=2.168). Comparatively, the low ACPA (A=0.085) sera had absorbance levels below the high ACPA sera for 15 μg/well of CCP. These results provided additional support to the findings by the Schellekens' group and affirmed CCP (15 μg/well) as a suitable assay control. Additional CCP ELISA optimization and testing was pursued by another member of the Larché group (Jing Bo Amy Wang), and their dissertation was consulted during the course of experimentation.

3.6 Peptidyl-Arginine Deiminase (PAD) Activity (*in vitro*)

3.6.1 Comparison of the Amount of Citrullinated Protein levels in Untransduced and Transduced Cells

To assess PAD4 enzyme functionality, HEPG2 and HEK-293 cells were transduced at an MOI of 160,000 and incubated for 96- to 144-hours. Following the incubation, supernatant and cell lysate were collected, and coated on 96-well ELISA plates at variable dilutions. An indirect ELISA system was performed. Pooled patient and control sera was added to the coated samples. In the initial iterations of this experiment, only high titre ACPA patient sera (HPS) was used.

As evident in **Figure 13A**, for HEPG2 cells harvested at the 96-hour mark, a higher absorbance signal [reported as mean (SD)] was observed with the supernatant collected from transduced cells across all four dilutions [e.g., *No dilution* (*100%*): A=0.387 (0.019)] compared to the untransduced (control) [A=0.157 (0.007)] condition (**Table 6**). Statistical analysis employing a one-way ANOVA (F-statistic (degrees of freedom), p-value), demonstrated a significant difference in the mean absorbance signals across the groups analyzed ($F(4)=84.18$, $p<0.0001$). To assess if the four experimental conditions were significantly different than the control group, Dunnett's multiple comparison test was conducted, and the test statistics results were provided in **Table 7**. It was found that the absorbance signal for all four experimental conditions of supernatant were significantly different ($p<0.0001$) than the negative control. For instance, when the *No dilution* (*100%*) condition was compared to the *Control*, the mean difference (MD) was MD=-0.229 [95% CI: -0.267, -0.192]. The negative mean difference indicated that the control group absorbance signal was less than each of the experimental conditions assessed (**Table**

7). Similarly for HEK-293 cells, also incubated for the 96-hour interval, had higher mean absorbance signals for the experimental conditions [e.g., *No dilution* (*100%*): A=0.382 (0.036)] than the control [A=0.171 (0.003)] (**Table 8**). This trend was present regardless of the length of incubation (96- or 144-hours) and across both cell types (**Figure 13A-B**). The results from a one-way ANOVA also indicated a significant difference among the means of the groups analyzed ($F(4)=20.81$, $p<0.0001$). While Dunnett's multiple comparison test supported that the control group mean absorbance signal was significantly lower than each of the experimental conditions [e.g., *No dilution* (*100%*) versus *Control*: MD=-0.211, 95% CI [-0.278, -0.144], $p<0.0001$] (**Table 9**).

After 144 hours of incubation (**Figure 13B**), the descriptive statistics of the absorbance signals for the supernatant of HEPG2 were described in **Table 10**. Statistical analysis employing the Kruskal-Wallis H test (since one of the groups was did not pass the test of normality), reported as the H-statistic (degrees of freedom) with the p-value, demonstrated that there was a significant difference in absorbance levels across all groups ($H(4)=11.65$, $p=0.001$). Further, Dunn's post hoc multiple comparisons test yielded a statistically significant difference in the mean ranks (mean rank difference=12.000, $p=0.004$) between the *No dilution* (*100%*) (mean rank=14.000) and *control* condition (mean rank=2.000), indicating that absorbance signals on average from the experimental condition tended to be higher than the control group for cell supernatant. All other pairwise analyses were non-significant ($p>0.05$) (**Table 11**). Moreover, for the supernatant of HEK-293 cells (normally distributed dataset), the mean (SD) signal values were reported in **Table 12**. Statistical analysis employing a one-way ANOVA indicated a statistically significant difference among the groups ($F(4)=54.87$, $p<0.0001$), with

Dunnett's multiple comparison test demonstrating that the mean absorbance of all four experimental conditions (supernatant) were significantly higher than the control group (supernatant) [e.g., *No dilution* (*100%*) versus *Control*: MD=-0.085, 95% CI [-0.101, -0.068], p<0.0001] (**Table 13**).

The absorbance signal also progressively declined at higher dilutions, as anticipated. However, there was no difference in signal when comparing cell lysate, except for HEPG2 at 96 hours using an unpaired (two-tailed) t test [t=4.226, p=0.013; MD (standard error of the mean; SEM)=0.016 (0.004)]. The Mann Whitney U test (two-tailed) comparing the medians of the transduced and untransduced lysate signals for HEK-293 cells was non-significant (U statistic=0, p=0.100). Interestingly, the trend observed across the varying dilutions of the supernatant when comparing transduced with untransduced cells, was reversed for the cell lysate of both cell types at lengthier incubations (144 hours), with a higher mean (SD) signal present for the uninfected condition [*HEPG2*: A=0.084 (0.003); *HEK-293*: A=0.106 (0.003)] over the infected [*HEPG2*: A=0.067 (0.000); *HEK-293*: A=0.097 (0.000)]. Notably, the overall absorbance levels also declined at the 144-hour mark compared to 96 hours, which could potentially indicate diminishing enzyme activity over time. Thus, these ELISA experiments at the two time points, using only the high ACPA titre, showed that transduced cell lysate did not contain a significantly different and biologically meaningful amount of citrullinated peptide over uninfected cell lysate, with the absorbance signals less than or nearly equal to that of the control (supernatant). Though the significant comparisons seen for the experimental supernatant relative to the control, warranted further investigation.

In a subsequent iteration of the experiment, at only one time-point (144 hours), pooled sera from ACPA-negative healthy controls (CPS) with no indications of inflammatory arthritis, along with the media used during the AAV infection process, were added to understand how much of the absorbance signal was attributable to substrates other than citrullinated peptides/proteins contained in the supernatant and cell lysates between transduced and untransduced cells and to assess any potential background effects. As a repeat ELISA, only the supernatant was tested given its statistically significant outcomes in the previous experiment (**Figure 13**). The descriptive statistics for the absorbance values of HEPG2 and HEK-293 supernatant with the high titre ACPA sera (HPS) and pooled control sera (CPS) were reported in **Tables 14 and 15**, respectively. Across both cell types, it was clear that the median [Mdn; Interquartile Range (IQR)] absorbance for all four experimental conditions interrogated with HPS were higher (1) than the control supernatant interrogated with HPS [e.g., HEPG2: *No dilution* (*100%*) (HPS): Mdn A=0.202 (0.016) versus *Control* (HPS): Mdn A=0.118 (0.020)] (**Table 14**) and (2) each of experimental conditions with CPS [e.g., HEK-293: *No dilution* (*100%*) (HPS): Mdn A=0.226 (0.009) versus *No dilution* (*100%*) (CPS): Mdn A=0.061 (0.001)] (**Table 15**).

Since each group was conducted in duplicates, normality could not be assessed (n was too small for the Shapiro-Wilk test), and non-parametric techniques were utilized. The Kruskal-Wallis H test (for HEPG2) demonstrated that the median absorbances of at least one of the different dilutions of supernatant was significantly different to the others ($H(4)=9.528$, $p=0.003$). While the post hoc multiple comparisons test highlighted that only the mean ranks difference between the *No dilution* (*100%*) (HPS) and *Control* (HPS) group was statistically significant (mean rank difference=9.000, $p=0.015$) (**Table 16**). To

directly compare if the signal attained by the HPS condition differed significantly from the CPS, independent Mann-Whitney U tests were applied. Across each of the dilutions, the absorbance signal under the HPS condition did not differ significantly from that with CPS (U statistic=0, p=0.333). For HEK-293 cells, the results of the Kruskal-Wallis H test (H(4)=9.958, p=0.001) followed by the post hoc analysis demonstrated that only the mean ranks of the *No dilution* (*100%*) (HPS) group differed significantly from the *Control* (HPS) (mean rank difference=9.000, p=0.015) (**Table 17**). In addition, the categories of supernatant from transduced cells interrogated with HPS were not statistically different from those interrogated with CPS (p=0.333). However, a large signal provided by the media alone condition (assay negative control) [HPS: Mdn A=0.098 (IQR=0.063); CPS: Mdn A=0.060 (IQR=0.097] demonstrated high background noise, questioning whether there was a 'true' statistically significant difference between the *No dilution* (*100%*) (HPS) and *Control* (HPS), as seen for both HEPG2 and HEK-293 (**Figure 14A-B**).

3.6.2 Citrullinated Protein levels in Untransduced and Transduced Cells – Examining Ionomycin and Calcium Supplementation on PAD Activity

As part of the troubleshooting process to understand the low absorbance signals from the in-house ELISA experiments, cells were supplemented with 1 μM of ionomycin and 2 mM of calcium (Ca^{2+}) for two hours prior to harvesting (following a 144-hour incubation) with the aim of assisting PAD4 activation and protein citrullination. Three separate conditions were investigated: 1. No ionomycin and no calcium; 2. Ionomycin without calcium; and 3. Both ionomycin and calcium present. Similar to previous experiments, supernatant at four dilutions (No dilution (100%), 50% dilution, 33% dilution, and 10% dilution) were plated, along with lysate from both transduced (MOI=160,000)

and untransduced (MOI=0) cells. However, the lysate only received high titre ACPA (HPS). In addition, a pooled peptide mixture consisted of the three RA-peptides encoded by the viral constructs (AAV6-V1 and AAV6-V2) were plated to assess the assay's ability, specifically the HPS, to recognize citrullinated proteins and not their native (unmodified) counterparts. While the signal provided by the CPS condition was expected to remain similar across both peptide mixtures.

The descriptive statistics for HEPG2 and HEK-293 cells across all three conditions, were reported in **Tables 18-23**. As evident in **Figure 15A**, the absorbance signals for all four dilutions of transduced cell supernatant interrogated with HPS, were higher than supernatant from untransduced cells [e.g., HEPG2: *No Dilution* (*100%*) Mdn A=0.197 (IQR=0.015) versus *Control* Mdn A=0.100 (IQR=0.013); HEK-293: *50% Dilution* Mdn A=0.139 (IQR=0.005) versus *Control* Mdn A=0.100 (IQR=0.014)]. This trend was present regardless of the presence or absence of ionomycin/calcium supplementation (**Figure 15A-C**). However, there was no significant difference in the absorbance levels when all four dilutions of supernatant of HEPG2 (no ionomycin and no calcium) were compared to the control supernatant ($H(4)=7.309$, $p=0.063$); and Dunn's post hoc multiple comparisons test was not conducted. The transduced cell lysate compared to untransduced lysate from the HEPG2, no ionomycin and no calcium condition, were also non-significant (U statistic=1, $p=0.667$).

In contrast to initial expectations, both HPS and CPS antibody sera detected the pooled peptide mixture (citrullinated and native), with a higher absorbance obtained with the native peptides than their citrullinated counterpart [e.g., pooled native (HPS) Mdn A=0.029 (0.002) versus pooled citrullinated (HPS) Mdn A=0.023 (0.002)]. Although there

was no significant difference (p=0.333) in their measures of central tendency, these findings highlighted the challenges posed by the ELISA assay to address the research questions of this project. Moreover, the results from the Kruskal-Wallis H test for HEK-293 (no ionomycin and no calcium) suggested that the absorbance levels of one or more groups differed significantly (H(4)=8.588, p=0.002), which upon further investigation demonstrated that only the supernatant with *No dilution* (*100%*) (HPS) was statistically different from the *Control* (HPS) group (mean rank difference=8.000, p=0.032) (**Table 24**). All other independent comparisons of the supernatant (CPS versus HPS), and untransduced versus transduced cell lysates were non-significant (p>0.05).

In the second condition, only ionomycin was added to both cell populations (**Figure 15B**). Regarding HEPG2, the median absorbance signal varied significantly across the different supernatant dilutions (H(4)=7.793, p=0.031). When Dunn's post hoc test was applied, the *Control* (HPS) group was statistically different than *No dilution* (*100%*) (HPS) (mean rank difference=8.00, p=0.032) (**Table 25**). Similarly for HEK-293, the hypothesis that there was no difference among the diluted supernatant groups and the control from uninfected cells was rejected (H(4)=7.930, p=0.023). However, all pairwise comparisons (experimental versus control) were non-significant (**Table 26**). For both cell populations receiving ionomycin and calcium (**Figure 15C**), there was a statistically significant difference in absorbance levels across the supernatant conditions interrogated with HPS (HEPG2: H(4)=7.923, p=0.025, and, HEK-293: H(4)=8.780, p=0.001), specifically for the *No dilution* (*100%*) (HPS) - *Control* (HPS) pair [HEPG2: mean rank difference=8.000, p=0.031 (**Table 27**); and, HEK-293: mean rank difference=8.000, p=0.032 (**Table 28**)]. The absorbance signals did not vary significantly when comparing the type of antibody

sera (HPS or CPS) used, the status of the lysate (from uninfected versus infected cells), or the presence of ionomycin alone or both ionomycin with calcium.

However, to examine the potential impact of a shorter incubation time (96 hours) and a higher calcium concentration (10 mM), an ELISA, comparing only two conditions: 1. No ionomycin and no calcium, and 2. Ionomycin and calcium, was repeated on HEPG2, HEK-293, and mouse splenocytes (**Figure 16A-B**). The addition of mouse cells as a third comparator, was intended to provide insight into the environment most appropriate for the encoded PAD4 enzyme, which is of mouse origin. The descriptive statistics for each cell type across both conditions were summarized in **Tables 29-34**. Importantly, although the Kruskal-Wallis H test for HEPG2 across both conditions was statistically significant (Condition 1 (No ionomycin/calcium): $H(4)=7.875$, $p=0.026$; Condition 2 (Ionomycin and calcium): $H(4)=7.745$, $p=0.032$), post hoc, there were no pairs [supernatant dilutions (No dilution (100%), 50% dilution, 33% dilution, and 10% dilution)] versus negative control supernatant] that differed statistically ($p>0.05$) (**Tables 35-36**). The Kruskal Wallis H test was non-significant for HEK-293 cell supernatant across both conditions (1. No ionomycin and No calcium: $H(4)=4.610$, $p=0.393$; 2. Ionomycin and calcium: $H(4)=6.545$, $p=0.134$), and hence, no multiple comparison test was conducted. Furthermore, the supernatant groups interrogated with HPS were not statistically different than their CPS counterpart, as was the case for both cell lines across both conditions analyzed; and the cell lysates (HPS) at different dilutions were also not significantly different from the negative control [e.g., HEPG2 (condition 1): $H(4)=6.072$, $p=0.067$; HEK-293 (condition 1): $H(4)=4.833$, $p=0.171$]. In fact, many of the trends observed in previous ELISAs were not repeated, such as, a decreasing average absorbance level with a less concentrated supernatant,

or the lysates from infected cells having a higher signal than the control (lysate from untransduced cells), as seen across all three cell lines tested.

In contrast, to HEK-293, the absorbance signals for mouse splenocytes were not the same (statistically different) across all supernatant groups (Condition 1 (no ionomycin/calcium): H(4)=7.745, p=0.032; Condition 2 (ionomycin and calcium): H(4)=8.204, p=0.009), with the *No dilution* (*100%*) (HPS) (Condition 1: mean rank difference=8.000, p=0.033) (**Table 37**) and *10% dilution* (Condition 2: mean rank difference=8.000, p=0.032) (**Table 38**) being significantly different than their respective negative *control* (HPS). The statistical analyses demonstrated that there was also a significant difference in the absorbance levels among the varying dilutions of lysate from mouse splenocytes (no ionomycin and no calcium) (H(4)=6.167, p=0.038). But no significant pairs could be identified post hoc (p>0.05) (**Table 39**). Therefore, the primary findings for this sequence of ELISA experiments, with a particular emphasis on the descriptive statistics were as follows:

A) HEPG2/HEK-293/Mouse Splenocytes (no ionomycin and no calcium; **Figure 16A**): although the median absorbance signal across all four dilutions of supernatant was greater than the control [e.g., HEPG2: *No dilution* (*100%*) (HPS): Mdn A=0.324 (IQR=0.008) versus *Control* (HPS): Mdn A=0.261 (IQR=0.015)] and their CPS pair, there was no clear decline in absorbance signal with higher dilutions. For the cell lysate, it was apparent that the lysate of uninfected cells produced greater absorbance values than infected cells for HEPG2, potentially indicating that the observed signal was not due to citrullinated proteins and could be the result of interaction of another cellular substrate. There were no clear trends in the lysate data for HEK-293 and mouse splenocytes.

B) HEPG2/HEK-293 (ionomycin and calcium; **Figure 16B**): through visual inspection, the higher absorbance signals with CPS [e.g., HEK-293: *50% dilution* (HPS): Mdn A=0.269 (IQR=0.003) versus *50% dilution* (CPS): Mdn A=0.326 (IQR=0.005)] could possibly indicate that the assay had low sensitivity whereby it cannot distinguish the two signals (HPS versus CPS). All the transduced lysates performed as expected relative to the control, but the pairwise comparisons were non-significant (HEPG2: $H(3)=4.500$, $p=0.267$; HEK-293: $H(3)=4.849$, $p=0.200$). Further, the addition of ionomycin and calcium, likely did not increase protein citrullination and PAD activation in comparison to no ionomycin and no calcium supplementation. However, further investigation is warranted as the assay may not have been able to detect citrullinated proteins/peptides other than the Schellekens' CCP peptide (described in *section 3.6.3*).

C) Mouse Splenocytes (ionomycin and calcium; **Figure 16B**): the supernatant groups interrogated with HPS had a higher absorbance level than the control (e.g., *No dilution* (*100%*): versus *Control*) and their CPS pairs. Though the changes in absorbance based on dilution did not follow a clear dose-response. Compared to the cells of human origin, the mouse cells also had absorbance signals within the 0.200 to 0.400 range, which may indicate that the origin of the cell may not be an important factor in PAD functionality, though future experiments comparing human and mouse cells should be considered.

D) Pooled Citrullinated and Native Peptide Mixtures (**Figure 16A**): the peptide mixtures, which as mentioned previously, consisted of the three RA-peptides encoded by the viral constructs AAV6-V1 and -V2, were also tested in this ELISA sequence. Although the absorbances were higher [e.g., pooled citrullinated peptide mixture (144 hours; **Table**

18): Mdn A=0.023 (0.002) versus pooled citrullinated peptide mixture interrogated with HPS (96 hours; **Table 29**): Mdn A=0.113 (0.044)] for both the pooled native and citrullinated peptide mixtures when the length of cell was reduced from 144 hours compared to 96 hours. However, the assay's ability to detect these linear analytes remained inconclusive, given the similar response to both native and citrullinated peptide mixtures with both antibody sera (CPS) and (HPS) (**Tables 18 and 29**).

Despite statistical significance, with the mouse splenocytes, the magnitude of the differences in absorbance signals between control and transduced supernatant (or lysate) appeared small, indicating that there was likely no strong effect from the addition of ionomycin and calcium. Again, these findings must be approached with caution, as a significant finding may not have clinical/translational relevance.

3.6.3 Citrullinated Protein levels in Untransduced and Transduced Cells – Addition of CCP as an Assay Control

A final repeat of the in-house ELISA experiments was conducted to ensure that the findings attained were not due to a non-functional assay. Maintaining the same cell types (HEPG2 and HEK-293) and conditions (1. no ionomycin and no calcium, 2. Ionomycin and calcium) ensured reproducibility of the experiment design and increasing the sample size per condition from duplicates to triplicates, strengthened the confidence in the conclusions drawn (**Figure 17**). Descriptive statistics for both cell lines were provided in **Tables 40-43**. For HEPG2 cells, there was no significant difference in absorbance levels across the supernatant groups ($H(4)=8.020$, $p=0.062$) (condition 1: no ionomycin/calcium); Dunn's multiple comparisons test was therefore not conducted. However, there were specific supernatant groups, where the sample interrogated with

HPS was statistically different and larger than the sample with CPS (unpaired (two-tailed) t test), such as, *50% dilution* (HPS) versus *50% dilution* (CPS): t=16.09, p<0.0001; MD (SEM)=0.119 (0.007); and, *33% dilution* (HPS) versus *33% dilution* (CPS): t=7.127, p=0.002; MD (SEM)=0.103 (0.014). The signals from cell lysates, however, did not follow a clear pattern, as the lysate from untransduced cells [HPS: A=0.109 (0.001) and CPS: A=0.185 (0.008)] and transduced cells interrogated with CPS [A=0.198 (0.006)], had higher average absorbance signals than the lysate from transduced cells interrogated with HPS [A=0.087 (0.008)]. For the samples supplemented with ionomycin and calcium (condition 2), the CPS interrogated with groups signalled higher than the HPS, across most categories, and apparent for both cell types (**Figure 17**).

Moreover, for HEK-293 cells, the absorbance levels did vary significantly across the dilutions of supernatant (condition 1: no ionomycin and no calcium) (H(4)=12.73, p<0.0001), with both the *No dilution* (*100%*) (HPS) (mean rank difference=9.667, p=0.032) and *10% dilution* (HPS) (mean rank difference=11.33, p=0.007) significantly different than the negative *control* (HPS) (**Table 44**). Interestingly, the higher dilution condition (*10%*, HPS) also had a slightly greater average absorbance [Mdn A=0.193 (IQR=0.004)] than the non-diluted group (HPS) [Mdn A=0.191 (IQR=0.003)]. This directly contrasts the decline in absorbance with seen with increasing dilutions, as observed previously, and the meaningfulness of this finding. It may also be the case of differences in the amount of protein collected during the harvesting phase and loaded into the wells, especially as the trends thus far demonstrate that the signal can be due to non-target antibodies binding non-target cellular substrates. Despite the supernatant from transduced cells interrogated with HPS differed significantly from CPS (unpaired (two-

tailed) t test) [e.g., *50% dilution* (HPS) versus *50% dilution* (CPS): t=11.41, p=0.0003; MD (SEM)=0.101 (0.009); *33% dilution* (HPS) versus *33% dilution* (CPS): t=16.80, p<0.0001; MD (SEM)=0.097 (0.006); and, *10% dilution* (HPS) versus *10% dilution* (CPS): t=5.397, p=0.006, MD (SEM)=0.079 (0.015)] (condition 1), again the effects of diluting the supernatant rarely changed the absorbance (**Figure 17**). More importantly, this assay included the cyclic citrullinated peptide (CCP), a single analyte which should have served as an assay control across all in-house ELISAs, based on the Schellekens' group (147) (**Figure 17**). The average (SD) absorbance signal with CCP interrogated with HPS was A=2.487 (0.048) [and Mdn A=2.506 (IQR=0.091)], which was several units greater than the peptide interrogated with CPS with a mean of A=0.186 (0.007) [and Mdn A=0.190 (IQR=0.012)] but also all other samples examined. Thus, despite the assay being functional, it was unable to demonstrate if the expressed PAD enzyme was active by way of detecting citrullinated peptides, using patient (HPS) and control (CPS) sera, in supernatant/lysate. The assay was designed based on the ability of ACPA antibodies to detect citrullinated substrate, but it may possibly be the case that the assay was sensitive enough to detect CCP only with the high titre ACPA. Thus, whether there was insufficient PAD activation *in vitro* and/or non-target substrates competing with possibly citrullinated/target peptides for limited availability on the plate's surface, remained elusive.

3.7 PAD Activity using the Commercial Detection Kit

To circumvent the challenges posed by the in-house ELISA, a commercial kit was used to assess the activity of the encoded mouse PAD4 from the viral constructs (AAV6-V1 and AAV6-V2) following incubation for 96 hours. The descriptive statistics were provided in **Table 45**. When only AAV6-V1 was used for infection, it was evident that

there was no significant difference in absorbance when comparing the lysates from transduced cells (with or without ionomycin/calcium) to untransduced (HEPG2: F(2)=0.188, p=0.833; HEK-293: F(2)=0.063, p=0.940) (**Figure 18A**). It was also noted that the addition of ionomycin/calcium only slightly elevated the outcome value but was statistically insignificant [HEPG2: t=0.333, p=0.756; MD (SEM)=0.076 (0.228); HEK-293: t=0.012, p=0.991; MD (SEM)=0.003 (0.254)]. However, there seemed to be high background noise based on how the negative control (assay buffer) [A=1.44 (0.298)] performed compared to the positive (PAD cocktail; 100ng) [A=1.647 (0.278)]. The mean (SEM) absorbance difference between the two controls was only, MD (SEM)=0.208 (0.235), and non-significant (t=0.885, p=0.426) (unpaired (two-tailed) t test). Thus, the conclusions drawn from the commercial kit could not be affirmed until the controls were working appropriately.

The positive control was tested at three separate concentrations (**Figure 18B**), 2 ng/μL (100 ng), 3 ng/μL (150 ng), and 4 ng/μL (200 ng). The average absorbance was A=2.421 (0.089) for 100 ng of PAD, followed by A=2.397 (0.300) for 150 ng and A=2.469 (0.700) for 200 ng. Despite doubling the amount of enzyme available to catalyze the reaction, the change in absorbance was minimal (ΔA=0.048) and decreased at the intermediate concentration. The negative control still gave a large signal [A=1.640 (0.114)]. In systematically addressing the high background and discussing with the manufacturer, there were two probable sources of error: 1. Insufficient washing after the use of a trypsin digestion reagent, or 2. The trypsin digestion reagent has lost enzymatic activity. Although the former was ruled out, the trypsin was replaced and re-tested.

The lysate was collected from cells (HEPG2, HEK-293, and HEPA1-6 – a mouse liver cell line) infected with either construct AAV6-V1 (old (A) and new (B) batch) or AAV6-V2. Further, as a second comparator to the PAD cocktail (assay positive control), a commercial mouse PAD4 was assessed (**Figure 19**). The descriptive statistics were summarized in **Table 46**. It was found that across all three cell types, there was no statistical difference in absorbance levels among the untransduced and transduced cell lysates [HEPG2: $H(4)=1.763$, $p=0.666$; HEK-293: $F(3)=0.835$, $p=0.511$; HEPA1-6: $F(3)=0.613$, $p=0.626$]. Together these findings suggested that there was minimal to no functional PAD4 being produced by the viruses above the basal PAD levels. Since the average absorbance of the commercial PAD4 was only slightly below the PAD cocktail, it indicates that the assay is suitable for mouse PAD, and supports the conclusions drawn. And given the stark difference in absorbance levels between the assay controls [positive: A=1.461 (0.145); negative: A=0.212 (0.017)], increases confidence in the patterns observed and interpreted.

4.0 Discussion

This thesis, presented as two linked projects under the concept of citrullination, focused on improving the current landscape of RA treatment by laying the groundwork for a potential future therapeutic vaccine (project 1) and by enhancing understanding of protein hypercitrullination in RA pathology (project 2). More specifically, project 1, in the form of a clinical study, recruited RA patients and healthy controls to assess T cell responses against a variety of RA-implicated proteins. While project 2, used AAV constructs for the delivery and subsequent expression of a PAD enzyme in RA

pathophysiology known to modify intra- and extracellular proteins, against which an autoimmune response occurs.

4.1 Project 1: Targeting Epitope Specific T Cells

4.1.1 The frequency of T cell responses is not similar between citrulline and glutamine peptides.

The first part of this thesis examined T cell responses against five different peptides in their unmodified/native, citrullinated, or glutamine-substituted forms following the recruitment of RA patients and healthy controls (n=17). This project assessed the suitability of glutamine, which shares functional group similarity and a neutral net charge with citrulline, in the potential design of a therapeutic mRNA vaccine for the amelioration of immunopathology in RA. The reason for assessing glutamine suitability for this purpose was that citrulline is not among the amino acids (AA) for which there are codons in humans. Thus, whilst mRNA vaccine approaches offer potential advantages for the development of epitope-specific immune modulation, it is not possible to generate mRNA vaccine payloads that encode proteins/peptides containing citrulline. As described in the Introduction to this thesis, the conversion of arginine residues to citrulline in certain protein is believed to play a key role in the immunopathology driving RA pathogenesis. In nucleotide-based vaccines, immunodominant epitopes can be encoded to target antigen(ag)-specific cells driving disease. In a recent study by Krienke and colleagues for the treatment of experimental autoimmune encephalomyelitis (EAE), a disease model of multiple sclerosis, the researchers devised a nucleoside-modified mRNA vaccine that reduced immunogenicity of the delivery vehicle and encoded disease autoantigens (153,154). Their disease model was based on an autoimmune response against a peptide

epitope of myelin oligodendrocyte glycoprotein (35-55) (MOG_{35-55}). It was reported that following vaccination with the modified antigen-encoding mRNA, MOG_{35-55}-specific T cells did not exhibit the same pro-inflammatory cytokine profile as the group immunized with the non-modified mRNA, along with a higher frequency of regulatory T cells and lower T_H1 MOG_{35-55}-specific $CD4^+$ T cells. The clinical signs of disease also decreased which demonstrated the therapeutic potential of their approach. More importantly, to appropriately suppress autoimmune diseases, recognizing the involvement of, and therefore targeting autoreactive T cells is a crucial step.

Studies focused on RA have accumulated a plethora of evidence elucidating key peptide epitopes for the activation of $CD4^+$ T cells (155). These included citrullinated vimentin, fibrinogen, alpha-enolase, aggrecan, and anti-thrombin, shown as relevant disease targets (149,156-158). As mentioned in the thesis rationale, the Larché group had short-listed several candidate autoantigens (T cell epitopes) for *ex vivo* testing, including those mentioned above. However, it was apparent that the frequency of antigen-specific T cells was low and is a challenge that is commonly recognized in antigen-specific T cell characterization given their rarity (157,159-161). For instance, James and colleagues quantified the overall frequency of citrulline-specific T cells per $1x10^6$ $CD4^+$ T cells [mean (SEM)], which was statistically higher for RA patients [5.4 (8.6)] than controls [1.9 (1.4)], p=0.007 (155). Similarly, data from another group investigating T cell responses for native and citrullinated alpha-enolase (*ex vivo*) reported frequencies between 1 and 10 ag-specific T cells per $1x10^6$ $CD4^+$ T cells (157).

In the current study, the magnitude of T cell responses tended to be low across all three versions of the five tested antigens, as consistent with the literature. Responses to

native and substituted peptides fluctuated between patients. Further, positive immune responses for a peptide did not always correlate between citrulline and glutamine variants. In another context, technical shortcomings of the ELISPOT immunoassay did not permit comparing the mean frequencies of IFN-γ secreting cells for each peptide among participants. In doing so, the effects of between-subject variability in cell viability would have been insufficiently considered. Along with the possibility that concomitant underlying infections may increase the background noise (i.e., non-specific T cell activation) (162). Although the chosen statistical method for analysis compared antigen-stimulated responses with the background responses for each participant, it reportedly comes with a 5% false-positive rate (148,163). However, this rate tended to be less than some of the other approaches considered when defining a positive response in ELISPOTs (148,163).

A three-point criteria list was devised to independently assess each participant's T cell responses. The parameters examined included equivalent or approximately equivalent frequency of ag-specific T cells between the glutamine and citrulline peptides, a higher immune response level for the two modified peptides compared to the native peptide, and the two modified peptides having a significant response, as obtained by the DFR(eq) tool. For instance, RA1 had an equivalent mean (SD) response against peptide 23 [4.67 (1.53)] for Cit23 and Glut23, though it was less than with Nat23 [5.67 (2.89)], satisfying only one of three parameters. Although it was hypothesized that responses to native peptides would be less than citrulline for both patients and controls, there is evidence suggesting that a T cell can cross-recognize both versions of the same peptide, which may help explain how some native peptide responses were similar in frequency to

their citrulline counterpart (e.g., the average cytokine-specific secreting cells for patient RA1 was 3.67 (2.08) for Nat.-28 and 3.67 (3.06) for Cit.-28). It is also important to note that the enrolled RA patients and healthy controls may have non-shared epitope class II HLA molecules that could potentially bind any of the three peptide variants tested and lead to a T cell response. A study by Kampstra and colleagues demonstrated that specific HLA-DQ (e.g., DQ7 and DQ8) molecules preferentially interacted with citrulline-containing peptides over their native variant (110). Thus, it was difficult to interpret whether the generated responses came from the antigens binding a SE+ HLA-DR or another HLA molecule that was present, as some studies have shown that the HLA-DQ molecule was also involved in RA (110,164-166).

Pieper and colleagues reported, using HLA-DR4 tetramers conjugated to either APC or PE fluorophores, on patient samples positive for HLA-DRB1*04:01, that some T cells cross-recognized both peptide forms (i.e., native and citrullinated) of alpha-enolase (157). It was proposed that the cross-reactivity observed may have been due to the position of the arginine residue modified to citrulline, happening at a site that was not critical for interacting with the binding groove of the HLA-DR molecule (157). Thus, the native and citrullinated alpha-enolase bound to the class II HLA molecule could similarly activate alpha-enolase-specific T cells. Another hypothesis put forward by the group was the presence of multiple types of T cell receptors (TCRs), each responding differently toward the antigens tested. For instance, it was suggested that one TCR would detect both peptides and others that would only recognize one form of the peptide (either native or citrullinated) (157).

In this thesis, the immune responses and magnitude of cytokine-secreting cells did not match for glutamine and citrulline peptides given their structural similarities (**Figure 3**), as the T cell response for the citrulline analogue was only equivalent for the glutamine analogue in 23% of participants of which no T cell response was positive. It was therefore concluded that glutamine is not a suitable surrogate for citrulline in designing a potential mRNA-based therapy. If, however, there had been a clear trend in peptide response supporting the recognition of both citrulline and glutamine analogues, the next step would have been to demonstrate whether the same T cell was responding to each of the peptides (since this cannot be determined at the level of the polyclonal cultures conducted in the present study) while also exploring the possibility of cross-reactivity. The analysis would aim to determine whether separate T cells responded to each of the three peptide analogues, or whether single TCRs can respond to both the citrulline-substituted and glutamine-substituted epitopes. In effect, PBMCs would be isolated from RA patients who had demonstrated a positive one-to-one response to a peptide, followed by *ex vivo* staining with two fluorescently labelled MHC class II tetramers bound to either the citrulline or glutamine version of the peptide. If it was evident that both tetramers bound to the same T cell, then this would be foundational in designing a nucleic acid-based vaccine for use in an inflammatory-arthritis mouse model (previously established within the Larché lab) and delivered in a non-inflammatory context, similar to the Krienke group (154).

4.2 Project 2: Modelling Protein Hypercitrullination

In project 2, two AAV constructs (AAV6-V1 and AAV6-V2) were tested to overexpress the PAD4 enzyme (*in vitro*) to attain substantial upregulation of citrullination. Both constructs contained a KDEL sequence, and it was necessary to investigate if the virus-encoded PAD4 localized to the endoplasmic reticulum (ER) or elsewhere in the cell, as PAD4 has an embedded nuclear localization signal. The expression of AAV-encoded PAD4 was confirmed by western blot, and its activity was assessed using in-house and commercial ELISAs.

4.2.1 PAD4 is not localized to the endoplasmic reticulum

To determine where the PAD4 protein localized, human and mouse cells were infected and stained for visualization via EVOS and confocal microscopy. The data from the EVOS microscope (**Figures 7-9**), supported by data from flow cytometry (**Figures 7-8**), confirmed the successful transduction of cells using AAV6-V1 (GFP-PAD fusion construct), with an increasing proportion of GFP-positive cells at higher MOIs. However, the EVOS microscope could not confirm PAD4 localization, as the entire cell fluoresced green. Following the immunocytochemical staining of cells for visualization of intracellular structures via confocal microscopy, it was apparent that the GFP-PAD4 fusion protein did not localize to the ER lumen, contrary to what was envisaged due to the presence of a downstream KDEL sequence at the C-terminal domain (added by collaborator Dr. Wootton during construct design). This tetrapeptide sequence retains proteins in the ER lumen after they are synthesized (167,168). Given the importance of calcium to PAD function, it was thought that restricting the protein to the ER could provide a higher source of the cofactor, as Ca^{2+} concentrations are approximately 10^4-fold greater than the

cytoplasm (169,170). Due to the lack of overlap in signal between the GFP and PE channels in green and red, respectively, with AF647 in cyan, it was concluded that the fusion protein was present in the cytoplasm and not the ER (**Figure 10**). This was consistent across the acquired confocal images and has been described as one of the locations where this protein is reportedly found following physiologic expression (171).

The PAD4 enzyme contains an embedded NLS (nuclear localization sequence) signal in residues 45 to 74 (172). This motif, on the surface of the N-terminal domain, is believed to be recognized by nuclear transporters for passage through the nuclear pore complex and consists of the sequence ^{56}PPAKKKST^{63} in humans, and ^{56}PPVKKST^{62} in mice (172,173). Nakashima and colleagues compared the NLS in human and murine PAD4 with 'classical monopartite' motifs (an alpha-helix disrupting residue, i.e., proline, and basic AA) and found similarities in the sequence with a proline residue at position 56 followed by double lysine residues at positions 59 and 60 (172,174-176). Previously, it has been shown that nuclear transport receptors recognize the basic clusters in the 'classical NLS' which are complemented by electrostatic and hydrophilic interactions, and certain AA substitutions in the NLS can completely prevent transport (174,177-179). Moreover, the lack of PAD retention in the ER may be the result of competing signals as the engineered protein contained a C-terminal KDEL sequence in addition to the NLS (180). It is possible that the PAD4 may shuttle among many locations within the cell, from the ER to the cytoplasm and nucleus. Thus, even though nucleocytoplasmic distribution is common for this protein (172,173,181-183), how the ER retention signal may influence its subcellular destination has not been elucidated in the literature. In comparable studies, there is evidence that suggests certain proteins are dually dispersed among many

compartments of a cell (184-188). For instance, Petrova and colleagues demonstrated that the catalase A enzyme in yeast, responsible for neutralizing or reducing the harmful effects of reactive oxygen species, was found in both the peroxisome and mitochondria by fusing a GFP moiety at its C-terminus (186). However, having a bulky fusion partner or interactions among proteins could also make one or more of the signal sequences inaccessible (189-191). As was the case for catalase A, where GFP 'masked' the peroxisomal targeting signal near the site of fusion (186). Although PAD4 localization to the nucleus was not determined by the current staining procedure, a proposed model of the GFP-PAD4 fusion protein demonstrated the spatial proximity of the reporter to the NLS, as well as the KDEL motif at the C-terminus of PAD4 (**Figure 20**). Together these findings may partially explain the minimal overlap between the ER (AF647) and GFP/PE signals.

4.2.2 Detection of PAD4 expression by western blotting.

The basal expression of the PAD4 enzyme is known to extend beyond the cells of the immune system (i.e., neutrophils and monocytes). There are reports demonstrating tonic PAD4 expression in the human and mouse cell lines used in the current study (192-195). Thus, it was expected that in non-infected cells, there would be some detectable PAD4, which was indeed the case (**Figure 11**). These findings were also supported by the staining experiment, in which negative control cells had a PE-signal, which indirectly targeted PAD. For instance, all cell lysates generated an anti-PAD4 antibody-reactive band near the 75 kDa mark, as 76 kDa is the molecular weight of mouse PAD4 (**Figure 11**). The data from the western blot did confirm transgene expression, especially for AAV6-V1, as a second band appeared close to 100 kDa which is indicative of the GFP-

PAD4 fusion protein. However, relative to untransduced cells, the band for PAD4 from cells infected with AAV6-V2 containing the WPRE (Woodchuck Hepatitis Virus posttranscriptional regulatory element) sequence was not increased in intensity, suggesting a failure of the construct to boost PAD4 expression. The underlying reason for the lack of enhanced protein expression is currently unknown. It was thought that components of the vector may be incompatible, such as WPRE and the CASI promoter, as some studies showed no benefit of WPRE on enhancing transgene expression with specific promoters (196-198). Whether or not the CASI promoter would behave similarly has not been elucidated in the literature. Interestingly, the protein bands were more pronounced with mouse HEPA1-6 cells in comparison to HEK-293 or HEPG2, across three independent experimental repeats (**Figure 11**). Previous studies have demonstrated efficient transduction of mouse cells by AAV6, which could have allowed for higher protein expression (199-201). The results from the western blots support PAD enzyme production from AAV6-V1, though, PAD4 produced by AAV6-V2 is indistinguishable from endogenous PAD.

4.2.3 Assessment of PAD Activity by ELISA.

In addressing Aim 2 of project 2, PAD4 activation and citrullination of proteins were compared across infected and uninfected cells over a series of ELISA experiments, with troubleshooting techniques applied systematically. Several dilutions of supernatant from transduced cells (experimental condition) were compared to untransduced cell supernatant serving as a negative control. At first, only high titre ACPA sera (HPS) from RA patients were pooled and used as the source of antibodies to detect citrullinated substrates. The higher absorbance signals for transduced cell supernatant were

statistically different than the control ($p<0.05$), seen across two different cell types (HEPG2 and HEK-293) and two time points (96- and 144-hours). While only the lysate for HEPG2 at 96 hours had a significant difference between the experimental and control conditions ($p=0.013$) (**Figure 13**). It was also worth noting that absorbance signals for cell supernatant decreased by half with a longer incubation (144 hours), with the negative control [*HEPG2*: A=0.084 (0.003); *HEK-293*: A=0.106 (0.003)] having a higher mean absorbance than the experimental lysate [*HEPG2*: A= 0.067 (0.000); *HEK-293*: A=0.097 (0.000)] (**Figure 13**). If the absorbance signals had increased from 96- to 144-hours, it would support the conclusion that the enzyme modified more substrate over time. Rather, it may be the case of diminishing enzyme activity and thereby less citrullinated peptides were detected.

A comparator serum (CPS) pooled from healthy controls (all ACPA negative, <18 units) was added to observe how much of the absorbance signal was attributable to citrullinated proteins and background noise. Statistical analyses revealed that the wells the HPS was assayed in did not differ statistically from the wells interrogated with CPS ($p=0.333$). However, the absorbance signal was higher for every experimental and control condition with HPS than CPS. Surprisingly, supernatant from untransduced cells [*Control*: median (Mdn) A=0.118 (Interquartile range; IQR=0.020)] or the media alone resulted in high background noise with the HPS sera [HPS: Mdn A=0.098 (IQR=0.063)]. Absorbance from the wells that CPS was assayed in was relatively minimal and ranged from 0.044 to 0.051 units for the experimental conditions of HEPG2 (**Figure 14**) as an example, which was all above the signal from untransduced cell supernatant interrogated with CPS [*Control*: Mdn A=0.039 (IQR=0.006)] (same trend observed for HEK-293). Taken

together, these findings suggested the following: 1. above the negative control (HPS) and media alone (HPS), there were substrates that the antibodies bound to, but the identity of these substrates is unknown and cannot be attributed to citrullinated peptides; and 2. overall there was a poor signal-to-noise ratio with low absorbance readings, as compared to the absorbance seen with the HPS bound to CCP [A=2.487 (0.048)] (**Figure 17**).

In RA, PAD4 activation has been observed following cell death as the latter allows for an ample supply of calcium influx from the extracellular environment and the release of the cation from intracellular stores, which is why citrullinated autoantigens can be found both in an out of cells (104,202-204). As a result, it was hypothesized that intracellular Ca^{2+} concentrations in intact cells were not conducive for PAD4 activation *in vitro*. In support of this hypothesis, studies elucidating the structure and mechanisms of action of the PAD4 enzyme, highlight the importance of elevated calcium concentrations for its activity (173,205). PAD4, with its five-calcium binding sites, requires supraphysiologic amounts of Ca^{2+} for activation (up to 10 mM), which is 10^5-fold larger than resting state intracellular Ca^{2+}concentrations (near 100 nM) (173,206-208). Andrade and colleagues conducted an *in vitro* citrullination assay co-incubating PAD4 with histone H3.1 in the presence of 10 mM $CaCl_2$ and demonstrated modification of the histone protein by an anti-modified citrulline (AMC) antibody (209). This requirement for high calcium levels served as the rationale behind incorporating a KDEL sequence into AAV6-V1 and AAV6-V2. Virally infected cells were incubated with calcium and ionomycin (a calcium ionophore) in an ‘activation phase’ prior to harvesting the cells. However, there was no apparent change in signal, especially in comparison to the cells that were not treated with both supplements. It may be possible that the calcium concentration used at first was too

low (2 mM) and the length of incubation (120 minutes) with the supplements was inadequate to stimulate PAD4-mediated citrullination. However, the demonstration by Andrade and colleagues that citrullination of protein incubated at 37^{o}C was detected in as little as 5 minutes, suggests that the length of incubation in the current experiments is unlikely to explain the observed lack of PAD4 activity (209).

When comparing cells with and without ionomycin/calcium supplementation, there were no clear trends in the data that would suggest that the calcium supported PAD4 activation *in vitro* and subsequent citrullination of proteins (**Figures 15-17**). For example, directly comparing the mean (SD) [or median (IQR) which are equivalent, aside from their measures of spread, as the samples were in duplicates] of the supernatant from the HEPG2 cell culture diluted 50% with coating buffer and interrogated with the HPS sera, the absorbance values were: A(no ionomycin and no calcium)=0.144 (0.016); A(ionomycin without no calcium)=0.140 (0.011); and A(ionomycin and calcium)=0.153 (0.013) (**Tables 18,20,22**). These results demonstrate very little change in absorbance indicative of a failure to detect citrullinated proteins, despite the modification of culture conditions to mimic those conducive for PAD activation through the addition of ionomycin/calcium.

It is established that a high calcium concentration is important for PAD activation. However, the cell lines initially investigated (i.e., HEPG2 and HEK-293) in this study were of human origin. It was reasonable to question whether these cells lacked the appropriate cofactors necessary for complete activity of a murine PAD4 enzyme. Thus, ELISA assays were performed on samples generated from transduced murine splenocytes (**Figure 16**). With no change in the amount of ionomycin (1 μM); a higher calcium concentration (10

mM as opposed to 2 mM); and longer incubation (4 hours as opposed to 2 hours); the absorbance signals remained consistent regardless of the cell type or the presence of ionomycin and/or Ca^{2+} (**Figures 15-16**). When the ELISA plates were coated with the same CCP peptide used by the Schellekens' group, a greater absorbance signal near 2.5 units was observed with the high titre ACPA patient sera (**Figure 17**). Despite the results remaining consistent from assay to assay demonstrating repeatability, none of the absorbance signals with the supernatant or lysate from virally infected cells were as high as the signal with CCP interrogated with HPS (**Figure 17**). In fact, the signals from experimental conditions were near the signal obtained with CCP interrogated with CPS. These findings provided a good indication that although the CCP substrate was detected by HPS, PAD4 activation by way of detecting other cellular or AAV6-encoded peptides was not possible using the current in-house ELISA system.

4.2.4 Assessment of PAD Activity with a commercial kit.

Despite several adaptations to improve the in-house ELISA, it was unable to confirm PAD4 activity. This led to the PAD commercial kit, where lysate from infected (AAV6-V1 and AAV6-V2) human and mouse cells was collected and compared with a PAD cocktail (positive control) and commercial mouse PAD4 (**Figure 19**). Across all three cell lines (i.e., HEPG2, HEK-293, and HEPA1-6), there was almost no change in absorbance signal for the virally infected lysate relative to untransduced cell lysate. All conditions were analogous with the assay negative control (buffer). Of importance, is to note the activity of the commercial mouse PAD in relation to the PAD cocktail. The cocktail consisted of five PAD isoforms, 1 through 4 and 6, while the mouse PAD was exclusively PAD4, and equivalent concentrations of both were tested in the assay at 4 ng/μL. The

PADs contained in the mixture, were of equal amounts, and of human (PAD1/3/4/6) and mouse (PAD2) origin. The absorbance level from the commercial mouse PAD4 was slightly below but not statistically different ($t=1.607$, $p=0.183$) than the signal obtained by the PAD mixture (**Figure 19**). However, both, the commercial mouse PAD4 and PAD cocktail, were significantly different than the background (negative control) (Mouse PAD versus Negative Control: $t=16.91$, $p<0.0001$; PAD cocktail versus Negative Control: $t=14.78$, $p=0.0001$), as found using a two-tailed t test. These results indicated that the kit was functional in detecting PAD activity, however, the virally infected samples did not appear to contain a functional PAD4 enzyme.

4.2.5 An exploration of the following project caveats: effects of fusion protein on functional activity, reading frame for PAD4, substrate specificities, detection of a limited array of autoantigens by RA sera, peptide conformation, and citrullination-induced inactivation of PAD.

For this project, two viral constructs were designed: AAV6-V1 – containing a GFP-PAD4 fusion protein, and AAV6-V2 – replacing the GFP protein and incorporating a WPRE sequence downstream to enhance gene expression. In order to address factors that might explain the lack of enzymatic activity observed, a series of potential study caveats were examined. First, a complete review of the genetic sequence was conducted and the PAD4 sequence was found to be in the correct reading frame; hence, a frameshift was unlikely to be an explanation for the lack of activity observed with the in-house ELISAs.

The AAV6-V1 construct encoded a fusion protein with a small four amino acid glycine-serine [Gly-Gly-Ser-Gly, (G-G-S-G)] linker between the C-terminus of GFP and

the N-terminal region of PAD4 which allowed for visual detection of the enzyme. The glycine-serine linker employed is flexible, given the smaller size of the residues (i.e., glycine) and solubility in aqueous environments (i.e., serine) (210,211). It has also been shown that glycine-rich linkers add stability to the fusion protein (212,213). However, as these inter-peptide linkers permit a certain degree of motion, there has been a report where a five AA [$(Gly)_4Ser$] flexible linker used to conjugate protein G to luciferase resulted in a non-functional chimeric protein (214). The researchers suggested that potential interactions between the two moieties interfered with protein's binding ability (214). In response, the group employed a rigid, alpha-helix based linker, that maintained spatial distance, and reduced potential interference (210,214,215). Thus, with shorter flexible linkers, one limitation is possible interactions between the two proteins fused together highlighting the importance of optimizing the design and length to meet research needs (212).

With the fusion protein reported in this thesis, it is very possible that the GFP moiety was interfering/interrupting PAD4 enzyme activity. For instance, since the GFP was expressed upstream of the PAD4 enzyme, incorrect folding may have impacted the intensity of the fluorescence signal and resulted in the formation of an unstable protein complex (216-218). However, even if the protein folded correctly, it remains possible that the large size of the GFP (27 kDa) could sterically hinder the active site(s) of PAD (216,219). To address this possibility, the crystal structure of human PAD4 was examined (as the mouse version has not been elucidated). Four sites actively involved in catalysis, included D350, H471, D473, C645, which are also conserved in the mouse PAD4 (confirmed using NCBI BLAST) (173,181). All four sites were localized in the C-terminal

domain of PAD4, residues 301-663 (human; 666 for mouse) (181,220). The N-terminal domain of PAD4 consisted of two subdomains, three out of five calcium-binding sites, and was comprised of residues 1-300 (181,220). By leveraging the AlphaFold2 software to develop a 3-D model of the chimeric protein (used in the current study) with high predictability (with a mean predicted local distance difference test above 90 indicative of very high confidence towards the residue's spatial orientation and position; **Figure 20E**) and confirmed using three additional programs: SWISS-MODEL, ModBase, the Protein Data Bank (each protein independently assessed), it was evident that the GFP protein was visually adjacent to the N-terminal domain of PAD4 (**Figure 20**) (221-223). Using the methods currently available, it was hypothesized that with the flexible linker and/or bulkier substrates, GFP was likely to have some interference with the active cleft of PAD4. However, the extent of the interference, especially in the system reported in this thesis, cannot be determined.

Furthermore, as the constructs contained the genetic information to produce a PAD4 enzyme of mouse origin, it was important to note that the three native-sequence 'substrate' peptides (from vimentin, aggrecan core, and alpha-enolase) encoded by the AAV6-V1 and AAV6-V2 constructs were of human origin, and that most of the experiments were conducted using human cells. By conducting comparative analyses of the two proteins, mouse and human PAD4, using the NCBI Basic Local Alignment Search Tool (BLAST), it was evident that the mouse PAD4 was 73% identical to the human version. This indicates that the mouse PAD was not an exact match of the human, and by extension, this could potentially translate into slight differences in substrate specificities and affinities, especially for the non-conserved regions (224). However,

complexities arise when comparing potential cellular substrates between human and mouse, as they tend to be highly analogous with greater than 85% AA sequence similarity. For instance, mouse vimentin had 97% overlap in sequence identity with human vimentin, when comparing whole protein using the NCBI BLAST tool. Thus, the origin of the substrate on PAD4-mediated citrullination warrants further investigation.

The substrate specificity profile for the PAD4 isoform may have important implications for the findings in the current study. As PAD4 tends to localize in the cytoplasm and is the only PAD isoform with an NLS, many of the intracellular substrates it deiminates are nuclear, such as histones H2A, H3 and H4 (171,172,225,226). There is substantial evidence that outlines the distinct substrates that PAD isoforms target and subsequently modify (227-229). To illustrate, Darrah and colleagues, collected lysates from HL-60 (human myeloid leukemia) cells and co-incubated with or without three different PAD isoforms, PAD2-4, and 10 mM $CaCl_2$ for 1 hour at 37^{o}C (228). Citrullinated proteins were detected using an anti-modified citrulline (AMC) antibody. It was found that there were differences in the protein targets for each enzyme, such as, histone H3 was citrullinated by PAD4 and not by PAD2 nor PAD3; or that PAD2, but not PAD3, another cytoplasmic enzyme, modified actin (228). Although there tended to be overlap between some of the substrates modified, specifically when comparing PAD2 and PAD4 (most prominent in RA), there are differences in the residue sites that each isoform modifies preferentially. For example, comparing the citrullinated sites of fibrinogen, the researchers reported that 9 sites were only modified by PAD2 and not PAD4, while 1 site was only modified by PAD4, out of the 21 sites recognized together (226). In an investigation comparing citrullination sites between PAD2 and PAD4 on a synthetic peptide, relative to

the target arginine, AA substitutions at residue sites 1 or 3 spaces upstream were critical for PAD2. While, for PAD4, substitution of the glycine residue one position downstream of the arginine residue considerably affected substrate citrullination (227). Taken together, these findings affirmed that specific substrates (and residue sites) are preferred by various PAD isoforms. Thus, it cannot be excluded that substrate specificity contributed to the negative enzyme function findings in the current study.

In RA, and well elucidated in the literature, many autoantigens have been found in the joint space. However, there are characteristic differences in the profile of arthritogenic antigens detected by patient sera, which partly explain the heterogeneity of the disease. For example, a study reported that RA sera detected different (and a minor subset of) citrullinated proteins in lysates from ionomycin-activated or control neutrophils (228). Similarly, another group demonstrated that out of 72 ACPA-positive RA patients, only 61% and 60% of sera detected citrullinated vimentin or fibrinogen, respectively (230). For the in-house ELISA experiments detailed in this thesis, the high titre ACPA patient sera (HPS) was pooled from three patients with a strong positive ACPA status (>124 units). There still exists the possibility that the grouped patient sera did not have the specific autoantibodies to bind and detect a modified citrulline of a particular substrate, assuming that the PAD, whether virally encoded or basally expressed was active to some degree. It is also important to note that sera can contain antibodies to non-target proteins, such as against native (or non-modified) peptides which are highly likely to be contained in cell lysate and could potentially compete for space on the ELISA plate (231-236). Snir and colleagues noticed that 13% of RA patients and 5% of control sera reacted positively towards a native (unmodified) type-II collagen epitope (231). Although this can partly

explain the low signals observed for infected and non-infected cells, further evidence and experimentation would need to be conducted to demonstrate that this is indeed the case.

Besides the comparable absorbance signals seen with RA patient and control sera, a potential explanation for the high absorbance signal obtained with HPS and commercial CCP, and a low signal for the peptide mixtures, may be attributable to differences in reactivity of autoantibodies against cyclic and linear peptides. As demonstrated by Schellekens and colleagues using an ELISA assay comparing two versions (linear and cyclic) of the same citrullinated peptide derived from filaggrin, patient sera were more reactive towards the cyclic variant over the linear, as seen by the higher optical density values (95,147). Accumulating evidence from other studies reinforced that a higher absorbance signal with RA patient sera is seen with cyclic as opposed to linear peptides (236,237). There also tends to be a greater proportion of reactivity with patient sera to cyclic (68%) citrullinated pro-filaggrin than linear (44%) (236). Thus, the conformation of the peptide can have important implications for and influence antibody recognition, as evident across a multitude of target antigens and studies (147,236-240). Some groups have shown that PADs can auto-citrullinate in a calcium-dependent manner and PADs can be recognized by ACPA (209,241-247). Although unsubstantiated and entirely speculative given that the current methods cannot conclude if PAD4 was secreted from the cells and present in the supernatant, a potential absorbance signal in the ELISA could possibly be due to ACPA reacting to PAD4 instead of the other substrates. Intriguingly, one group discovered that following the autocitrullination of the PAD4 enzyme and incubation with cell lysate containing several cellular targets, there was no detectable citrullinated peptides by the AMC antibody (209). The researchers described this

phenomenon as citrullination-induced inactivation of PAD4 (209). In contrast, other studies have suggested that autocitrullination of PAD4 does not inhibit its activity (241). There is no evidence from the findings presented in this thesis that PAD4 activity may have been altered as a result of autocitrullination.

4.3 The 'true' meaning of statistical significance and experimental design limitations.

This thesis presents qualitative data supported by quantitative measurements and corresponding statistical tests. As outlined in the results of Project 2, many of the analyses conducted, found statistically significant differences in one or more of the experimental groups as compared to the negative controls. For instance, the *10% dilution* supernatant, had a higher absorbance value than the *no dilution* (*100%*) sample and was significantly different ($p<0.05$) than the negative control (**Table 34 and Figure 16B**). However, these findings must be interpreted carefully as the significant result lacks logical coherence in the context of this study and its aims. Further, the reported measurements were in technical repeats (duplicates or triplicates). With duplicates, there was no way to assess if the data measurement passed normality (small 'n'), especially with the Shapiro-Wilk test. With such a small sample size, the challenge becomes having enough statistical power to detect a real (or meaningful) difference between compared groups, as seen with non-parametric testing; or in other words the likelihood of seeing a false positive increases (248-250). Thus, it is highly plausible that some of the statistical results obtained with the in-house and commercial ELISAs were misleading, especially when assessing their scientific relevance, because a small difference between two comparators could become statistically significant (248) without being biologically significant. A method to improve

confidence in the data, is to have all test samples conducted in triplicates, followed by multiple whole experiment repeats. This can present as a challenge, however, given the limited space on ELISA plates, reagents available, and total sample collected.

In addition to the statistical limitations discussed above, there were discernable limitations in the experimental design. In Project 1, RA patients and healthy controls were recruited, with a final sample size of 17 participants (13 patients and 4 controls). As a pilot investigation, there were fewer controls and an overall small sample size, which could lead to an underpowered study. Furthermore, during PBMC isolation, the viability of the samples sometimes varied, with low viabilities (<75%) impacting the performance of the assay owing to red blood cell contamination (251). Since assay repeats were not conducted, it could not be determined if the spot counts remained consistent, demonstrating reproducibility, or changed drastically for the same subject. Another limitation of this project relates to the composition of the participant pool, with more than two thirds of the sample comprised of females. As a result, the study may be susceptible to sex/gender bias, which may limit its external validity. Even though sex differences in T cell responses were not investigated in this paper, it can be a future avenue to explore, especially as the prevalence of RA is higher in females (39,40).

Moreover, in Project 2, specifically for the cell staining experiment, a multi-colour procedure was applied involving three different fluorophores, such as, GFP, PE, and AF647. As the AF647 conjugated anti-calreticulin antibody directly bound to calreticulin, there were instances where a signal was observed across the cell; most clearly seen in the negative controls (**Figure 10A-B**). The challenge posed by this chaperone is that it resides in abundance in the ER lumen but can still be found in other cellular

compartments, including the cytoplasm, nucleus, and vesicles (252). Therefore, targeting calreticulin led to widespread fluorescence signals that may not have always corresponded to labelling the structures of the ER. Another obstacle was being able to differentiate the level of media and cellular auto-fluorescence from that of the extrinsic fluorophores used during staining. Intracellular molecules, such as flavins in the mitochondria, and fluorescent tags like GFP, can both be excited with similar wavelengths near 490 nm and emit around 510 nm (253-256). By having overlapping absorption and emission spectra**,** it was critical comparing infected to control cells to assess background noise. It has been reported that certain fixatives, including paraformaldehyde, can increase auto-fluorescence (256,257), which could have also had a negative impact on the signal-to-noise ratio observed here. Although, GFP reporters, and aldehyde fixatives are commonly used for immunocytochemistry and immunofluorescence procedures, cellular auto-fluorescence can nonetheless present challenges impeding with target detection. Besides potential confounding of the signal, a very large MOI was required for infecting >50% of cells, which consumed reagents quickly, raising practicality concerns (258). Also, with repetitive experimentation and freeze-thaw cycles there was loss of vector activity, as supported by the literature and fewer fluorescent cells spotted with microscopy (*data not shown*) (259-261). AAVs have variable transduction efficiencies based on the tissues being infected. In a previous *in vitro* investigation, 46% of HEPG2 and 76% of HEK-293 cells were GFP-positive two days post-infection with AAV6 (124). Although comparable transduction rates were attained and reported in this thesis using the same cell types, it is important to note that the researchers had a 96-hour shorter incubation, and while expression levels are expected to increase over time, this may

indicate that the virus used in this project performed relatively poorly (142). In fact, the AAV6-V2 construct seemed to perform no different than untransduced cells, despite containing a WPRE element meant to increase transgene expression, as determined by western blot (**Figure 11**).

In relation to the activity assays, it was apparent that the use of patient and control sera was not specific enough to demonstrate the presence of citrullinated protein. By using an antibody either specifically meant to detect citrulline residues (e.g., AMC antibody) or against a particular autoantigen, such as one well-established as a PAD4 substrate (e.g., an anti-histone citrulline antibody) could circumvent the issue. In addition, adding ionomycin and calcium to induce PAD4-mediated citrullination intracellularly was not effective. An alternative approach, based on the experimental evidence synthesized in the literature, would be to collect the cell lysate containing PAD, and then co-incubate the enzyme and a substrate for 2-4 hours at 37^{o}C. A similar experiment was conducted but the findings were not reported in the Results section of this thesis. In brief, the experiment involved a commercial mouse PAD4 (1 μg/mL) incubated with human fibrinogen (1 mg/mL) for 60 minutes at 37^{o}C in citrullination buffer (100 mM Tris-HCl, 10 mM $CaCl_2$, 1 mM dithiothreitol, pH 7.5) (262), to assess the compatibility of the literature-supported experimental design combined with the in-house ELISA. It was found that the in-house ELISA was better suited for detecting CCP as opposed to linear peptides or whole proteins, as mentioned previously. The issue with whole proteins is that orientation and presentation of the epitope for linking with its target antibody may not always occur. Also, given the scope of this study, and in line with the arguments made above, it was

concluded that the patient and control sera were not an appropriate detection antibody, and an alternative should be explored.

5.0 Conclusion and Future Directions

This thesis presents and discusses the findings of two parallel investigations linked by the concept of PAD-mediated citrullination of peptides commonly implicated in RA. Despite limited success with glutamine serving as a surrogate for citrulline, it was clear that certain modified peptides were able to elicit positive T cell responses *ex vivo* as detected using the ELISPOT assay (Project 1). Though few responses were synonymous between the citrulline-glutamine pairs among RA patients and a healthy control, none were greater than the average spot count observed for the native/un-modified counterpart. As a result, the strategy, to substitute glutamine for citrulline as there are no naturally occurring codons for the latter, employed in the pilot investigation of co-culturing PBMCs with select peptides was concluded as unsuitable for targeting autoreactive T cells. Given the complexity of the disease however, another major player, which was not the focus of this paper, are the ACPA-producing B cells. As these immune cells can produce ACPA antibodies, which have been shown to exacerbate disease symptoms/severity, a potential therapeutic angle can involve neutralizing these autoantibodies to lay the foundation for a distinct inhibitor-based immunotherapy. Although not reported here, the preliminary findings seem promising. Further testing is required *in vitro* before shifting towards a preclinical inflammatory-arthritis disease model.

In the latter portion of this thesis (Project 2), there was evidence demonstrating AAV6-mediated production of PAD4 with AAV6-V1 (GFP-PAD fusion) but not AAV6-V2 (WPRE), as seen with the data from the EVOS and confocal microscope, along with flow

cytometry and western blots. Microscopic images and flow cytometry confirmed GFP signalling, and data from the western blots displayed two signals: basal PAD4 (~75 kDa) and the GFP-PAD4 chimeric protein (~100 kDa). However, the in-house and commercial ELISAs were unable to demonstrate consistent PAD4 activity above background levels even with ionomycin and calcium supplementation. Given the design of the ELISAs, the detection and citrullination of the three AAV-encoded native peptides could not be determined. Cumulatively, these results suggest that some of the recombinant AAV was able to produce some of the disease-associated targets, such as the PAD4 enzyme, though there were concerns surrounding if the detection systems were appropriate for achieving the stated research goals. For instance, high titre ACPA patient sera may be a more sensitive approach, but it lacks specificity, especially towards detecting the virally encoded peptides or other intracellular PAD4-substrates (e.g., histones). Further, many of the cited studies have shown that vector-encoded PADs can citrullinate proteins extracellularly when co-incubated in citrullination buffer (calcium-rich), while the assays reported in this paper primarily focused on the PAD's ability to citrullinate intracellularly. Thus, it may seem logical to first demonstrate the enzyme is expressed and functional in cell lysate incubated with a native peptide before assessing if it also citrullinates substrates intracellularly. Then a specific antibody towards the modified form of the incubated peptide can be used to confirm enzymatic activity. Since only transduction experiments were conducted, it would be interesting to compare transgene expression by transfecting with DNA plasmids. In conclusion, glutamine and citrulline did not show consistent positive T cell responses, and the AAV6 infection of human and mouse cells validated PAD4 production but not function.

6.0 Figures and Tables

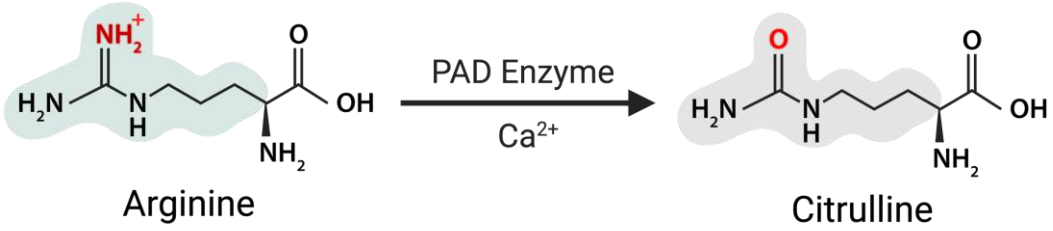

Figure 1. Arginine is converted into citrulline by a calcium (Ca^{2+})-dependent, peptidyl-arginine deiminase (PAD) enzyme. The positively charged arginine ('R') residue is hydrolyzed by water (H_2O), *not shown*, replacing the amino ($-NH_2$) functional group with a keto (=O) group (bolded in red). The end products are a neutral citrulline residue and an ammonium cation (NH_4^+; *not shown*). This figure was Created with BioRender.com.

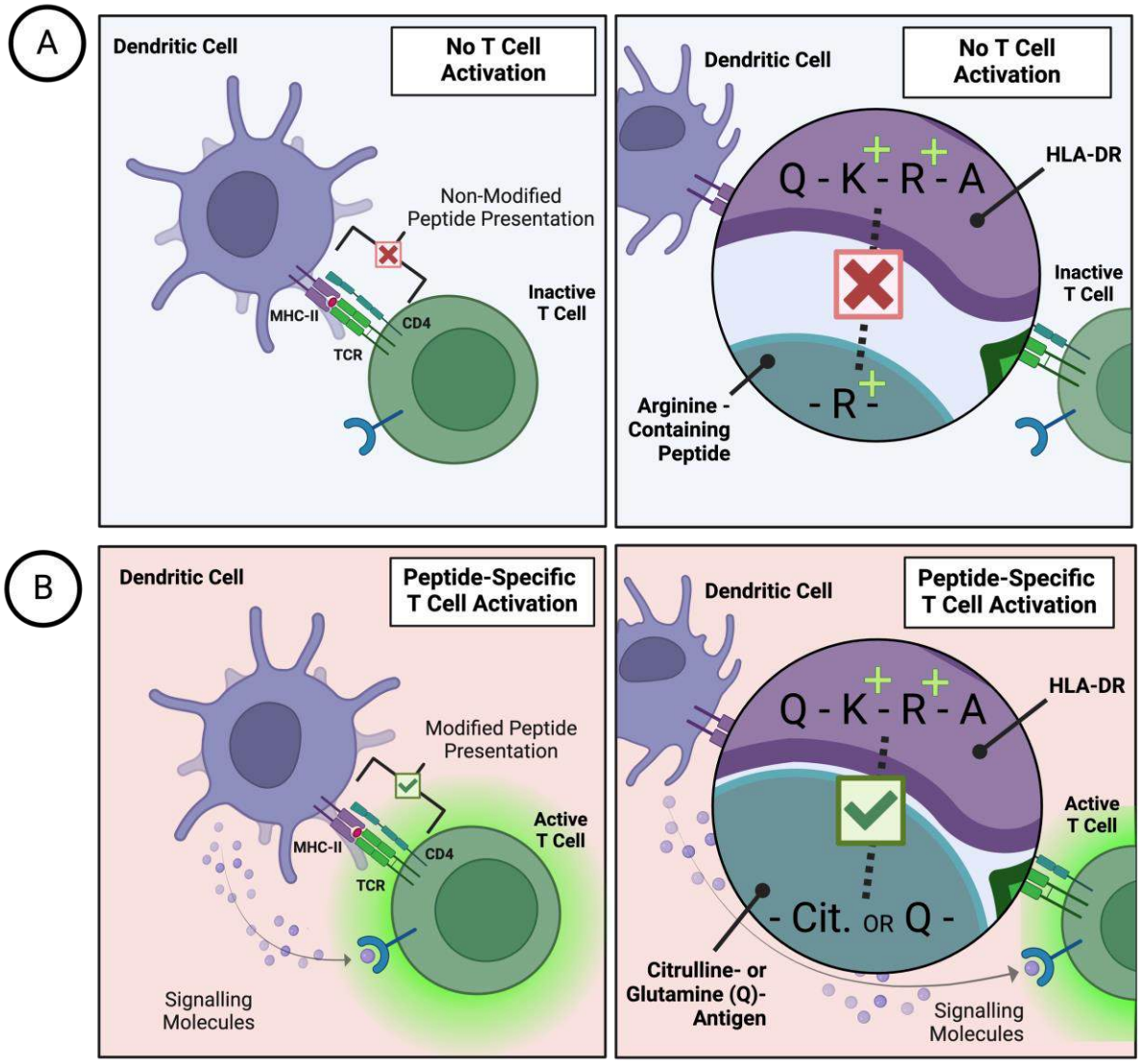

Figure 2. In an inflammatory-arthritic context, antigen (neoepitope) presentation by dendritic cells leads to autoreactive T cell activation. In healthy individuals (A), the presentation of a native/unmodified peptide by MHC class II (or HLA-DR) molecules does not lead to T cell activation. The unmodified substrate contains arginine, a positively charged residue, which does not interact favourably with the shared epitope (SE) motif in HLA-DR molecules. Following citrullination by a peptidyl-arginine deiminase enzyme, the arginine is replaced by a neutral citrulline, and the SE+ HLA-DR molecules show enhanced affinity to bind citrullinated epitopes (B), as seen in rheumatoid arthritis patients. The illustrations on the left in the panel figure, provide a broadened view of the interaction between antigen-presenting cells and an antigen-specific T cell, while the images on the right, are focused on showcasing the native and citrullinated (or glutamine-substituted – for project 1) epitopes binding with the SE+ HLA-DR groove. This figure was Created with BioRender.com.

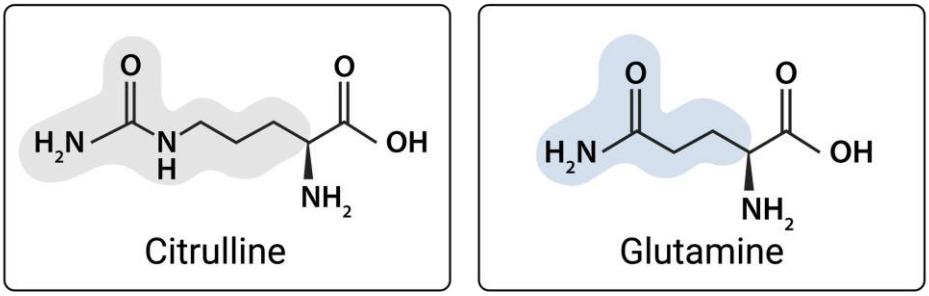

Figure 3. Glutamine and citrulline residues share a similar terminal amide (-C(=O)-NH_2) functional group and a net neutral charge at physiologic pH. This figure was Created with BioRender.com.

(A) AAV6-V1 cartoon construct.

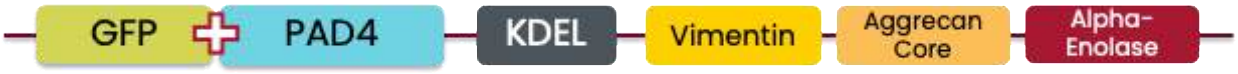

(A) AAV6-V1 plasmid map.

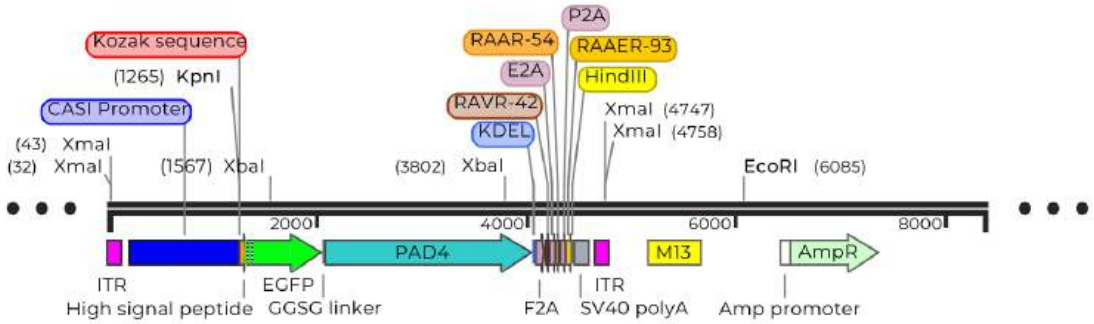

(B) AAV6-V2 cartoon construct.

(B) AAV6-V2 plasmid map.

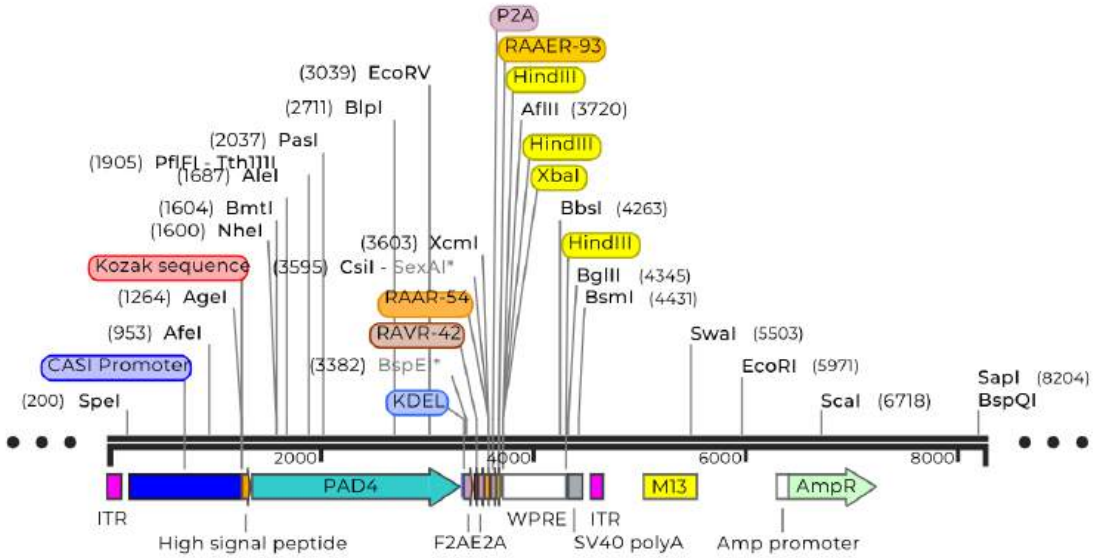

Figure 4. An overview of the two adeno-associated virus serotype 6 (AAV6) constructs developed; a cartoon depiction of the construct illustrated the key features of the vector, was followed by the plasmid map (SnapGene Viewer). In (A), the AAV6-V1 (vector 1) consisted of a green fluorescent protein (GFP) fused to the PAD4 enzyme by a GGSG flexible linker, which was followed by a downstream KDEL sequence for endoplasmic reticulum retention of the fusion protein, and three native/un-modified peptides implicated in rheumatoid arthritis, including vimentin (RAVR-42), aggrecan core (RAAR-54), and alpha-enolase (RAAER-93). In (B), the AAV6-V2 consisted of the PAD4 enzyme alone, not tagged with a fluorescent marker, followed by the same KDEL sequence as in AAV6-V1 and the three native/unmodified peptides. The AAV6-V2 construct replaced the GFP with a downstream WPRE (Woodchuck Hepatitis Virus Posttranscriptional Regulatory Element) sequence to enhance transgene expression. Both vectors were flanked by inverted terminal repeats (ITRs), and included a CASI promoter, a Kozak sequence, and a signal peptide (from the human growth hormone).

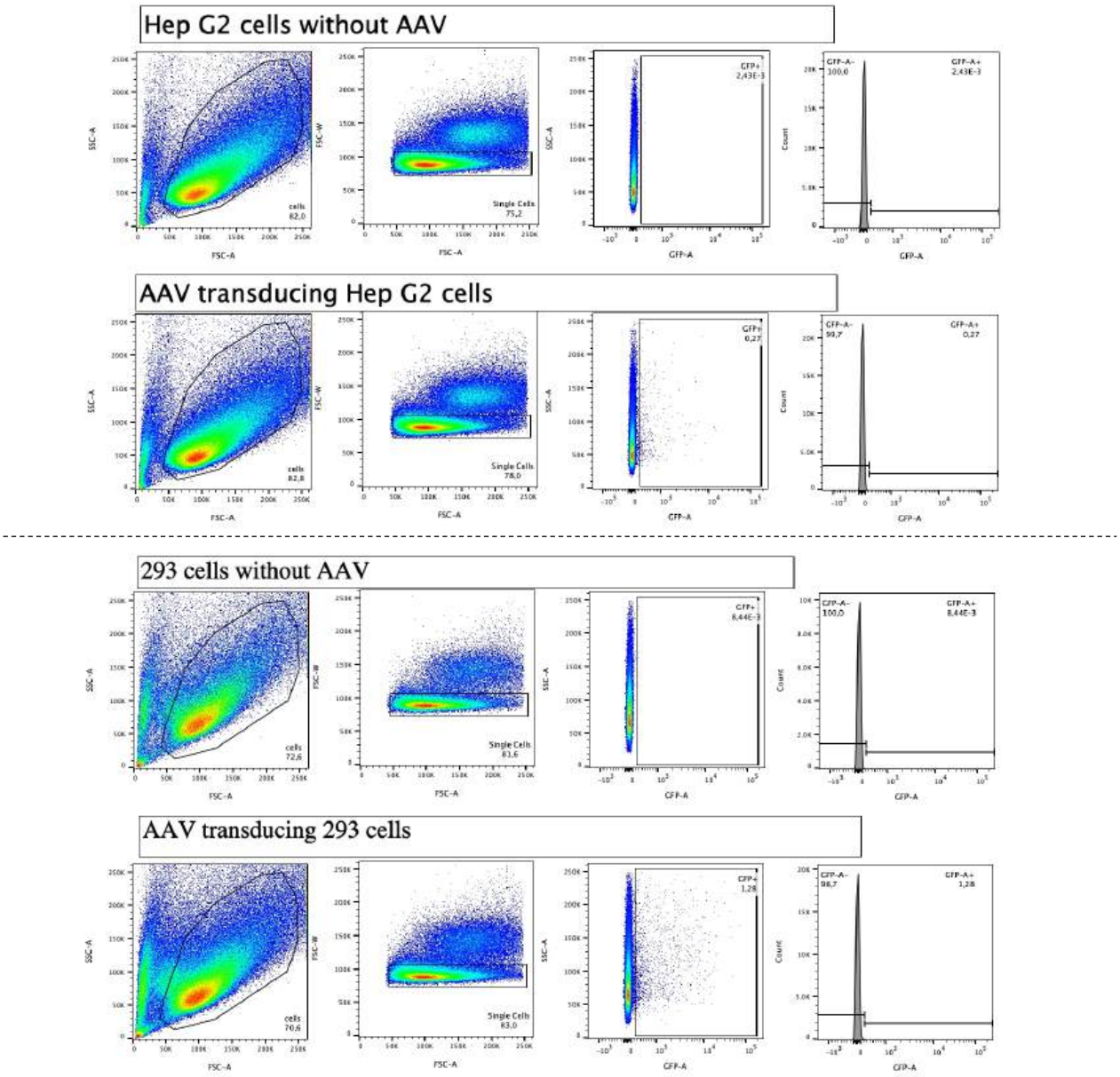

Figure 5. Flow Cytometry Gating Strategy. To confirm transduction of cells by way of detecting GFP expression, the following three step gating strategy was applied. First, side scatter-area (SSC-A) was compared against forward scatter-area (FSC-A) to detect the live cells in the sample. As SSC-A provides insight into the granularity of cells and FSC-A into cell size, live cells were farther along both axes. Second, FSC-A was compared against forward scatter-width (FSC-W) to remove any doublets. Then, using GFP fluorescence minus one (FMO), a sample of untransduced cells (negative control) was used to set the fluorescence gating boundary. Thus, when SSC-A was assessed alongside GFP, all cells successfully transduced with the virus and expressing GFP, were located within the fluorescence gate/area. *The multiplicity of infection (MOI) was 5000 for transduced cells, and the gating strategy is shown for both HEPG2 and HEK-293 cells. This figure was provided by Dr. Tom Mu.*

Table 1. Sample Characteristics (n=17), combined for RA patients (n=13) and healthy controls (n=4).

Age, mean (SD)	54.35 (14.87)
Patients	55.85 (12.86)
Healthy Controls	49.50 (21.83)
Biological Sex (%)	
Male	5/17 (29.41%)
Female	12/17 (70.59%)
Race (%)	
White	13/17 (76.47%)
Other	4/17 (23.53%)
CRP (%)	
High (≥10 mg/L)	3/16 (18.75%)
Low (<10 mg/L)	13/16 (81.25%)
ACPA Status (%)	
Positive (>20 U)	11/15 (73.33%)
Weak Positive (20-39 U)	0/15 (0.00%)
Positive (40-59 U)	1/15 (6.67%)
Strong Positive (≥60 U)	10/15 (66.67%)
Negative (<20 U)	4/15 (26.67%)
RF (%)	
High/Positive (≥20 U/mL)	9/15 (60.00%)
Low/Negative (<20 U/mL)	6/15 (40.00%)

CRP = c-reactive protein; ACPA = anti-citrullinated protein antibodies; RF = Rheumatoid Factor; mg/L = milligrams per liter; U = units; U/mL = units per milliliter. The serologic status (i.e., CRP, ACPA, RF) for two controls was unknown.

Table 2. An overview of the five peptides selected for assessing T cell responses.

Protein	Peptide Name*	Abbreviated Form	Region	Sequence
β-fibrinogen	RAFR-23	R23 or Nat23	69-83	GGYRA**R**PAKAAATQK
	RAFC-23	Cit23 or Cit23		GGYRA**{CIT}**PAKAAATQK
	RAFQ-23	Q23 or Glut23		GGYRA**Q**PAKAAATQK
	RAFR-28	R28 or Nat28	430-444	GGWWYN**R**CHAANPNG
	RAFC-28	Cit28 or Cit28		GGWWYN**{CIT}**CHAANPNG
	RAFQ-28	Q28 or Glut28		GGWWYN**Q**CHAANPNG
Aggrecan core	RAAR-54	R54 or Nat54	477-491	GVVFHY**R**PGPT**R**YSL
	RAAC-54	Cit54 or Cit54		GVVFHY**{CIT}**PGPT**{CIT}**YSL
	RAAQ-54	Q54 or Glut54		GVVFHY**Q**PGPT**Q**YSL
Anti-thrombin III	RAATR-69	R69 or Nat69	79-93	**R**VWELSKANS**R**FATT
	RAATC-69	Cit69 or Cit69		**{CIT}**VWELSKANS**{CIT}**FATT
	RAATQ-69	Q69 or Glut69		**Q**VWELSKANS**Q**FATT
	RAATR-76	R76 or Nat76	289-303	KFRY**RR**VAEGTQVLE
	RAATC-76	Cit76 or Cit76		KFRY**{CIT}{CIT}**VAEGTQVLE
	RAATQ-76	Q76 or Glut76		KFRY**QQ**VAEGTQVLE

The residue(s) modified among the peptides were bolded and underlined. *Decoding the Peptide Name: RA at the beginning stands for Rheumatoid Arthritis, which is followed by the specific protein (β-fibrinogen= F; Aggrecan Core= A; Anti-thrombin= AT), and the last letter corresponds to the configuration of the peptide (native=R; citrulline=C; glutamine=Q).

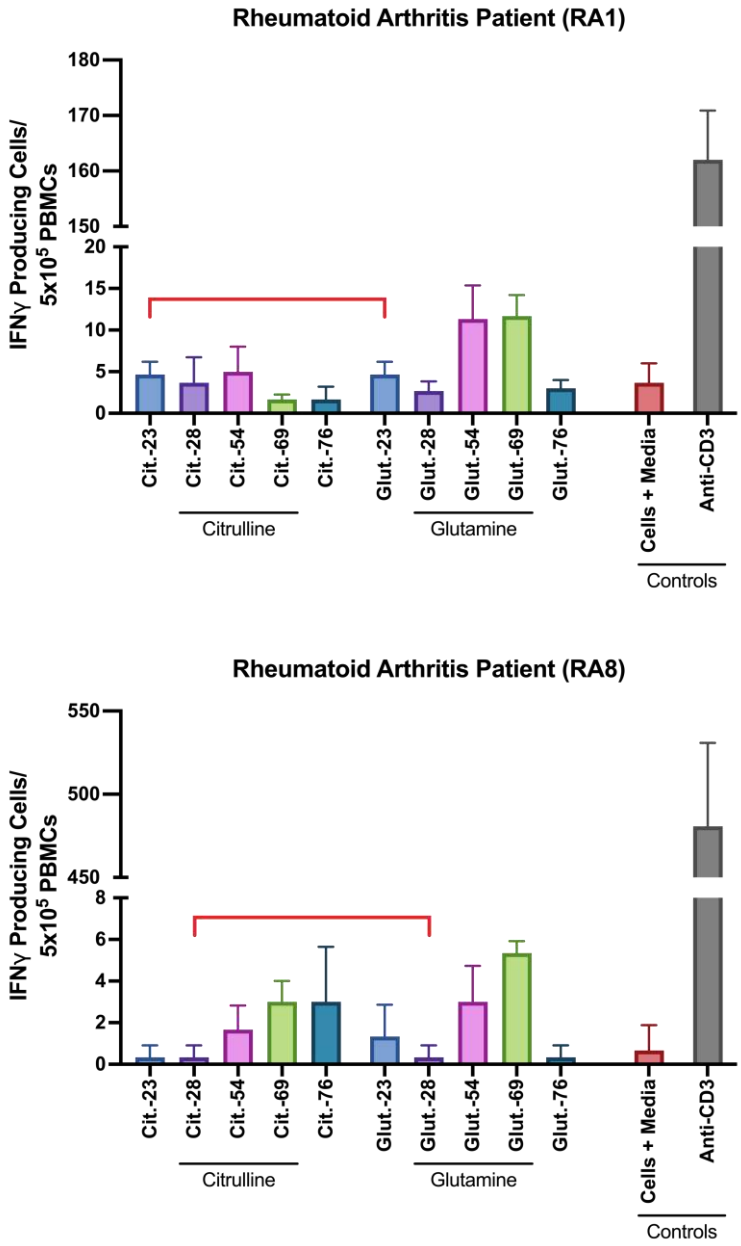

Figure 6. T cell responses of RA patients RA1 and RA8 demonstrated an equivalent immune response. For each participant, a corresponding graph comparing the native, citrullinated, and glutamine-substituted peptide responses were shown in the **Supplementary Figure 1**. Here, the graph focused only on the comparison between glutamine and its citrulline analogue, excluding T cell responses to the arginine-containing peptides. Although RA1 had an equivalent response for peptide 23, and RA8 had an equivalent response with peptide 28, these antigen-specific T cell responses were low and not significant based on the DFR(eq) test. The red bars were not used for significance, but to associate the two peptides with an equivalent magnitude of T cell response. Bar graphs plotted the mean with standard deviation for each condition.

Table 3. The average IFN-γ secreting cells across each peptide, analyzed in triplicates, are displayed for both RA patients (RA1-13) and controls (RA14-17).

This table only presents the magnitude of T cell responses to the 'Native' peptide version.

ID	R23	R28	R54	R69	R76	(-) Ctrl.	(+) Ctrl.
RA1	5.67 (2.89)	3.67 (2.08)	9.00 (2.65)	5.67 (3.51)	4.67 (1.15)	3.67 (2.34)	162.00 (8.89)
RA2	7.00 (4.58)	5.33 (2.52)	10.33 (5.03)	8.33 (4.16)	6.00 (3.00)	3.83 (2.48)	337.00 (26.3)
RA3	45.00 (5.57)	54.67 (7.51)	47.33 (13.20)	54.33 (12.66)	54.00 (6.56)	43.33 (5.16)	598.00 (26.6)
RA4	1.00 (1.00)	0.67 (0.58)	1.67 (1.53)	2.00 (1.00)	1.333 (0.58)	0.8333 (1.33)	177.70 (24.95)
RA5	0.00 (0.00)	1.67 (0.58)	4.00 (1.73)	1.33 (0.58)	1.33 (1.53)	1.17 (0.75)	524.00 (25.71)
RA6	1.67 (2.08)	1.00 (1.00)	4.33 (5.774)	0.33 (0.58)	1.33 (0.58)	0.50 (0.55)	577.70 (31.07)
RA7	0.00 (0.00)	0.00 (0.00)	0.00 (0.00)	0.00 (0.00)	0.00 (0.00)	0.00 (0.00)	217.00 (17.09)
RA8	0.33 (0.58)	0.33 (0.58)	1.13 (0.58)	0.00 (0.00)	0.00 (0.00)	0.67 (1.21)	480.70 (50.20)
RA9	0.33 (0.58)	0.00 (0.00)	0.33 (0.58)	0.00 (0.00)	0.00 (0.00)	0.00 (0.00)	413.30 (40.10)
RA10	0.33 (0.58)	0.33 (0.58)	0.00 (0.00)	0.00 (0.00)	0.67 (1.15)	1.33 (2.81)	159.00 (13.23)
RA11	1.33 (1.53)	0.00 (0.00)	0.33 (0.58)	0.00 (0.00)	0.67 (0.58)	0.00 (0.00)	24.67 (1.53)
RA12	0.67 (1.15)	2.00 (1.73)	2.33 (0.58)	0.67 (1.15)	2.00 (1.00)	1.00 (1.09)	393.30 (24.09)
RA13	1.00 (1.00)	0.00 (0.00)	2.00 (2.00)	0.33 (0.58)	1.33 (0.58)	0.83 (0.98)	140.70 (15.31)
RA14	1.67 (2.08)	0.333 (0.58)	1.33 (1.15)	2.00 (1.73)	1.33 (1.53)	1.33 (0.52)	173.30 (151.20)
RA15	1.33 (1.15)	1.33 (1.53)	1.67 (0.58)	3.33 (1.53)	1.33 (0.58)	1.50 (1.38)	41.33 (7.51)
RA16	5.00 (3.46)	4.00 (1.73)	11.33 (2.31)	4.00 (1.73)	3.00 (5.20)	6.00 (2.28)	348.00 (19.29)
RA17	2.67 (1.15)	0.67 (0.58)	1.33 (1.15)	0.67 (1.15)	1.67 (0.58)	1.00 (0.63)	53.00 (16.82)

All responses were reported as mean (standard deviation). The short forms of the peptides are abbreviated as 'R' indicating arginine or native conformation of the peptide, followed by the number of the peptide (23, 28, 54, 69, and 76). (-) Ctrl.=negative control (cells and media alone); (+) Ctrl.=positive control (anti-CD3).

This table only presents the magnitude of T cell responses to the 'Citrulline' containing peptide version.

ID	Cit23	Cit28	Cit54	Cit69	Cit76	(-) Ctrl.	(+) Ctrl.
RA1	4.67 (1.53)	3.67 (3.05)	5.00 (3.00)	1.67 (0.58)	1.67 (1.53)	3.67 (2.34)	162.00 (8.89)
RA2	7.00 (4.58)	4.00 (3.61)	8.67 (3.21)	5.00 (2.00)	3.00 (1.73)	3.83 (2.48)	337.00 (26.3)
RA3	61.67 (2.08)	49.00 (4.58)	68.00 (17.78)	32.67 (2.08)	27.00 (5.29)	43.33 (5.16)	598.00 (26.6)
RA4	0.67 (1.15)	1.33 (1.53)	1.67 (1.53)	1.00 (0.00)	0.67 (1.15)	0.83 (1.33)	177.70 (24.95)
RA5	2.00 (1.73)	2.33 (0.58)	2.67 (2.52)	0.33 (0.58)	0.00 (0.00)	1.17 (0.75)	524.00 (25.71)
RA6	0.33 (0.58)	2.00 (2.00)	1.67 (1.15)	2.67 (3.05)	0.33 (0.58)	0.50 (0.55)	577.70 (31.07)
RA7	0.00 (0.00)	0.00 (0.00)	1.67 (1.15)	0.00 (0.00)	0.00 (0.00)	0.00 (0.00)	217.00 (17.09)
RA8	0.33 (0.578)	0.33 (0.58)	1.67 (1.15)	3.00 (1.00)	3.00 (2.65)	0.67 (1.21)	480.70 (50.20)
RA9	0.33 (0.58)	0.00 (0.00)	0.33 (0.58)	0.00 (0.00)	0.00 (0.00)	0.00 (0.00)	413.30 (40.10)
RA10	1.00 (1.73)	0.00 (0.00)	3.67 (5.51)	0.00 (0.00)	0.00 (0.00)	1.33 (2.81)	159.00 (13.23)
RA11	0.33 (0.58)	0.33 (0.58)	1.33 (1.15)	0.00 (0.00)	0.33 (0.58)	0.00 (0.00)	24.67 (1.53)
RA12	0.33 (0.58)	0.33 (0.58)	7.33 (2.89)	2.33 (0.58)	3.00 (1.00)	1.00 (1.09)	393.30 (24.09)
RA13	0.33 (0.58)	0.67 (0.58)	3.00 (2.00)	0.00 (0.00)	0.33 (0.58)	0.83 (0.98)	140.70 (15.31)
RA14	1.00 (1.00)	0.00 (0.00)	5.33 (3.51)	0.33 (0.58)	0.33 (0.58)	1.33 (0.52)	173.30 (151.20)
RA15	1.33 (1.53)	1.00 (0.00)	3.00 (2.00)	1.33 (1.15)	2.00 (0.00)	1.50 (1.38)	41.33 (7.51)
RA16	7.67 (3.51)	5.00 (2.65)	6.00 (1.00)	4.67 (2.52)	16.33 (10.21)	6.00 (2.28)	348.00 (19.29)
RA17	3.67 (2.52)	0.67 (0.58)	1.33 (0.58)	0.67 (1.15)	0.67 (0.58)	1.00 (0.63)	53.00 (16.82)

All responses were reported as mean (standard deviation). The short forms of the peptides are abbreviated as 'Cit' indicating the citrulline-containing version of the peptide, followed by the number of the peptide (23, 28, 54, 69, and 76). (-) Ctrl.=negative control (cells and media alone); (+) Ctrl.=positive control (anti-CD3).

This table only presents the magnitude of T cell responses to the 'Glutamine' containing peptide version.

ID	Q23	Q28	Q54	Q69	Q76	(-) Ctrl.	(+) Ctrl.
RA1	4.67 (1.53)	2.67 (1.15)	11.33 (4.04)	11.67 (2.52)	3.00 (1.00)	3.67 (2.34)	162.00 (8.89)
RA2	4.67 (3.05)	4.67 (4.04)	71.33 (26.39)	25.33 (5.03)	8.00 (2.65)	3.83 (2.48)	337.00 (26.3)
RA3	61.33 (12.06)	64.67 (3.21)	64.67 (8.50)	53.00 (14.73)	65.33 (4.93)	43.33 (5.16)	598.00 (26.6)
RA4	1.33 (1.53)	2.00 (1.00)	3.67 (1.53)	5.33 (1.53)	1.00 (1.00)	0.83 (1.33)	177.70 (24.95)
RA5	2.67 (0.58)	0.33 (0.58)	2.33 (0.58)	3.00 (2.65)	1.67 (0.58)	1.17 (0.75)	524.00 (25.71)
RA6	1.00 (1.00)	7.33 (8.39)	2.33 (0.58)	1.67 (2.08)	1.67 (2.08)	0.50 (0.55)	577.70 (31.07)
RA7	0.00 (0.00)	0.00 (0.00)	0.00 (0.00)	0.00 (0.00)	4.00 (4.00)	0.00 (0.00)	217.00 (17.09)
RA8	1.33 (1.53)	0.33 (0.58)	3.00 (1.73)	5.33 (0.58)	0.33 (0.58)	0.67 (1.21)	480.70 (50.20)
RA9	0.00 (0.00)	1.00 (1.73)	0.67 (1.15)	0.33 (0.58)	1.33 (1.53)	0.00 (0.00)	413.30 (40.10)
RA10	0.00 (0.00)	0.33 (0.58)	2.67 (3.79)	0.67 (0.58)	3.33 (1.53)	1.33 (2.81)	159.00 (13.23)
RA11	0.00 (0.00)	0.00 (0.00)	0.33 (0.58)	0.00 (0.00)	1.33 (2.31)	0.00 (0.00)	24.67 (1.53)
RA12	0.00 (0.00)	2.33 (1.53)	1.00 (1.00)	0.33 (0.58)	1.67 (0.58)	1.00 (1.09)	393.30 (24.09)
RA13	1.00 (1.00)	0.67 (1.15)	0.00 (0.00)	2.00 (1.00)	1.67 (1.53)	0.83 (0.98)	140.70 (15.31)
RA14	1.67 (0.58)	1.67 (0.58)	1.33 (0.58)	3.67 (1.53)	2.33 (1.53)	1.33 (0.52)	173.30 (151.20)
RA15	0.33 (0.58)	1.00 (1.00)	2.00 (1.00)	2.00 (1.00)	2.33 (1.53)	1.50 (1.38)	41.33 (7.51)
RA16	3.33 (3.21)	21.67 (3.79)	5.00 (2.00)	30.67 (7.51)	6.33 (5.03)	6.00 (2.28)	348.00 (19.29)
RA17	2.00 (1.00)	1.33 (1.53)	1.00 (1.00)	2.00 (1.00)	1.33 (2.31)	1.00 (0.63)	53.00 (16.82)

All responses were reported as mean (standard deviation). The short forms of the peptides are abbreviated as 'Q' indicating the glutamine-containing version of the peptide, followed by the number of the peptide (23, 28, 54, 69, and 76). (-) Ctrl.=negative control (cells and media alone); (+) Ctrl.=positive control (anti-CD3).

Table 4. Summary of all positive (or significant) T cell responses for both RA patients (RA1-13) and controls (RA14-17).

ID	Cit23	Cit28	Cit54	Cit69	Cit76	Q23	Q28	Q54	Q69	Q76
RA1	-	-	-	-	-	-	-	+	+	-
RA2	-	-	-	-	-	-	-	+	+	-
RA3	+	-	+	-	-	+	+	+	-	+
RA4	-	-	-	-	-	-	-	+	+	-
RA5	-	-	-	-	-	-	-	-	-	-
RA6	-	-	-	-	-	-	+	-	-	-
RA7	-	-	-	-	-	-	-	-	-	-
RA8	-	-	-	-	-	-	-	-	+	-
RA9	-	-	-	-	-	-	-	-	-	-
RA10	-	-	-	-	-	-	-	-	-	-
RA11	-	-	-	-	-	-	-	-	-	-
RA12	-	-	+	-	-	-	-	-	-	-
RA13	-	-	-	-	-	-	-	-	-	-
RA14	-	-	+	-	-	-	-	-	+	-
RA15	-	-	-	-	-	-	-	-	-	-
RA16	-	-	-	-	+	-	+	-	+	-
RA17	-	-	-	-	-	-	-	-	-	-

The '+' sign is indicative of a positive/significant immune response based on the DFR(eq) statistical tool. Native peptide responses were *not shown*: only peptide R54 for RA1, RA2, RA5, and RA16 was significant.

Table 5. A summary for all RA patients (RA1-13) and controls (RA14-17) meeting the parameters of the ELISPOT assay.

ID	Criterion 1: An equivalent response between the same citrulline peptide and its glutamine-substituted variant. Met: Yes (Y) or No (N)	Peptide Pair Identity	Criterion 2: The citrulline-glutamine pair(s) have a higher T cell response than their native counterpart. Met: Yes (Y) or No (N)	Criterion 3: A positive response for the citrulline-glutamine peptide pair(s). Met: Yes (Y) or No (N)
RA1	Y	Cit23 – Glut23	N	N
RA2	N	-	N	N
RA3	N	-	N	N
RA4	N	-	N	N
RA5	N	-	N	N
RA6	N	-	N	N
RA7	N	-	N	N
RA8	Y	Cit28 – Glut28	N (equivalent)	N
RA9	N	-	N	N
RA10	N	-	N	N
RA11	N	-	N	N
RA12	N	-	N	N
RA13	Y	Cit28 – Glut28	N	N
RA14	N	-	N	N
RA15	Y	Cit28 – Glut28	N	N
RA16	N	-	N	N
RA17	N	-	N	N

The positive/significant immune response in criterion 3 was based on the results of the DFR(eq) statistical test.

A

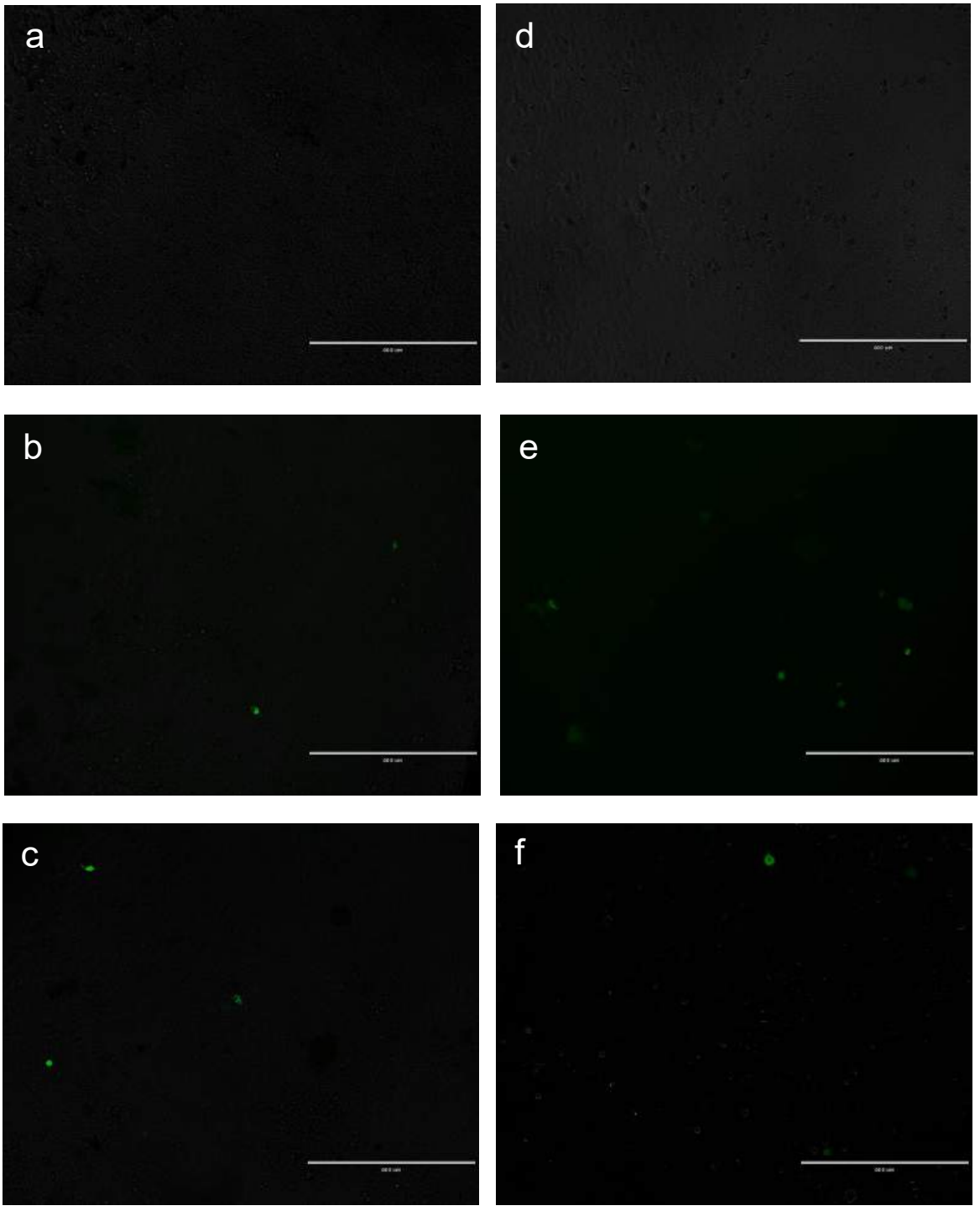

a: HEPG2 cells untransduced; b: HEPG2 cells 4-days post-transduction; c: HEPG2 cells 5-days post-transduction; d: HEK-293 cells untransduced; e: HEK-293 cells 4-days post-transduction; f: HEK-293 cells 5-days post-transduction.

B

HEPG2 cells without AAV

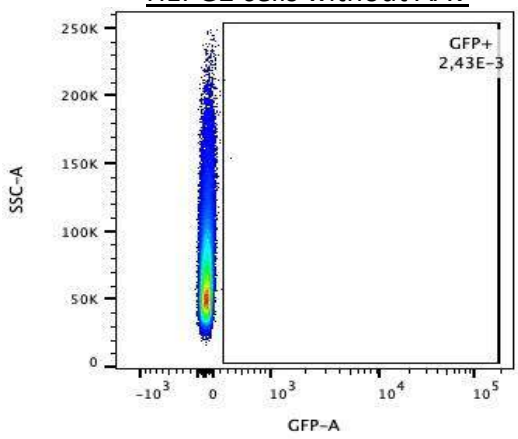

AAV transsduced HEPG2 cells

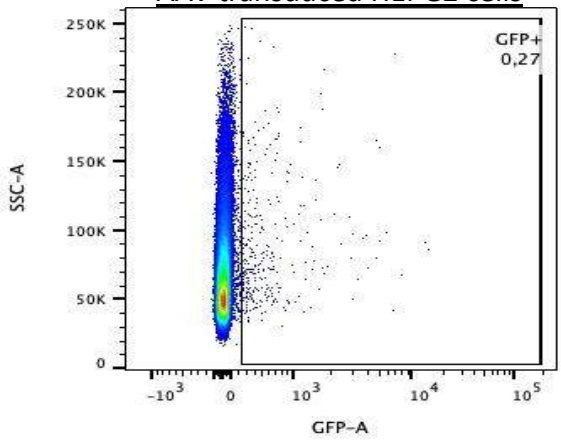

HEK-293 cells without AAV

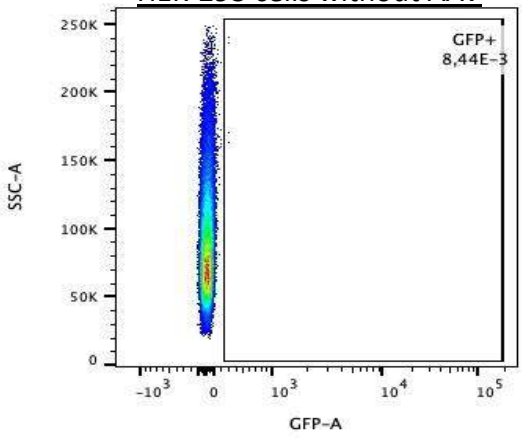

AAV transsduced HEK-293 cells

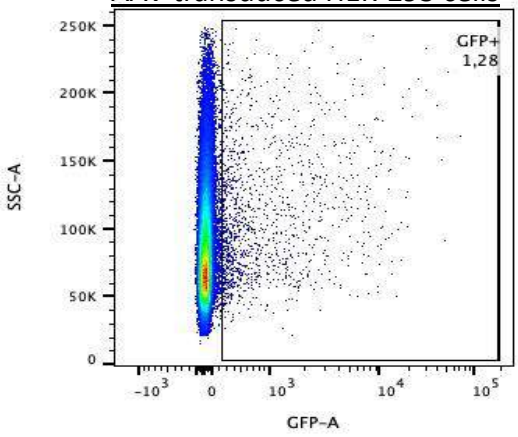

C

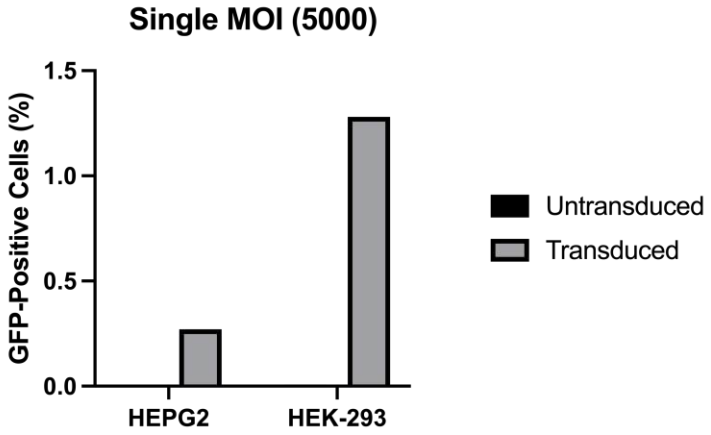

Figure 7. Detection of GFP-positive HEPG2 and HEK-293 cells. Both cell lines were infected at a single MOI of 5000 and (A) the EVOS microscope images (10x magnification) confirmed viral transduction through GFP detection (green spots) over 4 and 5 days of incubation, as compared to the untransduced cells in image a. (B) Data from Flow Cytometry showed that the proportion of GFP+ cells infected with the virus was 0.27% for HEPG2 and 1.28% for HEK-293 cells. (C) An alternative representation of the results from Flow Cytometry compared the percent of GFP+ cells across infected and uninfected cells.

A

48 Hours Post-Transduction

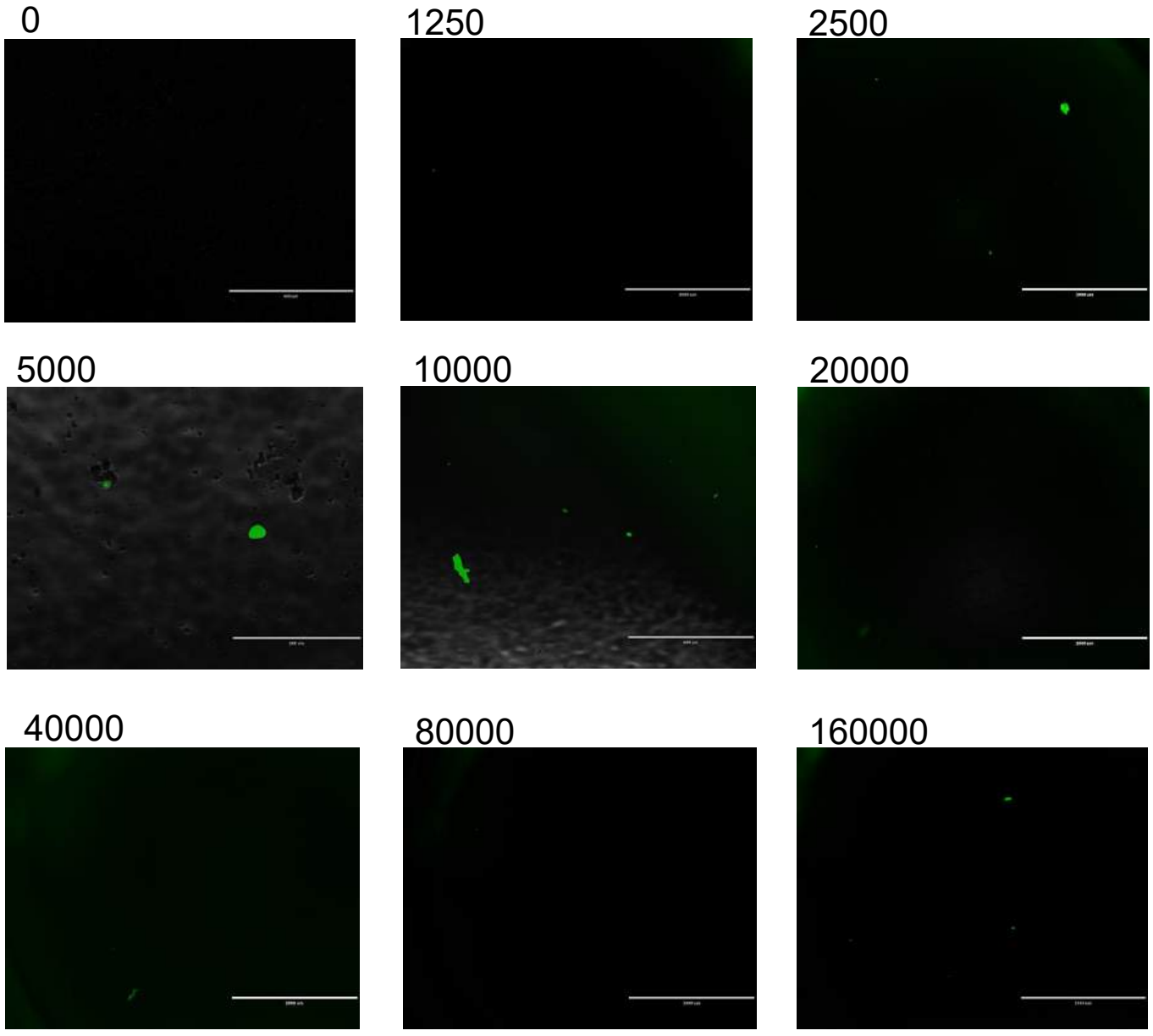

96 Hours Post-Transduction

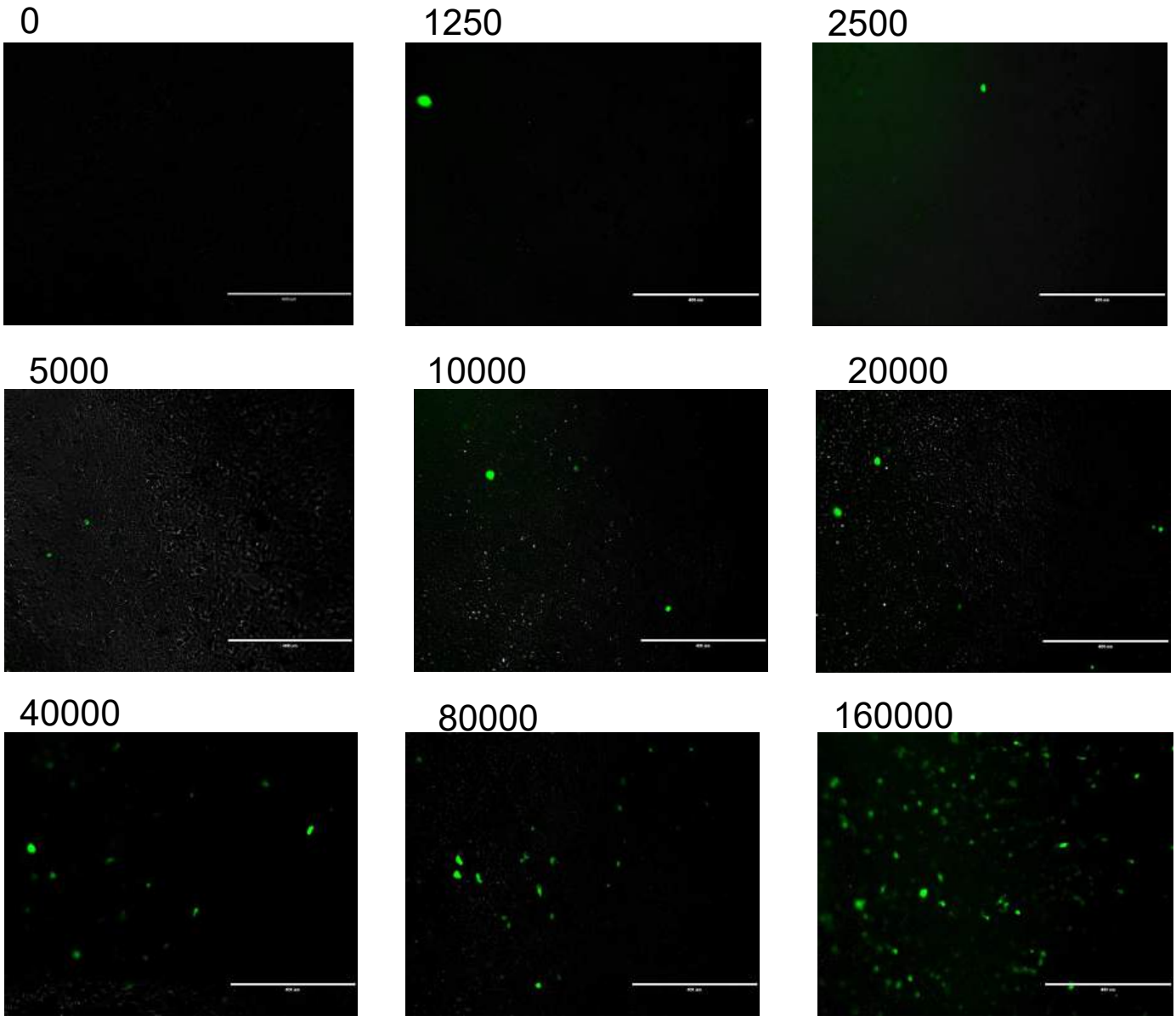

144 Hours Post-Transduction

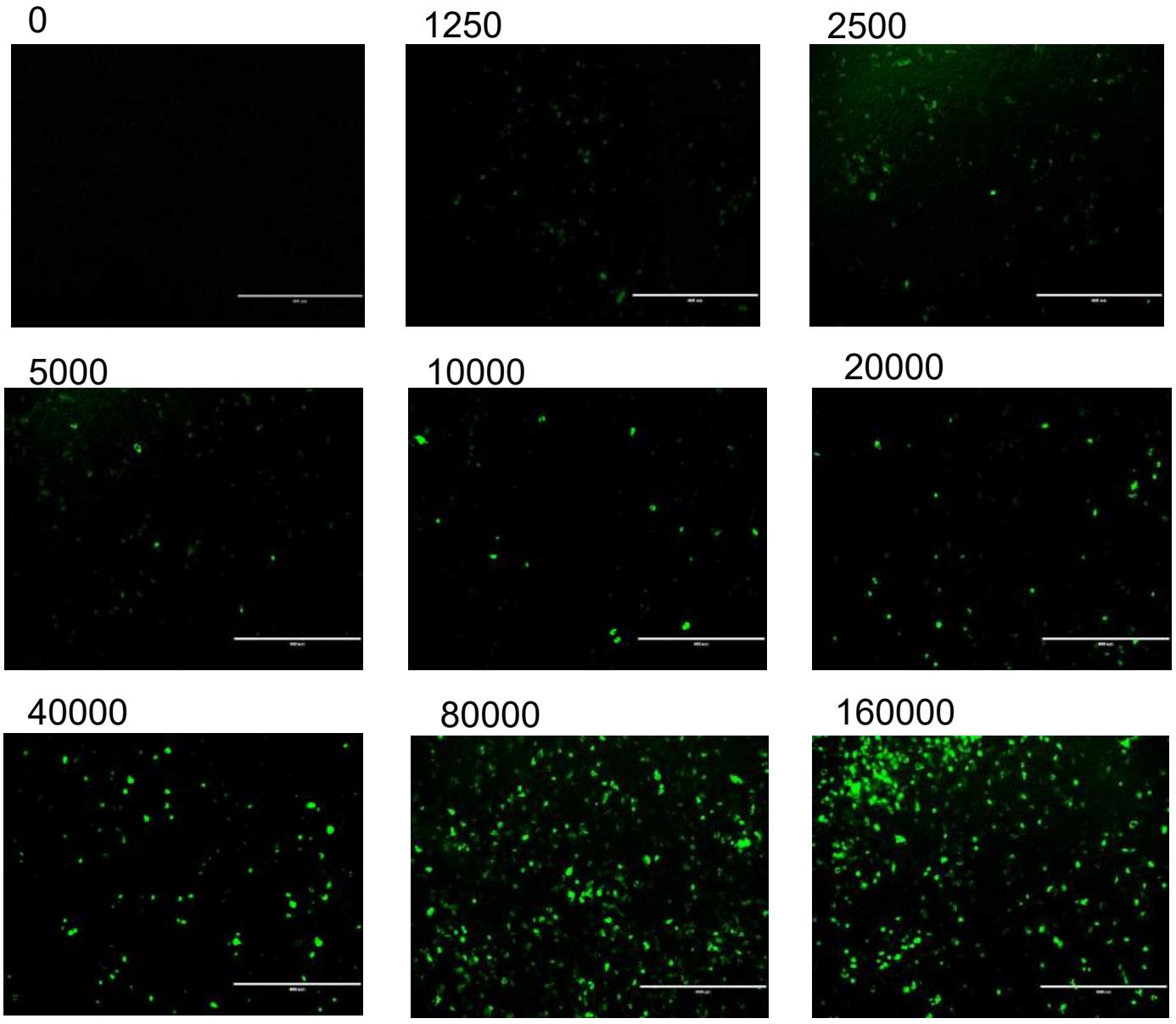

B

0

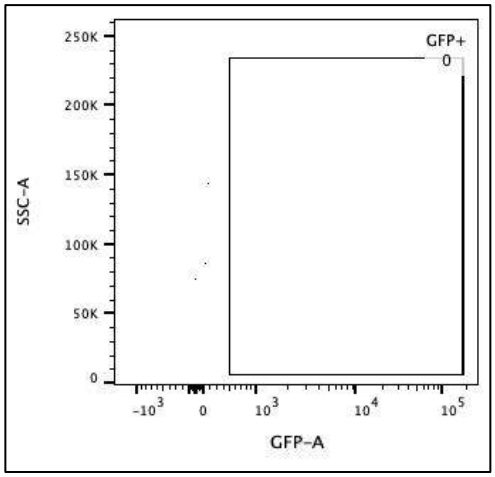

1250

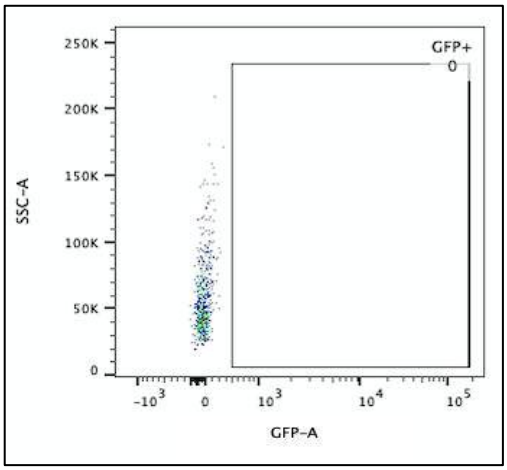

2500

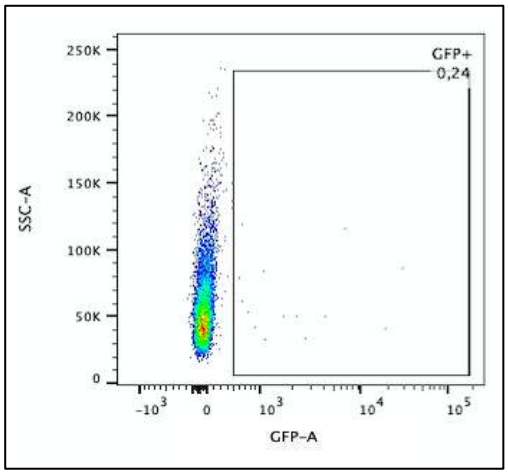

5000

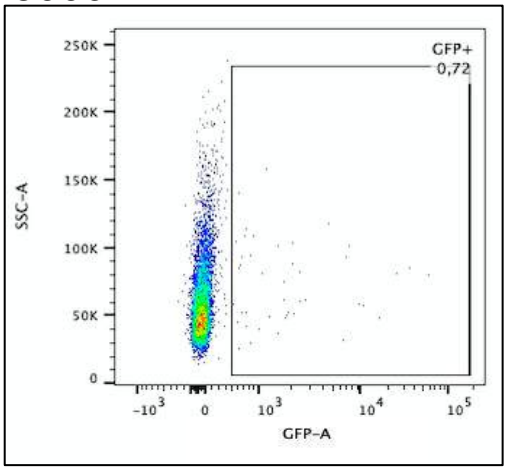

10000

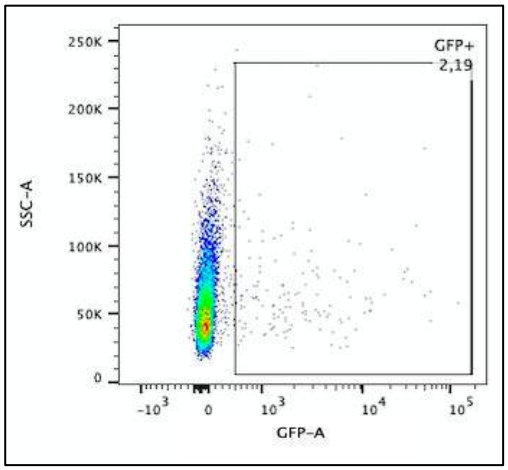

20000

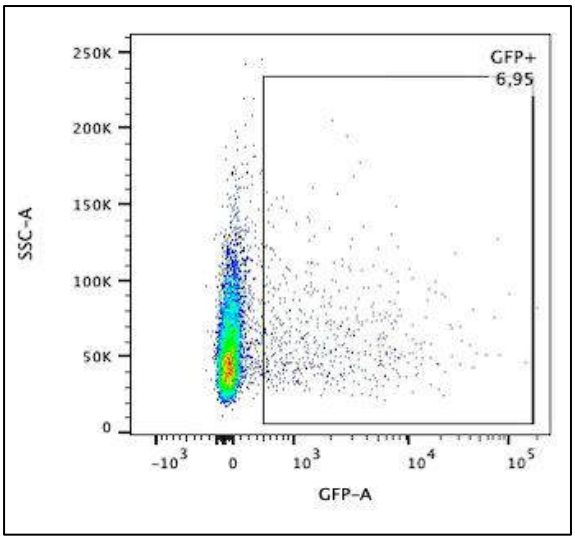

40000

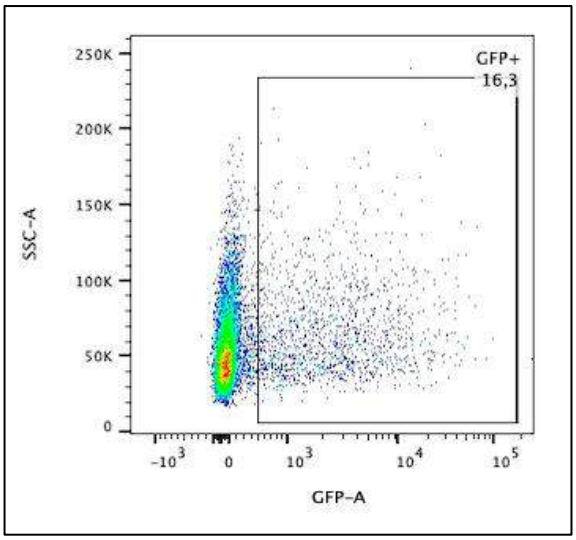

80000

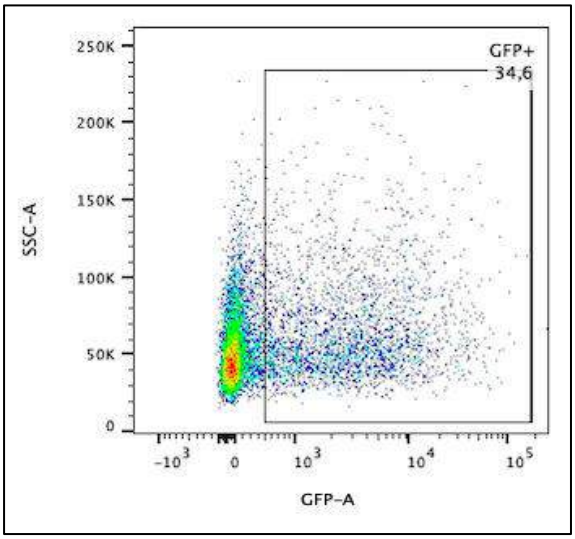

160000

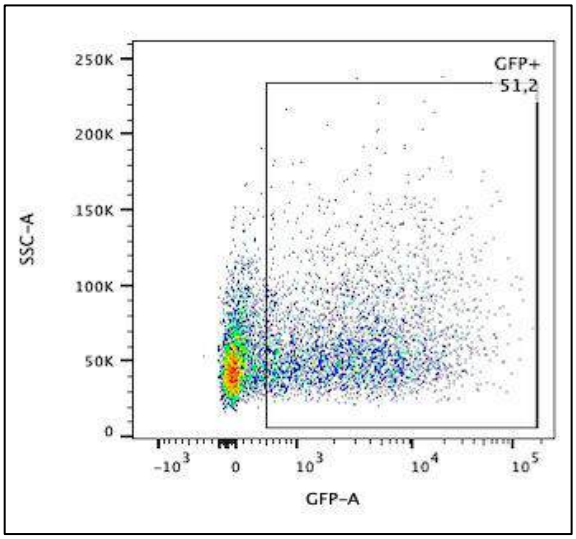

C

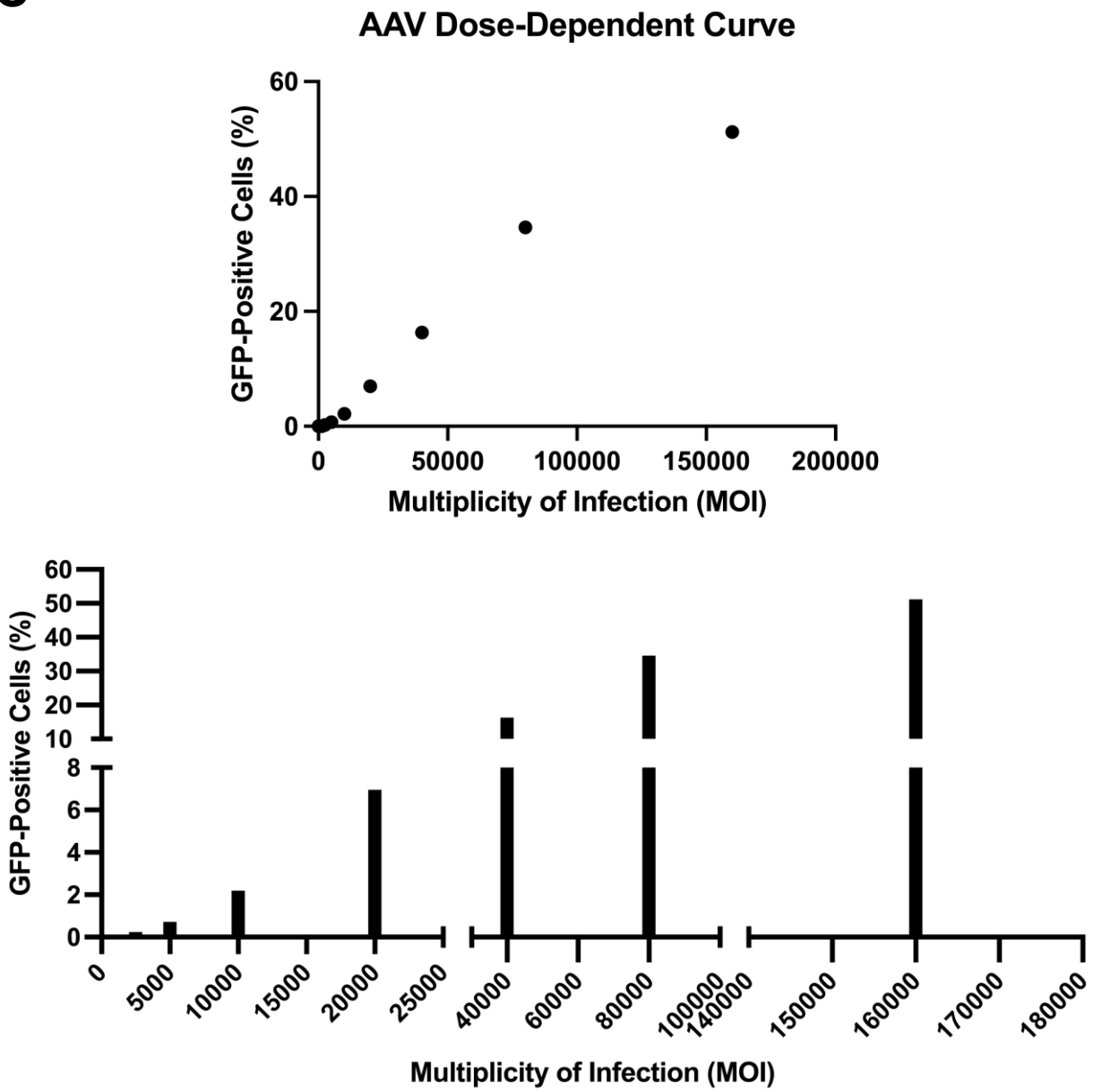

Figure 8. The proportion of GFP-positive HEPG2 cells increased with a higher multiplicity of infection (MOI). In (A), images taken with the EVOS microscope (10x magnification) at 48-, 96-, and 144-hours post-transduction demonstrated more detectable green-fluorescing cells as the MOI and length of incubation increased. In (B) each graph of Flow Cytometry data corresponds to the different MOIs tested and imaged in (A). Data from Flow cytometry confirmed expression of the fluorescent protein and revealed that about 51% of cells were transduced at an MOI of 160,000. In (C), a dose-dependent curve was evident for the AAV with increasing MOI that appears to begin plateauing near the 160,000 MOI mark. *The MOI for each condition analyzed was provided directly above the image or the corresponding flow cytometry graph, ranging from 0 (no infection) to 160,000.*

A

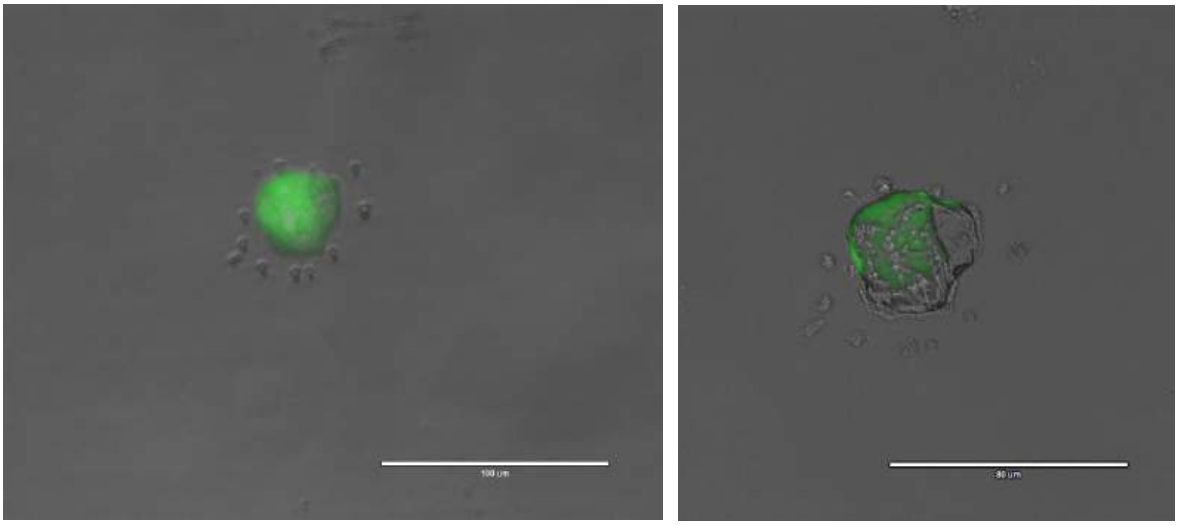

B

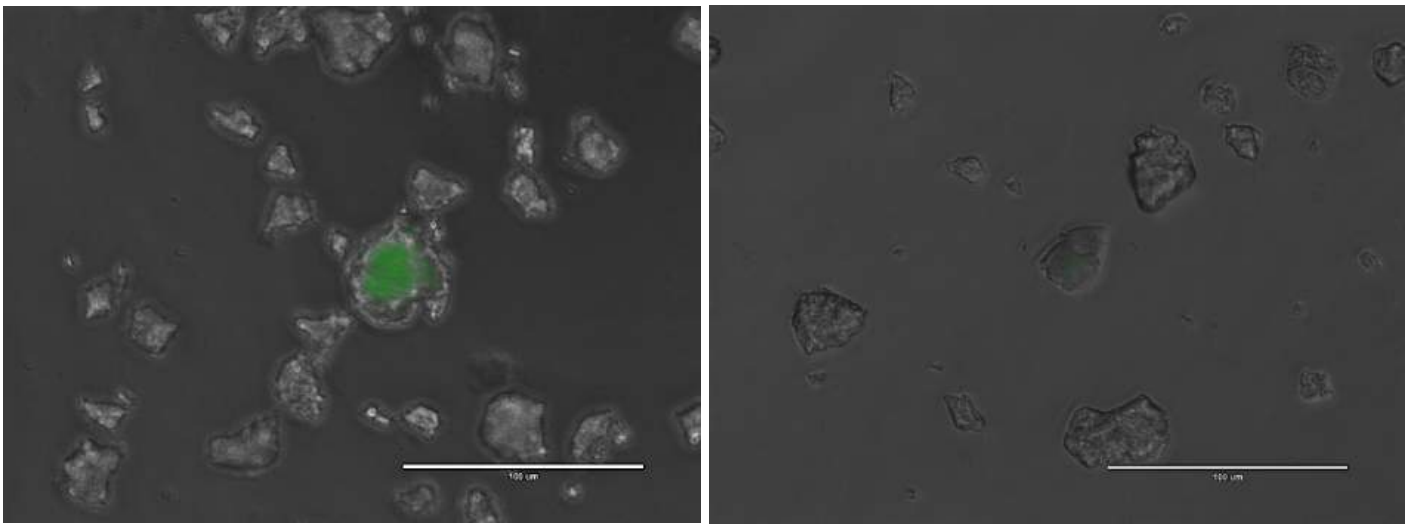

Figure 9. Assessing PAD4 subcellular location using higher magnifications of the EVOS microscope for both HEPG2 and HEK-293 cells 48 hours post-transduction. As evident in (A), HEPG2 cells were GFP+ following transduction with AAV6-V1. The image on the left was taken at a magnification of 40x, and the image on the right was 50x. Despite increasing the magnification, the subcellular location of the GFP-PAD4 fusion protein could not be confirmed. In (B), HEK-293 cells were imaged at 40x, and with most of the cell fluorescing, it was difficult to conclude intracellular PAD4 localization.

A

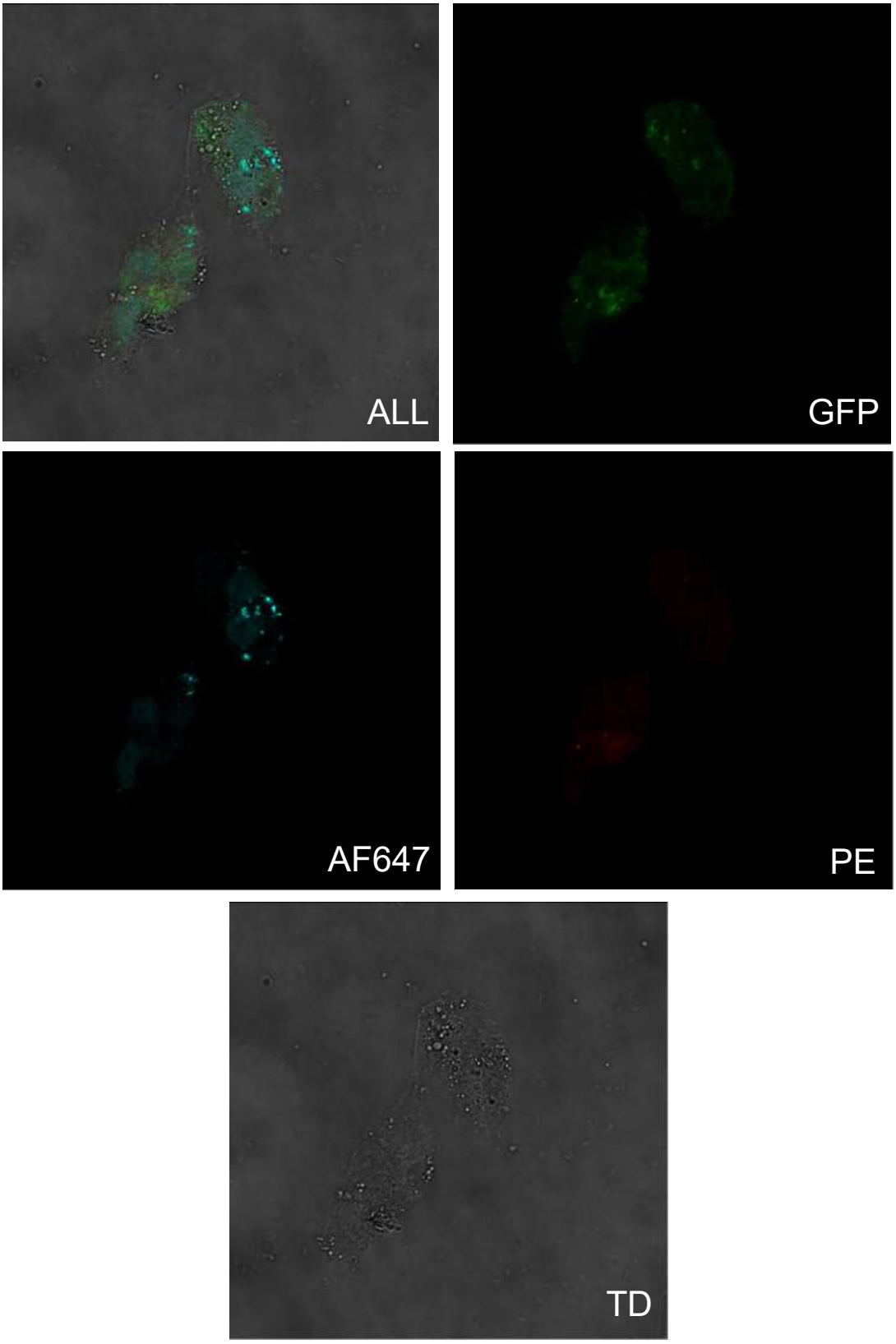

B

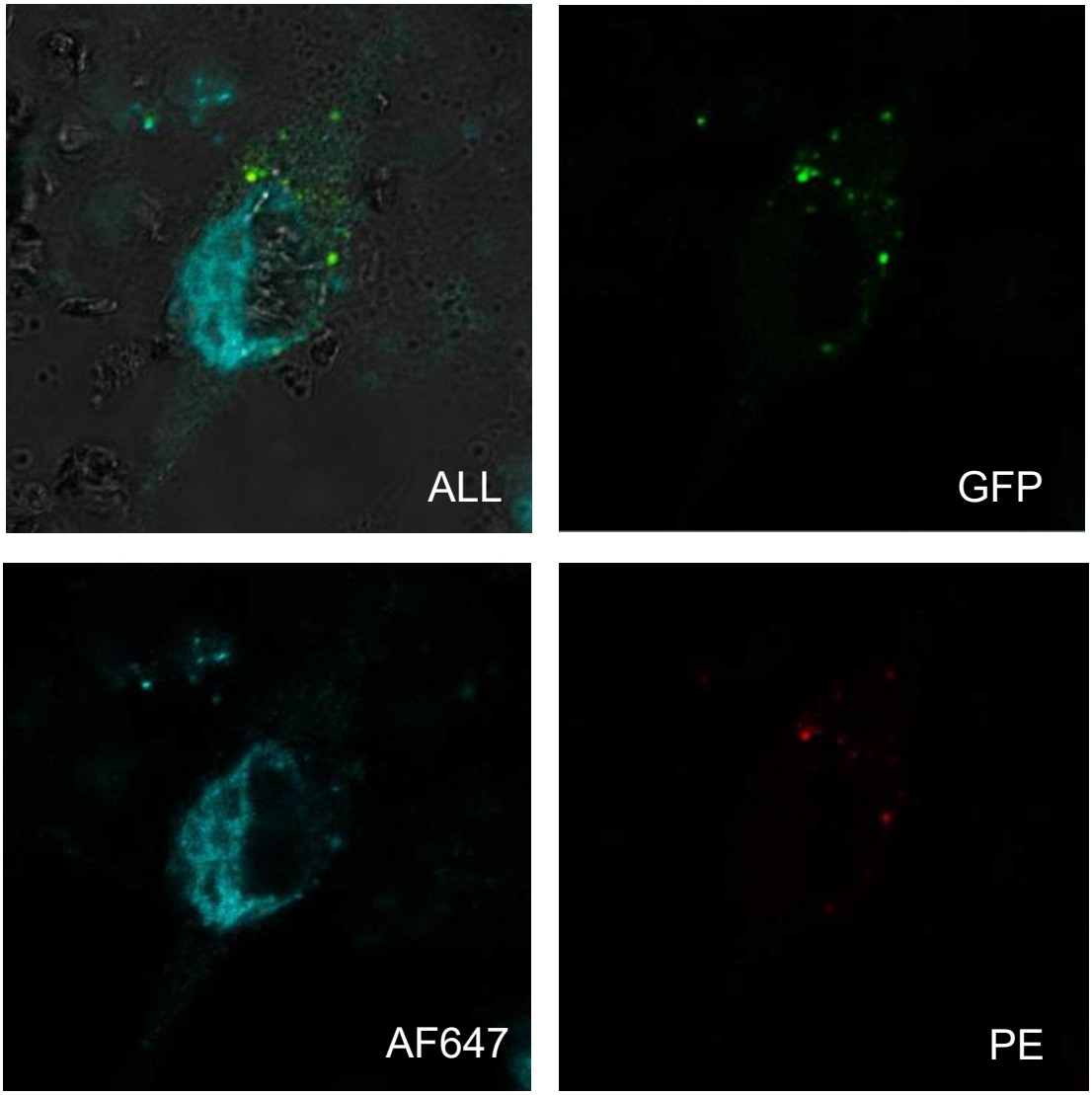

C

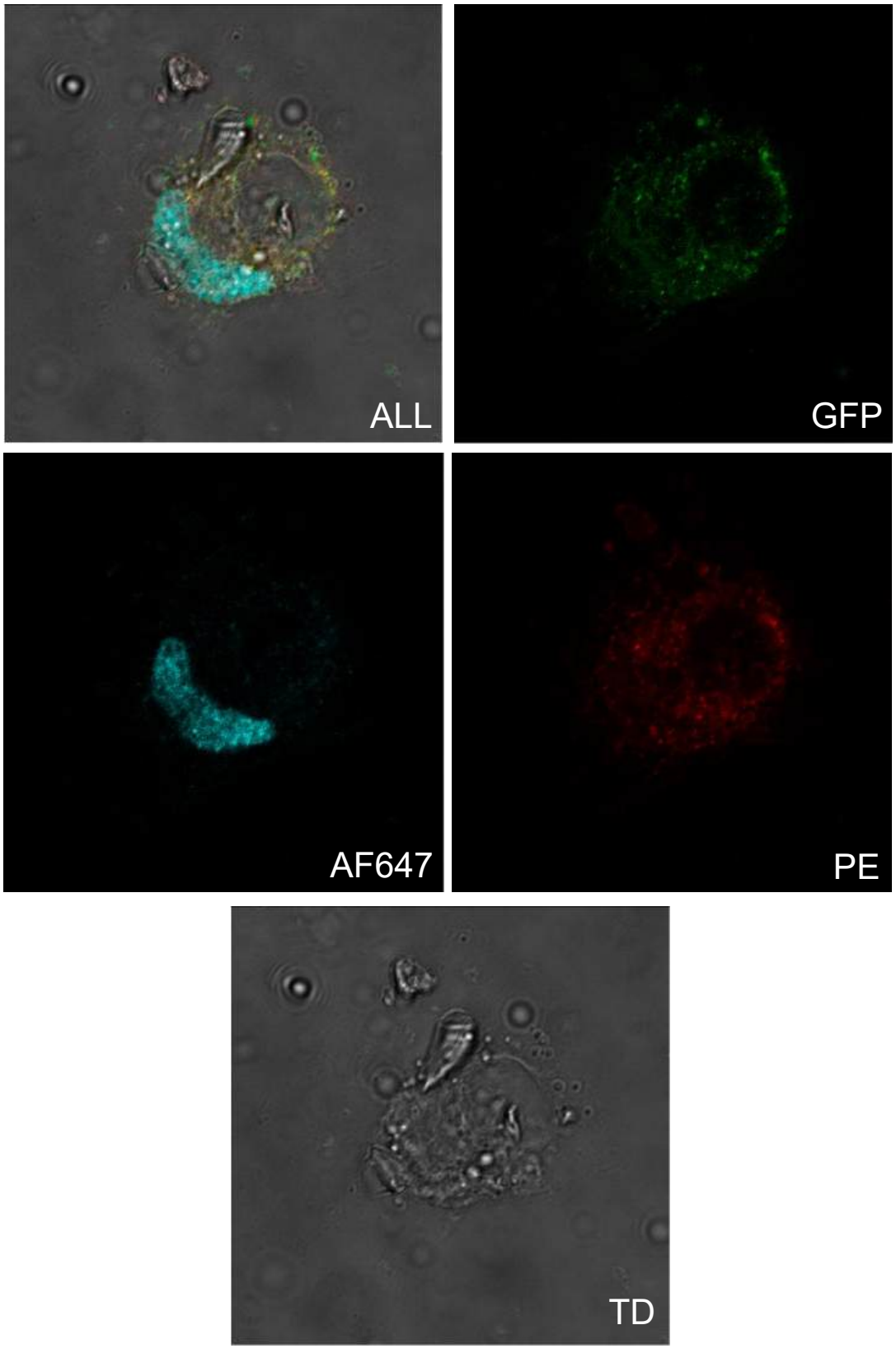

Figure 10. HEPG2 and HEPA1-6 cells were transduced with AAV6-V1 for 96 hours and imaged using a confocal microscope. Only the data for HEPG2 cells was shown here. Each subfigure contained five panels: ALL (which overlayed all the fluorescent channels into a single image); GFP (only presented the GFP fluorescence signal); PE (displayed only the PE signal); AF647 (displayed calreticulin binding in the ER and some other cellular locations); TD (transmitted detector; showed the cells without any fluorescent channels active). Although cannot be seen in the images, the scale was 10 μm. In (A), the negative control or untransduced cells (0 MOI) were stained with multiple antibodies including, an unconjugated rabbit anti-PAD4, a biotinylated anti-rabbit secondary, followed by a Streptavidin-PE (red) for the biotin secondary antibody, and a conjugated AF647 (cyan) anti-calreticulin antibody. These cells were not transduced with AAV6-V1, which encoded for the GFP-PAD4 fusion protein. As evident in (A), the GFP and PE images in the panel demonstrated a very faint signal owing to background noise due to cellular autofluorescence. The AF647 fluorophore demonstrated binding to the calreticulin protein and labelling the ER (endoplasmic reticulum). In (B), only the anti-calreticulin antibody was used for staining on non-infected cells to further confirm appropriate ER labelling. The GFP and PE images showed some autofluorescence, but the AF647 was able to outline the ER. In (C), virally infected cells at an MOI of 160,000, demonstrated a higher GFP and PE signal, as expected, given that both signals were targeting the same fusion protein. The lack of overlap between the ER-antibody conjugated with AF647 (cyan), and the GFP (green) and PE (red) signal for the fusion protein, demonstrated a non-ER distribution of the fusion protein.

A

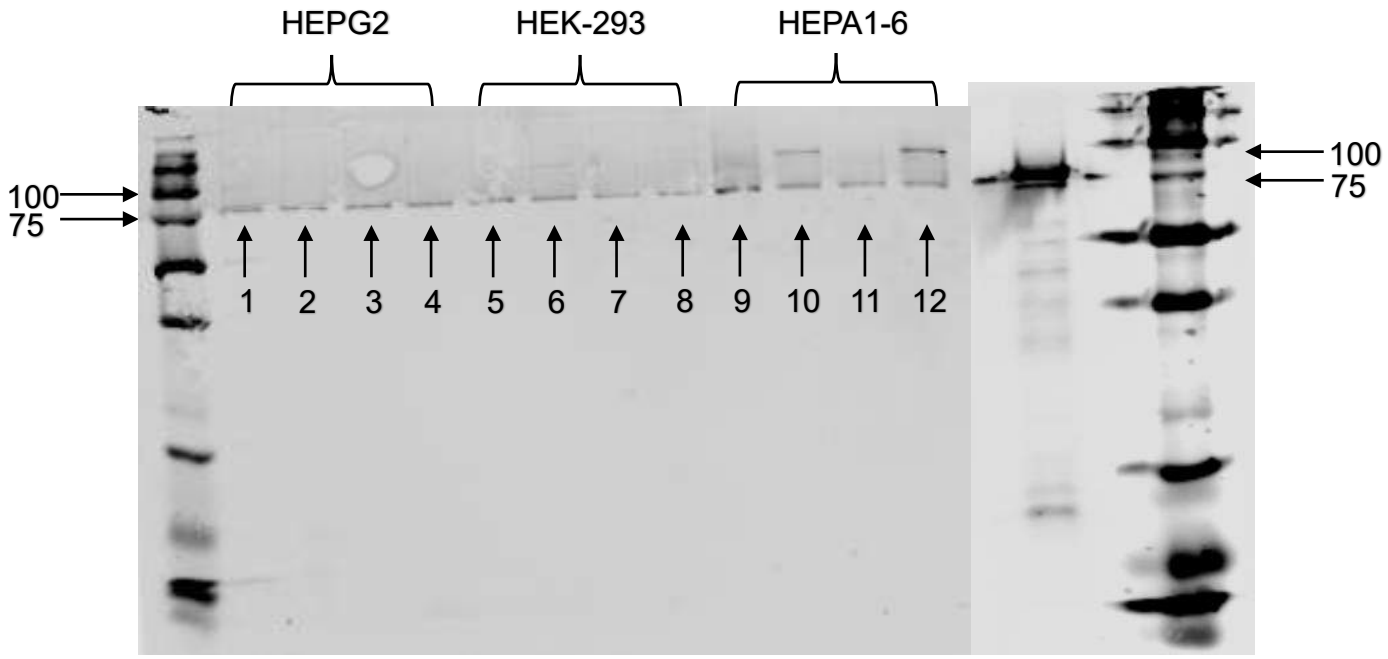
HEPG2
HEK-293
HEPA1-6
100
75
1 2 3 4 5 6 7 8 9 10 11 12
100
75

B

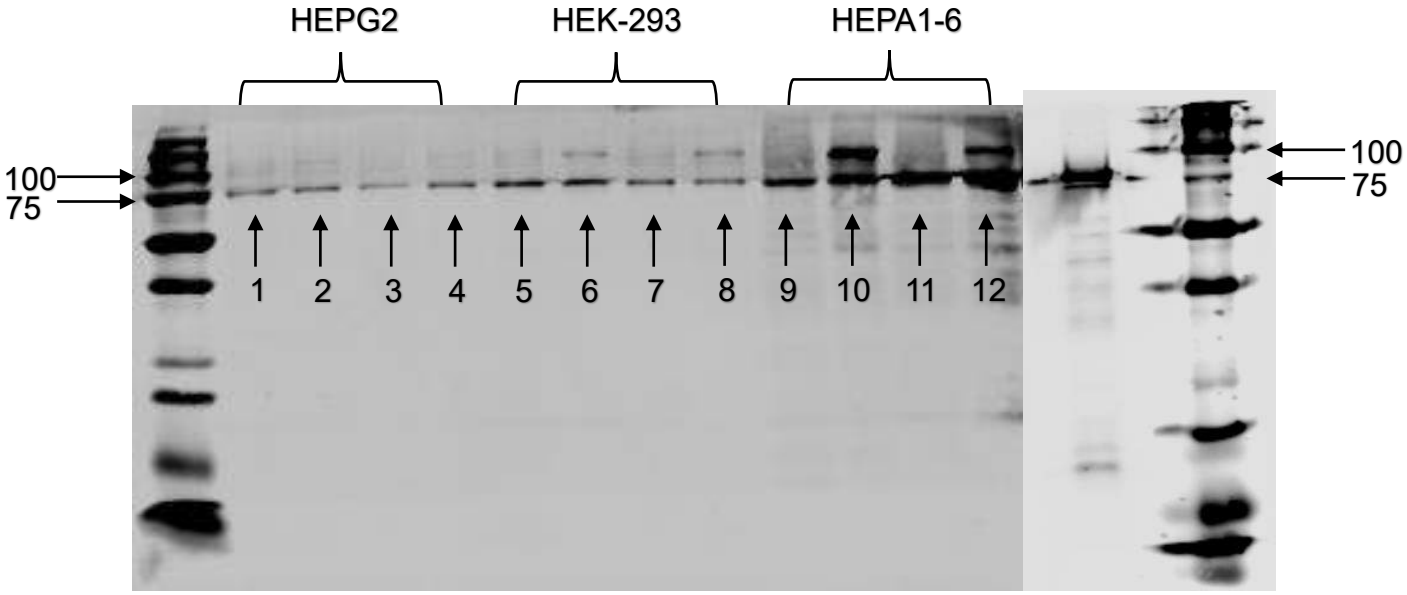
HEPG2
HEK-293
HEPA1-6
100
75
1 2 3 4 5 6 7 8 9 10 11 12
100
75

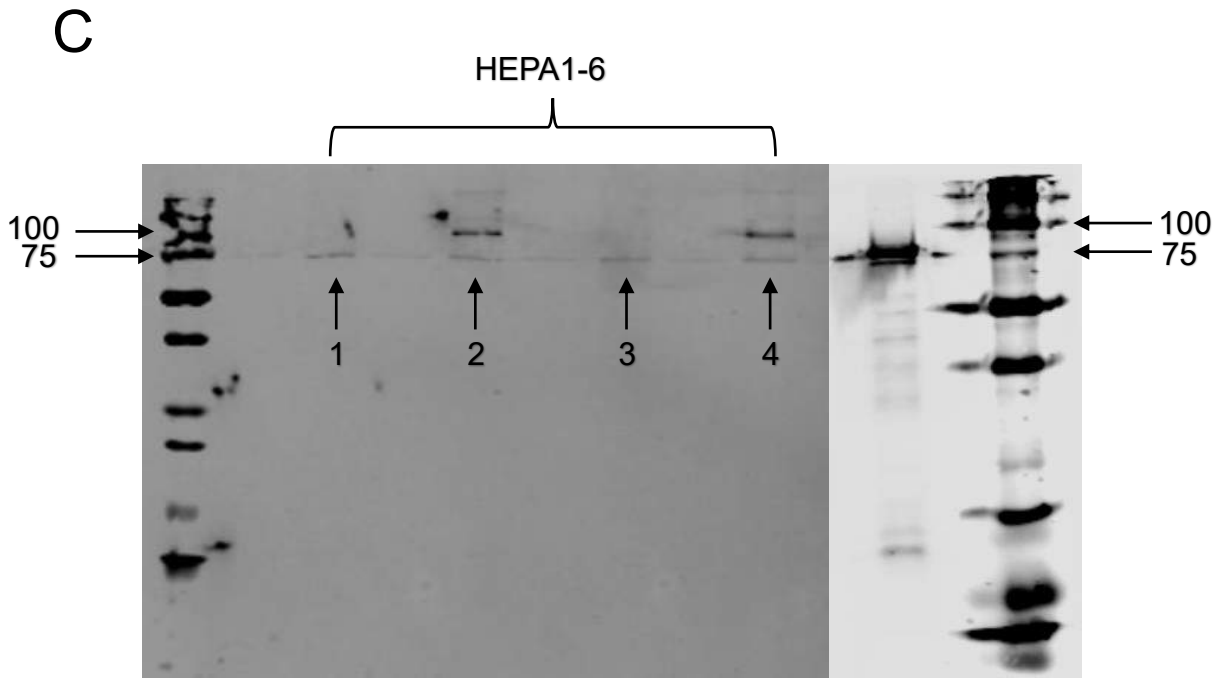

Figure 11. Three independent viral infection experiments confirmed basal PAD4 expression and production of the GFP-PAD4 fusion from AAV6-V1; no enhanced PAD4 expression was evident with AAV6-V2. In (A), three cell lines, HEPG2, HEK-293, and HEPA1-6, were transduced with AAV6-V1 or AAV6-V2, with a clear PAD4 expression band near the 75 kDa molecular weight, evident from virally infected cell lysate (lanes 2-4, 6-8, and 10-12, and for uninfected cell lysate (lanes 1, 5, and 9). Wells containing lysate from AAV6-V1 infected cells, lanes 2, 4, 6, 8, 10, and 12, demonstrated a second band near 100 kDa, indicative of the fusion protein (~76 kDa of the PAD4 + ~27 kDa of the GFP). In (B) a whole repeat experiment was conducted analogous to (A) and confirmed both endogenous PAD4 expression and the production of the fusion protein, but almost no difference in band intensity for the AAV6-V2 infected cells (construct contains a WPRE sequence) as compared to the controls. In (C) only the HEPA1-6 cells were repeated given their prominent signal in the first two infection experiments. A similar trend as with the data in subfigures (A) and (B) was also found in (C), with endogenous PAD4 expression near the 75 kDa mark and the fusion protein near 100 kDa, which demonstrated reproducibility of the findings.

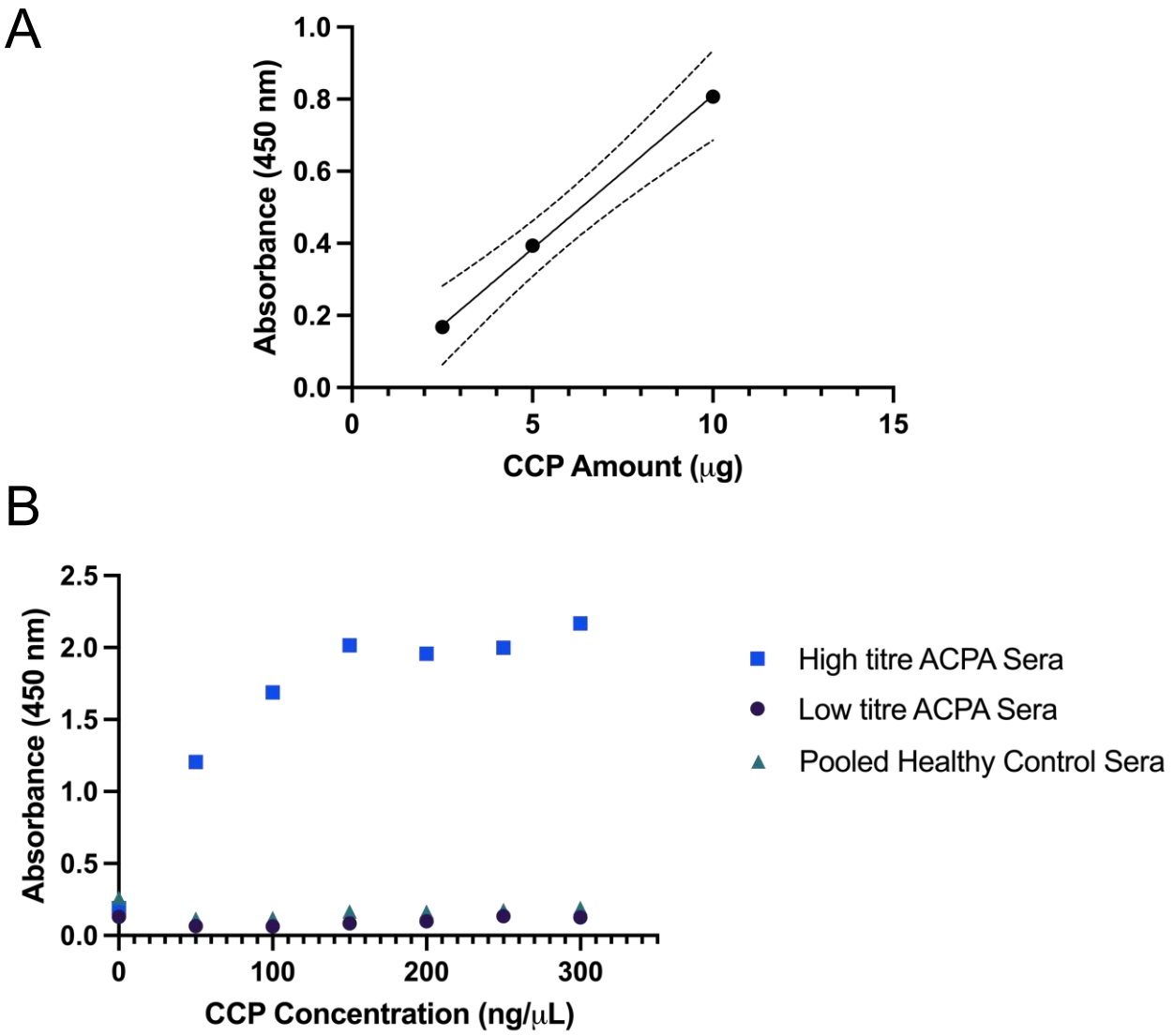

Figure 12. Optimizing the in-house ELISA for PAD activity detection and determining the optimal concentration of the cyclic citrullinated peptide (CCP) for experimentation. In (A) it was evident that with an increasing concentration of the CCP, from 2.5 μg/well to 10 μg/well, the absorbance demonstrated a linear correlation with CCP amounts. The 95% confidence interval bands were surrounding the line of best fit (Slope=0.08497 (95% CI of Slope: [0.06108, 0.1089]). In (B), absorbance signals of CCP plated at varying concentrations were compared with both pooled high titre ACPA (anti-citrullinated protein antibodies) sera (from RA patients), low titre ACPA (from RA patients), and pooled sera from healthy controls. The magnitude of the absorbance signal was consistently higher with the CCP interrogated with high titre ACPA, reaching signals over 2.00, but plateauing after 15 μg/well (150 ng/μL) of CCP, which was selected as the optimal amount for experimentation given the little change in signal from 15 to 30 μg/well of the substrate. While, CCP interrogated with low ACPA sera and pooled control sera had absorbances below 0.50.

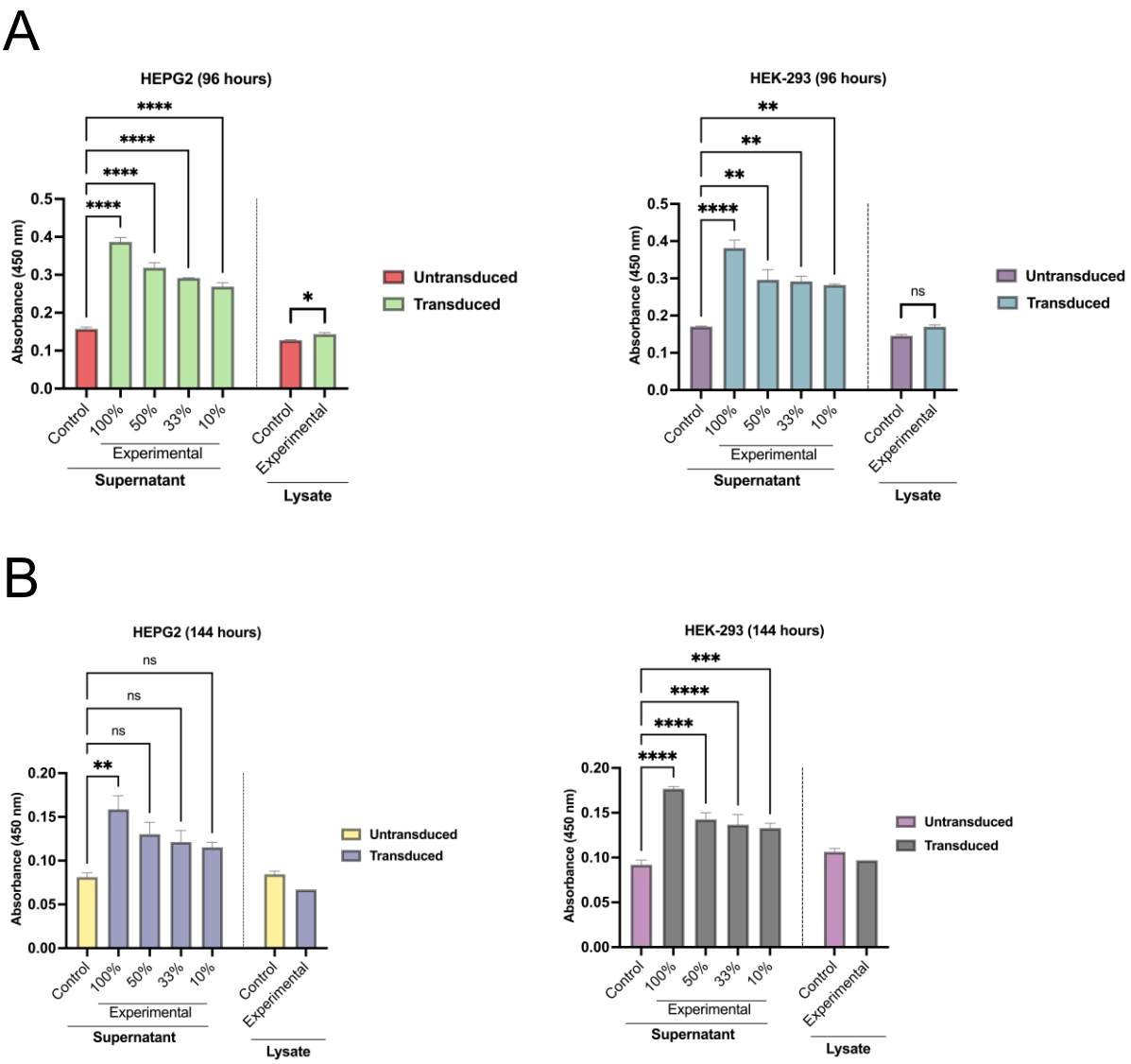

Figure 13. Comparing the amount of citrullinated protein levels between untransduced (0 MOI) and transduced (160,000 MOI) HEPG2 and HEK-293 cells after 96- and 144-hours post-transduction. For the data presented here, only the high titre ACPA Patient sera was used. In (A), the supernatants of HEPG2 and HEK-293 cells demonstrated significantly different absorbance levels as compared to the control supernatant from untransduced cells. Only the lysate of the experimental condition (transduced cells) for HEPG2 was statistically different from the control lysate. In (B), supernatant across all four dilutions (No dilution (100%), 50% dilution, 33% dilution, and 10% dilution) were significantly different than control supernatant from untransduced cells. In contrast to the trend observed in (A), in (B), the control lysate had a higher absorbance signal than the experimental lysate. The asterisks in the graphs were indicative of a significant difference among the two conditions compared: ****p≤0.0001; ***p≤0.001; **p≤0.01; *p<0.05. 'ns' = non-significant (statistically). Bar graphs plotted the mean with standard deviation for each condition.

Table 6: A summary of the descriptive statistics for HEPG2 cells.

	Condition	Mean (SD) Absorbance	95% CI of Mean [lower bound, upper bound]
Supernatant	Control	0.157 (0.007)	[0.139, 0.176]
	No Dilution (100%)	0.387 (0.019)	[0.338, 0.436]
	50% Dilution	0.318 (0.022)	[0.262, 0.374]
	33% Dilution	0.292 (0.001)	[0.289, 0.294]
	10% Dilution	0.269 (0.017)	[0.226, 0.312]
Lysate	Control	0.128 (0.002)	[0.123, 0.133]
	Experimental	0.144 (0.006)	[0.128, 0.159]

SD= Standard deviation; CI= confidence interval.

Table 7: A summary of the Dunnett's multiple comparison post hoc test for HEPG2 cells.

Pairwise Comparison	Mean Difference (MD)	95% CI of MD [lower bound, upper bound]	Adjusted p-value
No dilution* (*100%*) versus *Control	-0.229	[-0.267, -0.192]	p<0.0001
50% dilution* versus *Control	-0.161	[-0.198, -0.124]	p<0.0001
33% dilution* versus *Control	-0.134	[-0.172, -0.097]	p<0.0001
10% dilution* versus *Control	-0.112	[-0.149, -0.074]	p<0.0001

CI= confidence interval.

Table 8: A summary of the descriptive statistics for HEK-293 cells.

	Condition	Mean (SD) Absorbance	95% CI of Mean [lower bound, upper bound]
Supernatant	Control	0.171 (0.003)	[0.164, 0.177]
	No Dilution (100%)	0.382 (0.036)	[0.291, 0.472]
	50% Dilution	0.296 (0.047)	[0.180, 0.412]
	33% Dilution	0.292 (0.023)	[0.235, 0.350]
	10% Dilution	0.282 (0.005)	[0.271, 0.294]
Lysate	Control	0.146 (0.006)	[0.132, 0.160]
	Experimental	0.170 (0.009)	[0.148, 0.192]

SD= Standard deviation; CI= confidence interval.

Table 9: A summary of the Dunnett's multiple comparison post hoc test for HEK-293 cells.

Pairwise Comparison	Mean Difference (MD)	95% CI of MD [lower bound, upper bound]	Adjusted p-value
No dilution* (*100%*) versus *Control	-0.211	[-0.278, -0.144]	p<0.0001
50% dilution* versus *Control	-0.126	[-0.193, -0.058]	p=0.001
33% dilution* versus *Control	-0.122	[-0.189, -0.054]	p=0.001
10% dilution* versus *Control	-0.112	[-0.179, -0.044]	p=0.002

CI= confidence interval.

Table 10: A summary of the descriptive statistics for HEPG2 cells.

	Condition	Mean (SD) Absorbance	95% CI of Mean [lower bound, upper bound]	Median (IQR)	95% CI of Median [lower bound, upper bound]
Supernatant	Control	0.081 (0.005)	[0.069, 0.094]	0.079 (0.009)	[0.078, 0.087]
	No Dilution (100%)	0.159 (0.016)	[0.120, 0.198]	0.161 (0.031)	[0.142, 0.173]
	50% Dilution	0.130 (0.014)	[0.096, 0.164]	0.135 (0.026)	[0.115, 0.141]
	33% Dilution	0.121 (0.013)	[0.089, 0.154]	0.120 (0.026)	[0.109, 0.135]
	10% Dilution	0.115 (0.006)	[0.101, 0.130]	0.112 (0.010)	[0.112, 0.122]
Lysate	Control	0.084 (0.003)	[0.053, 0.116]	0.084 (0.005)	[0.082, 0.087]
	Experimental	0.067 (0.000)	-	0.067 (0.000)	-

SD= Standard deviation; IQR= interquartile range; CI= confidence interval.

Table 11: A summary of the Dunn's multiple comparison post hoc test for HEPG2 cells.

Pairwise Comparison	Mean Rank Difference	Adjusted p-value
No dilution* (*100%*) versus *Control	12.000	p=0.004
50% dilution* versus *Control	7.833	p=0.126
33% dilution* versus *Control	5.500	p=0.525
10% dilution* versus *Control	4.667	p=0.802

Table 12: A summary of the descriptive statistics for HEK-293 cells.

	Condition	Mean (SD) Absorbance	95% CI of Mean [lower bound, upper bound]
Supernatant	Control	0.092 (0.005)	[0.079, 0.105]
	No Dilution (100%)	0.177 (0.002)	[0.170, 0.183]
	50% Dilution	0.143 (0.007);	[0.124, 0.161]
	33% Dilution	0.137 (0.011);	[0.108, 0.165]
	10% Dilution	0.133 (0.005)	[0.120, 0.146]
Lysate	Control	0.106 (0.003)	[0.075, 0.138]
	Experimental	0.097 (0.000)	-

Standard Deviation= SD; CI= confidence interval.

Table 13. A summary of the Dunnett's multiple comparison post hoc test for HEK-293 cells.

Pairwise Comparison	Mean Difference (MD)	95% CI of MD [lower bound, upper bound]	Adjusted p-value
No dilution* (*100%*) versus *Control	-0.085	[-0.101, -0.068]	p<0.0001
50% dilution* versus *Control	-0.051	[-0.067, -0.034]	p<0.0001
33% dilution* versus *Control	-0.045	[-0.061, -0.028]	p<0.0001
10% dilution* versus *Control	-0.041	[-0.056, -0.024]	p=0.0001

Table 14. A summary of the descriptive statistics for HEPG2 cells.

	Sera Type	Condition	Median (IQR)	95% CI of Median [lower bound, upper bound]
Supernatant	HPS	Control	0.118 (0.020)	[0.114, 0.134]
		No Dilution (100%)	0.202 (0.016)	[0.194, 0.210]
		50% Dilution	0.169 (0.010)	[0.164, 0.174]
		33% Dilution	0.163 (0.006)	[0.160, 0.166]
		10% Dilution	0.163 (0.006)	[0.160, 0.166]
	CPS	Control	0.039 (0.006)	[0.037, 0.043]
		No Dilution (100%)	0.044 (0.001)	[0.044, 0.045]
		50% Dilution	0.045 (0.001)	[0.045, 0.046]
		33% Dilution	0.050 (0.003)	[0.049, 0.052]
		10% Dilution	0.051 (0.002)	[0.050, 0.052]
Media Alone	HPS		0.098 (0.063)	[0.052, 0.115]
	CPS		0.060 (0.097)	[0.040, 0.137]

IQR= interquartile range; CI= confidence interval; HPS= High titre ACPA sera; CPS= Control pooled (ACPA-negative) Sera.

Table 15. A summary of the descriptive statistics for HEK-293 cells.

	Sera Type	Condition	Median (IQR)	95% CI of Median [lower bound, upper bound]
Supernatant	HPS	Control	0.126 (0.007)	[0.121, 0.128]
		No Dilution (100%)	0.226 (0.009)	[0.222, 0.231]
		50% Dilution	0.186 (0.009)	[0.182, 0.192]
		33% Dilution	0.183 (0.010)	[0.178, 0.188]
		10% Dilution	0.178 (0.003)	[0.177, 0.180]
	CPS	Control	0.043 (0.009)	[0.039, 0.048]
		No Dilution (100%)	0.061 (0.001)	[0.061, 0.062]
		50% Dilution	0.075 (0.029)	[0.061, 0.090]
		33% Dilution	0.063 (0.004)	[0.061, 0.065]
		10% Dilution	0.057 (0.003)	[0.056, 0.059]
Media Alone	HPS		0.0985 (0.063)	[0.052, 0.115]
	CPS		0.060 (0.097)	[0.040, 0.137]

IQR= interquartile range; CI= confidence interval; HPS= High titre ACPA sera; CPS= Control pooled (ACPA-negative) Sera.

Table 16: A summary of the Dunn's multiple comparison post hoc test for HEPG2 cells.

Pairwise Comparison	Mean Rank Difference	Adjusted p-value
No dilution* (*100%*) versus *Control	9.000	p=0.015
50% dilution* versus *Control	6.000	p=0.215
33% dilution* versus *Control	4.500	p=0.592
10% dilution* versus *Control	4.500	p=0.592

Table 17: A summary of the Dunn's multiple comparison post hoc test for HEK-293 cells.

Pairwise Comparison	Mean Rank Difference	Adjusted p-value
No dilution* (*100%*) versus *Control	9.000	p=0.015
50% dilution* versus *Control	6.500	p=0.148
33% dilution* versus *Control	5.000	p=0.435
10% dilution* versus *Control	3.500	p>0.999

A

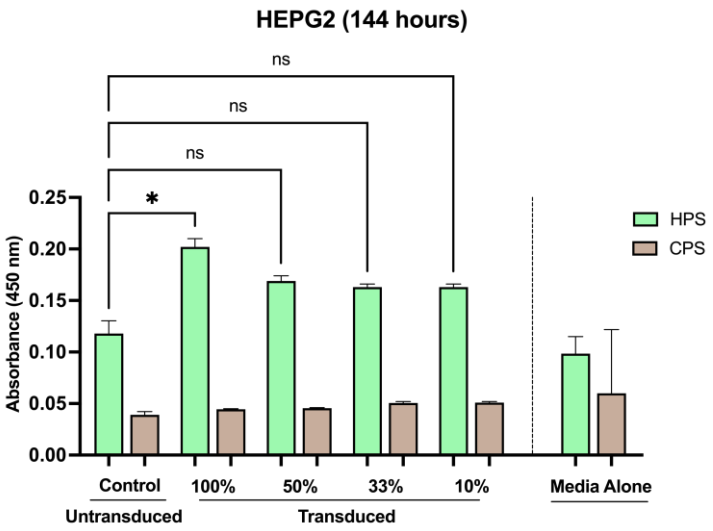

B

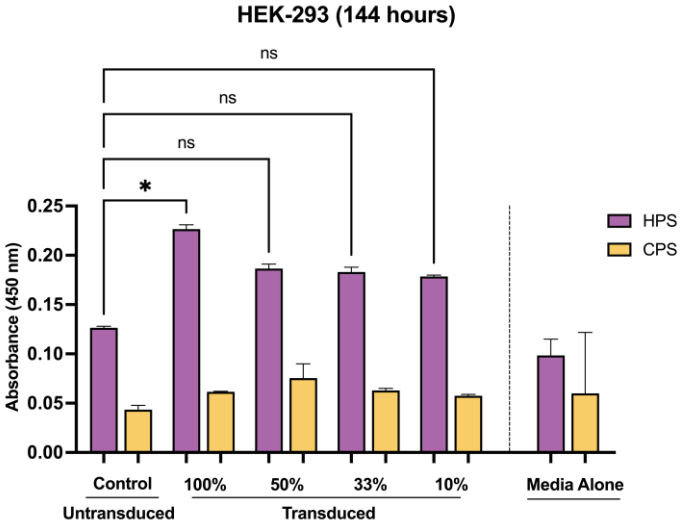

Figure 14. Comparing the amount of citrullinated protein levels between untransduced (0 MOI) and transduced (160,000 MOI) HEPG2 and HEK-293 cells after 144-hours post-transduction using high titre ACPA and control sera. In (A) and (B) a control serum (CPS) was added as a comparator to high titre ACPA sera (HPS). For both HEPG2 and HEK-293 cells, only the concentrated supernatant [No Dilution (100%)] was significantly different from control supernatant. All other pairwise comparisons were non-significant. As an assay control, the media alone condition was used to analyze background absorbance levels. It was evident that the samples interrogated with HPS likely had a lower signal-to-noise ratio given the high background absorbance from the media alone. The asterisks in the graphs were indicative of a significant difference among the two conditions compared: ****p≤0.0001; ***p≤0.001; **p≤0.01; *p<0.05. 'ns' = non-significant (statistically). Bar graphs plotted the median and interquartile range for each condition.

Table 18. A summary of the descriptive statistics for HEPG2 cells (condition: no ionomycin and no calcium).

	Sera Type	Condition	Median (IQR)	95% CI of Median [lower bound, upper bound]
Supernatant	HPS	Control	0.100 (0.013)	[0.094, 0.107]
		No Dilution (100%)	0.197 (0.015)	[0.190, 0.205]
		50% Dilution	0.144 (0.022)	[0.133, 0.155]
		33% Dilution	0.135 (0.008)	[0.131, 0.139]
		10% Dilution	0.140 (0.011)	[0.135, 0.146]
	CPS	Control	0.033 (0.000)	-
		No Dilution (100%)	0.055 (0.000)	-
		50% Dilution	0.043 (0.011)	[0.038, 0.049]
		33% Dilution	0.046 (0.010)	[0.041, 0.051]
		10% Dilution	0.048 (0.003)	[0.047, 0.050]
Lysate	HPS	Control	0.093 (0.011)	[0.088, 0.099]
		Experimental	0.102 (0.022)	[0.091, 0.113]
Peptide Mixtures	HPS	Pooled Nat.	0.029 (0.002)	[0.028, 0.030]
	CPS		0.046 (0.008)	[0.042, 0.050]
	HPS	Pooled Cit.	0.023 (0.002)	[0.022, 0.024]
	CPS		0.037 (0.004)	[0.035, 0.039]

IQR= interquartile range; CI= confidence interval; HPS= High titre ACPA sera; CPS= Control pooled (ACPA-negative) Sera; Pooled Nat.= Native (unmodified) peptides; Pooled Cit.= Citrullinated (modified) peptides.

Table 19. A summary of the descriptive statistics for HEK-293 cells (condition: no ionomycin and no calcium).

	Sera Type	Condition	Median (IQR)	95% CI of Median [lower bound, upper bound]
Supernatant	HPS	Control	0.100 (0.014)	[0.094, 0.107]
		No Dilution (100%)	0.176 (0.002)	[0.175, 0.177]
		50% Dilution	0.139 (0.005)	[0.137, 0.142]
		33% Dilution	0.134 (0.002)	[0.133, 0.135]
		10% Dilution	0.132 (0.001)	[0.132, 0.133]
	CPS	Control	0.036 (0.000)	[0.032, 0.041]
		No Dilution (100%)	0.045 (0.008)	[0.041, 0.049]
		50% Dilution	0.037 (0.008)	[0.033, 0.041]
		33% Dilution	0.048 (0.000)	[0.048, 0.048]
		10% Dilution	0.047 (0.003)	[0.046, 0.049]
Lysate	HPS	Control	0.072 (0.010)	[0.067, 0.077]
		Experimental	0.124 (0.00)	[0.124, 0.124]
	HPS	Pooled Nat.	0.029 (0.002)	[0.028, 0.030]

Peptide Mixtures	CPS		0.046 (0.008)	[0.042, 0.050]
	HPS	Pooled Cit.	0.023 (0.002)	[0.022, 0.024]
	CPS		0.037 (0.004)	[0.035, 0.039]

IQR= interquartile range; CI= confidence interval; HPS= High titre ACPA sera; CPS= Control pooled (ACPA-negative) Sera; Pooled Nat.= Native (unmodified) peptides; Pooled Cit.= Citrullinated (modified) peptides.

Table 20. A summary of the descriptive statistics for HEPG2 cells (condition: ionomycin and no calcium).

	Sera Type	**Condition**	**Median (IQR)**	**95% CI of Median [lower bound, upper bound]**
Supernatant	HPS	Control	0.098 (0.000)	[0.098, 0.098]
		No Dilution (100%)	0.172 (0.009)	[0.1680, 0.177]
		50% Dilution	0.140 (0.015)	[0.1330, 0.148]
		33% Dilution	0.129 (0.013)	[0.1230, 0.136]
		10% Dilution	0.127 (0.001)	[0.1270, 0.128]
	CPS	Control	0.039 (0.001)	[0.039, 0.040]
		No Dilution (100%)	0.044 (0.007)	[0.041, 0.048]
		50% Dilution	0.055 (0.006)	[0.052, 0.058]
		33% Dilution	0.052 (0.003)	[0.051, 0.054]
		10% Dilution	0.052 (0.003)	[0.051, 0.054]
Lysate	HPS	Control	0.104 (0.001)	[0.104, 0.105]
		Experimental	0.101 (0.000)	[0.101, 0.101]
Peptide Mixtures	HPS	Pooled Nat.	0.029 (0.002)	[0.028, 0.030]
	CPS		0.046 (0.008)	[0.042, 0.050]
	HPS	Pooled Cit.	0.023 (0.002)	[0.022, 0.024]
	CPS		0.037 (0.004)	[0.035, 0.039]

IQR= interquartile range; CI= confidence interval; HPS= High titre ACPA sera; CPS= Control pooled (ACPA-negative) Sera; Pooled Nat.= Native (unmodified) peptides; Pooled Cit.= Citrullinated (modified) peptides.

Table 21. A summary of the descriptive statistics for HEK-293 cells (condition: ionomycin and no calcium).

	Sera Type	**Condition**	**Median (IQR)**	**95% CI of Median [lower bound, upper bound]**
Supernatant	HPS	Control	0.095 (0.002)	[0.094, 0.096]
		No Dilution (100%)	0.142 (0.001)	[0.142, 0.143]
		50% Dilution	0.143 (0.010)	[0.138, 0.148]
		33% Dilution	0.124 (0.001)	[0.124, 0.125]
		10% Dilution	0.125 (0.003)	[0.124, 0.127]

	CPS	Control	0.045 (0.000)	[0.045, 0.045]
		No Dilution (100%)	0.048 (0.004)	[0.046, 0.050]
		50% Dilution	0.043 (0.003)	[0.042, 0.045]
		33% Dilution	0.044 (0.001)	[0.044, 0.045]
		10% Dilution	0.049 (0.004)	[0.047, 0.051]
Lysate	HPS	Control	0.085 (0.000)	[0.085, 0.085]
		Experimental	0.099 (0.008)	[0.095, 0.103]
Peptide Mixtures	HPS	Pooled Nat.	0.029 (0.002)	[0.028, 0.030]
	CPS		0.046 (0.008)	[0.042, 0.050]
	HPS	Pooled Cit.	0.023 (0.002)	[0.022, 0.024]
	CPS		0.037 (0.004)	[0.035, 0.039]

IQR= interquartile range; CI= confidence interval; HPS= High titre ACPA sera; CPS= Control pooled (ACPA-negative) Sera; Pooled Nat.= Native (unmodified) peptides; Pooled Cit.= Citrullinated (modified) peptides.

Table 22. A summary of the descriptive statistics for HEPG2 cells (condition: ionomycin and calcium).

	Sera Type	**Condition**	**Median (IQR)**	**95% CI of Median [lower bound, upper bound]**
Supernatant	HPS	Control	0.102 (0.000)	[0.102, 0.102]
		No Dilution (100%)	0.185 (0.012)	[0.179, 0.191]
		50% Dilution	0.153 (0.019)	[0.143, 0.162]
		33% Dilution	0.139 (0.004)	[0.137, 0.141]
		10% Dilution	0.142 (0.009)	[0.137, 0.146]
	CPS	Control	0.042 (0.003)	[0.040, 0.043]
		No Dilution (100%)	0.058 (0.011)	[0.052, 0.063]
		50% Dilution	0.053 (0.001)	[0.052, 0.053]
		33% Dilution	0.054 (0.010)	[0.049, 0.059]
		10% Dilution	0.060 (0.006)	[0.057, 0.063]
Lysate	HPS	Control	0.115 (0.013)	[0.108, 0.121]
		Experimental	0.105 (0.008)	[0.101, 0.109]
Peptide Mixtures	HPS	Pooled Nat.	0.029 (0.002)	[0.028, 0.030]
	CPS		0.046 (0.008)	[0.042, 0.050]
	HPS	Pooled Cit.	0.023 (0.002)	[0.022, 0.024]
	CPS		0.037 (0.004)	[0.035, 0.039]

IQR= interquartile range; CI= confidence interval; HPS= High titre ACPA sera; CPS= Control pooled (ACPA-negative) Sera; Pooled Nat.= Native (unmodified) peptides; Pooled Cit.= Citrullinated (modified) peptides.

Table 23. A summary of the descriptive statistics for HEK-293 cells (condition: ionomycin and calcium).

	Sera Type	Condition	Median (IQR)	95% CI of Median [lower bound, upper bound]
Supernatant	HPS	Control	0.103 (0.009)	[0.098, 0.107]
		No Dilution (100%)	0.166 (0.003)	[0.164, 0.167]
		50% Dilution	0.124 (0.000)	[0.124, 0.124]
		33% Dilution	0.130 (0.007)	[0.126, 0.133]
		10% Dilution	0.139 (0.006)	[0.136, 0.142]
	CPS	Control	0.041 (0.003)	[0.039, 0.042]
		No Dilution (100%)	0.044 (0.006)	[0.041, 0.047]
		50% Dilution	0.051 (0.003)	[0.049, 0.052]
		33% Dilution	0.0485 (0.004)	[0.046, 0.050]
		10% Dilution	0.052 (0.005)	[0.049, 0.054]
Lysate	HPS	Control	0.121 (0.004).	[0.119, 0.123]
		Experimental	0.113 (0.001)	[0.112, 0.113]
Peptide Mixtures	HPS	Pooled Nat.	0.029 (0.002)	[0.028, 0.030]
	CPS		0.046 (0.008)	[0.042, 0.050]
	HPS	Pooled Cit.	0.023 (0.002)	[0.022, 0.024]
	CPS		0.037 (0.004)	[0.035, 0.039]

IQR= interquartile range; CI= confidence interval; HPS= High titre ACPA sera; CPS= Control pooled (ACPA-negative) Sera; Pooled Nat.= Native (unmodified) peptides; Pooled Cit.= Citrullinated (modified) peptides.

Table 24. A summary of the Dunn's multiple comparison post hoc test for HEK-293 cells (condition: no ionomycin and no calcium).

Pairwise Comparison	Mean Rank Difference	Adjusted p-value
No dilution* (*100%*) versus *Control	8.000	p=0.032
50% dilution* versus *Control	6.000	p=0.187
33% dilution* versus *Control	3.750	p=0.856
10% dilution* versus *Control	2.250	p>0.999

Table 25. A summary of the Dunn's multiple comparison post hoc test for HEPG2 cells (condition: ionomycin and no calcium).

Pairwise Comparison	Mean Rank Difference	Adjusted p-value
No dilution* (*100%*) versus *Control	8.000	p=0.032
50% dilution* versus *Control	5.500	p=0.274
33% dilution* versus *Control	3.500	p=0.985
10% dilution* versus *Control	3.000	p>0.999

Table 26. A summary of the Dunn's multiple comparison post hoc test for HEK-293 cells (condition: ionomycin and no calcium).

Pairwise Comparison	Mean Rank Difference	Adjusted p-value
No dilution* (*100%*) versus *Control	7.000	p=0.082
50% dilution* versus *Control	7.000	p=0.082
33% dilution* versus *Control	2.750	p>0.999
10% dilution* versus *Control	3.250	p>0.999

Table 27. A summary of the Dunn's multiple comparison post hoc test for HEPG2 cells (condition: ionomycin and calcium).

Pairwise Comparison	Mean Rank Difference	Adjusted p-value
No dilution* (*100%*) versus *Control	8.000	p=0.031
50% dilution* versus *Control	5.500	p=0.270
33% dilution* versus *Control	2.750	p>0.999
10% dilution* versus *Control	3.750	p=0.851

Table 28. A summary of the Dunn's multiple comparison post hoc test for HEK-293 cells (condition: ionomycin and calcium).

Pairwise Comparison	Mean Rank Difference	Adjusted p-value
No dilution* (*100%*) versus *Control	8.000	p=0.032
50% dilution* versus *Control	2.000	p>0.999
33% dilution* versus *Control	4.000	p=0.740
10% dilution* versus *Control	6.000	p=0.187

A

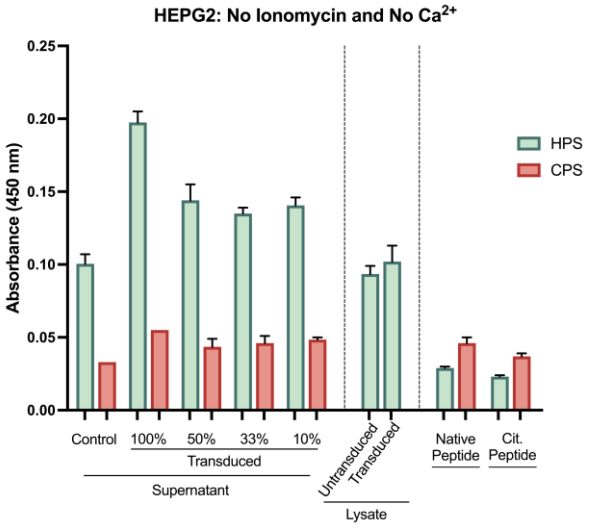
HEPG2: No Ionomycin and No Ca2+
Absorbance (450 nm)
0.25
0.20
0.15
0.10
0.05
0.00
HPS
CPS
Control
100%
50%
33%
10%
Transduced
Supernatant
Untransduced
Transduced
Lysate
Native Peptide
Cit. Peptide

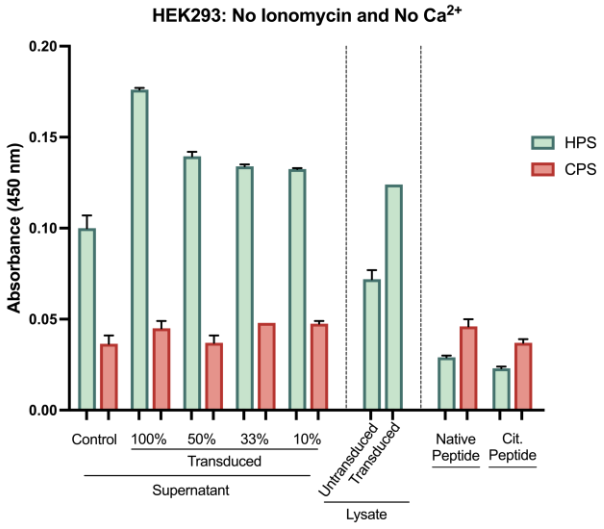
HEK293: No Ionomycin and No Ca2+
Absorbance (450 nm)
0.20
0.15
0.10
0.05
0.00
HPS
CPS
Control
100%
50%
33%
10%
Transduced
Supernatant
Untransduced
Transduced
Lysate
Native Peptide
Cit. Peptide

B

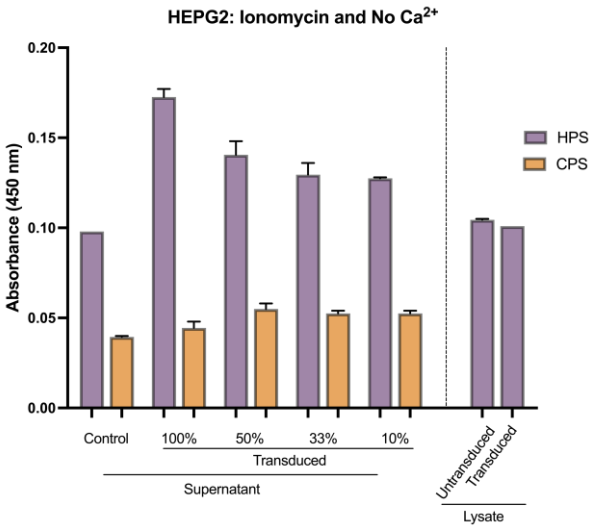
HEPG2: Ionomycin and No Ca2+
Absorbance (450 nm)
0.20
0.15
0.10
0.05
0.00
HPS
CPS
Control
100%
50%
33%
10%
Transduced
Supernatant
Untransduced
Transduced
Lysate

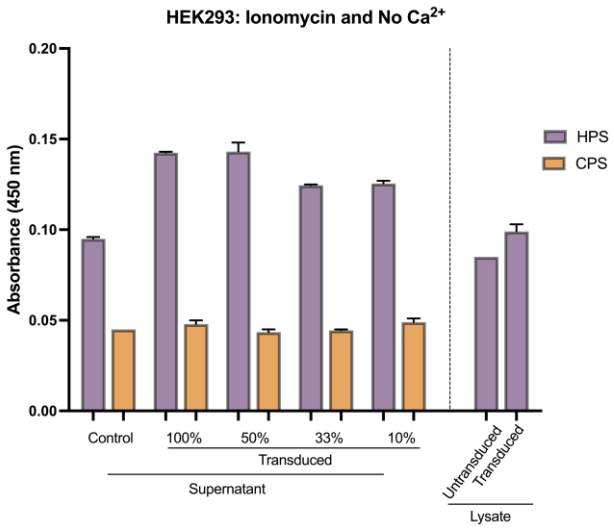
HEK293: Ionomycin and No Ca2+
Absorbance (450 nm)
0.20
0.15
0.10
0.05
0.00
HPS
CPS
Control
100%
50%
33%
10%
Transduced
Supernatant
Untransduced
Transduced
Lysate

C

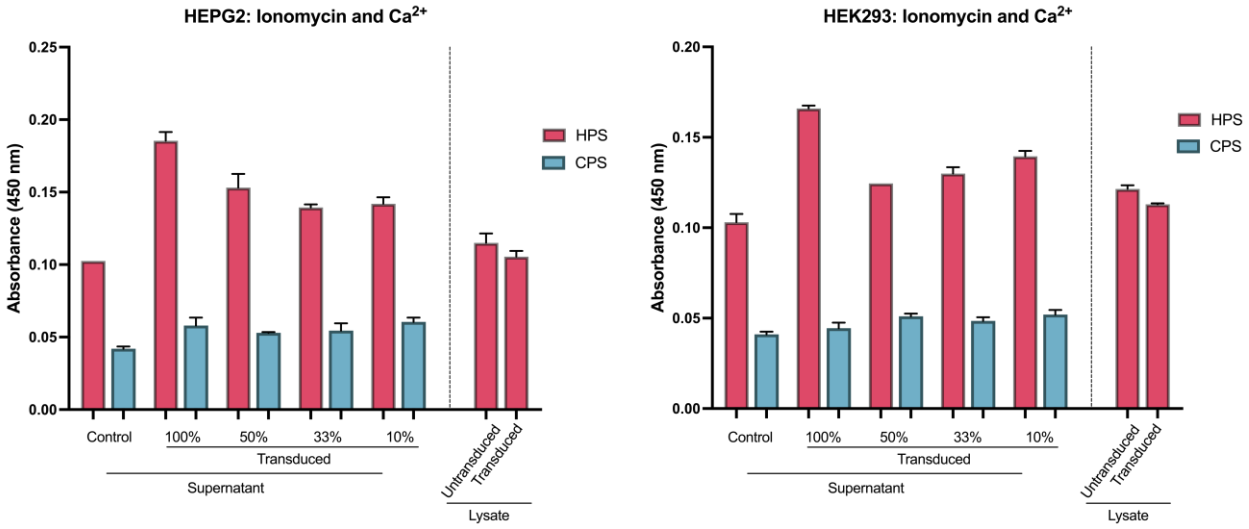

Figure 15. Comparing the amount of citrullinated protein levels between untransduced (0 MOI) and transduced (160,000 MOI) cells, after supplementation with ionomycin (1 μM) and calcium (2 mM) for 2 hours (activation phase), using high titre ACPA (HPS) and control sera (CPS). All cells were cultured for 144 hours before the activation phased was employed. In (A), HEPG2 and HEK-293 cells were not supplemented with ionomycin and calcium, and the absorbance signals between transduced cell lysate and supernatant (experimental conditions) were compared with respective controls. Absorbance signals for the pooled mixture of native (nat.) and citrullinated (cit.) peptides were compared across CPS and HPS categories. Interestingly, signals were higher with samples interrogated with CPS than HPS. In (B), cells received ionomycin but no calcium for the 2-hour incubation and there appeared to be no change in signal as compared to when ionomycin and calcium were absent (A). In (C), ionomycin and calcium were added to cells prior to lysate and supernatant collection. Again, there seemed to be no change in absorbance levels overall even in the presence of both reagents. However, the trend of decreasing in absorbance signal with higher dilutions of the cell supernatant was not apparent for HEK-293; and the signal for untransduced cell lysate was higher than transduced cell lysate interrogated with HPS. Bar graphs plotted the median and interquartile range for each condition.

Table 29: A summary of the descriptive statistics for HEPG2 cells (condition: no ionomycin and no calcium).

	Sera Type	Condition	Median (IQR)	95% CI of Median [lower bound, upper bound]
Supernatant	HPS	Control	0.261 (0.015)	[0.254, 0.269]
		No Dilution (100%)	0.324 (0.008)	[0.320, 0.328]
		50% Dilution	0.322 (0.006)	[0.319, 0.325]
		33% Dilution	0.314 (0.005)	[0.312, 0.317]
		10% Dilution	0.327 (0.001)	[0.327, 0.328]
	CPS	Control	0.112 (0.003)	[0.108, 0.117]
		No Dilution (100%)	0.113 (0.000)	[0.113, 0.113]
		50% Dilution	0.132 (0.001)	[0.132, 0.133]
		33% Dilution	0.148 (0.011)	[0.143, 0.154]
		10% Dilution	0.183 (0.004)	[0.181, 0.185]
Lysate	HPS	Control	0.228 (0.013)	[0.222, 0.235]
		No Dilution (100%)	0.185 (0.000)	[0.185, 0.185]
		50% Dilution	0.172 (0.009)	[0.168, 0.177]
		33% Dilution	0.172 (0.003)	[0.171, 0.174]
Peptide Mixtures	HPS	Pooled Nat.	0.111 (0.010)	[0.106, 0.116]
	CPS		0.147 (0.008)	[0.143, 0.151]
	HPS	Pooled Cit.	0.113 (0.044)	[0.091, 0.135]
	CPS		0.108 (0.027)	[0.095, 0.122]

IQR= interquartile range; CI= confidence interval; HPS= High titre ACPA sera; CPS= Control pooled (ACPA-negative) Sera; Pooled Nat.= Native (unmodified) peptides; Pooled Cit.= Citrullinated (modified) peptides.

Table 30: A summary of the descriptive statistics for HEK-293 cells (condition: no ionomycin and no calcium).

	Sera Type	Condition	Median (IQR)	95% CI of Median [lower bound, upper bound]
Supernatant	HPS	Control	0.262 (0.005)	[0.260, 0.265]
		No Dilution (100%)	0.298 (0.000)	[0.298, 0.298]
		50% Dilution	0.306 (0.019)	[0.297, 0.316]
		33% Dilution	0.301 (0.018)	[0.292, 0.310]
		10% Dilution	0.345 (0.107)	[0.292, 0.399]
	CPS	Control	0.114 (0.001)	[0.114, 0.115]
		No Dilution (100%)	0.109 (0.000)	[0.109, 0.109]
		50% Dilution	0.128 (0.003)	[0.126, 0.130]
		33% Dilution	0.153 (0.012)	[0.147, 0.159]
		10% Dilution	0.145 (0.013)	[0.139, 0.152]

Lysate	HPS	Control	0.216 (0.016)	[0.208, 0.224]
		No Dilution (100%)	0.235 (0.017)	[0.227, 0.244]
		50% Dilution	0.244 (0.004)	[0.242, 0.246]
		33% Dilution	0.230 (0.016)	[0.222, 0.238]
Peptide Mixtures	HPS	Pooled Nat.	0.111 (0.010)	[0.106, 0.116]
	CPS		0.147 (0.008)	[0.143, 0.151]
	HPS	Pooled Cit.	0.113 (0.044)	[0.091, 0.135]
	CPS		0.108 (0.027)	[0.095, 0.122]

IQR= interquartile range; CI= confidence interval; HPS= High titre ACPA sera; CPS= Control pooled (ACPA-negative) Sera; Pooled Nat.= Native (unmodified) peptides; Pooled Cit.= Citrullinated (modified) peptides.

Table 31: A summary of the descriptive statistics for mouse splenocytes (condition: no ionomycin and no calcium).

	Sera Type	**Condition**	**Median (IQR)**	**95% CI of Median [lower bound, upper bound]**
Supernatant	HPS	Control	0.279 (0.015)	[0.272, 0.287]
		No Dilution (100%)	0.331 (0.004)	[0.329, 0.333]
		50% Dilution	0.315 (0.007)	[0.312, 0.319]
		33% Dilution	0.309 (0.001)	[0.309, 0.310]
		10% Dilution	0.307 (0.015)	[0.300, 0.315]
	CPS	Control	0.116 (0.004)	[0.114, 0.118]
		No Dilution (100%)	0.124 (0.008)	[0.120, 0.128]
		50% Dilution	0.130 (0.025)	[0.118, 0.143]
		33% Dilution	0.121 (0.001)	[0.121, 0.122]
		10% Dilution	0.139 (0.008)	[0.135, 0.143]
Lysate	HPS	Control	0.292 (0.004)	[0.290, 0.294]
		No Dilution (100%)	0.285 (0.004)	[0.283, 0.287]
		50% Dilution	0.308 (0.009)	[0.304, 0.313]
		33% Dilution	0.313 (0.002)	[0.312, 0.314]
Peptide Mixtures	HPS	Pooled Nat.	0.111 (0.010)	[0.106, 0.116]
	CPS		0.147 (0.008)	[0.143, 0.151]
	HPS	Pooled Cit.	0.113 (0.044)	[0.091, 0.135]
	CPS		0.108 (0.027)	[0.095, 0.122]

IQR= interquartile range; CI= confidence interval; HPS= High titre ACPA sera; CPS= Control pooled (ACPA-negative) Sera; Pooled Nat.= Native (unmodified) peptides; Pooled Cit.= Citrullinated (modified) peptides.

Table 32: A summary of the descriptive statistics for HEPG2 (condition: ionomycin and calcium).

	Sera Type	Condition	Median (IQR)	95% CI of Median [lower bound, upper bound]
Supernatant	HPS	Control	0.181 (0.001)	[0.181, 0.182]
		No Dilution (100%)	0.198 (0.005)	[0.196, 0.201]
		50% Dilution	0.233 (0.031)	[0.218, 0.249]
		33% Dilution	0.247 (0.016)	[0.239, 0.255]
		10% Dilution	0.230 (0.007)	[0.227, 0.234]
	CPS	Control	0.252 (0.005)	[0.250, 0.255]
		No Dilution (100%)	0.234 (0.013)	[0.228, 0.241]
		50% Dilution	0.288 (0.005)	[0.286, 0.291]
		33% Dilution	0.121 (0.001)	[0.121, 0.122]
		10% Dilution	0.183 (0.011)	[0.178, 0.189]
Lysate	HPS	Control	0.253 (0.023)	[0.242, 0.265]
		No Dilution (100%)	0.276 (0.003)	[0.275, 0.278]
		50% Dilution	0.264 (0.003)	[0.263, 0.266]
		33% Dilution	0.260 (0.007)	[0.257, 0.264]
Peptide Mixtures	HPS	Pooled Nat.	0.111 (0.010)	[0.106, 0.116]
	CPS		0.147 (0.008)	[0.143, 0.151]
	HPS	Pooled Cit.	0.113 (0.044)	[0.091, 0.135]
	CPS		0.108 (0.027)	[0.095, 0.122]

IQR= interquartile range; CI= confidence interval; HPS= High titre ACPA sera; CPS= Control pooled (ACPA-negative) Sera; Pooled Nat.= Native (unmodified) peptides; Pooled Cit.= Citrullinated (modified) peptides.

Table 33: A summary of the descriptive statistics for HEK-293 (condition: ionomycin and calcium).

	Sera Type	Condition	Median (IQR)	95% CI of Median [lower bound, upper bound]
Supernatant	HPS	Control	0.201 (0.039)	[0.182, 0.221]
		No Dilution (100%)	0.202 (0.002)	[0.201, 0.203]
		50% Dilution	0.269 (0.003)	[0.254, 0.284]
		33% Dilution	0.269 (0.007)	[0.266, 0.273]
		10% Dilution	0.270 (0.047)	[0.247, 0.294]
	CPS	Control	0.276 (0.048)	[0.252, 0.300]
		No Dilution (100%)	0.233 (0.043)	[0.212, 0.255]
		50% Dilution	0.326 (0.005)	[0.324, 0.329]
		33% Dilution	0.285 (0.032)	[0.269, 0.301]
		10% Dilution	0.216 (0.005)	[0.214, 0.219]

Lysate	HPS	Control	0.254 (0.007)	[0.251, 0.258]
		No Dilution (100%)	0.262 (0.007)	[0.259, 0.266]
		50% Dilution	0.263 (0.003)	[0.262, 0.265]
		33% Dilution	0.267 (0.005)	[0.265, 0.270]
Peptide Mixtures	HPS	Pooled Nat.	0.111 (0.010)	[0.106, 0.116]
	CPS		0.147 (0.008)	[0.143, 0.151]
	HPS	Pooled Cit.	0.113 (0.044)	[0.091, 0.135]
	CPS		0.108 (0.027)	[0.095, 0.122]

IQR= interquartile range; CI= confidence interval; HPS= High titre ACPA sera; CPS= Control pooled (ACPA-negative) Sera; Pooled Nat.= Native (unmodified) peptides; Pooled Cit.= Citrullinated (modified) peptides

Table 34: A summary of the descriptive statistics for mouse splenocytes (condition: ionomycin and calcium).

	Sera Type	**Condition**	**Median (IQR)**	**95% CI of Median [lower bound, upper bound]**
Supernatant	HPS	Control	0.233 (0.002)	[0.232, 0.234]
		No Dilution (100%)	0.278 (0.008)	[0.274, 0.282]
		50% Dilution	0.272 (0.004)	[0.270, 0.274]
		33% Dilution	0.268 (0.005)	[0.266, 0.271]
		10% Dilution	0.286 (0.001)	[0.286, 0.287]
	CPS	Control	0.110 (0.011)	[0.105, 0.116]
		No Dilution (100%)	0.111 (0.010)	[0.106, 0.116]
		50% Dilution	0.137 (0.036)	[0.119, 0.155]
		33% Dilution	0.118 (0.001)	[0.118, 0.119]
		10% Dilution	0.173 (0.011)	[0.168, 0.179]
Lysate	HPS	Control	0.261 (0.003)	[0.260, 0.263]
		No Dilution (100%)	0.247 (0.016)	[0.239, 0.255]
		50% Dilution	0.251 (0.003)	[0.250, 0.253]
		33% Dilution	0.268 (0.004)	[0.266, 0.270]
Peptide Mixtures	HPS	Pooled Nat.	0.111 (0.010)	[0.106, 0.116]
	CPS		0.147 (0.008)	[0.143, 0.151]
	HPS	Pooled Cit.	0.113 (0.044)	[0.091, 0.135]
	CPS		0.108 (0.027)	[0.095, 0.122]

IQR= interquartile range; CI= confidence interval; HPS= High titre ACPA sera; CPS= Control pooled (ACPA-negative) Sera; Pooled Nat.= Native (unmodified) peptides; Pooled Cit.= Citrullinated (modified) peptides.

Table 35: A summary of the Dunn's multiple comparison post hoc test for HEPG2 cells (condition: no ionomycin and no calcium).

Pairwise Comparison	Mean Rank Difference	Adjusted p-value
No dilution* (*100%*) versus *Control	6.250	p=0.153
50% dilution* versus *Control	4.500	p=0.544
33% dilution* versus *Control	2.000	p>0.999
10% dilution* versus *Control	7.250	p=0.065

Table 36: A summary of the Dunn's multiple comparison post hoc test for HEPG2 cells (condition: ionomycin and calcium).

Pairwise Comparison	Mean Rank Difference	Adjusted p-value
No dilution* (*100%*) versus *Control	2.000	p>0.999
50% dilution* versus *Control	5.500	p=0.277
33% dilution* versus *Control	7.500	p=0.053
10% dilution* versus *Control	5.000	p=0.395

Table 37: A summary of the Dunn's multiple comparison post hoc test for mouse splenocytes cells (condition: no ionomycin and no calcium).

Pairwise Comparison	Mean Rank Difference	Adjusted p-value
No dilution* (*100%*) versus *Control	8.000	p=0.033
50% dilution* versus *Control	5.500	p=0.277
33% dilution* versus *Control	3.000	p>0.999
10% dilution* versus *Control	3.500	p=0.991

Table 38: A summary of the Dunn's multiple comparison post hoc test for mouse splenocytes cells (condition: ionomycin and calcium).

Pairwise Comparison	Mean Rank Difference	Adjusted p-value
No dilution* (*100%*) versus *Control	5.750	p=0.227
50% dilution* versus *Control	3.750	p=0.856
33% dilution* versus *Control	2.500	p>0.999
10% dilution* versus *Control	8.000	p=0.032

Table 39: A summary of the Dunn's multiple comparison post hoc test for mouse splenocytes cells (condition: no ionomycin and no calcium).

Pairwise Comparison (lysate)	Mean Rank Difference	Adjusted p-value
No dilution* (*100%*) versus *Control	2.000	p>0.999
50% dilution* versus *Control	-2.500	p=0.922
33% dilution* versus *Control	-3.500	p=0.459

A

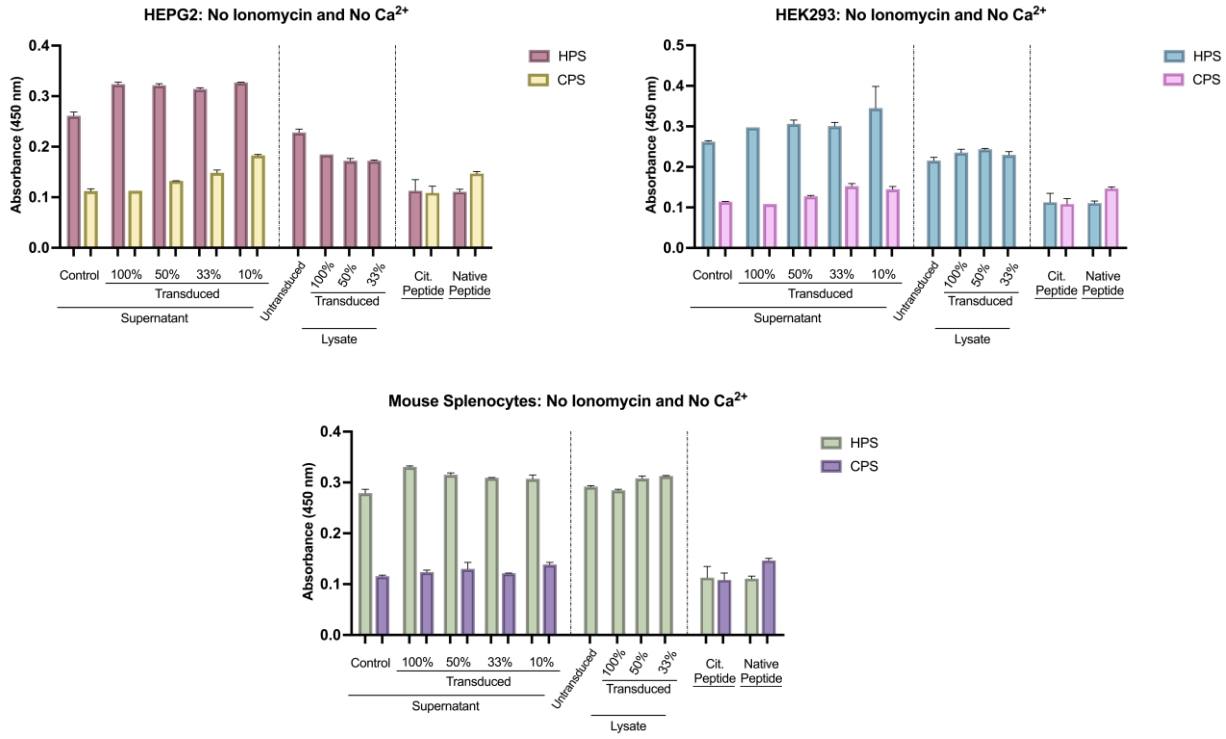
HEPG2: No Ionomycin and No Ca2+
HEK293: No Ionomycin and No Ca2+
Mouse Splenocytes: No Ionomycin and No Ca2+
HPS
CPS
Absorbance (450 nm)
Control
100%
50%
33%
10%
Transduced
Supernatant
Untransduced
Lysate
Cit. Peptide
Native Peptide

B

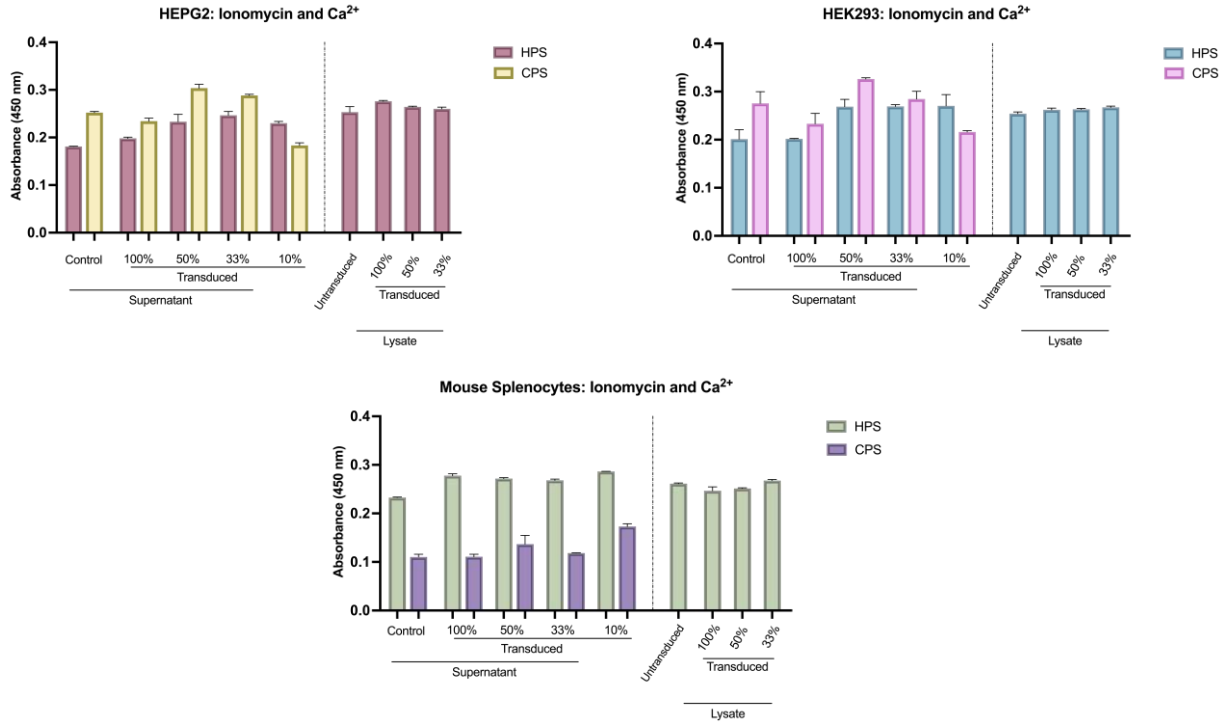
HEPG2: Ionomycin and Ca2+
HEK293: Ionomycin and Ca2+
Mouse Splenocytes: Ionomycin and Ca2+
HPS
CPS
Absorbance (450 nm)
Control
100%
50%
33%
10%
Transduced
Supernatant
Untransduced
Lysate

Figure 16. Comparing the amount of citrullinated protein levels between untransduced (0 MOI) and transduced (160,000 MOI) cells, after supplementation with ionomycin (1 μM) and calcium (10 mM) for 4 hours (activation phase), using high titre ACPA (HPS) and control sera (CPS). All cells were cultured for 96 hours before the activation phase was employed. In (A), HEPG2 and HEK-293 cells, and mouse splenocytes, not supplemented with ionomycin and calcium, demonstrated higher absorbance signals with transduced cell supernatant when comparing all four experimental dilutions with control supernatant, as well as when comparing the HPS interrogated experimental sample with its CPS counterpart. Only mouse splenocytes demonstrated a decreasing signal in absorbance (for supernatant) at higher dilutions. This trend was inconsistent for HEPG2 and reversed for HEK-293. Similarly, transduced cell lysate compared to control, did not demonstrate a clear relationship, as the control had a higher signal than some of the experimental samples, most prominent for HEPG2. Similarly, with the same peptide mixtures, as depicted in Figure 17, it was clear that the HPS did not detect the citrullinated peptides. In (B), cells received ionomycin and calcium for the 4-hour incubation, but it was evident that the samples interrogated with HPS did not differ from their CPS counterpart. In fact, it was unusual to see that that the samples detected with CPS had a higher absorbance signal. All three cell lines demonstrated that the addition of ionomycin and calcium did not appear to increase PAD activity and subsequent protein citrullination. Bar graphs plotted the median and interquartile range for each condition.

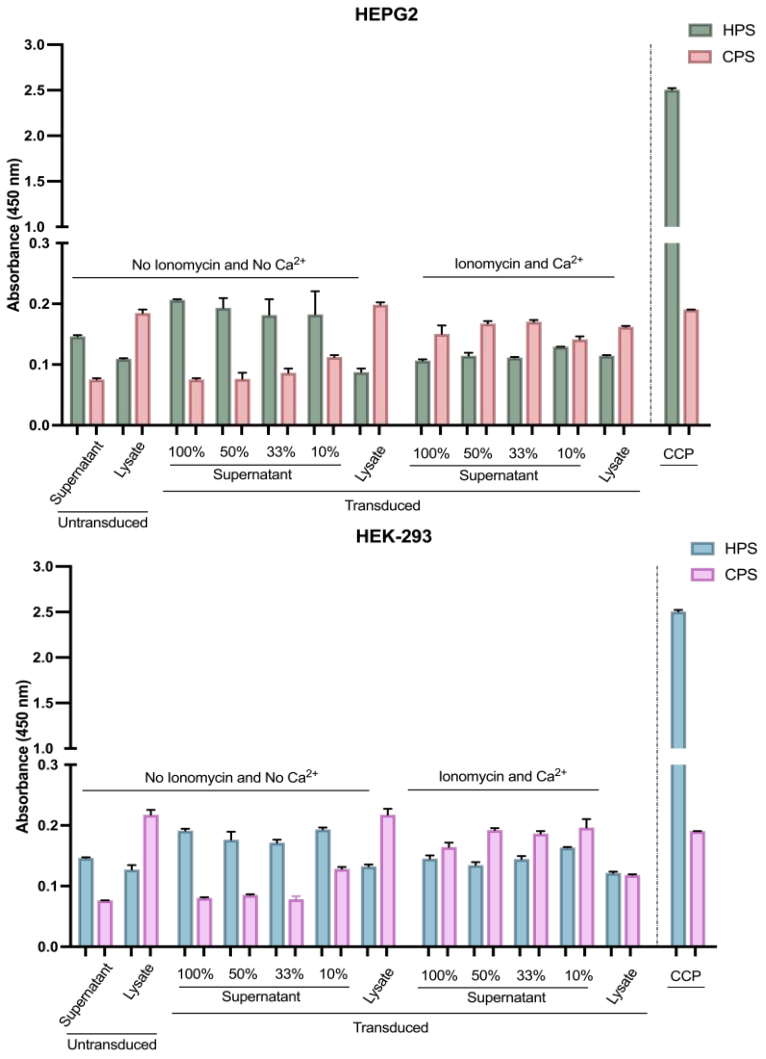

Figure 17. Examining the functionality of the in-house ELISA assay by using a commercial CCP peptide and comparing the amount of citrullinated protein levels between untransduced (0 MOI) and transduced (160,000 MOI) cells, after supplementation with ionomycin (1 μM) and calcium (2 mM) for 2 hours (activation phase), using high titre ACPA (HPS) and control sera (CPS). All cells were cultured for 96 hours before the activation phase was employed. An assay control, the CCP peptide, was used to assess whether the assay was unable to detect any citrullinated protein. 15 μg/well of CCP was coated, and the absorbance signal with HPS was over 2.00 units higher than the experimental conditions (transduced cell lysate and supernatant). Interestingly, CCP interrogated with CPS (Mdn A= 0.190) also had an absorbance that was comparable with the supernatant and lysate experimental samples, demonstrating that with or without ionomycin and calcium supplementation, the AAV-encoded PAD was non-functional and there was little to no citrullinated protein in the experimental samples over the controls. Bar graphs plotted the median and interquartile range for each condition.

Table 40: A summary of the descriptive statistics for HEPG2 (condition: no ionomycin and no calcium).

	Sera Type	Condition	Median (IQR)	95% CI of Median [lower bound, upper bound]
Supernatant	HPS	Control	0.146 (0.006)	[0.142, 0.148]
		No Dilution (100%)	0.206 (0.009)	[0.198, 0.207]
		50% Dilution	0.193 (0.020)	[0.189, 0.209]
		33% Dilution	0.182 (0.041)	[0.166, 0.207]
		10% Dilution	0.182 (0.039)	[0.181, 0.220]
	CPS	Control	0.076 (0.007)	[0.070, 0.077]
		No Dilution (100%)	0.076 (0.002)	[0.075, 0.077]
		50% Dilution	0.076 (0.014)	[0.072, 0.086]
		33% Dilution	0.086 (0.027)	[0.066, 0.093]
		10% Dilution	0.112 (0.042)	[0.073, 0.115]
Lysate	HPS	Control	0.109 (0.002)	[0.108, 0.110]
		Experimental	0.087 (0.012)	[0.081, 0.093]
	CPS	Control	0.185 (0.011)	[0.179, 0.190]
		Experimental	0.198 (0.008)	[0.194, 0.202]
Assay control	HPS	CCP	2.506 (0.091)	[2.432, 2.523]
	CPS	CCP	0.190 (0.012)	[0.178, 0.190]

IQR= interquartile range; CI= confidence interval; HPS= High titre ACPA sera; CPS= Control pooled (ACPA-negative) Sera.

Table 41: A summary of the descriptive statistics for HEPG2 (condition: ionomycin and calcium).

	Sera Type	Condition	Median (IQR)	95% CI of Median [lower bound, upper bound]
Supernatant	HPS	No Dilution (100%)	0.106 (0.004)	[0.104, 0.108]
		50% Dilution	0.114 (0.007)	[0.112, 0.119]
		33% Dilution	0.111 (0.005)	[0.107, 0.112]
		10% Dilution	0.129 (0.002)	[0.127, 0.129]
	CPS	No Dilution (100%)	0.150 (0.017)	[0.147, 0.164]
		50% Dilution	0.167 (0.012)	[0.159, 0.171]
		33% Dilution	0.170 (0.013)	[0.160, 0.173]
		10% Dilution	0.141 (0.005)	[0.141, 0.146]
Lysate	HPS	Experimental	0.114 (0.002)	[0.113, 0.115]
	CPS	Experimental	0.162 (0.003)	[0.160, 0.163]
Assay control	HPS	CCP	2.506 (0.091)	[2.432, 2.523]
	CPS	CCP	0.190 (0.012)	[0.178, 0.190]

IQR= interquartile range; CI= confidence interval; HPS= High titre ACPA sera; CPS= Control pooled (ACPA-negative) Sera.

Table 42: A summary of the descriptive statistics for HEK-293 (condition: no ionomycin and no calcium).

	Sera Type	Condition	Median (IQR)	95% CI of Median [lower bound, upper bound]
Supernatant	HPS	Control	0.146 (0.001)	[0.146, 0.147]
		No Dilution (100%)	0.191 (0.003)	[0.191, 0.194]
		50% Dilution	0.176 (0.017)	[0.172, 0.189]
		33% Dilution	0.171 (0.007)	[0.169, 0.176]
		10% Dilution	0.193 (0.004)	[0.192, 0.196]
	CPS	Control	0.076 (0.004)	[0.072, 0.076]
		No Dilution (100%)	0.080 (0.002)	[0.079, 0.081]
		50% Dilution	0.085 (0.022)	[0.064, 0.086]
		33% Dilution	0.078 (0.018)	[0.066, 0.083]
		10% Dilution	0.128 (0.045)	[0.086, 0.131]
Lysate	HPS	Control	0.127 (0.014)	[0.120, 0.134]
		Experimental	0.132 (0.006)	[0.129, 0.135]
	CPS	Control	0.217 (0.016)	[0.209, 0.225]
		Experimental	0.217 (0.020)	[0.207, 0.227]
Assay control	HPS	CCP	2.506 (0.091)	[2.432, 2.523]
	CPS	CCP	0.190 (0.012)	[0.178, 0.190]

IQR= interquartile range; CI= confidence interval; HPS= High titre ACPA sera; CPS= Control pooled (ACPA-negative) Sera.

Table 43: A summary of the descriptive statistics for HEK-293 (condition: ionomycin and calcium).

	Sera Type	Condition	Median (IQR)	95% CI of Median [lower bound, upper bound]
Supernatant	HPS	No Dilution (100%)	0.145 (0.009)	[0.141 to 0.150]
		50% Dilution	0.134 (0.006)	[0.133 to 0.139]
		33% Dilution	0.144 (0.008)	[0.141 to 0.149]
		10% Dilution	0.163 (0.004)	[0.160 to 0.164]
	CPS	No Dilution (100%)	0.164 (0.012)	[0.159 to 0.171]
		50% Dilution	0.192 (0.006)	[0.189 to 0.195]
		33% Dilution	0.186 (0.006)	[0.184 to 0.190]
		10% Dilution	0.196 (0.015)	[0.195 to 0.210]
Lysate	HPS	Experimental	0.121 (0.004)	[0.119, 0.123]
	CPS	Experimental	0.118 (0.002)	[0.117, 0.119]
Assay control	HPS	CCP	2.506 (0.091)	[2.432, 2.523]
	CPS	CCP	0.190 (0.012)	[0.178, 0.190]

IQR= interquartile range; CI= confidence interval; HPS= High titre ACPA sera; CPS= Control pooled (ACPA-negative) Sera.

Table 44. A summary of the Dunn's multiple comparison post hoc test for HEK-293 cells (condition: no ionomycin and no calcium).

Pairwise Comparison	Mean Rank Difference	Adjusted p-value
No dilution* (*100%*) versus *Control	9.667	p=0.032
50% dilution* versus *Control	5.500	p=0.524
33% dilution* versus *Control	3.500	p>0.999
10% dilution* versus *Control	11.330	p=0.007

Table 45. A summary of the descriptive statistics for the initial run of the PAD Activity Detection Kit.

	Condition	Mean (SD)	95% CI of Mean [lower bound, upper bound]
Hepg2	Control (untransduced)	1.370 (0.209)	[0.851 to 1.890]
	Experimental (No Ion/Ca^{2+})	1.423 (0.227)	[0.859 to 1.987]
	Experimental (Ion/Ca^{2+})	1.499 (0.324)	[0.694 to 2.304]
Hek-293	Control (untransduced)	1.525 (0.355)	[0.644, 2.406]
	Experimental (no Ion/Ca^{2+})	1.445 (0.299)	[0.701, 2.188]
	Experimental (Ion/Ca^{2+})	1.442 (0.322)	[0.643, 2.241]
Controls	Negative	1.438 (0.298)	[0.698, 2.178]
	Positive	1.647 (0.278)	[0.955, 2.339]

SD= Standard deviation; CI= confidence interval; Ion/Ca^{2+}= ionomycin/calcium; Negative Control= Assay buffer alone; Positive Control= PAD cocktail; Experimental= transduced cell lysate following infection of cells at an MOI of 160,000 with AAV6-V1 only.

Table 46. A summary of the descriptive statistics for the repeat run of the PAD Activity Detection Kit, comparing lysate from AAV6-V1 and AAV6-V2 infected cells.

	Condition	Mean (SD)	95% CI of Mean [lower bound, upper bound]
Hepg2	Control	0.214 (0.034)	[0.129, 0.300]
	AAV6-V1 (A)	0.214 (0.010)	[0.189, 0.240]
	AAV6-V1 (B)	0.224 (0.006)	[0.210, 0.238]
	AAV6-V2	0.210 (0.026)	[0.146, 0.273]
Hek-293	Control	0.209 (0.006)	[0.193, 0.224]
	AAV6-V1 (A)	0.214 (0.025)	[0.152, 0.276]
	AAV6-V1 (B)	0.203 (0.019)	[0.155, 0.251]
	AAV6-V2	0.230 (0.029)	[0.158, 0.302]
Hepa1-6	Control	0.208 (0.011)	[0.181, 0.234]
	AAV6-V1 (A)	0.227 (0.031)	[0.150, 0.304]
	AAV6-V1 (B)	0.224 (0.040)	[0.124, 0.323]
	AAV6-V2	0.246 (0.047)	[0.128, 0.364]
Controls	Mouse PAD4	1.292 (0.109)	[1.021, 1.553]
	Negative	0.212 (0.017)	[0.168, 0.255]
	Positive	1.461 (0.145)	[1.100, 1.822]

SD= Standard deviation; CI= confidence interval; Negative Control= Assay buffer alone; Positive Control= PAD cocktail; (A) refers to an older batch of AAV6-V1; (B) refers to a newer batch of AAV6-V1.

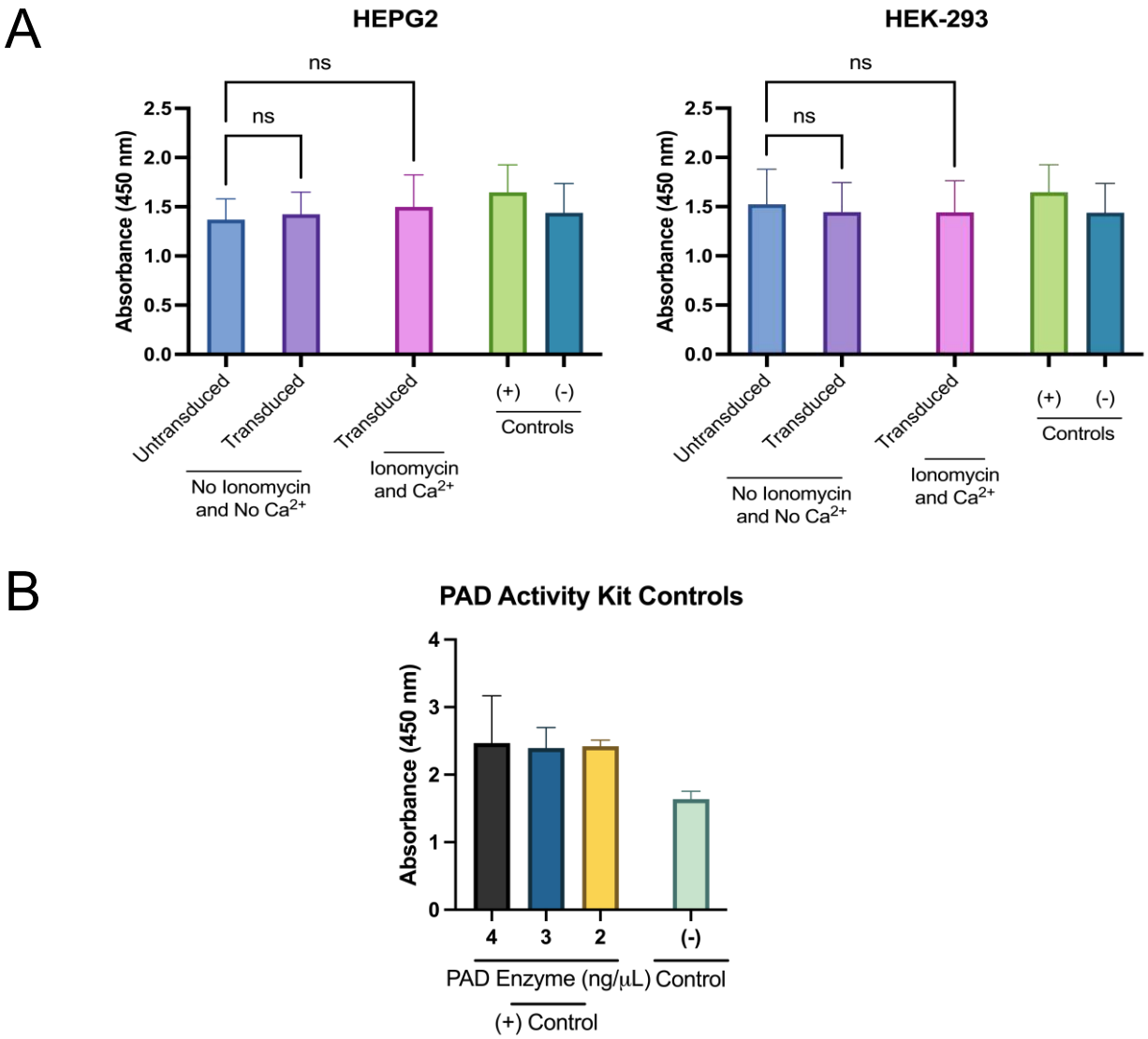

Figure 18. Assessing AAV-encoded PAD4 activity using a commercial kit. Both cell lines were cultured for 96 hours before lysates were collected. In (A), HEPG2 and HEK-293 cells were transduced (MOI 160,000) with only AAV6-V1 (GFP-PAD4 fusion protein) and lysate was collected for examining PAD functionality. Regardless of ionomycin and calcium supplementation, transduced cell lysate did not differ statistically from untransduced cell lysate. Assay negative control had an extremely high absorbance, comparable with the positive control, demonstrating the assay may not be working appropriately. In (B), the positive controls of the assay were assessed separately to understand the poor working conditions as seen in (A). The absorbance levels of the PAD cocktail (positive control) was compared across three concentrations 2 ng/μL, 3 ng/μL, and 4 ng/μL. The higher absorbance from the negative control led to the conclusion that there was a faulty reagent, which was replaced immediately. The asterisks in the graphs were indicative of a significant difference among the two conditions compared: ****p≤0.0001; ***p≤0.001; **p≤0.01; *p<0.05. 'ns' = non-significant (statistically). Bar graphs plotted the mean and standard deviation for each condition.

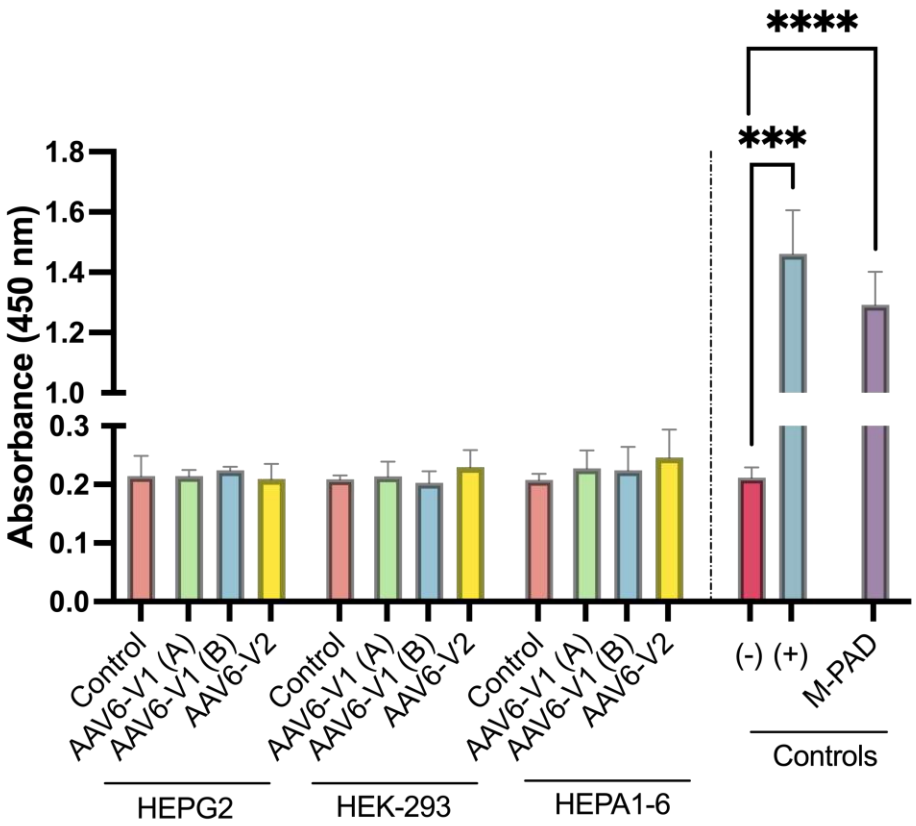

Figure 19. Assessing AAV-encoded PAD4 activity using a commercial kit and comparing both constructs: AAV6-V1 and AAV6-V2. All three cell lines (HEPG2, HEK-293, and HEPA1-6) were cultured for 96 hours before cells were harvested for the commercial kit. Cells were transduced with AAV6-V1 or AAV6-V2 at an MOI of 160,000. Evidently, the lysates from infected cells did not demonstrate any difference in activity relative to the controls, suggesting a non-functional AAV-encoded PAD enzyme. Interestingly, both M-PAD (commercial murine PAD4) and the assay positive control (PAD cocktail) at concentrations of 2 ng/μL, had significantly different absorbance levels than the negative control. Both AAV6-V1 (A) and AAV6-V1 (B) refer to the same constructs, just two different batches. The asterisks in the graphs are indicative of a significant difference among the two conditions compared: ****p≤0.0001; ***p≤0.001; **p≤0.01; *p<0.05. 'ns' = non-significant (statistically). Bar graphs plotted the mean and standard deviation for each condition.

A

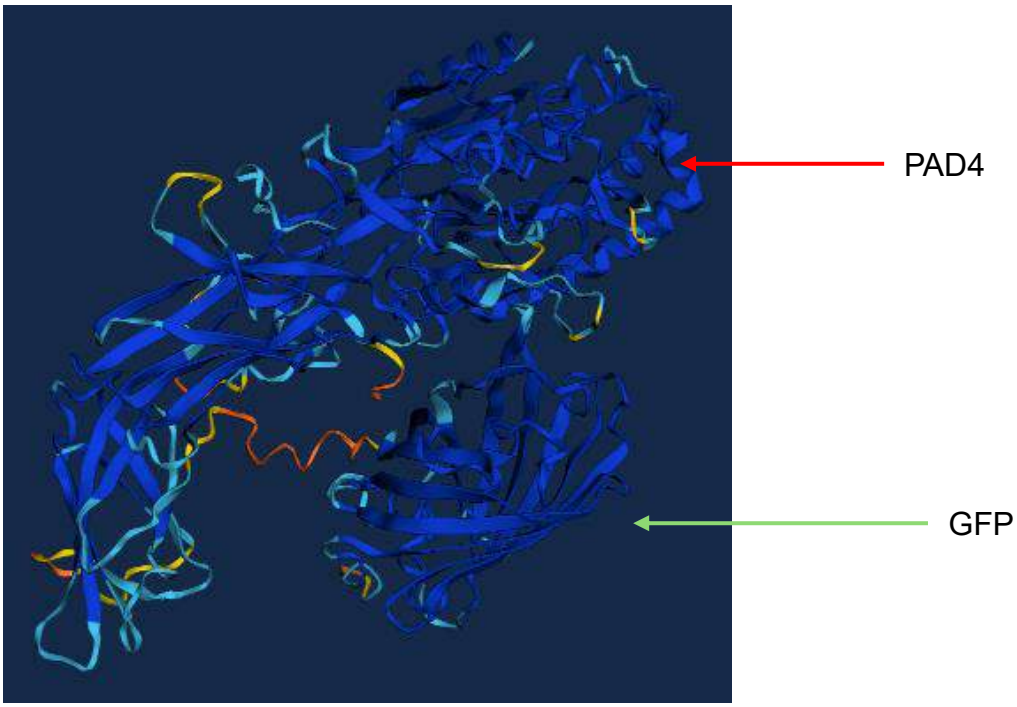

B

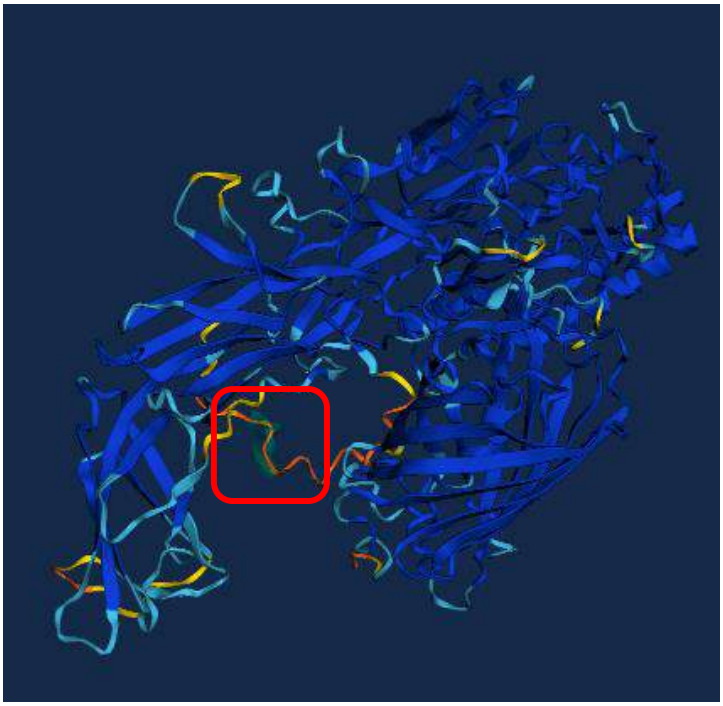

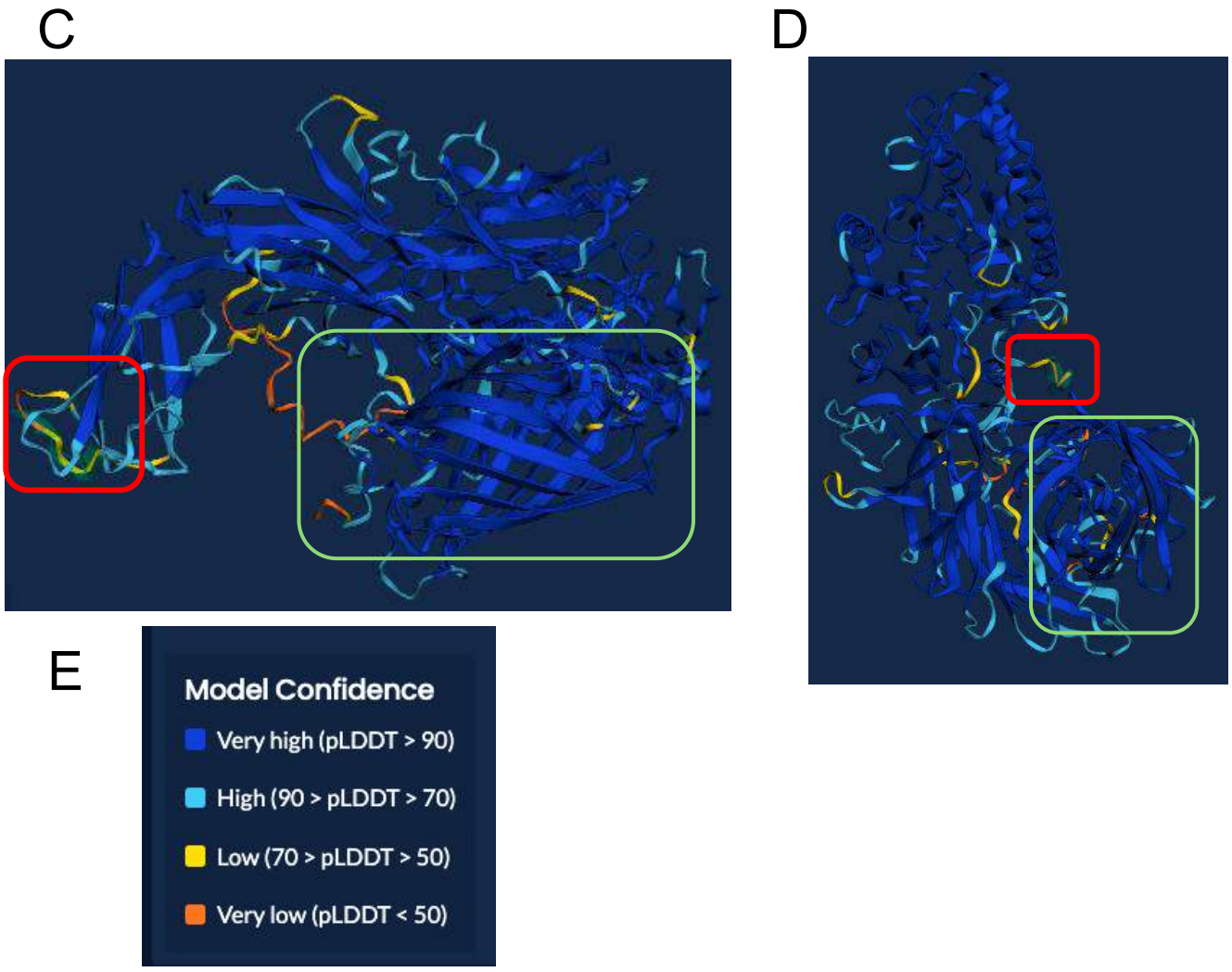

Figure 20. A predicted 3-D model of the GFP-PAD4 fusion protein produced by the AAV6-V1 construct. In (A), an overview of the chimeric protein is provided, highlighting the PAD4 protein (red arrow) and the GFP (green arrow). In (B), the GGSG flexible linker (red box) to demonstrate the spatial proximity of the two components of the chimeric protein, and the closeness of GFP to the C-terminal (active site) domain of PAD4. Given the large size of GFP, and the flexibility of the linker, it is highly likely that the orientation of GFP can interfere with PAD functionality. In (C), the nuclear localization signal of the murine PAD4 (red box) along with GFP (green box) is shown. It was hypothesized that the GFP could interfere with PAD4 localization to the nucleus as well, especially at the level of interaction of the chimeric protein with the nuclear pore complex for translocation. In (D), the position of the GFP (green box) in relation to the KDEL sequence (red box) for ER retention is assessed and it was also thought that the lack of retention of the fusion protein to the ER and a widespread cytoplasmic distribution observed from confocal microscopy, could be due to potential hindering of the sequence by the bulky GFP tag. (E) a breakdown of the prediction software's model confidence using the pLDDT (predicted local distance difference test), with higher scores indicating greater accuracy in predicting the positions of residues.

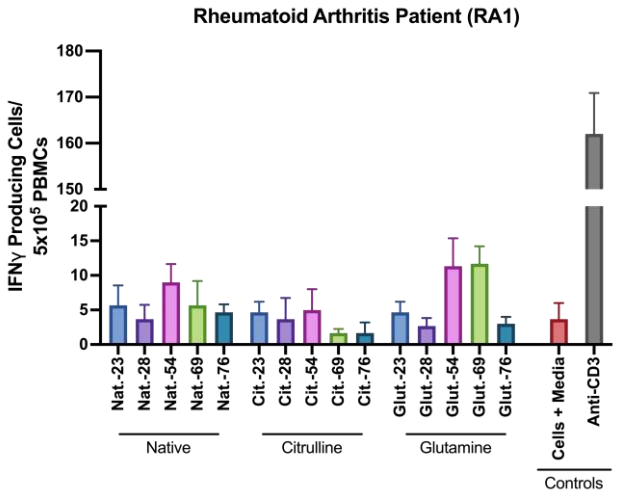
Rheumatoid Arthritis Patient (RA1)
IFNγ Producing Cells/ 5x10^5 PBMCs
Nat.-23
Nat.-28
Nat.-54
Nat.-69
Nat.-76
Cit.-23
Cit.-28
Cit.-54
Cit.-69
Cit.-76
Glut.-23
Glut.-28
Glut.-54
Glut.-69
Glut.-76
Cells + Media
Anti-CD3
Native
Citrulline
Glutamine
Controls

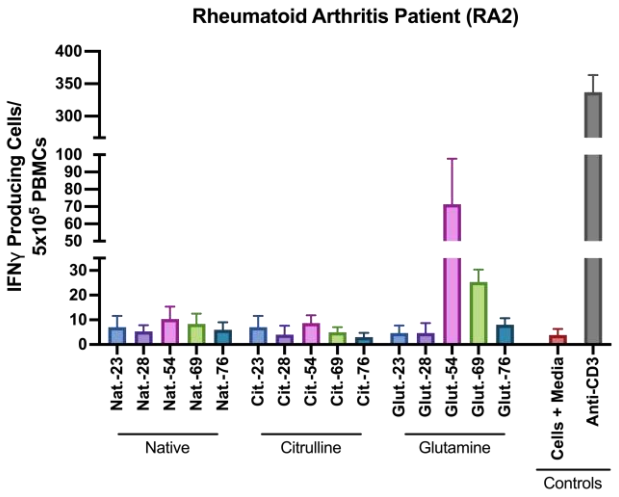
Rheumatoid Arthritis Patient (RA2)
IFNγ Producing Cells/ 5x10^5 PBMCs
Nat.-23
Nat.-28
Nat.-54
Nat.-69
Nat.-76
Cit.-23
Cit.-28
Cit.-54
Cit.-69
Cit.-76
Glut.-23
Glut.-28
Glut.-54
Glut.-69
Glut.-76
Cells + Media
Anti-CD3
Native
Citrulline
Glutamine
Controls

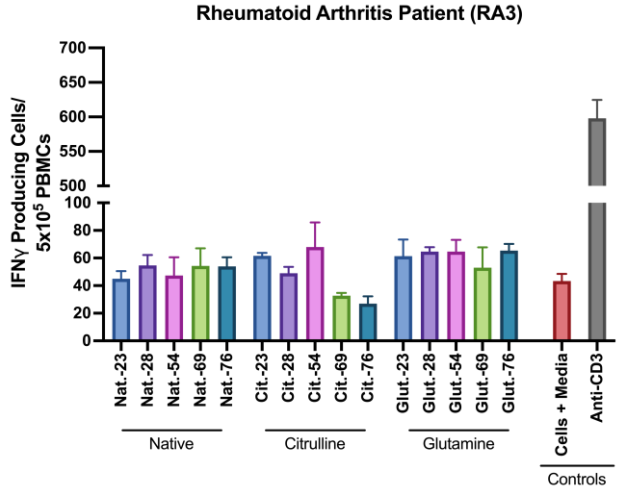
Rheumatoid Arthritis Patient (RA3)
IFNγ Producing Cells/ 5x10^5 PBMCs
Nat.-23
Nat.-28
Nat.-54
Nat.-69
Nat.-76
Cit.-23
Cit.-28
Cit.-54
Cit.-69
Cit.-76
Glut.-23
Glut.-28
Glut.-54
Glut.-69
Glut.-76
Cells + Media
Anti-CD3
Native
Citrulline
Glutamine
Controls

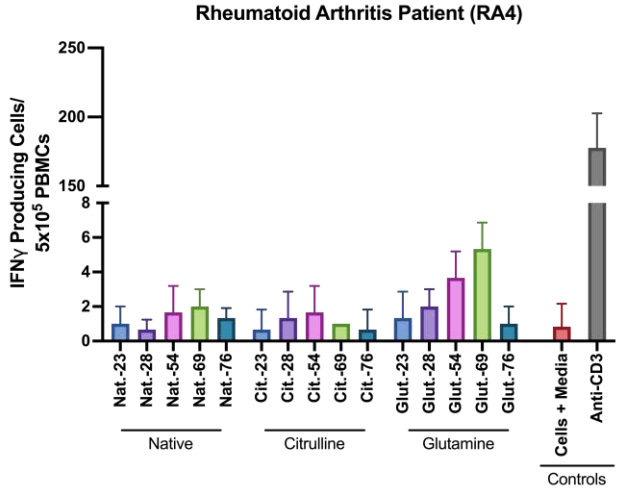
Rheumatoid Arthritis Patient (RA4)
IFNγ Producing Cells/ 5x10^5 PBMCs
Nat.-23
Nat.-28
Nat.-54
Nat.-69
Nat.-76
Cit.-23
Cit.-28
Cit.-54
Cit.-69
Cit.-76
Glut.-23
Glut.-28
Glut.-54
Glut.-69
Glut.-76
Cells + Media
Anti-CD3
Native
Citrulline
Glutamine
Controls

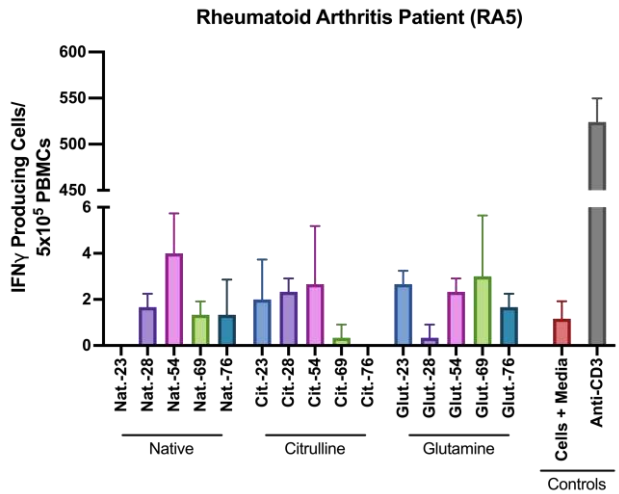
Rheumatoid Arthritis Patient (RA5)
IFNγ Producing Cells/ 5x10^5 PBMCs
Nat.-23
Nat.-28
Nat.-54
Nat.-69
Nat.-76
Cit.-23
Cit.-28
Cit.-54
Cit.-69
Cit.-76
Glut.-23
Glut.-28
Glut.-54
Glut.-69
Glut.-76
Cells + Media
Anti-CD3
Native
Citrulline
Glutamine
Controls

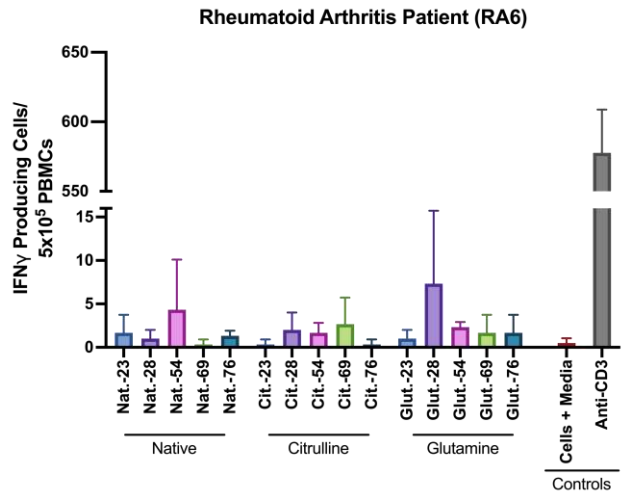
Rheumatoid Arthritis Patient (RA6)
IFNγ Producing Cells/ 5x10^5 PBMCs
Nat.-23
Nat.-28
Nat.-54
Nat.-69
Nat.-76
Cit.-23
Cit.-28
Cit.-54
Cit.-69
Cit.-76
Glut.-23
Glut.-28
Glut.-54
Glut.-69
Glut.-76
Cells + Media
Anti-CD3
Native
Citrulline
Glutamine
Controls

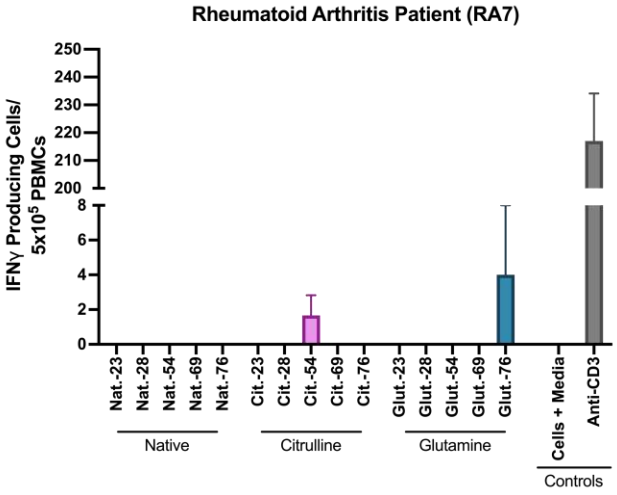
Rheumatoid Arthritis Patient (RA7)
IFNγ Producing Cells/ 5x10^5 PBMCs
Nat.-23
Nat.-28
Nat.-54
Nat.-69
Nat.-76
Cit.-23
Cit.-28
Cit.-54
Cit.-69
Cit.-76
Glut.-23
Glut.-28
Glut.-54
Glut.-69
Glut.-76
Cells + Media
Anti-CD3
Native
Citrulline
Glutamine
Controls

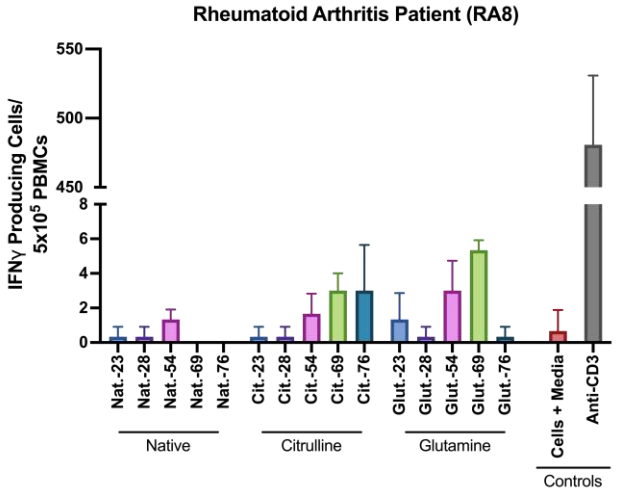
Rheumatoid Arthritis Patient (RA8)
IFNγ Producing Cells/ 5x10^5 PBMCs
Nat.-23
Nat.-28
Nat.-54
Nat.-69
Nat.-76
Cit.-23
Cit.-28
Cit.-54
Cit.-69
Cit.-76
Glut.-23
Glut.-28
Glut.-54
Glut.-69
Glut.-76
Cells + Media
Anti-CD3
Native
Citrulline
Glutamine
Controls

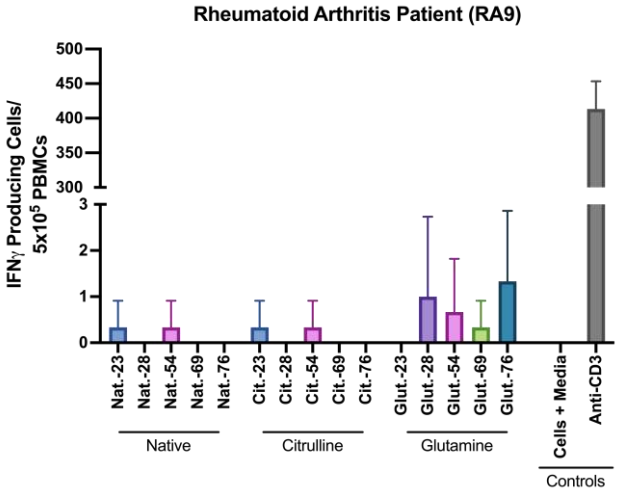
Rheumatoid Arthritis Patient (RA9)
IFNγ Producing Cells/ 5x10^5 PBMCs
Nat.-23
Nat.-28
Nat.-54
Nat.-69
Nat.-76
Cit.-23
Cit.-28
Cit.-54
Cit.-69
Cit.-76
Glut.-23
Glut.-28
Glut.-54
Glut.-69
Glut.-76
Cells + Media
Anti-CD3
Native
Citrulline
Glutamine
Controls

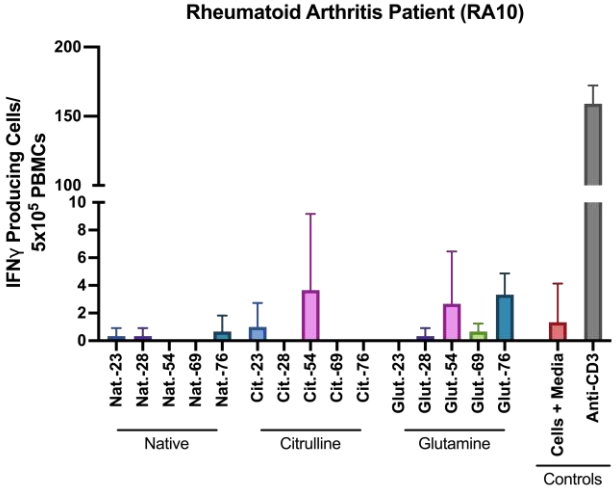
Rheumatoid Arthritis Patient (RA10)
IFNγ Producing Cells/ 5x10^5 PBMCs
Nat.-23
Nat.-28
Nat.-54
Nat.-69
Nat.-76
Cit.-23
Cit.-28
Cit.-54
Cit.-69
Cit.-76
Glut.-23
Glut.-28
Glut.-54
Glut.-69
Glut.-76
Cells + Media
Anti-CD3
Native
Citrulline
Glutamine
Controls

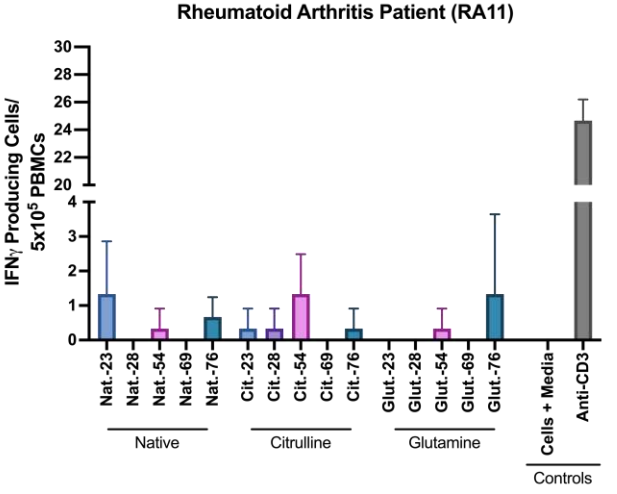
Rheumatoid Arthritis Patient (RA11)
IFNγ Producing Cells/ 5x10^5 PBMCs
Nat.-23
Nat.-28
Nat.-54
Nat.-69
Nat.-76
Cit.-23
Cit.-28
Cit.-54
Cit.-69
Cit.-76
Glut.-23
Glut.-28
Glut.-54
Glut.-69
Glut.-76
Cells + Media
Anti-CD3
Native
Citrulline
Glutamine
Controls

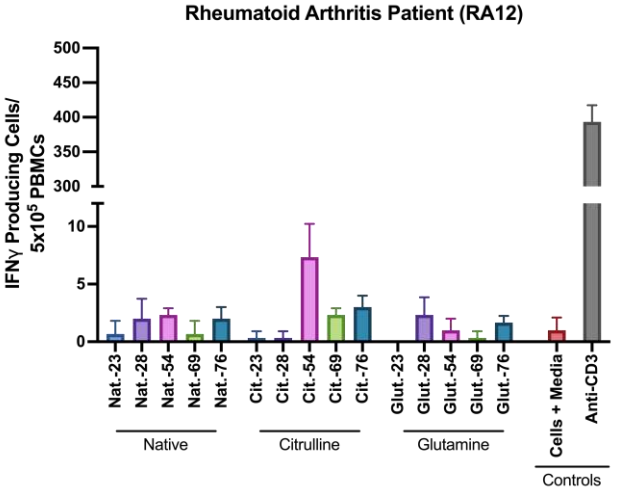
Rheumatoid Arthritis Patient (RA12)
IFNγ Producing Cells/ 5x10^5 PBMCs
Nat.-23
Nat.-28
Nat.-54
Nat.-69
Nat.-76
Cit.-23
Cit.-28
Cit.-54
Cit.-69
Cit.-76
Glut.-23
Glut.-28
Glut.-54
Glut.-69
Glut.-76
Cells + Media
Anti-CD3
Native
Citrulline
Glutamine
Controls

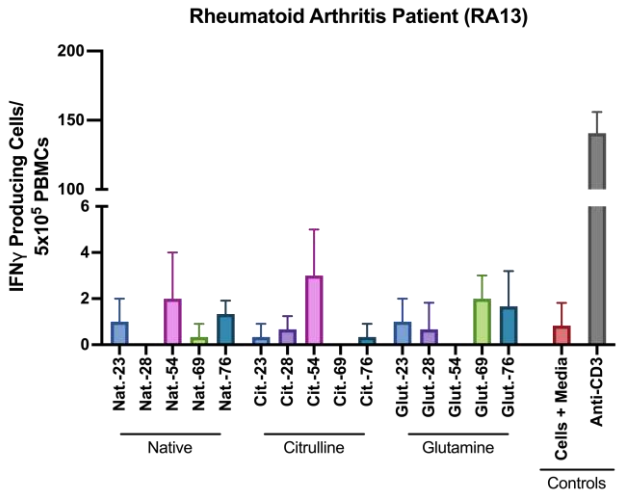
Rheumatoid Arthritis Patient (RA13)
IFNγ Producing Cells/ 5x10^5 PBMCs
Nat.-23
Nat.-28
Nat.-54
Nat.-69
Nat.-76
Cit.-23
Cit.-28
Cit.-54
Cit.-69
Cit.-76
Glut.-23
Glut.-28
Glut.-54
Glut.-69
Glut.-76
Cells + Media
Anti-CD3
Native
Citrulline
Glutamine
Controls

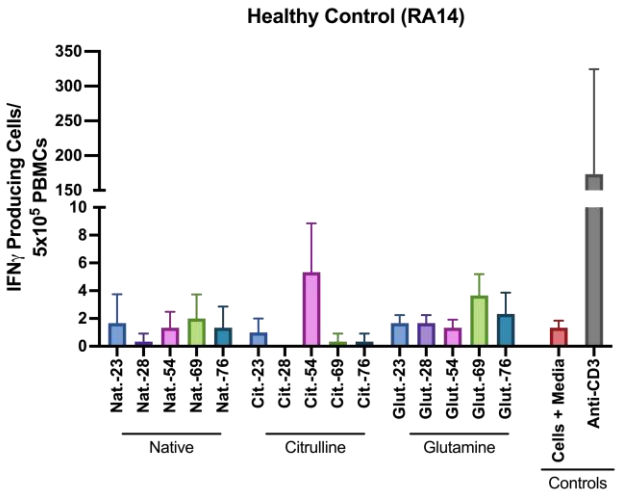
Healthy Control (RA14)
IFNγ Producing Cells/ 5x10^5 PBMCs
Nat.-23
Nat.-28
Nat.-54
Nat.-69
Nat.-76
Cit.-23
Cit.-28
Cit.-54
Cit.-69
Cit.-76
Glut.-23
Glut.-28
Glut.-54
Glut.-69
Glut.-76
Cells + Media
Anti-CD3
Native
Citrulline
Glutamine
Controls

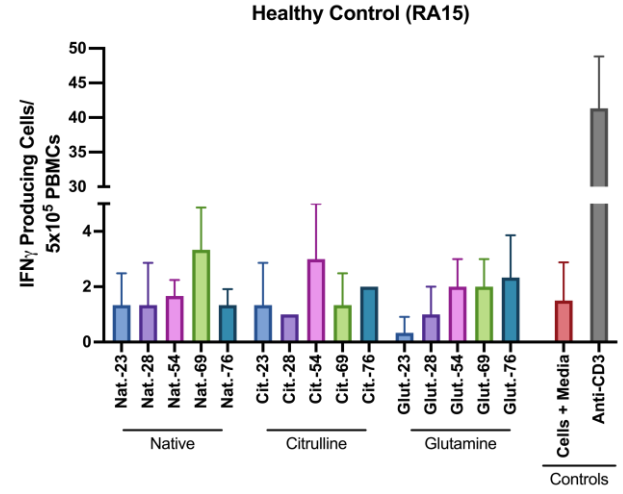
Healthy Control (RA15)
IFNγ Producing Cells/ 5x10^5 PBMCs
Nat.-23
Nat.-28
Nat.-54
Nat.-69
Nat.-76
Cit.-23
Cit.-28
Cit.-54
Cit.-69
Cit.-76
Glut.-23
Glut.-28
Glut.-54
Glut.-69
Glut.-76
Cells + Media
Anti-CD3
Native
Citrulline
Glutamine
Controls

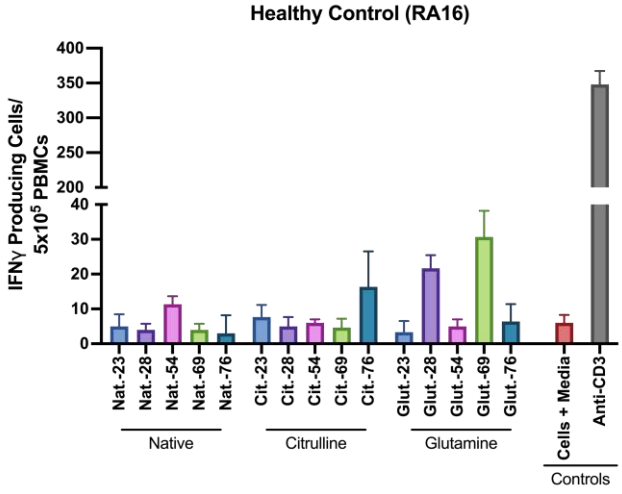
Healthy Control (RA16)
IFNγ Producing Cells/ 5x10^5 PBMCs
Nat.-23
Nat.-28
Nat.-54
Nat.-69
Nat.-76
Cit.-23
Cit.-28
Cit.-54
Cit.-69
Cit.-76
Glut.-23
Glut.-28
Glut.-54
Glut.-69
Glut.-76
Cells + Media
Anti-CD3
Native
Citrulline
Glutamine
Controls

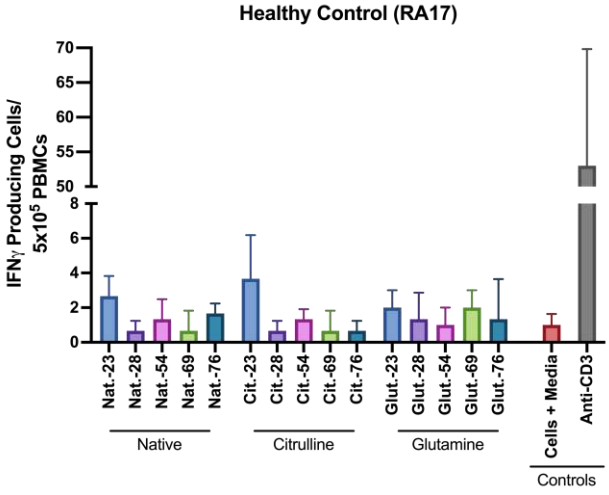
Healthy Control (RA17)
IFNγ Producing Cells/ 5x10^5 PBMCs
Nat.-23
Nat.-28
Nat.-54
Nat.-69
Nat.-76
Cit.-23
Cit.-28
Cit.-54
Cit.-69
Cit.-76
Glut.-23
Glut.-28
Glut.-54
Glut.-69
Glut.-76
Cells + Media
Anti-CD3
Native
Citrulline
Glutamine
Controls

Supplementary Figure 1. T cell responses for all RA patients (n=13; RA1-13) and Healthy Controls (n=4; RA14-17). The frequency of antigen-specific T cell responses were assessed against three versions of five peptides which included β-fibrinogen (peptides 23 and 28), aggrecan core (peptide 54), and anti-thrombin III (peptides 69 and 76). Bar graphs plotted the mean with standard deviation for each condition. Negative control=cells and media alone; Positive control=anti-CD3.

7.0 References

1. Marshall JS, Warrington R, Watson W, Kim HL. An introduction to immunology and immunopathology. Allergy Asthma Clin Immunol. 2018 Sep 12;14(Suppl 2):49. doi: 10.1186/s13223-018-0278-1. PMID: 30263032; PMCID: PMC6156898.
2. Arango Duque G, Descoteaux A. Macrophage cytokines: involvement in immunity and infectious diseases. Front Immunol. 2014 Oct 7;5:491. doi: 10.3389/fimmu.2014.00491. PMID: 25339958; PMCID: PMC4188125.
3. Sckisel GD, Bouchlaka MN, Monjazeb AM, Crittenden M, Curti BD, Wilkins DE, Alderson KA, Sungur CM, Ames E, Mirsoian A, Reddy A, Alexander W, Soulika A, Blazar BR, Longo DL, Wiltrout RH, Murphy WJ. Out-of-Sequence Signal 3 Paralyzes Primary CD4(+) T-Cell-Dependent Immunity. Immunity. 2015 Aug 18;43(2):240-50. doi: 10.1016/j.immuni.2015.06.023. Epub 2015 Jul 28. PMID: 26231116; PMCID: PMC4770886.
4. Tai Y, Wang Q, Korner H, Zhang L, Wei W. Molecular Mechanisms of T Cells Activation by Dendritic Cells in Autoimmune Diseases. Front Pharmacol. 2018 Jun 26;9:642. doi: 10.3389/fphar.2018.00642. PMID: 29997500; PMCID: PMC6028573.
5. Cruz-Tapias P, Castiblanco J, Anaya JM. Major histocompatibility complex: Antigen processing and presentation. In: Anaya JM, Shoenfeld Y, Rojas-Villarraga A, et al., editors. Autoimmunity: From Bench to Bedside [Internet]. Bogota (Colombia): El Rosario University Press; 2013 Jul 18. Chapter 10. Available from: https://www.ncbi.nlm.nih.gov/books/NBK459467/
6. Appleman LJ, Boussiotis VA. T cell anergy and costimulation. Immunol Rev. 2003 Apr;192:161-80. doi: 10.1034/j.1600-065x.2003.00009.x. PMID: 12670403.
7. Schietinger A, Greenberg PD. Tolerance and exhaustion: defining mechanisms of T cell dysfunction. Trends Immunol. 2014 Feb;35(2):51-60. doi: 10.1016/j.it.2013.10.001. Epub 2013 Nov 6. PMID: 24210163; PMCID: PMC3946600.
8. Sprent J, Kishimoto H. The thymus and central tolerance. Philos Trans R Soc Lond B Biol Sci. 2001 May 29;356(1409):609-16. doi: 10.1098/rstb.2001.0846. PMID: 11375064; PMCID: PMC1088448.
9. Sykes M. Immune tolerance: mechanisms and application in clinical transplantation. J Intern Med. 2007 Sep;262(3):288-310. doi: 10.1111/j.1365-2796.2007.01855.x. PMID: 17697153.
10. Audiger C, Rahman MJ, Yun TJ, Tarbell KV, Lesage S. The importance of dendritic cells in maintaining immune tolerance. The Journal of Immunology. 2017 Mar 15;198(6):2223-31.
11. Nemazee, D. Mechanisms of central tolerance for B cells. *Nat Rev Immunol* **17,** 281–294 (2017). https://doi.org/10.1038/nri.2017.19
12. Anderton S, Burkhart C, Metzler B, Wraith D. Mechanisms of central and peripheral T-cell tolerance: lessons from experimental models of multiple sclerosis. Immunol Rev. 1999 Jun;169:123-37. doi: 10.1111/j.1600-065x.1999.tb01311.x. PMID: 10450513.
13. Cibotti R, Kanellopoulos JM, Cabaniols JP, Halle-Panenko O, Kosmatopoulos K, Sercarz E, Kourilsky P. Tolerance to a self-protein involves its immunodominant but does not involve its subdominant determinants. Proc Natl Acad Sci U S A. 1992

Jan 1;89(1):416-20. doi: 10.1073/pnas.89.1.416. PMID: 1370355; PMCID: PMC48248.

14. Harrington CJ, Paez A, Hunkapiller T, Mannikko V, Brabb T, Ahearn M, Beeson C, Goverman J. Differential tolerance is induced in T cells recognizing distinct epitopes of myelin basic protein. Immunity. 1998 May;8(5):571-80. doi: 10.1016/s1074-7613(00)80562-2. PMID: 9620678.
15. Walker, L., Abbas, A. The enemy within: keeping self-reactive T cells at bay in the periphery. *Nat Rev Immunol* **2,** 11–19 (2002). https://doi.org/10.1038/nri701
16. Gatzka, Martina; Walsh, Craig M. (2007). Apoptotic signal transduction and T cell tolerance. Autoimmunity, 40(6), 442–452. doi:10.1080/08916930701464962
17. Alderson MR, Tough TW, Davis-Smith T, Braddy S, Falk B, Schooley KA, Goodwin RG, Smith CA, Ramsdell F, Lynch DH. Fas ligand mediates activation-induced cell death in human T lymphocytes. J Exp Med. 1995 Jan 1;181(1):71-7. doi: 10.1084/jem.181.1.71. PMID: 7528780; PMCID: PMC2191813.
18. Akimzhanov AM, Wang X, Sun J, Boehning D. T-cell receptor complex is essential for Fas signal transduction. Proc Natl Acad Sci U S A. 2010 Aug 24;107(34):15105-10. doi: 10.1073/pnas.1005419107. Epub 2010 Aug 9. PMID: 20696918; PMCID: PMC2930531.
19. Sakaguchi S, Sakaguchi N, Asano M, Itoh M, Toda M. Immunologic self-tolerance maintained by activated T cells expressing IL-2 receptor alpha-chains (CD25). Breakdown of a single mechanism of self-tolerance causes various autoimmune diseases. J Immunol. 1995 Aug 1;155(3):1151-64. Doi: 10.4049/jimmunol.155.3.1151. PMID: 7636184.
20. Josefowicz SZ, Lu LF, Rudensky AY. Regulatory T cells: mechanisms of differentiation and function. Annu Rev Immunol. 2012;30:531-64. doi: 10.1146/annurev.immunol.25.022106.141623. Epub 2012 Jan 6. PMID: 22224781; PMCID: PMC6066374.
21. Dieckmann D, Plottner H, Berchtold S, Berger T, Schuler G. Ex vivo isolation and characterization of CD4(+)CD25(+) T cells with regulatory properties from human blood. J Exp Med. 2001 Jun 4;193(11):1303-10. doi: 10.1084/jem.193.11.1303. PMID: 11390437; PMCID: PMC2193384.
22. Grossman WJ, Verbsky JW, Barchet W, Colonna M, Atkinson JP, Ley TJ. Human T regulatory cells can use the perforin pathway to cause autologous target cell death. Immunity. 2004 Oct;21(4):589-601. doi: 10.1016/j.immuni.2004.09.002. PMID: 15485635.
23. Schmidt A, Oberle N, Krammer PH. Molecular mechanisms of treg-mediated T cell suppression. Front Immunol. 2012 Mar 21;3:51. doi: 10.3389/fimmu.2012.00051. PMID: 22566933; PMCID: PMC3341960.
24. Dieckmann D, Plöttner H, Dotterweich S, Schuler G. Activated CD4+ CD25+ T cells suppress antigen-specific CD4+ and CD8+ T cells but induce a suppressive phenotype only in CD4+ T cells. Immunology. 2005 Jul;115(3):305-14. doi: 10.1111/j.1365-2567.2005.02144.x. PMID: 15946248; PMCID: PMC1782171
25. Jenkins, M. K. (1987). Antigen presentation by chemically modified splenocytes induces antigen- specific T cell unresponsiveness in vitro and in vivo. Journal of Experimental Medicine, 165(2), 302–319. doi:10.1084/jem.165.2.302

26. Fathman, C., Lineberry, N. Molecular mechanisms of $CD4^+$ T-cell anergy. *Nat Rev Immunol* **7,** 599–609 (2007). https://doi.org/10.1038/nri2131
27. Mondino A, Whaley CD, DeSilva DR, Li W, Jenkins MK, Mueller DL. Defective transcription of the IL-2 gene is associated with impaired expression of c-Fos, FosB, and JunB in anergic T helper 1 cells. J Immunol. 1996 Sep 1;157(5):2048-57. PMID: 8757326.
28. Wang L, Wang FS, Gershwin ME. Human autoimmune diseases: a comprehensive update. J Intern Med. 2015 Oct;278(4):369-95. doi: 10.1111/joim.12395. Epub 2015 Jul 25. PMID: 26212387.
29. Klareskog L, Rönnelid J, Lundberg K, Padyukov L, Alfredsson L. Immunity to Citrullinated Proteins in Rheumatoid Arthritis. Annu. Rev. Immunol. 2008; 26:651–75. doi: 10.1146/annurev.immunol.26.021607.090244. PMID: 18173373.
30. Biga LM, Dawson S, Harwell A, Hopkins R, Kaufmann J, LeMaster M, Matern P; Morrison-Graham K, Quick D, Runyeon J. Anatomy & Physiology. OpenStax/Oregon State University; 2019. 497-501 p.
31. Iwanaga T, Shikichi M, Kitamura H, Yanase H, Nozawa-Inoue K. Morphology and functional roles of synoviocytes in the joint. Arch Histol Cytol. 2000 Mar;63(1):17-31. doi: 10.1679/aohc.63.17. PMID: 10770586.
32. Iqbal K, Kelly C. Treatment of rheumatoid arthritis-associated interstitial lung disease: a perspective review. Ther Adv Musculoskelet Dis. 2015;7(6):247-67. doi: 10.1177/1759720X15612250.
33. Guo Q, Wang Y, Xu D, Nossent J, Pavlos NJ, Xu J. Rheumatoid arthritis: pathological mechanisms and modern pharmacologic therapies. Bone Res. 2018 Apr 27;6:15. doi: 10.1038/s41413-018-0016-9. PMID: 29736302; PMCID: PMC5920070.
34. Cojocaru M, Cojocaru IM, Silosi I, Vrabie CD, Tanasescu R. Extra-articular Manifestations in Rheumatoid Arthritis. Maedica (Bucur). 2010 Dec;5(4):286-91. PMID: 21977172; PMCID: PMC3152850.
35. Widdifield J, Paterson JM, Bernatsky S, Tu K, Tomlinson G, Kuriya B, Thorne JC, Bombardier C. The epidemiology of rheumatoid arthritis in Ontario, Canada. Arthritis Rheumatol. 2014 Apr;66(4):786-93. doi: 10.1002/art.38306. PMID: 24757131.
36. Boots AM, Maier AB, Stinissen P, Masson P, Lories RJ, De Keyser F. The influence of ageing on the development and management of rheumatoid arthritis. Nat Rev Rheumatol. 2013 Oct;9(10):604-13. doi: 10.1038/nrrheum.2013.92. Epub 2013 Jun 18. PMID: 23774902.
37. Hitchon CA, Khan S, Elias B, Lix LM, Peschken CA. Prevalence and Incidence of Rheumatoid Arthritis in Canadian First Nations and Non–First Nations People, JCR: Journal of Clinical Rheumatology: August 2020 - Volume 26 - Issue 5 - p 169-175 doi: 10.1097/RHU.0000000000001006
38. Kvien TK, Uhlig T, Ødegård S, Heiberg MS. Epidemiological aspects of rheumatoid arthritis: the sex ratio. Ann N Y Acad Sci. 2006 Jun;1069:212-22. doi: 10.1196/annals.1351.019. PMID: 16855148.
39. Linos A, Worthington JW, O'Fallon WM, Kurland LT. The epidemiology of rheumatoid arthritis in Rochester, Minnesota: a study of incidence, prevalence, and

mortality. Am J Epidemiol. 1980 Jan;111(1):87-98. doi: 10.1093/oxfordjournals.aje.a112878. PMID: 7352462.

40. Cross M, Smith E, Hoy D, Carmona L, Wolfe F, Vos T, Williams B, Gabriel S, Lassere M, Johns N, Buchbinder R, Woolf A, March L. The global burden of rheumatoid arthritis: estimates from the global burden of disease 2010 study. Ann Rheum Dis. 2014 Jul;73(7):1316-22. doi: 10.1136/annrheumdis-2013-204627. Epub 2014 Feb 18. PMID: 24550173.
41. Chaojie Yu, Chong Liu, Jie Jiang, Hao Li, Jiarui Chen, Tianyou Chen, Xinli Zhan, "Gender Differences in Rheumatoid Arthritis: Interleukin-4 Plays an Important Role", *Journal of Immunology Research*, vol. 2020, Article ID 4121524, 12 pages, 2020. https://doi.org/10.1155/2020/4121524
42. Deshiré Alpízar-Rodríguez, Nicola Pluchino, Geraldine Canny, Cem Gabay, Axel Finckh, The role of female hormonal factors in the development of rheumatoid arthritis, *Rheumatology*, Volume 56, Issue 8, August 2017, Pages 1254–1263, https://doi.org/10.1093/rheumatology/kew318
43. MacGregor AJ, Snieder H, Rigby AS, Koskenvuo M, Kaprio J, Aho K, Silman AJ. Characterizing the quantitative genetic contribution to rheumatoid arthritis using data from twins. Arthritis Rheum. 2000 Jan;43(1):30-7. doi: 10.1002/1529-0131(200001)43:1<30::AID-ANR5>3.0.CO;2-B. PMID: 10643697.
44. Silman AJ, MacGregor AJ, Thomson W, Holligan S, Carthy D, Farhan A, Ollier WE. Twin concordance rates for rheumatoid arthritis: results from a nationwide study. Br J Rheumatol. 1993 Oct;32(10):903-7. doi: 10.1093/rheumatology/32.10.903. PMID: 8402000.
45. Aho K, Koskenvuo M, Tuominen J, Kaprio J. Occurrence of rheumatoid arthritis in a nationwide series of twins. J Rheumatol. 1986 Oct;13(5):899-902. PMID: 3820198.
46. Stahl EA, Raychaudhuri S, Remmers EF, Xie G, Eyre S, Thomson BP, Li Y, Kurreeman FA, Zhernakova A, Hinks A, Guiducci C, Chen R, Alfredsson L, Amos CI, Ardlie KG; BIRAC Consortium, Barton A, Bowes J, Brouwer E, Burtt NP, Catanese JJ, Coblyn J, Coenen MJ, Costenbader KH, Criswell LA, Crusius JB, Cui J, de Bakker PI, De Jager PL, Ding B, Emery P, Flynn E, Harrison P, Hocking LJ, Huizinga TW, Kastner DL, Ke X, Lee AT, Liu X, Martin P, Morgan AW, Padyukov L, Posthumus MD, Radstake TR, Reid DM, Seielstad M, Seldin MF, Shadick NA, Steer S, Tak PP, Thomson W, van der Helm-van Mil AH, van der Horst-Bruinsma IE, van der Schoot CE, van Riel PL, Weinblatt ME, Wilson AG, Wolbink GJ, Wordsworth BP; YEAR Consortium, Wijmenga C, Karlson EW, Toes RE, de Vries N, Begovich AB, Worthington J, Siminovitch KA, Gregersen PK, Klareskog L, Plenge RM. Genome-wide association study meta-analysis identifies seven new rheumatoid arthritis risk loci. Nat Genet. 2010 Jun;42(6):508-14. doi: 10.1038/ng.582. Epub 2010 May 9. PMID: 20453842; PMCID: PMC4243840.
47. Clarke, F., Purvis, H.A., Sanchez-Blanco, C. *et al.* The protein tyrosine phosphatase PTPN22 negatively regulates presentation of immune complex derived antigens. *Sci Rep* **8,** 12692 (2018). https://doi.org/10.1038/s41598-018-31179-x
48. Begovich AB, Carlton VE, Honigberg LA, Schrodi SJ, Chokkalingam AP, Alexander HC, Ardlie KG, Huang Q, Smith AM, Spoerke JM, Conn MT, Chang M,

Chang SY, Saiki RK, Catanese JJ, Leong DU, Garcia VE, McAllister LB, Jeffery DA, Lee AT, Batliwalla F, Remmers E, Criswell LA, Seldin MF, Kastner DL, Amos CI, Sninsky JJ, Gregersen PK. A missense single-nucleotide polymorphism in a gene encoding a protein tyrosine phosphatase (PTPN22) is associated with rheumatoid arthritis. Am J Hum Genet. 2004 Aug;75(2):330-7. doi: 10.1086/422827. Epub 2004 Jun 18. PMID: 15208781; PMCID: PMC1216068.

49. Kerlan-Candon S, Combe B, Vincent R, Clot J, Pinet V, Eliaou JF. HLA-DRB1 gene transcripts in rheumatoid arthritis. Clin Exp Immunol. 2001 Apr;124(1):142-9. doi: 10.1046/j.1365-2249.2001.01498.x. PMID: 11359453; PMCID: PMC1906025.
50. Gregersen PK, Silver J, Winchester RJ. The shared epitope hypothesis. An approach to understanding the molecular genetics of susceptibility to rheumatoid arthritis. Arthritis Rheum. 1987 Nov;30(11):1205-13. doi: 10.1002/art.1780301102. PMID: 2446635.
51. Ting YT, Petersen J, Ramarathinam SH, Scally SW, Loh KL, Thomas R, Suri A, Baker DG, Purcell AW, Reid HH, Rossjohn J. The interplay between citrullination and HLA-DRB1 polymorphism in shaping peptide binding hierarchies in rheumatoid arthritis. J Biol Chem. 2018 Mar 2;293(9):3236-3251. doi: 10.1074/jbc.RA117.001013. Epub 2018 Jan 9. PMID: 29317506; PMCID: PMC5836122.
52. Fugger L, Rothbard JB, Sonderstrup-McDevitt G. Specificity of an HLA-DRB1*0401-restricted T cell response to type II collagen. Eur J Immunol. 1996 Apr;26(4):928-33. doi: 10.1002/eji.1830260431. PMID: 8625990.
53. Rosloniec EF, Brand DD, Myers LK, Whittington KB, Gumanovskaya M, Zaller DM, Woods A, Altmann DM, Stuart JM, Kang AH. An HLA-DR1 transgene confers susceptibility to collagen-induced arthritis elicited with human type II collagen. J Exp Med. 1997 Mar 17;185(6):1113-22. doi: 10.1084/jem.185.6.1113. PMID: 9091584; PMCID: PMC2196244.
54. Restrepo JF, del Rincón I, Battafarano DF, Haas RW, Doria M, Escalante A. Clinical and laboratory factors associated with interstitial lung disease in rheumatoid arthritis. Clin Rheumatol. 2015 Sep;34(9):1529-36. doi: 10.1007/s10067-015-3025-8. Epub 2015 Aug 9. PMID: 26255186.
55. Esposito AJ, Chu SG, Madan R, Doyle TJ, Dellaripa PF. Thoracic Manifestations of Rheumatoid Arthritis. Clin Chest Med. 2019 Sep;40(3):545-560. doi: 10.1016/j.ccm.2019.05.003. Epub 2019 Jul 6. PMID: 31376890; PMCID: PMC6994971.
56. Zhao R, Zhang YW, Guo JC, Qiao J, Song S, Zhang TT, Zhang HY, Zhang SX. Genetic evidence reveals a causal relationship between rheumatoid arthritis and interstitial lung disease. Front Genet. 2024 May 14;15:1395315. doi: 10.3389/fgene.2024.1395315. PMID: 38808332; PMCID: PMC11130360.
57. Jacobsson LT, Jacobsson ME, Askling J, Knowler WC. Perinatal characteristics and risk of rheumatoid arthritis. BMJ. 2003 May 17;326(7398):1068-9. doi: 10.1136/bmj.326.7398.1068. PMID: 12750209; PMCID: PMC155691.
58. Bengtsson C, Nordmark B, Klareskog L, Lundberg I, Alfredsson L; EIRA Study Group. Socioeconomic status and the risk of developing rheumatoid arthritis: results from the Swedish EIRA study. Ann Rheum Dis. 2005 Nov;64(11):1588-94.

doi: 10.1136/ard.2004.031666. Epub 2005 Apr 20. PMID: 15843455; PMCID: PMC1755268.

59. Kharlamova N, Jiang X, Sherina N, Potempa B, Israelsson L, Quirke AM, Eriksson K, Yucel-Lindberg T, Venables PJ, Potempa J, Alfredsson L, Lundberg K. Antibodies to Porphyromonas gingivalis Indicate Interaction Between Oral Infection, Smoking, and Risk Genes in Rheumatoid Arthritis Etiology. Arthritis Rheumatol. 2016 Mar;68(3):604-13. doi: 10.1002/art.39491. PMID: 26554752; PMCID: PMC4767537.
60. Makrygiannakis D, Hermansson M, Ulfgren AK, Nicholas AP, Zendman AJ, Eklund A, Grunewald J, Skold CM, Klareskog L, Catrina AI. Smoking increases peptidylarginine deiminase 2 enzyme expression in human lungs and increases citrullination in BAL cells. Ann Rheum Dis. 2008 Oct;67(10):1488-92. doi: 10.1136/ard.2007.075192. Epub 2008 Apr 15. PMID: 18413445.
61. J. R. Glossop, P. T. Dawes, D. L. Mattey, Association between cigarette smoking and release of tumour necrosis factor α and its soluble receptors by peripheral blood mononuclear cells in patients with rheumatoid arthritis, *Rheumatology*, Volume 45, Issue 10, October 2006, Pages 1223–1229, https://doi.org/10.1093/rheumatology/kel094
62. Stolt P, Bengtsson C, Nordmark B, Lindblad S, Lundberg I, Klareskog L, Alfredsson L; EIRA study group. Quantification of the influence of cigarette smoking on rheumatoid arthritis: results from a population based case-control study, using incident cases. Ann Rheum Dis. 2003 Sep;62(9):835-41. doi: 10.1136/ard.62.9.835. PMID: 12922955; PMCID: PMC1754669.
63. Rafiei M, Kiani F, Sayehmiri F, Sayehmiri K, Sheikhi A, Zamanian Azodi M. Study of *Porphyromonas gingivalis* in periodontal diseases: A systematic review and meta-analysis. Med J Islam Repub Iran. 2017 Sep 12;31:62. doi: 10.18869/mjiri.31.62. PMID: 29445691; PMCID: PMC5804457.
64. Totaro MC, Cattani P, Ria F, Tolusso B, Gremese E, Fedele AL, D'Onghia S, Marchetti S, Di Sante G, Canestri S, Ferraccioli G. Porphyromonas gingivalis and the pathogenesis of rheumatoid arthritis: analysis of various compartments including the synovial tissue. Arthritis Res Ther. 2013 Jun 18;15(3):R66. doi: 10.1186/ar4243. PMID: 23777892; PMCID: PMC4060366.
65. Blank M, Barzilai O, Shoenfeld Y. Molecular mimicry and auto-immunity. Clin Rev Allergy Immunol. 2007 Feb;32(1):111-8. doi: 10.1007/BF02686087. PMID: 17426366.
66. Vanderlugt CL, Miller SD. Epitope spreading in immune-mediated diseases: implications for immunotherapy. Nat Rev Immunol. 2002 Feb;2(2):85-95. doi: 10.1038/nri724. PMID: 11910899.
67. Damian R.T. Molecular Mimicry: Antigen Sharing by Parasite and Host and Its Consequences. Am. Nat. 1964;98:129–149. doi: 10.1086/282313
68. Lundberg K, Kinloch A, Fisher BA, Wegner N, Wait R, Charles P, Mikuls TR, Venables PJ. Antibodies to citrullinated alpha-enolase peptide 1 are specific for rheumatoid arthritis and cross-react with bacterial enolase. Arthritis Rheum. 2008 Oct;58(10):3009-19. doi: 10.1002/art.23936. PMID: 18821669.
69. Ascough S, Ingram RJ, Chu KK, Musson JA, Moore SJ, Gallagher T, Baillie L, Williamson ED, Robinson JH, Maillere B, Boyton RJ, Altmann DM. CD4+ T Cells

Targeting Dominant and Cryptic Epitopes from Bacillus anthracis Lethal Factor. Front Microbiol. 2016 Jan 5;6:1506. doi: 10.3389/fmicb.2015.01506. PMID: 26779161; PMCID: PMC4700811.

70. Aletaha D, Neogi T, Silman AJ, Funovits J, Felson DT, Bingham CO 3rd, Birnbaum NS, Burmester GR, Bykerk VP, Cohen MD, Combe B, Costenbader KH, Dougados M, Emery P, Ferraccioli G, Hazes JM, Hobbs K, Huizinga TW, Kavanaugh A, Kay J, Kvien TK, Laing T, Mease P, Ménard HA, Moreland LW, Naden RL, Pincus T, Smolen JS, Stanislawska-Biernat E, Symmons D, Tak PP, Upchurch KS, Vencovský J, Wolfe F, Hawker G. 2010 Rheumatoid arthritis classification criteria: an American College of Rheumatology/European League Against Rheumatism collaborative initiative. Arthritis Rheum. 2010 Sep;62(9):2569-81. doi: 10.1002/art.27584. PMID: 20872595.
71. Sparks JA. Rheumatoid Arthritis. Ann Intern Med. 2019 Jan 1;170(1):ITC1-ITC16. doi: 10.7326/AITC201901010. PMID: 30596879.
72. Gulati M, Farah Z, Mouyis M. Clinical features of rheumatoid arthritis. Medicine: Elsevier; 46:211-215; 2018. doi:10.1016/j.mpmed.2018.01.008
73. Baecklund E, Iliadou A, Askling J, Ekbom A, Backlin C, Granath F, Catrina AI, Rosenquist R, Feltelius N, Sundström C, Klareskog L. Association of chronic inflammation, not its treatment, with increased lymphoma risk in rheumatoid arthritis. Arthritis Rheum. 2006 Mar;54(3):692-701. doi: 10.1002/art.21675. PMID: 16508929.
74. Ingegnoli F, Castelli R, Gualtierotti R. Rheumatoid factors: clinical applications. Dis Markers. 2013;35(6):727-34. doi: 10.1155/2013/726598. Epub 2013 Nov 13. PMID: 24324289; PMCID: PMC3845430.
75. Nielen MM, van Schaardenburg D, Reesink HW, van de Stadt RJ, van der Horst-Bruinsma IE, de Koning MH, Habibuw MR, Vandenbroucke JP, Dijkmans BA. Specific autoantibodies precede the symptoms of rheumatoid arthritis: a study of serial measurements in blood donors. Arthritis Rheum. 2004 Feb;50(2):380-6. doi: 10.1002/art.20018. PMID: 14872479.
76. Rantapää-Dahlqvist S, de Jong BA, Berglin E, Hallmans G, Wadell G, Stenlund H, Sundin U, van Venrooij WJ. Antibodies against cyclic citrullinated peptide and IgA rheumatoid factor predict the development of rheumatoid arthritis. Arthritis Rheum. 2003 Oct;48(10):2741-9. doi: 10.1002/art.11223. PMID: 14558078.
77. Lee DM, Schur PH. Clinical utility of the anti-CCP assay in patients with rheumatic diseases. Ann Rheum Dis. 2003 Sep;62(9):870-4. doi: 10.1136/ard.62.9.870. PMID: 12922961; PMCID: PMC1754666.
78. Nishimura K, Sugiyama D, Kogata Y, Tsuji G, Nakazawa T, Kawano S, Saigo K, Morinobu A, Koshiba M, Kuntz KM, Kamae I, Kumagai S. Meta-analysis: diagnostic accuracy of anti-cyclic citrullinated peptide antibody and rheumatoid factor for rheumatoid arthritis. Ann Intern Med. 2007 Jun 5;146(11):797-808. doi: 10.7326/0003-4819-146-11-200706050-00008. PMID: 17548411.
79. Whiting PF, Smidt N, Sterne JA, Harbord R, Burton A, Burke M, Beynon R, Ben-Shlomo Y, Axford J, Dieppe P. Systematic review: accuracy of anti-citrullinated Peptide antibodies for diagnosing rheumatoid arthritis. Ann Intern Med. 2010 Apr 6;152(7):456-64; W155-66. doi: 10.7326/0003-4819-152-7-201004060-00010. PMID: 20368651.

80. Pope JE, Choy EH. C-reactive protein and implications in rheumatoid arthritis and associated comorbidities. Semin Arthritis Rheum. 2021 Feb;51(1):219-229. doi: 10.1016/j.semarthrit.2020.11.005. Epub 2020 Dec 17. PMID: 33385862.
81. Bullock J, Rizvi SAA, Saleh AM, Ahmed SS, Do DP, Ansari RA, Ahmed J. Rheumatoid Arthritis: A Brief Overview of the Treatment. Med Princ Pract. 2018;27(6):501-507. doi: 10.1159/000493390. Epub 2018 Sep 2. PMID: 30173215; PMCID: PMC6422329.
82. Gaffo A, Saag KG, Curtis JR. Treatment of rheumatoid arthritis. Am J Health Syst Pharm. 2006 Dec 15;63(24):2451-65. doi: 10.2146/ajhp050514. PMID: 17158693.
83. Barnes PJ. How corticosteroids control inflammation: Quintiles Prize Lecture 2005. Br J Pharmacol. 2006 Jun;148(3):245-54. doi: 10.1038/sj.bjp.0706736. PMID: 16604091; PMCID: PMC1751559.
84. Ebina K, Hashimoto M, Yamamoto W, Hirano T, Hara R, Katayama M, Onishi A, Nagai K, Son Y, Amuro H, Yamamoto K, Maeda Y, Murata K, Jinno S, Takeuchi T, Hirao M, Kumanogoh A, Yoshikawa H. Drug tolerability and reasons for discontinuation of seven biologics in 4466 treatment courses of rheumatoid arthritis-the ANSWER cohort study. Arthritis Res Ther. 2019 Apr 11;21(1):91. doi: 10.1186/s13075-019-1880-4. Erratum in: Arthritis Res Ther. 2019 May 6;21(1):114. PMID: 30971306; PMCID: PMC6458752.
85. Lopez-Olivo MA, Tayar JH, Martinez-Lopez JA, Pollono EN, Cueto JP, Gonzales-Crespo MR, Fulton S, Suarez-Almazor ME. Risk of malignancies in patients with rheumatoid arthritis treated with biologic therapy: a meta-analysis. JAMA. 2012 Sep 5;308(9):898-908. doi: 10.1001/2012.jama.10857. PMID: 22948700.
86. Partridge AH, Avorn J, Wang PS, Winer EP. Adherence to therapy with oral antineoplastic agents. J Natl Cancer Inst. 2002 May 1;94(9):652-61. doi: 10.1093/jnci/94.9.652. PMID: 11983753.
87. Tarp S, Furst DE, Boers M, Luta G, Bliddal H, Tarp U, Asmussen KH, Brock B, Dossing A, Jørgensen TS, Thirstrup S, Christensen R. Risk of serious adverse effects of biological and targeted drugs in patients with rheumatoid arthritis: a systematic review meta-analysis. Rheumatology. 2017; 56(3):417–425. doi.org/10.1093/rheumatology/kew442.
88. Möttönen T, Hannonen P, Leirisalo-Repo M, Nissilä M, Kautiainen H, Korpela M, Laasonen L, Julkunen H, Luukkainen R, Vuori K, Paimela L, Blåfield H, Hakala M, Ilva K, Yli-Kerttula U, Puolakka K, Järvinen P, Hakola M, Piirainen H, Ahonen J, Pälvimäki I, Forsberg S, Koota K, Friman C. Comparison of combination therapy with single-drug therapy in early rheumatoid arthritis: a randomised trial. FIN-RACo trial group. Lancet. 1999 May 8;353(9164):1568-73. doi: 10.1016/s0140-6736(98)08513-4. PMID: 10334255.
89. Korpela M, Laasonen L, Hannonen P, Kautiainen H, Leirisalo-Repo M, Hakala M, Paimela L, Blåfield H, Puolakka K, Möttönen T; FIN-RACo Trial Group. Retardation of joint damage in patients with early rheumatoid arthritis by initial aggressive treatment with disease-modifying antirheumatic drugs: five-year experience from the FIN-RACo study. Arthritis Rheum. 2004 Jul;50(7):2072-81. doi: 10.1002/art.20351. PMID: 15248204.
90. Chen BK, Yang YT, Bennett CL. Why Biologics and Biosimilars Remain So Expensive: Despite Two Wins for Biosimilars, the Supreme Court's Recent Rulings

do not Solve Fundamental Barriers to Competition. Drugs. 2018 Nov;78(17):1777-1781. doi: 10.1007/s40265-018-1009-0. PMID: 30446980.

91. Kremer JM, Westhovens R, Leon M, Di Giorgio E, Alten R, Steinfeld S, Russell A, Dougados M, Emery P, Nuamah IF, Williams GR, Becker JC, Hagerty DT, Moreland LW. Treatment of rheumatoid arthritis by selective inhibition of T-cell activation with fusion protein CTLA4Ig. N Engl J Med. 2003 Nov 13;349(20):1907-15. doi: 10.1056/NEJMoa035075. PMID: 14614165.
92. Van Steendam, K., Tilleman, K., De Ceuleneer, M. *et al.* Citrullinated vimentin as an important antigen in immune complexes from synovial fluid of rheumatoid arthritis patients with antibodies against citrullinated proteins. *Arthritis Res Ther* **12,** R132 (2010). https://doi.org/10.1186/ar3070
93. Raijmakers R, van Beers JJ, El-Azzouny M, Visser NF, Božič B, Pruijn GJ, Heck AJ. Elevated levels of fibrinogen-derived endogenous citrullinated peptides in synovial fluid of rheumatoid arthritis patients. Arthritis Res Ther. 2012 May 14;14(3):R114. doi: 10.1186/ar3840. PMID: 22584083; PMCID: PMC3446491.
94. Lundberg K, Nijenhuis S, Vossenaar ER, Palmblad K, van Venrooij WJ, Klareskog L, Zendman AJ, Harris HE. Citrullinated proteins have increased immunogenicity and arthritogenicity and their presence in arthritic joints correlates with disease severity. Arthritis Res Ther. 2005;7(3):R458-67. doi: 10.1186/ar1697. Epub 2005 Feb 21. PMID: 15899032; PMCID: PMC1174941.
95. Schellekens GA, de Jong BA, van den Hoogen FH, van de Putte LB, van Venrooij WJ. Citrulline is an essential constituent of antigenic determinants recognized by rheumatoid arthritis-specific autoantibodies. J Clin Invest. 1998 Jan 1;101(1):273-81. doi: 10.1172/JCI1316. PMID: 9421490; PMCID: PMC508564.
96. Wang F, Chen FF, Gao WB, Wang HY, Zhao NW, Xu M, Gao DY, Yu W, Yan XL, Zhao JN, Li XJ. Identification of citrullinated peptides in the synovial fluid of patients with rheumatoid arthritis using LC-MALDI-TOF/TOF. Clin Rheumatol. 2016 Sep;35(9):2185-94. doi: 10.1007/s10067-016-3247-4. Epub 2016 Apr 8. PMID: 27060082; PMCID: PMC4989008.
97. Tabushi, Y., Nakanishi, T., Takeuchi, T., Nakajima, M., Ueda, K., Kotani, T., Makino, S., Shimizu, A., Hanafusa, T., & Takubo, T. (2008). Detection of citrullinated proteins in synovial fluids derived from patients with rheumatoid arthritis by proteomics-based analysis. *Annals of Clinical Biochemistry*, *45*(4), 413–417. https://doi.org/10.1258/acb.2007.007205
98. Fouda, A.I., Rageh, I., Hashaad, N.I. *et al.* Synovial fluid anti-citrulline-containing peptide antibody and its role in the diagnosis of rheumatoid arthritis. *Egypt Rheumatol Rehabil* **44,** 97–102 (2017). https://doi.org/10.4103/err.err_5_17
99. Kuhn KA, Kulik L, Tomooka B, Braschler KJ, Arend WP, Robinson WH, Holers VM. Antibodies against citrullinated proteins enhance tissue injury in experimental autoimmune arthritis. J Clin Invest. 2006 Apr;116(4):961-73. doi: 10.1172/JCI25422. PMID: 16585962; PMCID: PMC1421345.
100. Foulquier C, Sebbag M, Clavel C, Chapuy-Regaud S, Al Badine R, Méchin MC, Vincent C, Nachat R, Yamada M, Takahara H, Simon M, Guerrin M, Serre G. Peptidyl arginine deiminase type 2 (PAD-2) and PAD-4 but not PAD-1, PAD-3, and PAD-6 are expressed in rheumatoid arthritis synovium in close association with

tissue inflammation. Arthritis Rheum. 2007 Nov;56(11):3541-53. doi: 10.1002/art.22983. PMID: 17968929.

101. Samara KD, Trachalaki A, Tsitoura E, Koutsopoulos AV, Lagoudaki ED, Lasithiotaki I, Margaritopoulos G, Pantelidis P, Bibaki E, Siafakas NM, Tzanakis N, Wells AU, Antoniou KM. Upregulation of citrullination pathway: From Autoimmune to Idiopathic Lung Fibrosis. Respir Res. 2017 Dec 29;18(1):218. doi: 10.1186/s12931-017-0692-9. PMID: 29287593; PMCID: PMC5747943.
102. Curran, A.M., Naik, P., Giles, J.T. *et al.* PAD enzymes in rheumatoid arthritis: pathogenic effectors and autoimmune targets. *Nat Rev Rheumatol* **16,** 301–315 (2020). https://doi.org/10.1038/s41584-020-0409-1
103. Baeten D, Peene I, Union A, Meheus L, Sebbag M, Serre G, Veys EM, De Keyser F. Specific presence of intracellular citrullinated proteins in rheumatoid arthritis synovium: relevance to antifilaggrin autoantibodies. Arthritis Rheum. 2001 Oct;44(10):2255-62. doi: 10.1002/1529-0131(200110)44:10<2255::aid-art388>3.0.co;2-#. PMID: 11665966.
104. Zhou Y, Chen B, Mittereder N, Chaerkady R, Strain M, An LL, Rahman S, Ma W, Low CP, Chan D, Neal F, Bingham CO 3rd, Sampson K, Darrah E, Siegel RM, Hasni S, Andrade F, Vousden KA, Mustelin T, Sims GP. Spontaneous Secretion of the Citrullination Enzyme PAD2 and Cell Surface Exposure of PAD4 by Neutrophils. Front Immunol. 2017 Sep 25;8:1200. doi: 10.3389/fimmu.2017.01200. PMID: 28993780; PMCID: PMC5622307.
105. Carmona-Rivera C, Carlucci PM, Goel RR, James E, Brooks SR, Rims C, Hoffmann V, Fox DA, Buckner JH, Kaplan MJ. Neutrophil extracellular traps mediate articular cartilage damage and enhance cartilage component immunogenicity in rheumatoid arthritis. JCI Insight. 2020 Jul 9;5(13):e139388. doi: 10.1172/jci.insight.139388. PMID: 32484790; PMCID: PMC7406272.
106. Willis VC, Gizinski AM, Banda NK, Causey CP, Knuckley B, Cordova KN, Luo Y, Levitt B, Glogowska M, Chandra P, Kulik L, Robinson WH, Arend WP, Thompson PR, Holers VM. N-α-benzoyl-N5-(2-chloro-1-iminoethyl)-L-ornithine amide, a protein arginine deiminase inhibitor, reduces the severity of murine collagen-induced arthritis. J Immunol. 2011 Apr 1;186(7):4396-404. doi: 10.4049/jimmunol.1001620. Epub 2011 Feb 23. PMID: 21346230; PMCID: PMC3085980.
107. McInnes IB, Schett G. The pathogenesis of rheumatoid arthritis. N Engl J Med. 2011 Dec 8;365(23):2205-19. doi: 10.1056/NEJMra1004965. PMID: 22150039.
108. Law SC, Street S, Yu CH, Capini C, Ramnoruth S, Nel HJ, van Gorp E, Hyde C, Lau K, Pahau H, Purcell AW, Thomas R. T-cell autoreactivity to citrullinated autoantigenic peptides in rheumatoid arthritis patients carrying HLA-DRB1 shared epitope alleles. Arthritis Res Ther. 2012 ;14(3):R118. doi: 10.1186/ar3848
109. Tarcsa E, Marekov LN, Mei G, Melino G, Lee SC, Steinert PM. Protein unfolding by peptidylarginine deiminase. Substrate specificity and structural relationships of the natural substrates trichohyalin and filaggrin. J Biol Chem. 1996 Nov 29;271(48):30709-16. doi: 10.1074/jbc.271.48.30709. PMID: 8940048.

110. Kampstra AS, van Heemst J, Moustakas AK, Papadopoulos GK, Huizinga TW, Toes RE. The increased ability to present citrullinated peptides is not unique to HLA-SE molecules: arginine-to-citrulline conversion also enhances peptide affinity for HLA-DQ molecules. Arthritis Res Ther. 2016 Nov 3;18(1):254. doi: 10.1186/s13075-016-1153-4. PMID: 27809896; PMCID: PMC5094042.
111. Wegner N, Wait R, Sroka A, Eick S, Nguyen KA, Lundberg K, Kinloch A, Culshaw S, Potempa J, Venables PJ. Peptidylarginine deiminase from Porphyromonas gingivalis citrullinates human fibrinogen and α-enolase: implications for autoimmunity in rheumatoid arthritis. Arthritis Rheum. 2010 Sep;62(9):2662-72. doi: 10.1002/art.27552. PMID: 20506214; PMCID: PMC2941529.
112. Kurowska W, Kuca-Warnawin EH, Radzikowska A, Maśliński W. The role of anti-citrullinated protein antibodies (ACPA) in the pathogenesis of rheumatoid arthritis. Cent Eur J Immunol. 2017;42(4):390-398. doi: 10.5114/ceji.2017.72807.
113. Lu MC, Lai NS, Yu HC, Huang HB, Hsieh SC, Yu CL. Anti-citrullinated protein antibodies bind surface-expressed citrullinated Grp78 on monocyte/macrophages and stimulate tumor necrosis factor alpha production. Arthritis Rheum. 2010 May;62(5):1213-23. doi: 10.1002/art.27386. PMID: 20213805.
114. Kay J, Upchurch KS. ACR/EULAR 2010 rheumatoid arthritis classification criteria. Rheumatology (Oxford). 2012 Dec;51 Suppl 6:vi5-9. doi: 10.1093/rheumatology/kes279. PMID: 23221588.
115. Lin YJ, Anzaghe M, Schülke S. Update on the Pathomechanism, Diagnosis, and Treatment Options for Rheumatoid Arthritis. Cells. 2020 Apr 3;9(4):880. doi: 10.3390/cells9040880. PMID: 32260219; PMCID: PMC7226834.
116. Chemin K, Gerstner C, Malmström V. Effector Functions of CD4+ T Cells at the Site of Local Autoimmune Inflammation-Lessons From Rheumatoid Arthritis. Front Immunol. 2019 Mar 12;10:353. doi: 10.3389/fimmu.2019.00353. PMID: 30915067; PMCID: PMC6422991.
117. Yoshitomi H. Regulation of Immune Responses and Chronic Inflammation by Fibroblast-Like Synoviocytes. Front Immunol. 2019 Jun 19;10:1395. doi: 10.3389/fimmu.2019.01395. PMID: 31275325; PMCID: PMC6593115.
118. Kotake S, Udagawa N, Takahashi N, Matsuzaki K, Itoh K, Ishiyama S, Saito S, Inoue K, Kamatani N, Gillespie MT, Martin TJ, Suda T. IL-17 in synovial fluids from patients with rheumatoid arthritis is a potent stimulator of osteoclastogenesis. J Clin Invest. 1999 May;103(9):1345-52. doi: 10.1172/JCI5703. PMID: 10225978; PMCID: PMC408356.
119. Nakae S, Nambu A, Sudo K, Iwakura Y. Suppression of immune induction of collagen-induced arthritis in IL-17-deficient mice. J Immunol. 2003 Dec 1;171(11):6173-7. doi: 10.4049/jimmunol.171.11.6173. PMID: 14634133.
120. Wang D, Tai PWL, Gao G. Adeno-associated virus vector as a platform for gene therapy delivery. Nat Rev Drug Discov. 2019;18**,** 358–378. doi.org/10.1038/s41573-019-0012-9.
121. Naso MF, Tomkowicz B, Perry WL 3rd, Strohl WR. Adeno-Associated Virus (AAV) as a Vector for Gene Therapy. BioDrugs. 2017;31(4):317-334. doi: 10.1007/s40259-017-0234-5.

122. Ronzitti G, Gross DA, Mingozzi F. (2020). Human Immune Responses to Adeno-Associated Virus (AAV) Vectors. Frontiers in Immunology, 2020;11:670. doi:10.3389/fimmu.2020.00670.
123. Issa SS, Shaimardanova AA, Solovyeva VV, Rizvanov AA. Various AAV Serotypes and Their Applications in Gene Therapy: An Overview. Cells. 2023 Mar 1;12(5):785. doi: 10.3390/cells12050785.
124. Ellis BL, Hirsch ML, Barker JC, Connelly JP, Steininger RJ 3rd, Porteus MH. A survey of ex vivo/in vitro transduction efficiency of mammalian primary cells and cell lines with Nine natural adeno-associated virus (AAV1-9) and one engineered adeno-associated virus serotype. Virol J. 2013 Mar 6;10:74. doi: 10.1186/1743-422X-10-74. PMID: 23497173; PMCID: PMC3607841.
125. Fisher KJ, Jooss K, Alston J, Yang Y, Haecker SE, High K, Pathak R, Raper SE, Wilson JM. Recombinant adeno-associated virus for muscle directed gene therapy. Nat Med. 1997 Mar;3(3):306-12. doi: 10.1038/nm0397-306. PMID: 9055858.
126. Snyder RO, Miao CH, Patijn GA, Spratt SK, Danos O, Nagy D, Gown AM, Winther B, Meuse L, Cohen LK, Thompson AR, Kay MA. Persistent and therapeutic concentrations of human factor IX in mice after hepatic gene transfer of recombinant AAV vectors. Nat Genet. 1997 Jul;16(3):270-6. doi: 10.1038/ng0797-270. PMID: 9207793.
127. Xiao W, Chirmule N, Berta SC, McCullough B, Gao G, Wilson JM. Gene therapy vectors based on adeno-associated virus type 1. J Virol. 1999 May;73(5):3994-4003. doi: 10.1128/JVI.73.5.3994-4003.1999. PMID: 10196295; PMCID: PMC104178.
128. Kotterman MA, Schaffer DV. Engineering adeno-associated viruses for clinical gene therapy. Nat Rev Genet. 2014 Jul;15(7):445-51. doi: 10.1038/nrg3742. Epub 2014 May 20. PMID: 24840552; PMCID: PMC4393649.
129. Choi VW, McCarty DM, Samulski RJ. Host cell DNA repair pathways in adeno-associated viral genome processing. J Virol. 2006 Nov;80(21):10346-56. doi: 10.1128/JVI.00841-06. PMID: 17041215; PMCID: PMC1641795.
130. Manno CS, Pierce GF, Arruda VR, Glader B, Ragni M, Rasko JJ, Ozelo MC, Hoots K, Blatt P, Konkle B, Dake M, Kaye R, Razavi M, Zajko A, Zehnder J, Rustagi PK, Nakai H, Chew A, Leonard D, Wright JF, Lessard RR, Sommer JM, Tigges M, Sabatino D, Luk A, Jiang H, Mingozzi F, Couto L, Ertl HC, High KA, Kay MA. Successful transduction of liver in hemophilia by AAV-Factor IX and limitations imposed by the host immune response. Nat Med. 2006 Mar;12(3):342-7. doi: 10.1038/nm1358. Epub 2006 Feb 12. Erratum in: Nat Med. 2006 May;12(5):592. Rasko, John [corrected to Rasko, John JE]; Rustagi, Pradip K [added]. PMID: 16474400.
131. Ogbonmide T, Rathore R, Rangrej SB, Hutchinson S, Lewis M, Ojilere S, Carvalho V, Kelly I. Gene Therapy for Spinal Muscular Atrophy (SMA): A Review of Current Challenges and Safety Considerations for Onasemnogene Abeparvovec (Zolgensma). Cureus. 2023 Mar 15;15(3):e36197. doi: 10.7759/cureus.36197. PMID: 37065340; PMCID: PMC10104684.
132. Thornburg CD, Simmons DH, von Drygalski A. Evaluating Gene Therapy as a Potential Paradigm Shift in Treating Severe Hemophilia. BioDrugs. 2023

Sep;37(5):595-606. doi: 10.1007/s40259-023-00615-4. Epub 2023 Jul 25. PMID: 37490225; PMCID: PMC10432364.

133. Tonti E, Duvvuri B, Dhar S, Haaland D, Larche M, Larché M. Role of CD4+ T Cells in the Pathogenesis of RA: Immunization with Citrullinated T Cell Epitopes Is Sufficient to Induce Immunological and Clinical Manifestations of Arthritis in DR4-Transgenic Mice [abstract]. Arthritis Rheumatol. 2021; 73 (suppl 9). https://acrabstracts.org/abstract/role-of-cd4-t-cells-in-the-pathogenesis-of-ra-immunization-with-citrullinated-t-cell-epitopes-is-sufficient-to-induce-immunological-and-clinical-manifestations-of-arthritis-in-dr4-transgenic-mice/.

134. Musse AA, Li Z, Ackerley CA, Bienzle D, Lei H, Poma R, Harauz G, Moscarello MA, Mastronardi FG. Peptidylarginine deiminase 2 (PAD2) overexpression in transgenic mice leads to myelin loss in the central nervous system. Dis Model Mech. 2008 Nov-Dec;1(4-5):229-40. doi: 10.1242/dmm.000729. Epub 2008 Nov 6. PMID: 19093029; PMCID: PMC2590822.

135. Zendman AJW, Horstman WAM, Arntz AJ, Bennink MB, Vossenaar ER, van Venrooij WJ, van den Berg WB, van de Loo FAJ, Pruijn GJM. Effects of overexpression of PAD4 enzyme in mouse synovium. Arthritis Res Ther. 2005;7(Suppl 1):P45. doi: 10.1186/ar1566. Epub 2005 Feb 17. PMCID: PMC2834044.

136. Kaur J, Kumar A, Kaur J. Strategies for optimization of heterologous protein expression in E. coli: Roadblocks and reinforcements. Int J Biol Macromol. 2018 Jan;106:803-822. doi: 10.1016/j.ijbiomac.2017.08.080. Epub 2017 Aug 19. PMID: 28830778.

137. van Haasteren J, Hyde SC, Gill DR. Lessons learned from lung and liver in-vivo gene therapy: implications for the future. Expert Opin Biol Ther. 2018 Sep;18(9):959-972. doi: 10.1080/14712598.2018.1506761. Epub 2018 Aug 10. PMID: 30067117; PMCID: PMC6134476.

138. Kozak M. An analysis of 5'-noncoding sequences from 699 vertebrate messenger RNAs. Nucleic Acids Res. 1987 Oct 26;15(20):8125-48. doi: 10.1093/nar/15.20.8125. PMID: 3313277; PMCID: PMC306349.

139. Xie J, Zhuang Z, Gou S, Zhang Q, Wang X, Lan T, Lian M, Li N, Liang Y, Ouyang Z, Ye Y, Wu H, Lai L, Wang K. Precise genome editing of the Kozak sequence enables bidirectional and quantitative modulation of protein translation to anticipated levels without affecting transcription. Nucleic Acids Res. 2023 Oct 13;51(18):10075-10093. doi: 10.1093/nar/gkad687. PMID: 37650635; PMCID: PMC10570039.

140. Liu, Z., Chen, O., Wall, J.B.J., Zheng, M., Zhou, Y., Wang, L., Vaseghi, H.R., Qian, L., Liu, J. Systematic comparison of 2A peptides for cloning multi-genes in a polycistronic vector. Nature Sci Rep 7. 2017 May 2193. doi: 10.1038/s41598-017-02460-2

141. Grimm D, Zhou S, Nakai H, Thomas CE, Storm TA, Fuess S, Matsushita T, Allen J, Surosky R, Lochrie M, Meuse L, McClelland A, Colosi P, Kay MA. Preclinical in vivo evaluation of pseudotyped adeno-associated virus vectors for liver gene therapy. Blood. 2003 Oct 1;102(7):2412-9. doi: 10.1182/blood-2003-02-0495. Epub 2003 Jun 5. PMID: 12791653.

142. Zincarelli C, Soltys S, Rengo G, Rabinowitz JE. Analysis of AAV serotypes 1-9 mediated gene expression and tropism in mice after systemic injection. Mol Ther. 2008 Jun;16(6):1073-80. doi: 10.1038/mt.2008.76. Epub 2008 Apr 15. PMID: 18414476.
143. Donato MT, Tolosa L, Gómez-Lechón MJ. Culture and Functional Characterization of Human Hepatoma HepG2 Cells. Methods Mol Biol. 2015;1250:77-93. doi: 10.1007/978-1-4939-2074-7_5. PMID: 26272135.
144. Molinaro A, Becattini B, Solinas G. Insulin signaling and glucose metabolism in different hepatoma cell lines deviate from hepatocyte physiology toward a convergent aberrant phenotype. Sci Rep. 2020 Jul 21;10(1):12031. doi: 10.1038/s41598-020-68721-9. PMID: 32694512; PMCID: PMC7374613.
145. Weinberg MS, Nicolson S, Bhatt AP, McLendon M, Li C, Samulski RJ. Recombinant adeno-associated virus utilizes cell-specific infectious entry mechanisms. J Virol. 2014 Nov;88(21):12472-84. doi: 10.1128/JVI.01971-14. Epub 2014 Aug 20. PMID: 25142580; PMCID: PMC4248914.
146. Douar AM, Poulard K, Stockholm D, Danos O. Intracellular trafficking of adeno-associated virus vectors: routing to the late endosomal compartment and proteasome degradation. J Virol. 2001 Feb;75(4):1824-33. doi: 10.1128/JVI.75.4.1824-1833.2001. PMID: 11160681; PMCID: PMC114092.
147. Schellekens GA, Visser H, de Jong BA, van den Hoogen FH, Hazes JM, Breedveld FC, van Venrooij WJ. The diagnostic properties of rheumatoid arthritis antibodies recognizing a cyclic citrullinated peptide. Arthritis Rheum. 2000 Jan;43(1):155-63. doi: 10.1002/1529-0131(200001)43:1<155::AID-ANR20>3.0.CO;2-3. PMID: 10643712.
148. Moodie Z, Price L, Gouttefangeas C, Mander A, Janetzki S, Löwer M, Welters MJ, Ottensmeier C, van der Burg SH, Britten CM. Response definition criteria for ELISPOT assays revisited. Cancer Immunol Immunother. 2010 Oct;59(10):1489-501. doi: 10.1007/s00262-010-0875-4. Epub 2010 Jun 15. PMID: 20549207; PMCID: PMC2909425.
149. Rims C, Uchtenhagen H, Kaplan MJ, Carmona-Rivera C, Carlucci P, Mikecz K, Markovics A, Carlin J, Buckner JH, James EA. Citrullinated Aggrecan Epitopes as Targets of Autoreactive CD4+ T Cells in Patients With Rheumatoid Arthritis. Arthritis Rheumatol. 2019 Apr;71(4):518-528. doi: 10.1002/art.40768. Epub 2019 Mar 8. Erratum in: Arthritis Rheumatol. 2019 Jun;71(6):907. doi: 10.1002/art.40926. PMID: 30390384; PMCID: PMC6438725.
150. Takizawa Y, Suzuki A, Sawada T, Ohsaka M, Inoue T, Yamada R, Yamamoto K. Citrullinated fibrinogen detected as a soluble citrullinated autoantigen in rheumatoid arthritis synovial fluids. Ann Rheum Dis. 2006 Aug;65(8):1013-20. doi: 10.1136/ard.2005.044743. Epub 2006 Jan 31. PMID: 16449316; PMCID: PMC1798256.
151. Ho PP, Lee LY, Zhao X, Tomooka BH, Paniagua RT, Sharpe O, BenBarak MJ, Chandra PE, Hueber W, Steinman L, Robinson WH. Autoimmunity against fibrinogen mediates inflammatory arthritis in mice. J Immunol. 2010 Jan 1;184(1):379-90. doi: 10.4049/jimmunol.0901639. Epub 2009 Nov 30. PMID: 19949094; PMCID: PMC3412066.

152. von Delwig A, Locke J, Robinson JH, Ng WF. Response of Th17 cells to a citrullinated arthritogenic aggrecan peptide in patients with rheumatoid arthritis. Arthritis Rheum. 2010 Jan;62(1):143-9. doi: 10.1002/art.25064. PMID: 20039419.
153. Constantinescu CS, Farooqi N, O'Brien K, Gran B. Experimental autoimmune encephalomyelitis (EAE) as a model for multiple sclerosis (MS). Br J Pharmacol. 2011 Oct;164(4):1079-106. doi: 10.1111/j.1476-5381.2011.01302.x. PMID: 21371012; PMCID: PMC3229753.
154. Krienke C, Kolb L, Diken E, Streuber M, Kirchhoff S, Bukur T, Akilli-Öztürk Ö, Kranz LM, Berger H, Petschenka J, Diken M, Kreiter S, Yogev N, Waisman A, Karikó K, Türeci Ö, Sahin U. A noninflammatory mRNA vaccine for treatment of experimental autoimmune encephalomyelitis. Science. 2021 Jan 8;371(6525):145-153. doi: 10.1126/science.aay3638. PMID: 33414215.
155. James EA, Rieck M, Pieper J, Gebe JA, Yue BB, Tatum M, Peda M, Sandin C, Klareskog L, Malmström V, Buckner JH. Citrulline-specific Th1 cells are increased in rheumatoid arthritis and their frequency is influenced by disease duration and therapy. Arthritis Rheumatol. 2014 Jul;66(7):1712-22. doi: 10.1002/art.38637. PMID: 24665079; PMCID: PMC4248674.
156. Kinloch A, Tatzer V, Wait R, Peston D, Lundberg K, Donatien P, Moyes D, Taylor PC, Venables PJ. Identification of citrullinated alpha-enolase as a candidate autoantigen in rheumatoid arthritis. Arthritis Res Ther. 2005;7(6):R1421-9. doi: 10.1186/ar1845. Epub 2005 Oct 19. PMID: 16277695; PMCID: PMC1297593.
157. Pieper J, Dubnovitsky A, Gerstner C, James EA, Rieck M, Kozhukh G, Tandre K, Pellegrino S, Gebe JA, Rönnblom L, Sandalova T, Kwok WW, Klareskog L, Buckner JH, Achour A, Malmström V. Memory T cells specific to citrullinated α-enolase are enriched in the rheumatic joint. J Autoimmun. 2018 Aug;92:47-56. doi: 10.1016/j.jaut.2018.04.004. Epub 2018 May 28. PMID: 29853344; PMCID: PMC8259322.
158. Snir O, Rieck M, Gebe JA, Yue BB, Rawlings CA, Nepom G, Malmström V, Buckner JH. Identification and functional characterization of T cells reactive to citrullinated vimentin in HLA-DRB1*0401-positive humanized mice and rheumatoid arthritis patients. Arthritis Rheum. 2011 Oct;63(10):2873-83. doi: 10.1002/art.30445. PMID: 21567378; PMCID: PMC3174345.
159. Wölfl M, Greenberg PD. Antigen-specific activation and cytokine-facilitated expansion of naive, human CD8+ T cells. Nat Protoc. 2014 Apr;9(4):950-66. doi: 10.1038/nprot.2014.064. Epub 2014 Mar 27. PMID: 24675735; PMCID: PMC4312138.
160. Eming R, Büdinger L, Riechers R, Christensen O, Bohlen H, Kalish R, Hertl M. Frequency analysis of autoreactive T-helper 1 and 2 cells in bullous pemphigoid and pemphigus vulgaris by enzyme-linked immunospot assay. Br J Dermatol. 2000 Dec;143(6):1279-82. doi: 10.1046/j.1365-2133.2000.03901.x. PMID: 11122034.
161. Lucas M, Day CL, Wyer JR, Cunliffe SL, Loughry A, McMichael AJ, Klenerman P. Ex vivo phenotype and frequency of influenza virus-specific CD4 memory T cells. J Virol. 2004 Jul;78(13):7284-7. doi: 10.1128/JVI.78.13.7284-7287.2004. PMID: 15194806; PMCID: PMC421690.

162. Shim CH, Cho S, Shin YM, Choi JM. Emerging role of bystander T cell activation in autoimmune diseases. BMB Rep. 2022 Feb;55(2):57-64. doi: 10.5483/BMBRep.2022.55.2.183. PMID: 35000675; PMCID: PMC8891623.
163. Moodie Z, Price L, Janetzki S, Britten CM. Response determination criteria for ELISPOT: toward a standard that can be applied across laboratories. Methods Mol Biol. 2012;792:185-96. doi: 10.1007/978-1-61779-325-7_15. PMID: 21956511.
164. Singal DP, D'Souza M, Reid B, Bensen WG, Kassam YB, Adachi JD. HLA-DQ beta-chain polymorphism in HLA-DR4 haplotypes associated with rheumatoid arthritis. Lancet. 1987 Nov 14;2(8568):1118-20. doi: 10.1016/s0140-6736(87)91548-0. PMID: 2890022.
165. van Heemst J, Jansen DT, Polydorides S, Moustakas AK, Bax M, Feitsma AL, Bontrop-Elferink DG, Baarse M, van der Woude D, Wolbink GJ, Rispens T, Koning F, de Vries RR, Papadopoulos GK, Archontis G, Huizinga TW, Toes RE. Crossreactivity to vinculin and microbes provides a molecular basis for HLA-based protection against rheumatoid arthritis. Nat Commun. 2015 May 5;6:6681. doi: 10.1038/ncomms7681. PMID: 25942574.
166. Ali AA, Khalid KE, Mohammed SE, Akhtar MS, Saeed OK. Association of Human Leukocyte Antigen (HLA) class II (DRB1 and DQB1) alleles and haplotypes with Rheumatoid Arthritis in Sudanese patients. Front Immunol. 2023 Jun 22;14:1178546. doi: 10.3389/fimmu.2023.1178546. PMID: 37426636; PMCID: PMC10324672.
167. Munro S, Pelham HR. A C-terminal signal prevents secretion of luminal ER proteins. Cell. 1987 Mar 13;48(5):899-907. doi: 10.1016/0092-8674(87)90086-9. PMID: 3545499.
168. Sönnichsen B, Füllekrug J, Nguyen Van P, Diekmann W, Robinson DG, Mieskes G. Retention and retrieval: both mechanisms cooperate to maintain calreticulin in the endoplasmic reticulum. J Cell Sci. 1994 Oct;107 (Pt 10):2705-17. doi: 10.1242/jcs.107.10.2705. PMID: 7876339.
169. Raffaello A, Mammucari C, Gherardi G, Rizzuto R. Calcium at the Center of Cell Signaling: Interplay between Endoplasmic Reticulum, Mitochondria, and Lysosomes. Trends Biochem Sci. 2016 Dec;41(12):1035-1049. doi: 10.1016/j.tibs.2016.09.001. Epub 2016 Sep 28. PMID: 27692849; PMCID: PMC5123979.
170. Solovyova N, Verkhratsky A. Monitoring of free calcium in the neuronal endoplasmic reticulum: an overview of modern approaches. J Neurosci Methods. 2002 Dec 31;122(1):1-12. doi: 10.1016/s0165-0270(02)00300-x. PMID: 12535760.
171. Mastronardi FG, Wood DD, Mei J, Raijmakers R, Tseveleki V, Dosch HM, Probert L, Casaccia-Bonnefil P, Moscarello MA. Increased citrullination of histone H3 in multiple sclerosis brain and animal models of demyelination: a role for tumor necrosis factor-induced peptidylarginine deiminase 4 translocation. J Neurosci. 2006 Nov 1;26(44):11387-96. doi: 10.1523/JNEUROSCI.3349-06.2006. PMID: 17079667; PMCID: PMC6674531.
172. Nakashima K, Hagiwara T, Yamada M. Nuclear localization of peptidylarginine deiminase V and histone deimination in granulocytes. J Biol

Chem. 2002 Dec 20;277(51):49562-8. doi: 10.1074/jbc.M208795200. Epub 2002 Oct 18. PMID: 12393868.

173. Arita K, Hashimoto H, Shimizu T, Nakashima K, Yamada M, Sato M. Structural basis for Ca(2+)-induced activation of human PAD4. Nat Struct Mol Biol. 2004 Aug;11(8):777-83. doi: 10.1038/nsmb799. Epub 2004 Jul 11. PMID: 15247907.
174. Conti E, Uy M, Leighton L, Blobel G, Kuriyan J. Crystallographic analysis of the recognition of a nuclear localization signal by the nuclear import factor karyopherin alpha. Cell. 1998 Jul 24;94(2):193-204. doi: 10.1016/s0092-8674(00)81419-1. PMID: 9695948.
175. Cokol M, Nair R, Rost B. Finding nuclear localization signals. EMBO Rep. 2000 Nov;1(5):411-5. doi: 10.1093/embo-reports/kvd092. PMID: 11258480; PMCID: PMC1083765.
176. Lange A, Mills RE, Lange CJ, Stewart M, Devine SE, Corbett AH. Classical nuclear localization signals: definition, function, and interaction with importin alpha. J Biol Chem. 2007 Feb 23;282(8):5101-5. doi: 10.1074/jbc.R600026200. Epub 2006 Dec 14. PMID: 17170104; PMCID: PMC4502416.
177. Kalderon D, Roberts BL, Richardson WD, Smith AE. A short amino acid sequence able to specify nuclear location. Cell. 1984 Dec;39(3 Pt 2):499-509. doi: 10.1016/0092-8674(84)90457-4. PMID: 6096007.
178. Lu J, Wu T, Zhang B, Liu S, Song W, Qiao J, Ruan H. Types of nuclear localization signals and mechanisms of protein import into the nucleus. Cell Commun Signal. 2021 May 22;19(1):60. doi: 10.1186/s12964-021-00741-y. PMID: 34022911; PMCID: PMC8140498.
179. Lanford RE, Butel JS. Construction and characterization of an SV40 mutant defective in nuclear transport of T antigen. Cell. 1984 Jul;37(3):801-13. doi: 10.1016/0092-8674(84)90415-x. PMID: 6086146.
180. Karniely S, Pines O. Single translation--dual destination: mechanisms of dual protein targeting in eukaryotes. EMBO Rep. 2005 May;6(5):420-5. doi: 10.1038/sj.embor.7400394. PMID: 15864293; PMCID: PMC1299304.
181. Rohrbach AS, Slade DJ, Thompson PR, Mowen KA. Activation of PAD4 in NET formation. Front Immunol. 2012 Nov 29;3:360. doi: 10.3389/fimmu.2012.00360. PMID: 23264775; PMCID: PMC3525017.
182. Asaga H, Nakashima K, Senshu T, Ishigami A, Yamada M. Immunocytochemical localization of peptidylarginine deiminase in human eosinophils and neutrophils. J Leukoc Biol. 2001 Jul;70(1):46-51. PMID: 11435484.
183. Thomas MA, Kim SY, Curran AM, Smith B, Antiochos B, Na CH, Darrah E. An unbiased proteomic analysis of PAD4 in human monocytes: novel substrates, binding partners and subcellular localizations. Philos Trans R Soc Lond B Biol Sci. 2023 Nov 20;378(1890):20220477. doi: 10.1098/rstb.2022.0477. Epub 2023 Oct 2. PMID: 37778379; PMCID: PMC10542449.
184. Jiao W, Datta J, Lin HM, Dundr M, Rane SG. Nucleocytoplasmic shuttling of the retinoblastoma tumor suppressor protein via Cdk phosphorylation-dependent nuclear export. J Biol Chem. 2006 Dec 8;281(49):38098-108. doi: 10.1074/jbc.M605271200. Epub 2006 Oct 16. PMID: 17043357.

185. Kiefer P, Acland P, Pappin D, Peters G, Dickson C. Competition between nuclear localization and secretory signals determines the subcellular fate of a single CUG-initiated form of FGF3. EMBO J. 1994 Sep 1;13(17):4126-36. doi: 10.1002/j.1460-2075.1994.tb06730.x. PMID: 8076608; PMCID: PMC395335.
186. Petrova VY, Drescher D, Kujumdzieva AV, Schmitt MJ. Dual targeting of yeast catalase A to peroxisomes and mitochondria. Biochem J. 2004 Jun 1;380(Pt 2):393-400. doi: 10.1042/BJ20040042. PMID: 14998369; PMCID: PMC1224190.
187. Anandatheerthavarada HK, Biswas G, Mullick J, Sepuri NB, Otvos L, Pain D, Avadhani NG. Dual targeting of cytochrome P4502B1 to endoplasmic reticulum and mitochondria involves a novel signal activation by cyclic AMP-dependent phosphorylation at ser128. EMBO J. 1999 Oct 15;18(20):5494-504. doi: 10.1093/emboj/18.20.5494. PMID: 10523294; PMCID: PMC1171618.
188. Robin MA, Anandatheerthavarada HK, Biswas G, Sepuri NB, Gordon DM, Pain D, Avadhani NG. Bimodal targeting of microsomal CYP2E1 to mitochondria through activation of an N-terminal chimeric signal by cAMP-mediated phosphorylation. J Biol Chem. 2002 Oct 25;277(43):40583-93. doi: 10.1074/jbc.M203292200. Epub 2002 Aug 20. PMID: 12191992; PMCID: PMC3800117.
189. Vongsamphanh R, Fortier PK, Ramotar D. Pir1p mediates translocation of the yeast Apn1p endonuclease into the mitochondria to maintain genomic stability. Mol Cell Biol. 2001 Mar;21(5):1647-55. doi: 10.1128/MCB.21.5.1647-1655.2001. PMID: 11238901; PMCID: PMC86710.
190. Frechin M, Senger B, Brayé M, Kern D, Martin RP, Becker HD. Yeast mitochondrial Gln-tRNA(Gln) is generated by a GatFAB-mediated transamidation pathway involving Arc1p-controlled subcellular sorting of cytosolic GluRS. Genes Dev. 2009 May 1;23(9):1119-30. doi: 10.1101/gad.518109. PMID: 19417106; PMCID: PMC2682957.
191. Cranfill PJ, Sell BR, Baird MA, Allen JR, Lavagnino Z, de Gruiter HM, Kremers GJ, Davidson MW, Ustione A, Piston DW. Quantitative assessment of fluorescent proteins. Nat Methods. 2016 Jul;13(7):557-62. doi: 10.1038/nmeth.3891. Epub 2016 May 30. PMID: 27240257; PMCID: PMC4927352.
192. Henna Khalid, PAD4 inhibitors: potential sensitizers of tumour cells to TRAIL-induced apoptosis, Bioscience Horizons: The International Journal of Student Research, Volume 9, 2016, hzw003, https://doi.org/10.1093/biohorizons/hzw003
193. Guo Q, Bedford MT, Fast W. Discovery of peptidylarginine deiminase-4 substrates by protein array: antagonistic citrullination and methylation of human ribosomal protein S2. Mol Biosyst. 2011 Jul;7(7):2286-95. doi: 10.1039/c1mb05089c. Epub 2011 May 16. PMID: 21584310; PMCID: PMC3251905.
194. Chang X, Han J, Pang L, Zhao Y, Yang Y, Shen Z. Increased PADI4 expression in blood and tissues of patients with malignant tumors. BMC Cancer. 2009 Jan 30;9:40. doi: 10.1186/1471-2407-9-40. PMID: 19183436; PMCID: PMC2637889.

195. Chang X, Han J. Expression of peptidylarginine deiminase type 4 (PAD4) in various tumors. Mol Carcinog. 2006 Mar;45(3):183-96. doi: 10.1002/mc.20169. PMID: 16355400.
196. Fagoe ND, Eggers R, Verhaagen J, Mason MR. A compact dual promoter adeno-associated viral vector for efficient delivery of two genes to dorsal root ganglion neurons. Gene Ther. 2014 Mar;21(3):242-52. doi: 10.1038/gt.2013.71. Epub 2013 Nov 28. PMID: 24285216.
197. Ramezani A, Hawley TS, Hawley RG. Lentiviral vectors for enhanced gene expression in human hematopoietic cells. Mol Ther. 2000 Nov;2(5):458-69. doi: 10.1006/mthe.2000.0190. PMID: 11082319.
198. Klein R, Ruttkowski B, Knapp E, Salmons B, Günzburg WH, Hohenadl C. WPRE-mediated enhancement of gene expression is promoter and cell line specific. Gene. 2006 May 10;372:153-61. doi: 10.1016/j.gene.2005.12.018. Epub 2006 Feb 20. PMID: 16488559.
199. Limberis MP, Vandenberghe LH, Zhang L, Pickles RJ, Wilson JM. Transduction efficiencies of novel AAV vectors in mouse airway epithelium in vivo and human ciliated airway epithelium in vitro. Mol Ther. 2009 Feb;17(2):294-301. doi: 10.1038/mt.2008.261. Epub 2008 Dec 9. PMID: 19066597; PMCID: PMC2835069.
200. Li W, Zhang L, Wu Z, Pickles RJ, Samulski RJ. AAV-6 mediated efficient transduction of mouse lower airways. Virology. 2011 Sep 1;417(2):327-33. doi: 10.1016/j.virol.2011.06.009. Epub 2011 Jul 14. PMID: 21752418; PMCID: PMC3163804.
201. Halbert CL, Allen JM, Miller AD. Adeno-associated virus type 6 (AAV6) vectors mediate efficient transduction of airway epithelial cells in mouse lungs compared to that of AAV2 vectors. J Virol. 2001 Jul;75(14):6615-24. doi: 10.1128/JVI.75.14.6615-6624.2001. PMID: 11413329; PMCID: PMC114385.
202. Kinloch A, Lundberg K, Wait R, Wegner N, Lim NH, Zendman AJ, Saxne T, Malmström V, Venables PJ. Synovial fluid is a site of citrullination of autoantigens in inflammatory arthritis. Arthritis Rheum. 2008 Aug;58(8):2287-95. doi: 10.1002/art.23618. PMID: 18668562.
203. Damgaard D, Senolt L, Nielsen MF, Pruijn GJ, Nielsen CH. Demonstration of extracellular peptidylarginine deiminase (PAD) activity in synovial fluid of patients with rheumatoid arthritis using a novel assay for citrullination of fibrinogen. Arthritis Res Ther. 2014 Dec 5;16(6):498. doi: 10.1186/s13075-014-0498-9. PMID: 25475141; PMCID: PMC4298085.
204. Zhou Y, An LL, Chaerkady R, Mittereder N, Clarke L, Cohen TS, Chen B, Hess S, Sims GP, Mustelin T. Evidence for a direct link between PAD4-mediated citrullination and the oxidative burst in human neutrophils. Sci Rep. 2018 Oct 15;8(1):15228. doi: 10.1038/s41598-018-33385-z. PMID: 30323221; PMCID: PMC6189209.
205. Liu X, Arfman T, Wichapong K, Reutelingsperger CPM, Voorberg J, Nicolaes GAF. PAD4 takes charge during neutrophil activation: Impact of PAD4 mediated NET formation on immune-mediated disease. J Thromb Haemost. 2021 Jul;19(7):1607-1617. doi: 10.1111/jth.15313. Epub 2021 May 12. PMID: 33773016; PMCID: PMC8360066.

206. Bagur R, Hajnóczky G. Intracellular Ca2+ Sensing: Its Role in Calcium Homeostasis and Signaling. Mol Cell. 2017 Jun 15;66(6):780-788. doi: 10.1016/j.molcel.2017.05.028. PMID: 28622523; PMCID: PMC5657234.
207. Liu YL, Lee CY, Huang YN, Chen HY, Liu GY, Hung HC. Probing the Roles of Calcium-Binding Sites during the Folding of Human Peptidylarginine Deiminase 4. Sci Rep. 2017 May 25;7(1):2429. doi: 10.1038/s41598-017-02677-1. PMID: 28546558; PMCID: PMC5445078.
208. Vossenaar ER, Radstake TR, van der Heijden A, van Mansum MA, Dieteren C, de Rooij DJ, Barrera P, Zendman AJ, van Venrooij WJ. Expression and activity of citrullinating peptidylarginine deiminase enzymes in monocytes and macrophages. Ann Rheum Dis. 2004 Apr;63(4):373-81. doi: 10.1136/ard.2003.012211. PMID: 15020330; PMCID: PMC1754951.
209. Andrade F, Darrah E, Gucek M, Cole RN, Rosen A, Zhu X. Autocitrullination of human peptidyl arginine deiminase type 4 regulates protein citrullination during cell activation. Arthritis Rheum. 2010 Jun;62(6):1630-40. doi: 10.1002/art.27439. PMID: 20201080; PMCID: PMC2951335.
210. Chen X, Zaro JL, Shen WC. Fusion protein linkers: property, design and functionality. Adv Drug Deliv Rev. 2013 Oct;65(10):1357-69. doi: 10.1016/j.addr.2012.09.039. Epub 2012 Sep 29. PMID: 23026637; PMCID: PMC3726540.
211. Argos P. An investigation of oligopeptides linking domains in protein tertiary structures and possible candidates for general gene fusion. J Mol Biol. 1990 Feb 20;211(4):943-58. doi: 10.1016/0022-2836(90)90085-Z. PMID: 2313701.
212. Robinson CR, Sauer RT. Optimizing the stability of single-chain proteins by linker length and composition mutagenesis. Proc Natl Acad Sci U S A. 1998 May 26;95(11):5929-34. doi: 10.1073/pnas.95.11.5929. PMID: 9600894; PMCID: PMC34497.
213. Reddy Chichili VP, Kumar V, Sivaraman J. Linkers in the structural biology of protein-protein interactions. Protein Sci. 2013 Feb;22(2):153-67. doi: 10.1002/pro.2206. Epub 2013 Jan 8. PMID: 23225024; PMCID: PMC3588912.
214. Maeda Y, Ueda H, Kazami J, Kawano G, Suzuki E, Nagamune T. Engineering of functional chimeric protein G-Vargula luciferase. Anal Biochem. 1997 Jul 1;249(2):147-52. doi: 10.1006/abio.1997.2181. PMID: 9212866.
215. Klein JS, Jiang S, Galimidi RP, Keeffe JR, Bjorkman PJ. Design and characterization of structured protein linkers with differing flexibilities. Protein Eng Des Sel. 2014 Oct;27(10):325-30. doi: 10.1093/protein/gzu043. PMID: 25301959; PMCID: PMC4191447.
216. Snapp E. Design and use of fluorescent fusion proteins in cell biology. Curr Protoc Cell Biol. 2005 Jul;Chapter 21:21.4.1-21.4.13. doi: 10.1002/0471143030.cb2104s27. PMID: 18228466; PMCID: PMC2875081.
217. Evanko D. Training GFP to fold. Nat Methods. 2006 Feb;3(2):76. doi: 10.1038/nmeth0206-76. PMID: 16468177.
218. Waldo GS, Standish BM, Berendzen J, Terwilliger TC. Rapid protein-folding assay using green fluorescent protein. Nat Biotechnol. 1999 Jul;17(7):691-5. doi: 10.1038/10904. PMID: 10404163.

219. Hink MA, Griep RA, Borst JW, van Hoek A, Eppink MH, Schots A, Visser AJ. Structural dynamics of green fluorescent protein alone and fused with a single chain Fv protein. J Biol Chem. 2000 Jun 9;275(23):17556-60. doi: 10.1074/jbc.M001348200. PMID: 10748019.
220. Arita K, Shimizu T, Hashimoto H, Hidaka Y, Yamada M, Sato M. Structural basis for histone N-terminal recognition by human peptidylarginine deiminase 4. Proc Natl Acad Sci U S A. 2006 Apr 4;103(14):5291-6. doi: 10.1073/pnas.0509639103. Epub 2006 Mar 27. PMID: 16567635; PMCID: PMC1459348.
221. Waterhouse A, Bertoni M, Bienert S, Studer G, Tauriello G, Gumienny R, Heer FT, de Beer TAP, Rempfer C, Bordoli L, Lepore R, Schwede T. SWISS-MODEL: homology modelling of protein structures and complexes. Nucleic Acids Res. 2018 Jul 2;46(W1):W296-W303. doi: 10.1093/nar/gky427. PMID: 29788355; PMCID: PMC6030848.
222. Pieper U, Webb BM, Dong GQ, Schneidman-Duhovny D, Fan H, Kim SJ, Khuri N, Spill YG, Weinkam P, Hammel M, Tainer JA, Nilges M, Sali A. ModBase, a database of annotated comparative protein structure models and associated resources. Nucleic Acids Res. 2014 Jan;42(Database issue):D336-46. doi: 10.1093/nar/gkt1144. Epub 2013 Nov 23. PMID: 24271400; PMCID: PMC3965011.
223. Jumper J, Evans R, Pritzel A, Green T, Figurnov M, Ronneberger O, Tunyasuvunakool K, Bates R, Žídek A, Potapenko A, Bridgland A, Meyer C, Kohl SAA, Ballard AJ, Cowie A, Romera-Paredes B, Nikolov S, Jain R, Adler J, Back T, Petersen S, Reiman D, Clancy E, Zielinski M, Steinegger M, Pacholska M, Berghammer T, Bodenstein S, Silver D, Vinyals O, Senior AW, Kavukcuoglu K, Kohli P, Hassabis D. Highly accurate protein structure prediction with AlphaFold. Nature. 2021 Aug;596(7873):583-589. doi: 10.1038/s41586-021-03819-2. Epub 2021 Jul 15. PMID: 34265844; PMCID: PMC8371605.
224. Puranen T, Poutanen M, Ghosh D, Vihko R, Vihko P. Origin of substrate specificity of human and rat 17beta-hydroxysteroid dehydrogenase type 1, using chimeric enzymes and site-directed substitutions. Endocrinology. 1997 Aug;138(8):3532-9. doi: 10.1210/endo.138.8.5303. PMID: 9231808.
225. Amin B, Voelter W. Human Deiminases: Isoforms, Substrate Specificities, Kinetics, and Detection. Prog Chem Org Nat Prod. 2017;106:203-240. doi: 10.1007/978-3-319-59542-9_2. PMID: 28762090.
226. Nakayama-Hamada M, Suzuki A, Kubota K, Takazawa T, Ohsaka M, Kawaida R, Ono M, Kasuya A, Furukawa H, Yamada R, Yamamoto K. Comparison of enzymatic properties between hPADI2 and hPADI4. Biochem Biophys Res Commun. 2005 Feb 4;327(1):192-200. doi: 10.1016/j.bbrc.2004.11.152. PMID: 15629448.
227. Assohou-Luty C, Raijmakers R, Benckhuijsen WE, Stammen-Vogelzangs J, de Ru A, van Veelen PA, Franken KL, Drijfhout JW, Pruijn GJ. The human peptidylarginine deiminases type 2 and type 4 have distinct substrate specificities. Biochim Biophys Acta. 2014 Apr;1844(4):829-36. doi: 10.1016/j.bbapap.2014.02.019. Epub 2014 Mar 2. PMID: 24594197.

228. Darrah E, Rosen A, Giles JT, Andrade F. Peptidylarginine deiminase 2, 3 and 4 have distinct specificities against cellular substrates: novel insights into autoantigen selection in rheumatoid arthritis. Ann Rheum Dis. 2012 Jan;71(1):92-8. doi: 10.1136/ard.2011.151712. Epub 2011 Aug 21. PMID: 21859690; PMCID: PMC3302156.
229. Zhu D, Lu Y, Wang Y, Wang Y. PAD4 and Its Inhibitors in Cancer Progression and Prognosis. Pharmaceutics. 2022 Nov 8;14(11):2414. doi: 10.3390/pharmaceutics14112414. PMID: 36365233; PMCID: PMC9699117.
230. Ioan-Facsinay A, Willemze A, Robinson DB, Peschken CA, Markland J, van der Woude D, Elias B, Ménard HA, Newkirk M, Fritzler MJ, Toes RE, Huizinga TW, El-Gabalawy HS. Marked differences in fine specificity and isotype usage of the anti-citrullinated protein antibody in health and disease. Arthritis Rheum. 2008 Oct;58(10):3000-8. doi: 10.1002/art.23763. PMID: 18821680.
231. Snir O, Widhe M, von Spee C, Lindberg J, Padyukov L, Lundberg K, Engström A, Venables PJ, Lundeberg J, Holmdahl R, Klareskog L, Malmström V. Multiple antibody reactivities to citrullinated antigens in sera from patients with rheumatoid arthritis: association with HLA-DRB1 alleles. Ann Rheum Dis. 2009 May;68(5):736-43. doi: 10.1136/ard.2008.091355. Epub 2008 Jul 17. PMID: 18635594.
232. Barakat S, Briand JP, Weber JC, van Regenmortel MH, Muller S. Recognition of synthetic peptides of Sm-D autoantigen by lupus sera. Clin Exp Immunol. 1990 Aug;81(2):256-62. doi: 10.1111/j.1365-2249.1990.tb03327.x. PMID: 2387092; PMCID: PMC1535060.
233. Charpin C, Arnoux F, Martin M, Toussirot E, Lambert N, Balandraud N, Wendling D, Diot E, Roudier J, Auger I. New autoantibodies in early rheumatoid arthritis. Arthritis Res Ther. 2013 Jul 25;15(4):R78. doi: 10.1186/ar4255. PMID: 23886014; PMCID: PMC3978570.
234. van Beers JJ, Willemze A, Stammen-Vogelzangs J, Drijfhout JW, Toes RE, Pruijn GJ. Anti-citrullinated fibronectin antibodies in rheumatoid arthritis are associated with human leukocyte antigen-DRB1 shared epitope alleles. Arthritis Res Ther. 2012 Feb 17;14(1):R35. doi: 10.1186/ar3744. PMID: 22339947; PMCID: PMC3392834.
235. Li Q, Li Y, Liang B, Xu R, Xu B, Lönnblom E, Feng H, Bai J, Stawikowska R, Ge C, Lu A, Fields GB, Xiao L, Holmdahl R. Rheumatoid arthritis sera antibodies to citrullinated collagen type II bind to joint cartilage. Arthritis Res Ther. 2022 Nov 22;24(1):257. doi: 10.1186/s13075-022-02945-0. PMID: 36419093; PMCID: PMC9682822.
236. Fanelli I, Rovero P, Hansen PR, Frederiksen J, Houen G, Trier NH. Specificity of Anti-Citrullinated Protein Antibodies to Citrullinated α-Enolase Peptides as a Function of Epitope Structure and Composition. Antibodies (Basel). 2021 Jul 21;10(3):27. doi: 10.3390/antib10030027. PMID: 34449533; PMCID: PMC8395424.
237. Trier NH, Holm BE, Heiden J, Slot O, Locht H, Lindegaard H, Svendsen A, Nielsen CT, Jacobsen S, Theander E, Houen G. Antibodies to a strain-specific citrullinated Epstein-Barr virus peptide diagnoses rheumatoid arthritis. Sci Rep.

2018 Feb 27;8(1):3684. doi: 10.1038/s41598-018-22058-6. PMID: 29487382; PMCID: PMC5829227.

238. Trier NH, Holm BE, Slot O, Locht H, Lindegaard H, Svendsen A, Houen G. Physical Characteristics of a Citrullinated Pro-Filaggrin Epitope Recognized by Anti-Citrullinated Protein Antibodies in Rheumatoid Arthritis Sera. PLoS One. 2016 Dec 21;11(12):e0168542. doi: 10.1371/journal.pone.0168542. PMID: 28002483; PMCID: PMC5176188.
239. Soutullo A, Santi MN, Perin JC, Beltramini LM, Borel IM, Frank R, Tonarelli GG. Systematic epitope analysis of the p26 EIAV core protein. J Mol Recognit. 2007 Jul-Aug;20(4):227-37. doi: 10.1002/jmr.825. PMID: 17705340.
240. Nogueira L, Parra E, Larrieu M, Verrouil E, Cornillet M. Are antibodies to fine specificities of citrullinated peptides/proteins useful for stratification of rheumatoid arthritis patients? Clin Transl Immunology. 2021 Jul 5;10(7):e1288. doi: 10.1002/cti2.1288. PMID: 34257966; PMCID: PMC8256671.
241. Slack JL, Jones LE Jr, Bhatia MM, Thompson PR. Autodeimination of protein arginine deiminase 4 alters protein-protein interactions but not activity. Biochemistry. 2011 May 17;50(19):3997-4010. doi: 10.1021/bi200309e. Epub 2011 Apr 20. PMID: 21466234; PMCID: PMC3091952.
242. Méchin MC, Coudane F, Adoue V, Arnaud J, Duplan H, Charveron M, Schmitt AM, Takahara H, Serre G, Simon M. Deimination is regulated at multiple levels including auto-deimination of peptidylarginine deiminases. Cell Mol Life Sci. 2010 May;67(9):1491-503. doi: 10.1007/s00018-010-0262-5. Epub 2010 Jan 29. PMID: 20111885; PMCID: PMC11115946.
243. Auger I, Martin M, Balandraud N, Roudier J. Rheumatoid arthritis-specific autoantibodies to peptidyl arginine deiminase type 4 inhibit citrullination of fibrinogen. Arthritis Rheum. 2010 Jan;62(1):126-31. doi: 10.1002/art.27230. PMID: 20039406.
244. Darrah E, Giles JT, Ols ML, Bull HG, Andrade F, Rosen A. Erosive rheumatoid arthritis is associated with antibodies that activate PAD4 by increasing calcium sensitivity. Sci Transl Med. 2013 May 22;5(186):186ra65. doi: 10.1126/scitranslmed.3005370. PMID: 23698378; PMCID: PMC3740946.
245. Darrah E, Giles JT, Davis RL, Naik P, Wang H, Konig MF, Cappelli LC, Bingham CO 3rd, Danoff SK, Andrade F. Autoantibodies to Peptidylarginine Deiminase 2 Are Associated With Less Severe Disease in Rheumatoid Arthritis. Front Immunol. 2018 Nov 20;9:2696. doi: 10.3389/fimmu.2018.02696. PMID: 30515171; PMCID: PMC6255931.
246. Nissinen R, Paimela L, Julkunen H, Tienari PJ, Leirisalo-Repo M, Palosuo T, Vaarala O. Peptidylarginine deiminase, the arginine to citrulline converting enzyme, is frequently recognized by sera of patients with rheumatoid arthritis, systemic lupus erythematosus and primary Sjögren syndrome. Scand J Rheumatol. 2003;32(6):337-42. doi: 10.1080/03009740410004990. PMID: 15080264.
247. Halvorsen EH, Pollmann S, Gilboe IM, van der Heijde D, Landewé R, Ødegård S, Kvien TK, Molberg Ø. Serum IgG antibodies to peptidylarginine deiminase 4 in rheumatoid arthritis and associations with disease severity. Ann

Rheum Dis. 2008 Mar;67(3):414-7. doi: 10.1136/ard.2007.080267. Epub 2007 Nov 15. PMID: 18006540.

248. Whitley E, Ball J. Statistics review 6: Nonparametric methods. Crit Care. 2002 Dec;6(6):509-13. doi: 10.1186/cc1820. Epub 2002 Sep 13. PMID: 12493072; PMCID: PMC153434.
249. Sidney Siegel (1957) Nonparametric Statistics, The American Statistician, 11:3, 13-19, DOI: 10.1080/00031305.1957.10501091
250. Christley RM. Power and Error: Increased Risk of False Positive Results in Underpowered Studies. The Open Epidemiology Journal: 3, 16-19; 2010.
251. Chan LL, Laverty DJ, Smith T, Nejad P, Hei H, Gandhi R, Kuksin D, Qiu J. Accurate measurement of peripheral blood mononuclear cell concentration using image cytometry to eliminate RBC-induced counting error. J Immunol Methods. 2013 Feb 28;388(1-2):25-32. doi: 10.1016/j.jim.2012.11.010. Epub 2012 Nov 29. PMID: 23201386.
252. Gold LI, Eggleton P, Sweetwyne MT, Van Duyn LB, Greives MR, Naylor SM, Michalak M, Murphy-Ullrich JE. Calreticulin: non-endoplasmic reticulum functions in physiology and disease. FASEB J. 2010 Mar;24(3):665-83. doi: 10.1096/fj.09-145482. Epub 2009 Nov 25. PMID: 19940256; PMCID: PMC2830142.
253. Surre J, Saint-Ruf C, Collin V, Orenga S, Ramjeet M, Matic I. Strong increase in the autofluorescence of cells signals struggle for survival. Sci Rep. 2018 Aug 14;8(1):12088. doi: 10.1038/s41598-018-30623-2. PMID: 30108248; PMCID: PMC6092379.
254. Monici M. Cell and tissue autofluorescence research and diagnostic applications. Biotechnol Annu Rev. 2005;11:227-56. doi: 10.1016/S1387-2656(05)11007-2. PMID: 16216779.
255. Teuscher AC, Ewald CY. Overcoming Autofluorescence to Assess GFP Expression During Normal Physiology and Aging in Caenorhabditis elegans. Bio Protoc. 2018 Jul 20;8(14):e2940. doi: 10.21769/BioProtoc.2940. PMID: 30073182; PMCID: PMC6067662.
256. Billinton N, Knight AW. Seeing the wood through the trees: a review of techniques for distinguishing green fluorescent protein from endogenous autofluorescence. Anal Biochem. 2001 Apr 15;291(2):175-97. doi: 10.1006/abio.2000.5006. PMID: 11401292.
257. Zhang Z, Fan H, Richardson W, Gao BZ, Ye T. Management of autofluorescence in formaldehyde-fixed myocardium: choosing the right treatment. Eur J Histochem. 2023 Oct 2;67(4):3812. doi: 10.4081/ejh.2023.3812. PMID: 37781779; PMCID: PMC10614721.
258. Porteus MH, Cathomen T, Weitzman MD, Baltimore D. Efficient gene targeting mediated by adeno-associated virus and DNA double-strand breaks. Mol Cell Biol. 2003 May;23(10):3558-65. doi: 10.1128/MCB.23.10.3558-3565.2003. PMID: 12724414; PMCID: PMC164769.
259. Howard DB, Harvey BK. Assaying the Stability and Inactivation of AAV Serotype 1 Vectors. Hum Gene Ther Methods. 2017 Feb;28(1):39-48. doi: 10.1089/hgtb.2016.180. PMID: 28192678; PMCID: PMC5314999.

260. Bee JS, Zhang Y, Finkner S, O'Berry K, Kaushal A, Phillippi MK, DePaz RA, Webber K, Marshall T. Mechanistic Studies and Formulation Mitigations of Adeno-associated Virus Capsid Rupture During Freezing and Thawing: Mechanisms of Freeze/Thaw Induced AAV Rupture. J Pharm Sci. 2022 Jul;111(7):1868-1878. doi: 10.1016/j.xphs.2022.03.018. Epub 2022 Mar 26. PMID: 35351496.
261. Srivastava A, Mallela KMG, Deorkar N, Brophy G. Manufacturing Challenges and Rational Formulation Development for AAV Viral Vectors. J Pharm Sci. 2021 Jul;110(7):2609-2624. doi: 10.1016/j.xphs.2021.03.024. Epub 2021 Apr 2. Erratum in: J Pharm Sci. 2021 Sep;110(9):3324. doi: 10.1016/j.xphs.2021.07.006. PMID: 33812887.
262. Won P, Kim Y, Jung H, Rim YA, Sohn DH, Robinson WH, Moon SJ, Ju JH. Pathogenic Role of Circulating Citrullinated Antigens and Anti-Cyclic Monoclonal Citrullinated Peptide Antibodies in Rheumatoid Arthritis. Front Immunol. 2021 Jun 30;12:692242. doi: 10.3389/fimmu.2021.692242. PMID: 34305925; PMCID: PMC8294326.